IL
NUOVO CIMENTO
ORGANO DELLA SOCIETÀ ITALIANA DI FISICA
SOTTO GLI AUSPICI DEL CONSIGLIO NAZIONALE DELLE RICERCHE

VOL. VIII, N. 2 *Serie decima* 16 Aprile 1958

The Range-Energy Relation in Emulsion.

PART. I. – Range Measurements (*).

W. H. BARKAS, P. H. BARRETT, P. CÜER, H. HECKMAN,
F. M. SMITH and H. K. TICHO

Radiation Laboratory, University of California - Berkeley, California

(ricevuto il 25 Maggio 1957)

Summary. — Simultaneous exposures have been made of Ilford G.5 emulsion to magnetically analyzed mesons as well as to hydrogen and helium nuclei of various velocities. Measurements of the particle ranges have been made for equivalent proton energies of 1.295 MeV to 700 MeV. Individual particle momenta were known to better than one part in a thousand. Especial care was taken to maintain the emulsion density at an accurately measured value. Curves and formulae used for converting particle ranges to their proton equivalents at other emulsion densities are given. Detailed procedures for correcting ranges of particles that traverse gaps between pellicles are described. Various effects that influence range measurements are discussed. Comparisons with existing data are made. Good agreement is found to exist only when the emulsion densities are known, and a correct procedure is employed to adjust the measured ranges to standard conditions. An empirical correction of the Vigneron range table is made.

1. – Introduction.

For some time it has been realized that a complete experimental restudy of the range energy relation in emulsion would be desirable. The technique of stacked emulsion pellicles has been developed so that emulsion now is a

(*) This work was done under the auspices of the U. S. Atomic Energy Commission.

most important instrument for high-energy physics, but empirical range-energy data have not been available for very high particel velocities. Even at low energies the range curve has not been known well, because the density of the emulsion from which most of the information came [1] was not known, or was known to differ from that of the stacked emulsion. Recently, the need for reliable data at very high as well as at low velocities for measuring the decay energies of hyperons and of K-mesons became acute, making this work imperative.

Some possible pitfalls in a range-energy experiment are reliance on secondary standards or unproven methods for the estimate of particle energies, and failure to measure true rectified particle ranges. Mesaurement of the momenta of particles by deflecting them through 180° in an accurately measured magnetic field greatly reduces the first uncertainty. Also, by measurement of the visible length of particle tracks in emulsion, one may avoid a scattering correction in measuring the rectified range. The advantages of incorporating these features in a range-energy experiment were obvious, therefore when we undertook new measurements we introduced these techniques as well as precise knowledge of the emulsion density. In another respect the experiment described below deviates from convention. It is usual to collimate beams strongly to obtain a group of monoenergetic particles by bending in a magnetic field. This, however, leads to slit scattering. We prefer to use a small source and an open geometry. We calculate momenta from the known source position and the observed point and direction of intersection of each particle trajectory with the emulsion. This enables us to calculate individual momenta to a part in one thousand, or better, and every track provides useful range data. The investigation was designed primarily to yield information regarding the *mean ranges*; their statistical distribution has been the subject of another study [2].

2. – Measurement of emulsion density and shrinkage factor.

The Ilford G-5 emulsion used in this experiment was from a single manufacturing batch (Z9299). Prior to use it was stored 50 feet underground for several weeks in the manufasturer's tight packaging. Equilibrium with respect to the water content of the emulsion therefore was approached [3]. Seventeen samples were taken, just after exposure, from throughout the emulsion volume,

[1] See the compilation by L. VIGNERON: *Journ. Phys. Rad.*, **14**, 145 (1953).
[2] W. H. BARKAS, F. M. SMITH and W. BIRNBAUM: *Phys. Rev.*, **98**, 605 (1955).
[3] A. OLIVER: *Rev. Sci. Instr.*, **25**, 326 (1954).

and exterior edges were trimmed from them. The density of each piece (of about 1 g) was determined by weighing in air, in carbon tetrachloride, and again in air to check the original weight, by the method developed in this laboratory ([3]). The individual densities in g/cm^3 were: 3.824, 3.834, 3.838, 3.832, 3.814, 3,836, 3,810, 3.810, 3.821, 3.819, 3.808, 3.827, 3.828, 3.825, 3.828, 3,813, 3.815 (Av. 3.8225). The fluctuations are real, and their existence has previously been mentioned in connection with the measurement of range straggling ([2]). They have important implications. In this study the samples taken were each about 4 cm^2 of 600 μm emulsion. In smaller volume elements even greater variations must take place. For short ranges, density fluctuation of the order of 1% therefore may be expected, and data from any one emulsion plate cannot be relied upon to be better than this no matter how many ranges are measured. (It is suggested that this effect may be one reason why a number of observers have found an apparent difference between ranges in samples of G-5 and of C-2 emulsion, which at the same density should not be detectably different in stopping power.) Long ranges, which sample a large part of the emulsion volume, are less affected by local density fluctuations, but a contribution to the range straggling from the emulsion heterogeneity may nevertheless be expected.

The area and weight of each piece of emulsion, along with the density, gave the average thickness. This agreed to within $\frac{1}{2}$% with the average thickness of the sheets determined from the over-all dimensions of the stacks into which the emulsion was assembled.

After the processing in the usual way with 5% glycerine in the alcohol drying baths, the emulsion thicknesses were measured again. The various estimates of the shrinkage factor all are included in the interval 1.97 to 2.02. (This includes one measurement derived statistically from the ranges of μ-mesons originating in π-μ decays with varying dip angles, which gave 2.02 ± 0.03.)

3. – Apparatus and exposure.

The experiment was carried out in the vacuum chamber of the 184 inch cyclotron. Pions, protons, triton, deuterons, ^{3}He, and α-particles of various velocities originating simultaneously in a small target were deflected through 180° and intercepted by emulsion. The slightly non-uniform magnetic field was mapped at the time of the experiment by use of the proton-moment magnetometer of Varian Associates. The distances from the target to the various emulsion stacks and pellicles were known to within 0.1% or better.

To insure that the density of the emulsion remained unchanged when it was introduced into the vacuum, the following steps were taken.

(*a*) For detecting long-range particles the emulsion was made up into tightly clamped stacks. An edge of each was milled flat. The stacks were exposed to particles incident normal to the milled surfaces. From the theory of water diffusion in emulsion we know that the thickness of emulsion that is dried out when such a stack is left in vacuum for the half hour required to carry out the experiment is negligible compared with the particle ranges.

(*b*) For tracks of less than a centimeter a more difficult problem was presented. To solve it two devices known as « mousetraps » were constructed, which clamped emulsion surfaces together tightly until a few seconds before the exposure to the beam (which lasted only 3 s). Just before exposure an

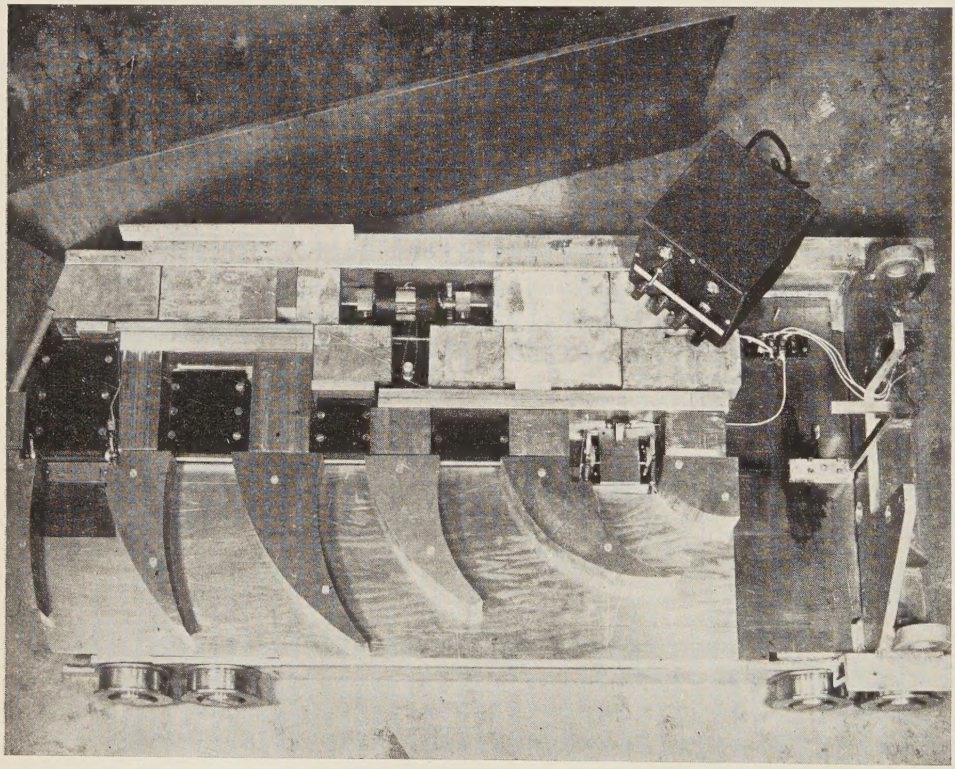

Fig. 1. – Photograph of the apparatus. It is mounted on a cart which enters the cyclotron vacuum chamber through an air lock. The target is the small polystyrene parallelopiped suspended on the right. The emulsion stacks are clamped between bakelite boards. The control box shown operates the armature, which rotates in the cyclotron field and provides the power for tripping the « mousetraps », one of which is shown to the right in the line of the four stacks. The proton beam of the cyclotron circulates above the cart and only the target is in the median plane to intercept the beam. The target support is not bombarded because the cyclotron beam is radially clipped by other probes.

electric signal cause the « trap » to snap open and expose a fresh surface of emulsion to the beam, which entered the emulsion with a small angle of dip.

Particles emitted forward from the polystyrene target were deflected through 180° and detected below the plane of the circulating proton beam. The apparatus for doing this was developed on the basis of experience gained in earlier work in which the problems were similar ([4,5]). Fig. 1 shows the apparatus used.

4. – Calculation of momenta.

The calculation of the momenta followed closely the method developed in connection with the measurement of meson masses ([5]). The target dimensions were kept sufficiently small that when the secondary-particle momenta were calculated on the assumption that the particles came from the center of the target, the mean values would never be in error by as much as 0.1%. In

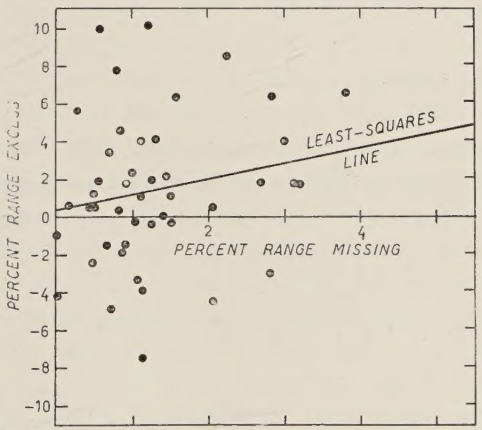

Fig. 2. – Illustration of method for eliminating effect of air spaces in stack. The percent range excess (100 μ) plotted against the percent range missing (100 α) for each track measured in an emulsion stack. The scatter of points in this diagram illustrates well the chief problem encountered in making precise range measurements in stacked emulsion. A correct treatment of it is essential for carrying out competent emulsion measurements. The horizontal displacements of the points from zero represent the track lengths which are unaccounted for in passing between pellicles, while the vertical dispersion is brought about by this effect coupled with the usual range straggling. This method of analysis has been devised to eliminate the systematic error in the range measurement, and reduce the calculation of the statistical error to the determination of the standard deviation of the ordinate at which the inclined line intersects the axis of ordinates.

(4) W. H. Barkas and H. Tyren: *Phys. Rev.*, **89**, 1 (1952).
(5) W. H. Barkas, W. Birnbaum and F. M. Smith: *Phys. Rev.*, **101**, 778 (1956).

addition, the dimensions were chosen so that the calculated momentum spread caused by the finite target size would increase the apparent range straggling only inappreciably. The actual dimensions were: height (parallel to the magnetic field), $\frac{1}{2}$ in.; length (parallel to the proton beam, $\frac{3}{8}$ in.; thickness (the radial dimension), 1/16 in. The thickness is the most critical, since this dimension directly affects the diameter of the secondary-particle orbits. So that the length could be kept reasonably large, and in order than the precession of the orbits might have a negligible effect, only those particle tracks were included in the analysis for which the angle θ' was in the interval $\pm 5°$. (The angle θ' is the horizontal projection of the angle between the particle orbit and the perpendicular to the edge of the emulsion stack (coincident with the radial line) at the point where the particle enters the emulsion. (See Fig. 2, ref. ( ).) This also reduced the momentum uncertainty caused by errors of about $\pm 1°$ in the measured of θ', since the momentum formula is insensitive to θ' when it is near zero.

5. – Measurement of ranges.

The range is defined ([2]) by $R_0 = \int (\mathrm{d}x_0^2 + \mathrm{d}y_0^2 + \mathrm{d}z_0^2)^{\frac{1}{2}}$. The integration is considered to be taken along the locus of the latent image of the particle track in the unprocessed emulsion. After processing, the range is found in good approximation from

$$R_1 = \int (\mathrm{d}x^2 + \mathrm{d}y^2 + S^2\,\mathrm{d}z^2)^{\frac{1}{2}} ,$$

when the distortion, aside from shrinkage, is small, and the z dimension (normal to the emulsion surface) shrinks in processing by a factor S.

Each long track was measured independent by two or more observers. The measurement of the range is carried out by breaking up the trajectory into a number of segments. Each segment approximates a straight line. The number of separate segments measured is determined by a general consideration of the amount of measurement error that can be tolerated. This was set at about 0.1% in this experiment. The x, y and z projections of the length of each segment are measured either by an eyepiece reticle calibrated to 0.1% or by a mechanical stage with a screw motion of similar accuracy. Calling the projections of the i-th segment Δx_i, Δy_i, and Δz_i, one computes an estimate of the range from

$$R_s = \sum_i (\Delta x_i^2 + \Delta y_i^2 + S^2 \Delta z_i^2)^{\frac{1}{2}} .$$

The track is taken to extend between the extremities of the first and last grains in the track. Tracks that show evidence of inelastic scattering are discarded. It is required that the distribution of ranges be consistent with the expected range straggling ([6]).

Consider a co-ordinate frame in which the beginning of the track is at the origin and the terminus of the track lies near the x axis. The co-ordinates of the terminus are designated X, Y, and Z. As a check of the range measurements, the independently measured sum $\sum \Delta x_i \equiv R_x$ may be compared with X. For tracks that lie in a single sheet of emulsion, the measured difference $X - R_x$ is a random variable of expectation value zero. The situation is more complicated when a track traverses several pellicles. The finite grain spacing, the possibility of surface erosion, surface graininess, imperfect matching of the co-ordinate frames in the two pellicles, loss of sensitivity at the surface, and the possibility of air gaps between surfaces, all may introduce systematic contributions to the expectation value of $X - R_x$: (In some important published researches, tissue paper has been packed between pellicles, but we avoided such a further complication.) We find that a systematic effect generally exists, and the expectation value of $X - R_x$ is normally positive. Whereas R_s is a lower limit for the true range, $R_t \equiv R_s + (X - R_x)$ is an approximate upper limit; R_s will be less than the true range if some of the path in emulsion is not seen and measured, and R_t will exceed the true range if gaps exist between pellicles. The meaning of R_t is made clearer if it is written $X + (R_s - R_x)$. The quantity X is then the main contribution to the measurement, but, because of scattering, a contribution to the range (given to sufficient accuracy by $R_s - R_x$) comes from the y and z components of the particle motion. To investigate the existence of air gaps, a statistical approach may be taken. If air gaps exist, the magnitude of R_t should be positively correlated with the magnitude of $X - R_x$. To make particles of slightly different momenta comparable, one utilizes as a standard an existing range-momentum curve from which the measured ranges deviate only by small amounts. Suppose R is the standard range for a particle of momentum p, and R_s, X, R_x, and R_t are the corresponding quantities introduced above. Then we define $\mu \equiv (R_t - R)/R$, and $\alpha \equiv (X - R_x)/R$.

If gaps occur between the pellicles, a functional relationship exists between

([6]) W. H. BARKAS: *Phys. Rev.*, **89**, 1019 (1953). In this experiment ^{8}Li and ^{8}B ranges were measured as well as ranges, in the same emulsion plates, of hydrogen and helium isotopes that had been magnetically analyzed along with the heavy ions. This enables one to make precise comparisons of ranges of various particles at the same velocity. Although it was stated in this paper that neither the emulsion density nor the absolute value of the magnetic field was accurately known, the ranges measured in this experiment are sometimes cited as if they were absolute measurements.

$\langle\mu\rangle$ and α, where $\langle\mu\rangle$ (in a small velocity interval) is the average value of μ as a function of α.

The intercept $\langle\mu\rangle_0$ is the value of $\langle\mu\rangle$ that would be obtained were there no gaps. Although it cannot be shown rigoroulsy that the relation between $\langle\mu\rangle$ and α is always linear, our data do not justify a more refined analysis. In Fig. 2 is shown the least-squares straight line calculated from measured values of μ and α for pions in a small stack. The true range is taken to be

$$R[1 + \langle\mu\rangle_0] .$$

When only a limited numbers of tracks are measured, as for the long-range groups, the data may be insufficient to define well the slope of the line, and another procedure is preferred. The value of α tells one how accurately the measurement of the depth of penetration, X, agrees with the measured $\sum \Delta x_i$. Large values of α correspond to large possible errors. Tracks giving large α's may be discarded without biasing the range measurement. If this is done, the mean value $\langle\alpha\rangle$ calculated for the remaining tracks is an indication of the possible systematic error introduced by the air spaces in the stack. In these cases we have discarded the tracks with values of α exceeding 0.007 and corrected the over-all mean value, $\ll\mu\gg$, of μ to $\ll\mu\gg - (\langle\alpha\rangle\, 2)$. Then we have compounded the quantity $\langle\alpha\rangle\, 3$ with the range straggling in calculating the standard deviation of the point.

For the long-range groups of tracks a correction was necessary because the probability of scattering out of the stack became important. Since near the end of the range the two highest-energy groups had characteristic survival lengths of only 3.5 and 2 cm, a correction of 0.2 % was found necessary for each of these ranges.

Measurement of the range in emulsion stacks is complicated by a number of additional effects. Because the particles enter the edge of the stack, the range measurement must be carried out to the original position of the edge. The edges of the stack were milled flat, and before processing a 1 mm grid was contact-printed on each pellicle. The grid position was the same with respect to the track to within a few microns on each sheet. After the pellicles are mounted and processed, the edge is of course distorted and blackened, but we have found, by using the grid as a reference system, that the line of contact of the emulsion edge with the glass (when viewed by a long-focus objective through the glass) is a reliable indication of the original edge position. Of course if the emulsion has pulled away from the glass, or if the pellicle has been mounted so wet and warm that it is distorted, this will not be true. By milling two opposite edges of the stacks, we discovered an effect for which corrections were required. Clamping the stack causes an outward

distortion or flow of the emulsion which is at least partially reversible on releasing the pressure. Therefore the X and Y components of particle ranges shrink when the compressive force is relieved. This effect was found to amount to 0.2% in the largest stacks to 0.5% in the smallest stack employed in this experiment. This correction was made, but no other distortion effects were found that could significantly affect the ranges.

In order that the rate of energy loss as calculated theoretically may be compared with the slope of the empirical energy-range curve, we require that the technique of measurement yield the true integral of the path in standard unprocessed emulsion. It is possible, of course, to adopt other conventions on what is meant by the range in emulsion, and « ranges » differing from ours could be obtained by measurements on the same tracks. Some observers, for example, disregard scattering in the vertical plane in rectifying ranges. Another approximation that is sometimes made in adjusting ranges to standard conditions is to assume that the product of the density obtained from the overall weight and volume of the stack and the total distance traversed by the particle in coming to rest in the stack is a constant. This is correct, however, only if the voids in the stack are homogeneously distributed and if the actual emulsion density is standard.

6. – Adjustment of data to equivalent proton ranges under standard conditions of density.

All our measured ranges have been converted to equivalent proton ranges. The conversion is made through the quantity $\lambda \equiv (z^2 R/M) - B_z$. This quantity is a function solely of the particle velocity, βc. (It is the actual range in centimeters of an antiproton of this velocity). R is the range in centimeters of any heavy positive particle of velocity βc, charge Ze, and mass M in units of the proton mass. The term B_z is added to correct for the range extension caused by the neutralization of positively charged particles by electron attachment at low velocities. At velocities sufficiently high that the ion remains stripped, B_z is a constant. An estimate of it has been made by BARKAS [6]:

$$B_z \approx 1.2 \cdot 10^{-5} z^3 \text{ cm} .$$

The particle kinetic energy we symbolize by T. The quantity $\tau = T/M$ is the kinetic energy of a proton of velocity βc. This experiment is designed to determine the relationship between τ and λ. It yields, therefore, range-energy relations for all heavy charged particles. In the conversion of ranges

to an equivalent range at a standard emulsion density, changes in density are not correctly allowed for by taking the range to vary inversely with the density. The variations of density of emulsion arise chiefly from changes in its water content, and the stopping behavior of water is appreciably different from that of standard emulsion. Water is relatively more effective in stopping at low particle velocities. We do not quote emulsion ranges in g/cm² because such ranges would not be independent of the water content of the emulsion.

We have made some studies of the variation of the emulsion volume with changes of the water content, and have found that emulsion behaves somewhat as if it were a porous structure containing voids that may absorb water. Normally the volume change of an emulsion sample is not as great as the volume of water added or removed, but if sufficient time elapses for adjustments in the emulsion structure to take place, additivity of the volumes is improved. By waiting two weeks between changes of the ambient humidity we found, for 600 μm G-5 emulsion, that the volume increments in cm³ averaged 94% of the weight increments in grams. Ilford Ltd. have estimated this to be 84% (⁷).

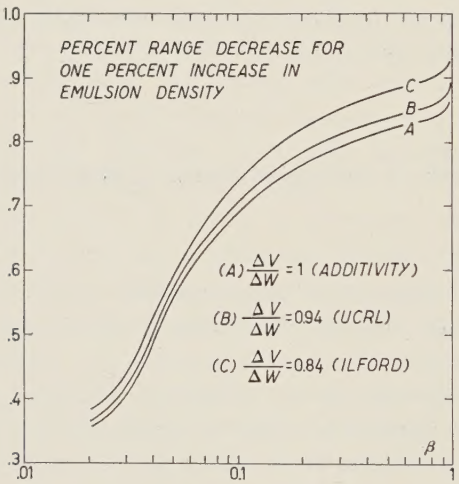

Fig. 3. – Curves for adjusting measured ranges to equivalent ranges in standard emulsion. The correction depends on the particle velocity, βc.

Let us select a density d_0 g/cm³ as the density of « standard » emulsion. To obtain a simple and accurate formula for the range in emulsion of some other density, d g/cm³, we make the rather good approximations: $d\lambda_d/d\lambda \approx \lambda_d/\lambda$, and $d\lambda_w/d\lambda \approx \lambda_w/\lambda$. Here λ_p is the range in emulsion of density d and λ_w

(⁷) Letter of 24 January 1956 from C. WALLER to E. GROSS.

is the range in water. Then we have

$$\frac{\lambda}{\lambda_l} = \frac{rd - 1}{rd_0 - 1} + \frac{r(d_0 - d)}{rd_0 - 1} \frac{\lambda}{\lambda_w},$$

where r $(= \Delta V / \Delta W)$ is the ratio of the volume increment in cubic centimeters to the weight increment in grams brought about by the addition of moisture to emulsion. The range curve for water has been calculated as described in Part 2 of this report. With this one may determine the correction required to adjust ranges measured in Ilford G-5 emulsion of arbitrary density to the corresponding ranges in standard emulsion. The correction factors are graphed in Fig. 3 for the three cases (*a*) $r = 1$ cm^3/g (additivity of volumes), (*b*) $r = 0.94$ cm^3/g (from our measurements), (*c*) $r = 0.84$ cm^3/g (from Ilford measurements). The correction factor is seen to depend rather strongly on β and to a less extent on r. We have made our range corrections using $r = 0.94$ cm^3/g.

7. – Results.

In a previous publication some meson ranges measured in this program were reported ([8]). In this article we include several new velocity points derived from the ranges of hydrogen and helium isotopes as well as more extended meson data. A re-examination of the possible sources of error has also been made. The inclusion of several small corrections described in Sect. 5 has had the general effect of increasing the ranges. The particle-mass ratios ([5]) are known well enough so that no appreciable error is introduced by them in the conversion to equivalent proton ranges. Since may of the ranges deviate considerably from those reported in the literature for emulsion plates, an independent investigation ([9]) was carried out to check our results by different methods ([4]). Table I, which is the most recent and most complete list of our measured ranges, contains these results in addition to the data obtained in the experiment described here. Some of the measurements were made in Strasbourg.

([8]) W. H. Barkas, P. H. Barrett, P. Cüer, H. Heckman, F. M. Smith and H. K. Ticho: *Phys. Rev.*, **102**, 583 (1956).

([9]) W. H. Barkas, F. M. Smith and H. Heckman: *Range-Energy Measurements in Emulsion*, UCRL-3513 (Aug. 1956).

TABLE I. – *Range points derived from the measurements.*

The errors indicated are standard deviations. Because many different kinds of particles were measured, normalized quantities are tabulated:

$$\tau = T/M \qquad \text{and} \qquad \lambda = z^2 R/M - 1.2 \cdot 10^{-5} z^3 .$$

The particle kinetic energy is symbolized by T. The quantity M is the mass of the particle in units of the proton, R is the range in centimeters, and z is the number of units of positive electric charge carried by the particle.

Particle	τ (MeV)	λ (cm)
α	1.295	$20.7 \pm 0.2 \cdot 10^{-4}$ (*)
p	2.421	$53.9 \pm 0.6 \cdot 10^{-4}$ (*)
t	2.450	$55.67 \pm 0.34 \cdot 10^{-4}$
d, t, ^{3}He, α	5.00	$175.1 \pm 2.0 \cdot 10^{-4}$ (+)
d	5.477	$204.6 \pm 0.64 \cdot 10^{-4}$
α	5.477	$205.5 \pm 1.1 \cdot 10^{-4}$
^{3}He	10.00	$562.7 \pm 2.6 \cdot 10^{-4}$
p	13.96	$988.3 \pm 7.4 \cdot 10^{-4}$ (*)
p	21.21	$2056 \pm 5 \cdot 10^{-4}$
μ^+	36.55	$5345 \pm 22 \cdot 10^{-4}$
π^+	200	10.31 ± 0.07
π^+	340	24.74 ± 0.10
π^+	540	51.15 ± 0.45
π^+	700	74.97 ± 0.36

(*) From Reference (9).
(+) Ranges measured in Strasbourg.

8. – Discussion and comparison with other measurements.

Many emulsion-range data for low velocities have been published, and the emulsion densities corresponding to some of these range measurements probably are known fairly well. Some experiments that we have performed indicate that, if the emulsion came to equilibrium in vacuum, the density was probably 4.00 to 4.03 g/cm^3. Ilford Ltd. give 4.033 g/cm^3 for the mean density of many samples of G-5 emulsion dried over H_2SO_4 (7). For thin layers (50 μm or less)

of C-2, E-1, and G-5 emulsion in vacuum for 2 or 3 hours, this condition probably was approached. In any case the surface layer, containing the tracks of the slowest grazing-incident particles, will have dried out. For longer ranges, where greater depths of penetration into emulsion are experienced, it is no longer certain that the emulsion has dried out completely. In reference ([3]) the theory of the drying is given, and it is shown that very long times in vacuum are required for emulsion to reach its maximum density. In connection with the range measurements now being reported we performed drying experiments with pellicles of 600 μm emulsion suspended in vacuum with both surfaces free. (This makes the unmounted pellicle equivalent in drying behavior to a 300 μm plate.) Table II shows how the mean density of one pellicle varied with time. Evidently the density of the deepest layers in this pellicle was little affected for perhaps the whole first day of evacuation.

TABLE II. – *Vacuum desiccation of emulsion. Mean density of a sample of unmounted* 600 μm G.5 *emulsion as a function of time in vacuum. (For mounted emulsion multiply all time intervals by four).*

Time in vacuum (h)	Mean density	Time in vacuum (h)	Mean density
0	3.812	45.5	3.962
2.75	3.853	69.5	3.986
4.5	3.871	172	4.010
21.0	3.927	334	4.021
27.5	3.946	502	4.022

Accurate range data were obtained by CÜER and JUNG for proton energies up to 5.2 MeV ([1]). As they used thin emulsion layers in vacuum for long periods, we may assume that the emulsion attained a density of ≈ 4.01 g/cm^3.

ROTBLAT ([11]) and GIBSON, PROWSE, and ROTBLAT ([12]) have also made many range measurements in the low-velocity region. They have published a smoothed table derived from their measurements on emulsion that had been kept in vacuum for certain times depending on the thickness. Although it was thought that the time in vacuum was sufficiently long in each case for an equilibrium to be attained, the times cited were, we think, insufficient for the greater thicknesses. They estimated the density of their emulsion as

([10]) P. CÜER and J. J. JUNG: *Sci. et Ind. Phot.*, **22**, 401 (1951).
([11]) J. ROTBLAT: *Nature*, **167**, 550 (1951).
([12]) W. M. GIBSON, D. Y. PROWSE and J. ROTBLAT: *Nature*, **173**, 1180 (1954).

3.94 g cm^3. This figure does not correspond to dryness, and the deep layers of emulsion probably had a lower density, while the surface layer was certainly rather dry. The differences between our measurements and those by GIBSON *et al.* for protons above 5 MeV can be entirely attributed to incorrect assumptions regarding what emulsion densities to associate with their various measured points. In an early study BRADNER *et al.* demonstrated the effect on the range of varying the emulsion dryness, ([13]), but—although an attempt was made to maintain normal laboratory humidity conditions—no measurements of the emulsion densities were obtainable, and their data cannot be cited because of this important deficiency. This remark applies equally to many other measurements that we do not quote for the same reason.

The range of the μ-meson from the decay of the pion is an important point of comparison. Here we are in virtually perfect agreement with the measurements made in the G-Stack ([11]) when allowance for the emulsion density is made. The adjusted range from the G-stack is (602.2 ± 2.1 μm) and our measurement is (602.2 ± 2.2) μm. The μ-meson range in standard emulsion then is known to be (602.2 ± 1.5) μm, Although the range straggling is large for μ-mesons, if a few hundred flat tracks are measured in a sample of emulsion, its density can be obtained reasonably well by comparing the measured range with 602.2 μm and calculating the density ratio, using Fig. 3.

By an ingenious use of the momentum balance in the decay of the π-meson, G. L. BACCHELLA *et al.* have found a way to develop an emulsion range curve beyond the π-μ decay point without making momentum measurements ([15]). An objection in principle to their method is that they assume a form for the range-energy relation that cannot have the same shape as the theoretical curve and, in fact, crosses it at two points. At 200 MeV our measured range is $(1.5 \pm 0.7)\%$ higher than their curve, andat 340 MeV it is $(0.4 \pm 0.4)\%$ lower, when allowance for the emulsion density difference is made by means of the μ-meson ranges.

There are no emulsion range measurements in the literature at higher velocities for which the particle energy has been measured in a direct way. A number of measurements in which the range in emulsion has been compared with the range in copper are available, but since by the method of measurement the actual rectified particles ranges are not seen, and the stopping power of copper is not well known in any case, we shall not undertake detailed comparisons with these measurements.

([13]) H. BRADNER, F. M. SMITH, W. H. BARKAS and A. S. BISHOP: *Phys. Rev.*, **77**, 462 (1950).

([14]) G-STACK COLLABORATION: *Nuovo Cimento*, **2**, 1063 (1955).

([15]) G. L. BACCHELLA, A. BERTHELOT, M. DI CORATO, O. GOUSSU, R. LEVI-SETTI, M. RENÉ, D. REVEL, L. SCARSI, G. TOMASINI and G. VANDERHAEGHE: *Nuovo Cimento*, **4**, 1529 (1956).

9. – The empirical range-energy relation.

Too few points were measured in this work alone to define a continuous empirical range-energy relation, but the new points are sufficient to correct to standard conditions an existing smooth table such as that of VIGNERON [1] (and its extension by BARKAS and YOUNG [16]) using Vigneron's mean ionization potential without shell corrections. This mean ionization potential was first proposed by CÜER and JUNG [10]). Table III lists the corrections as a

TABLE III. – *Percentage by which the measured ranges exceed Vigneron's. The values of* τ *are the equivalent proton energies at which our measurements are made.*

τ (MeV)	Percentage	τ (MeV)	Percentage
1.295	2.0 ± 1.0	13.96	0.9 ± 0.8
2.421	2.2 ± 1.1	21.21	1.3 ± 0.2
2.45	3.7 ± 0.6	36.55	1.2 ± 0.4
5.00	2.6 ± 1.2	200	0.7 ± 0.7
5.477	3.0 ± 0.3	340	1.0 ± 0.4
5.477	3.4 ± 0.6	540	1.4 ± 0.9
10.00	2.2 ± 0.5	700	1.3 ± 0.5

function of particle energy. In Part 2 of this report it is found that the measured ranges determine a mean ionization potential for emulsion of (331 ± 6) eV when the K- and L-shell corrections for the various elements are included in the Bethe-Bloch stopping formula. It is well to remember that small differences in the technique of measurement can easily affect the measured ranges by 1% or so. For the greatest accuracy, therefore, this range-energy relation must be used in conujnction with the range-measurement procedure and the corrections described above.

* * *

The cyclotron work in connection with this program was aided by the helpful co-operation of JAMES VALE and LLOYD HOUSER. Many of the range

[16] W. H. BARKAS and D. M. YOUNG: *Emulsion Tables. - I. Heavy-Particle Functions*, UCRL-2579 (rev.), (Sept. 1954).

measurements were made by NANCY FREED, HESTER LOWE, ROBERTA SPEER, JOHN DYER, and RENÉE FELDMAN, while MILDRED JOHNSON and CARL COLE aided in the emulsion-density studies.

This work was done under the auspices of the U. S. Atomic Energy Commission.

RIASSUNTO (*)

Emulsioni Ilford G.5 sono state simultaneamente esposte a mesoni analizzati magneticamente, nonchè a nuclei di idrogeno e di elio di differenti velocità. Si sono eseguite misure dei range delle particelle per energie protoniche equivalenti da 1295 MeV a 700 MeV. Gli impulsi delle singole particelle si conoscevano con esattezza superiore all'1 ‰. Ci si è specialmente curati di mantenere la densità dell'emulsione ad un valore esattamente misurato. Si danno le formule e le curve usate per convertire i range delle particelle nei loro equivalenti protonici ad altre densità dell'emulsione. Si descrivono dettagliati procedimenti per correggere i range delle particelle che traversano spazi fra pellicole adiacenti. Si discutono alcuni effetti che hanno influenza sulla misure di range. Si fanno confronti con dati già esistenti. Si trova un buon accordo solo se le densità delle emulsioni sono note e si impiega un procedimento corretto per aggiustare i range misurati a condizioni standard. Si esegue una correzione empirica della tabella dei range di Vigneron.

(*) *Traduzione a cura della Redazione.*

IL NUOVO CIMENTO Vol. VIII, N. 2 16 Aprile 1958

The Range-Energy Relation in Emulsion.

Part. II. – The Theoretical Range (*).

W. H. Barkas

Radiation Laboratory, University of California - Berkeley, California

(ricevuto il 25 Maggio 1957)

Summary. — The Bethe-Bloch theory of stopping, including shell corrections and the density-effect correction, is used to calculate theoretical ranges for standard Ilford G.5 emulsion. Only the mean ionization potential is an adjustable parameter. Making corrections for the K shells of all emulsion atoms except hydrogen, and also correcting for the L shells of iodine, silver, and bromine, one can obtain a fit to the measured ranges for protons of 1 to 700 MeV. The mean ionization potential found is (331 ± 6) eV, and I/Z has a value of (12.1 ± 0.2) eV as an average for all emulsion elements except hydrogen. At low velocities the hydrogenlike atomic model used in the shell-correction calculations appears to overaccentuate the shell effects. A better agreement with the experimental data for proton energies below 40 MeV is obtained semiempirically. A range table for emulsion of standard density is given. A calculated range table for water, useful for adjusting ranges measured under nonstandard density conditions, is also included.

1. – Introduction.

In Table I Part I we have listed our measured particle ranges with their associated statistical errors [1]. It is now proposed to draw on theoretical considerations as well as on other experimental data to obtain the best continuous functional relationship between the particle energy and its range in

(*) This work was done under the auspices of the U. S. Atomic Energy Commission.

(1) W. H. Barkas, P. H. Barrett, P. Cüer, H. Heckman, F. M. Smith and H. K. Ticho: *Phys. Rev.*, **102**, 583 (1956).

emulsion. The same notation as in Part I is used throughout. The appropriately corrected Bethe-Bloch theory of stopping contains only one adjustable parameter, the mean ionization potential ([2]). By means of the theory we use all the experimental points to improve our knowledge of the range for each particular velocity. The theoretical relation provides a means of interpolating between the experimental pointsm and of extrapolating to energies beyond those for which ranges have been measured.

2. – Characterization of the stopping medium.

Nuclear track emulsion is a complex substance. It consists of heavy inorganic crystals a few tenths of a micron in diameter suspended in an organic medium. The matrix material, which is largely gelatin, readily absorbs water, and the density of the emulsion varies with its water content, and also locally as the statistical ratio of heavy to light components fluctuates. The rate at which a charged particle loses energy in the heavy component varies with velocity in a different way from that in the light component.

We assume the average composition ([3]) of emulsion having a density of 3.815 g/cm^3 to be that given in Table I. This « standard » density of emulsion is arbitrary, but it has been chosen near that normally found for Ilford G-5 emulsion in equilibrium at a relative humidity of 60% ([3]).

3. – Stopping theory.

For particles of low velocity, NIELS BOHR ([4]) has theoretically deduced Geiger's empirical law that the rangse increases with the cube of the particle velocity. This suggests plotting the low ranges in emulsion against the $\frac{3}{2}$ power of the kinetic energy. In Fig. 1 the data are seen to define straight lines. It should be noted, however, that finite intercepts are obtained if the lines are extended to zero energy. The intercept consists of (*a*) the term B_l, which allows for the range extension caused by capture of electrons at low particle velocities ([5]), and (*b*) the overestimate of the ranges commonly intro-

([2]) H. A. BETHE and J. ASHKIN: *Passage of Radiation through Matter*, in *Experimental Nuclear Physics*. E. SEGRÈ, Ed., vol. I (New York); also E. A. UEHLING: *Ann. Rev. of Nucl. Sci.*, **4**, 315 (1954).

([3]) Letter from C. WALLER to E. GROSS of 24 January 1956.

([4]) N. BOHR: *Det. Kgl. Danske Vid. Selskab Mat.-fys. Medd.*, **18**, 8 (1948).

([5]) W. H. BARKAS: *Phys. Rev.*, **89**, 1019 (1953).

duced when one measures a saturated track between the extremities of the first and last grains. The measured length of the track of a particle cannot, of course, be less than one grain diameter. Very short ranges are meaningless because of the granular two-component structure of emulsion. Adjusting the ranges to standard emulsion, we obtain the following range-energy relation for $\tau<1$ MeV:

$$(1) \qquad \lambda = (0.00006 + 0.00138\ \tau^{\frac{3}{2}})\ \text{cm}\ .$$

The Bethe-Bloch theory is usually employed to calculate the rate of energy loss of a fast charged particle penetrating matter. The uncorrected theory is valid, however, only in the velocity interval extending from a point well above the velocity of the fastest

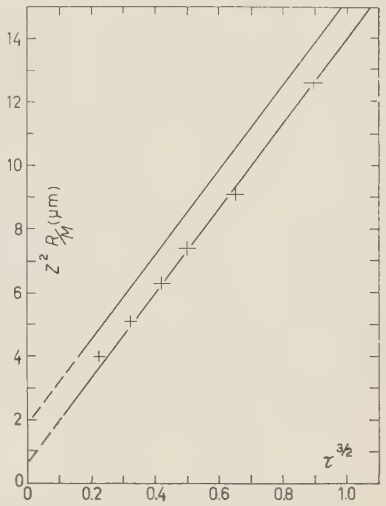

Fig. 1. – The range-energy data for $\tau < 1$ MeV. The straight lines are found when the (presumably smoothed) ranges from ROTBLAT (6) are plotted against $\tau^{\frac{3}{2}}$. The upper line is for α particles and the lower line is for protons. The dotted extension of the lines give intercepts of 1.9 μm and 0.74 μm, respectively. The crosses shown are experimental points for protons found by CÜER and JUNG (7) with the errors indicated. The data are for vacuum-desiccated emulsion.

TABLE I. – *Composition of « standard » emulsion.*

Element	Z_i	g/cm³	N_i ($\cdot 10^{-20}$)	$N_i Z_i$ ($\cdot 10^{-22}$)
Ag	47	1.808 8	101.01	47.476
Br	35	1.331 9	100.41	35.143
I	53	0.011 9	0.565	0.299
C	6	0.275 7	138.30	8.298
N	7	0.073 7	31.68	2.218
S	16	0.007 2	1.353	0.216
H	1	0.053 8	321.56	3.216
O	8	0.252 2	94.97	7.597

Totals: 3.815 g/cm³; $1.044\,6 \cdot 10^{24}$ electrons/cm³

(6) J. ROTBLAT: *Nature.*, **167**, 550 (1951).
(7) P. CÜER and J. J. JUNG: *Sc. et Ind. Phot.*, **22**, 401 (1951).

electron in the stopping material to a point near the minimum of ionization. In this interval the stopping behavior of an element, Z_i, is characterized by the electron density N_iZ_i and a « mean ionization potential » I_i. (N_i is the number of atoms per cubic centimeter.) According to the Bethe-Bloch theory the mean space rate of energy loss, $\mathcal{J}_i$, of a particle carrying z electronic units of charge is given by

$$\mathcal{J}_i = \frac{2\pi z^2 e^4}{mc^2\beta^2}(N_iZ_i)\left[\ln\left(\frac{2mc^2\beta^2\gamma^2 t}{I_i^2}\right) - 2\beta^2\right] \text{ erg/cm} . \tag{2}$$

Here $t \equiv ((\gamma^2-1)\mu c^2)/(\mu/2m + m/2\mu + \gamma)$ is the maximum energy transfer possible to an (assumed stationary) electron of mass m by the particle of mass μ, velocity βc, and kinetic energy $\mu c^2(\gamma^2-1)$. In the approximation to which the theory is usually carried, the particle-structure-dependent effects as well as the spin and sign-of-charge effects in the stopping cross section are neglected. If the stopping particle is heavy compared with an electron, and γ is small compared with this mass ratio, one obtains a simpler formula which does not contain the particle mass. This is

$$\mathcal{J}_i = \frac{4\pi z^2 r_0^2}{\beta^2} N_iZ_i \left[\ln\left(\frac{2mc^2}{I_i}\beta^2\gamma^2\right) - \beta^2\right] \text{ mc}^2/\text{cm} , \tag{3}$$

where $r_0 = e^2/mc^2$.

Even when a medium (such as emulsion) that contains several different kinds of atoms is used as the stopping material, the form of the energy-loss equation remains unchanged:

$$\mathcal{J} = \frac{4\pi z^2 r_0^2 n}{\beta^2}\left[\ln\left(\frac{2mc^2}{I}\beta^2\gamma^2\right) - \beta^2\right] \text{ mc}^2/\text{cm} . \tag{4}$$

Here n, the total number of electrons per cubic centimeter, is given by $n = \sum_i N_i Z_i$, and the mean ionization potential, I, is found from

$$n \ln I = \sum_i N_i Z_i \ln I_i .$$

For heavy atoms, described by the Fermi-Thomas model, F. Bloch found that I_i/Z_i is a constant, K, with a value of about one Rydberg ([8]). This is a useful concept despite the fact that small variations from constancy doubtless occur as the electronic shell structure is built up, and the precise value of the constant has not proved easy to measure.

([8]) F. Bloch: *Zeits. Phys.*, **81**, 363 (1933).

On the other hand, there is little reason to doubt that for sufficiently high—but not too high—velocities an expression of the form of Eq. (4) is capable of giving the rate of energy loss with good accuracy.

When the particle velocity is lowered so that it is comparable to the velocities of some of the electrons in the stopping atoms. Eq. (4) becomes progressively less valid. The tightly bound electrons are perturbed only adiabatically by the moving particle, and become ineffective in stopping. The behavior of the logarithm at low velocities is also wrong. K- and L-shell corrections have been calculated by WALSKE ([9,10]) which extend the usability of the theory toward lower velocities, but when applied to the heavy-component elements of emulsion, the corrections are large for proton energies of even several MeV. This part of the range energy curve is perhaps the most used, and the lack of an exact theory in this region is a serious misfortune. At low velocities other effects also set in. The stopping of a positive particle is influenced by the neutralization of its charge by electrons that it captures ([5]), and for heavy particles at low velocities, nuclear collisions become important ([1]).

At very high velocities the unlimited rise of the ionization implied by Eq. (4) is curtailed by the polarizability of the medium. This effect has been most thoroughly evaluated by STERNHEIMER ([11]).

For a particular element one may, in principle, write an exact expression for $\mathcal{J}_i$ by including an additive term, which is usually small:

$$\mathcal{J}_i = \frac{4\pi z^2 r_0^2}{\beta^2} N_i Z_i \left[\ln\left(\frac{2mc^2}{I_i}\beta^2\gamma^2\right) - \beta^2 - \frac{C_i(\beta)}{Z_i} \right] \mathrm{mc^2/cm} . \tag{5}$$

Here C_t is the sum of all the individual corrections for the element in question.

The corresponding expression for emulsion is

$$\iota = \mathcal{J}/z^2 = \frac{4\pi r_0^2 n}{\beta^2} \left[\ln\left(\frac{2mc^2}{I}\beta^2\gamma^2\right) - \beta^2 - C(\beta) \right] \mathrm{mc^2/cm} . \tag{6}$$

In this form I is considered a fixed constants. It has a characteristic value which may be determined at moderately high energies where $C(\beta)$ approaches zero. At very high velocities $C(\beta)$ is interpreted as one half of Sternehimer's δ, and at low velocities.

$$C(\beta) = \frac{\sum_i N_i C_i}{n} . \tag{7}$$

([9]) M. C. WALSKE: *Phys. Rev.*, **88**, 1283 (1952).
([10]) M. C. WALSKE: *Phys. Rev.*, **101**, 940 (1956).
([11]) R. M. STERNHEIMER: *Phys. Rev.*, **103**, 511 (1956).

The *effective* mean ionization potential deviates from the constant I by an approximate percentage 100 $C(\beta)$.

4. – Evaluation of $C(\beta)$.

By utilization of the curves of WALKSE ([9,10]) the shell correction contributions to $C(\beta)$ have been evaluated. For the i-th element we have

$$C_i = (C_K + C_L + \ldots)_i \,. \tag{8}$$

K-shell corrections were made for all the elements in emulsion except hydrogen, and L-shell corrections also were included for iodine, silver, and bromine. With these additions the usefulness of the Bethe-Bloch theory is extended down to about 1 MeV for protons, but it is difficult to estimate the possible errors remaining from the uncorrected shells and from the approximations in the atomic model used. Since Walske's calculation is non-relativistic, the curves do not behave correctly at high velocities. Following a suggestion of Dr. WALSKE, we have used $\beta\gamma$ to replace β wherever it appears in his formulas.

STERNHAIMER ([11]) has given an empirical formula for δ which estimates the density-effect correction at high velocities. The constants in the formula

TABLE II. – $C(\beta)$ *calculated from the theories of Walske and Sternheimer.*

τ (MeV)	C	τ (MeV)	C	τ (MeV)	C
1.2	— 0.081	5.0	0.072	200	0.016
1.4	— 0.059	5.4	0.075	260	0.011
1.6	— 0.040	6.0	0.079	300	0.009
1.8	— 0.023	7.0	0.084	400	0.006
2.0	— 0.009	8.0	0.085	500	0.005
2.2	+ 0.003	9.0	0.086	700	0.004
2.4	0.014	10.0	0.088	1 000	0.002
2.6	0.023	12.0	0.087	1 200	0.004
2.8	0.031	16.0	0.083	1 400	0.009
3.0	0.038	20.0	0.078	1 600	0.020
3.2	0.043	24.0	0.073	1 800	0.033
3.4	0.048	28.0	0.067	2 000	0.046
3.6	0.053	30.0	0.065	3 000	0.115
3.8	0.057	40.0	0.055	4 000	0.184
4.0	0.060	50.0	0.048	5 000	0.250
4.2	0.063	70.0	0.038	10 000	0.524
4.4	0.065	100.0	0.030	20 000	0.902
4.6	0.067	140.0	0.023	30 000	1.167
4.8	0.070				

depend on the mean ionization potential of the stopping material. From our measurements (Part I) at velocities at which the density effect is negligible, we have found $I = 331$ eV. For this value the density correction is

$$C = \delta/2 = 2.303 \log_{10} \beta\gamma - 2.66 + 0.103 (3 - \log_{10} \beta\gamma)^{2.97} .$$

The shell corrections are already vanishingly small at the high velocities at which the density effect must be taken into consideration, so that two different functions for C are applicable—one at low velocities and the other at high. Numerical values $C(\beta)$ are listed in Table II.

5. – Evaluation of the mean ionization potential.

By integrating $\lambda = \lambda_1 + \int_{\tau_1}^{\tau} d\tau/\iota$ one may predict the range for an energy τ in an interval, where (with an assumed mean ionization potential) ι may be calculated from Eq. (6). Each range measurement in Part I provides an almost independent estimate of the mean ionization potential. The best value of the mean ionization potential may be derived in this way from the measured points. Our range measurements are in satisfactory agreement with the adjusted dry-emulsion measurements of earlier experiments for $\tau < 5$ MeV. As a most probable value we take $\lambda_1 = 176.5$ μm for $\tau_1 = 5$ MeV. There is also good agreement between measurements of the π-μ decay range. Here we take $\tau = 36.55$ MeV and $\lambda = (5345 \pm 22)$ μm. From these points we obtain a mean ionization potential of (330 ± 7) eV. The highest-energy point was obtained with good accuracy, and it is the least influenced by shell-correction effects. From the 5 MeV point and this measurement we derive a mean ionization potential of (332 ± 13) eV. The other measured points give values both above and below these values, and the over-all weighted average, considering only statistical errors, is $I = (327 \pm 4)$ eV. In view of the several corrections that were found necessary, however, small systematic errors may remain in some of the experimental points. The possible influences of inexact corrections to the various points have been reviewed, and I prefer to quote (331 ± 6) eV for the mean ionization potential of emulsion. The sensitivity of the range to the mean ionization potential is shown in Fig. 2 which can be used to estimate the uncertainty in the range curve arising from the remaining uncertainty in the mean ionization potential.

If one assumes that I_i/Z_i is a constant, K, we may evaluate it, knowing the emulsion composition. For $I = (331 \pm 6)$ eV K is (12.25 ± 0.22) eV. Actually the hydrogen of the emulsion should probably be treated separately. If the mean ionization potential attributed [11] to hydrogen is 17.6 eV, we obtain

$K = (12.1 \pm 0.2)$ eV for the remaining elements of the emulsion. Since only about 18% of the emulsion electrons are in the light atoms of the C. N. O group, this value of K should be substantially that applying to the heavy element of the Ag, Br, I group.

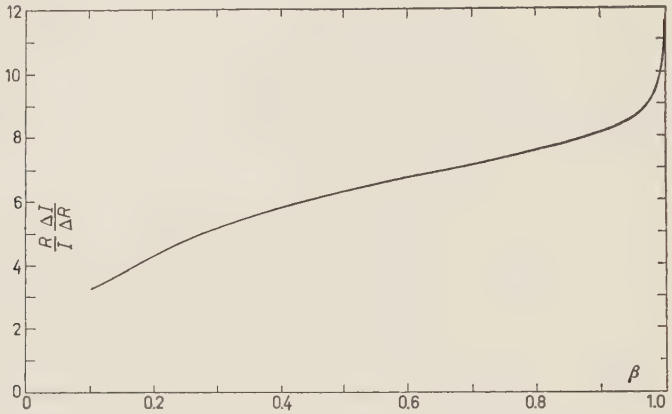

Fig. 2. – Graph of $(R/I)(\Delta I/\Delta R)$, the percent increase in mean ionization potential to bring about a 1 percent increase in emulsion range. βc is the particle velocity.

The value $K = 12.1$ eV is in fairly good agreement with the results of BURKIG and MCKENZIE [12] and BICHSEL, MOZLEY, and ARON [13], while CALDWELL [14] has proposed an even higher I/Z ratio. It is not, however, in accord with the lower ratios of MATHER and SEGRÈ [15].

[12] V. C. BURKIG and K. R. MCKENZIE: private communication (preprint).

[13] H. BICHSEL, R. F. MOZLEY and W. A. ARON: *Phys. Rev.*, **105**, 1788 (1957).

[14] D. O. CALDWELL: *Phys. Rev.*, **100**, 291 (1955).

[15] R. MATHER and E. SEGRÈ: *Phys. Rev.*, **84**, 191 (1951). See also C. J. BAKKER and E. SEGRÈ: *Phys. Rev.*, **81**, 489 (1951). It is important to try to understand this discrepancy. Although the velocity-measuring technique developed by MATHER is ingenious and probably sound, it has as yet not been compared directly with other methods. One need not question this phase of the experiment, however, to find a probable reason for the difference. Determination of the true range of a charged particle may be ambiguous unless, as in emulsion, one can measure the length of a visible track by breaking it up into essentially straight segments. Ranges determined from ionization measurements in an experimental arrangement that does not have « good geometry », such as that of Mather and Segrè, require difficult corrections for scattering, and sometimes also for secondary ionizing effects. This is particularly the case when the range is not small compared with the free path for nuclear interaction in the stopping material. Protons with ranges as great as those of Mather and Segrè will usually have suffered at least one diffraction scattering interaction. Their correction allowed only for the Coulomb scattering of a noninteracting particle. The data of

6. – Range calculations.

A theoretical range-energy relation for standard emulsion was calculated by using the table of $C(\beta)$, and the following formulas

(*a*) for $\tau < 1$ MeV,

$$\lambda = 0.00006 + 0.00138\,\tau^{\frac{3}{2}} \text{ cm} ;$$

(*b*) for $\tau > 1$ MeV,

$$\lambda = 0.00144 + \int_{1}^{\tau} \frac{\mathrm{d}\tau}{\iota} \text{ cm} ,$$

$$\iota = \frac{0.5326}{\beta^2} [\ln (3\,088\,\beta^2\gamma^2) - \beta^2 - C] \text{ MeV/cm} .$$

In order that ranges in emulsion of other than standard density may be corrected, the range in water has also been calculated. The *K*-shell correction for oxygen and the density effect have been included. This was done by finding an empirical function to fit $C_K(\beta)$. The formulas are:

(*a*) for $\tau > 0.1$ MeV,

$$\lambda_w = 0.00011 + \int_{.1}^{\tau} \frac{\mathrm{d}\tau}{\iota_w},$$

$$\iota_w = \frac{0.170}{\beta^2} [\ln (1.38 \cdot 10^1 \beta^2\gamma^2) - \beta^2 - C] \text{ MeV/cm} ,$$

with C given by

$$C \approx \frac{1}{880\beta^2} \exp\left(-\frac{1}{227\beta^2}\right) \text{ (at low velocities)};$$

Mather and Segrè give evidence of the presence of an additional scattering effect, and they themselves remarked that they were unable to explain the shapes of their ionization curves. It may also be worth pointing out in this connection that successive diffraction scattering events are not independent, as one usually assumes in plural — and multiple — scattering theory. Correlations will exist between successive scattering events when the particle can be polarized. The resultant scattering angles will then be even larger than estimated from the simple theory.

(*b*) for $\beta > 0.86$, we have

$$C \approx \ln \beta\gamma - 1.735 + 2.75 \cdot 10^{-2} (4.606 - \ln \beta\gamma)^{2.69} .$$

Table III is the calculated range-energy relation for water. In Fig. 3 the theoretically calculated ranges in emulsion are compared with the measurements. The agreement on the whole is remarkably good. Of the 14 experimental points, just the expected number, 4, depart from the theoretical curve

TABLE III. – *Calculated range-energy relation for water.*

τ (MeV)	λ_w (cm)	τ (MeV)	λ_w (cm)	τ (MeV)	λ_w (cm)	τ (MeV)	λ_w
0.2	$2.3 \cdot 10^{-4}$	6.8	$620.2 \cdot 10^{-4}$	64	$3.480 \cdot 10^{0}$	500	$117.2 \cdot 10^{0}$
0.4	5.8	7.6	755.3	68	3.880	600	155.1
0.6	10.5	8.4	902.1	72	4.299	700	195.4
0.8	16.3	9.2	1 061	76	4.737	800	237.5
1.0	23.4	10.0	1 230	80	5.192	900	281.1
1.2	31.4	12	1 704	84	5.666	1 000	325.9
1.4	40.6	14	2 246	88	6.156	1 200	418.3
1.6	50.7	16	2 855	92	6.664	1 400	513.4
1.8	61.9	18	3 529	96	7.189	1 600	610.3
2.0	74.0	20	4 266	100	7.730	1 800	708.5
2.4	101.0	24	5 927	120	10.68	2 000	807.4
2.8	131.6	28	7 829	140	14.00	4 000	1 805
3.2	165.7	32	9 965	160	17.68	6 000	2 785
3.6	203.3	36	$1.233 \cdot 10^{0}$	180	21.69	8 000	3 745
4.0	244.2	40	1.491	200	26.00	10 000	4 686
4.4	288.5	44	1.771	240	35.47	14 000	6 527
4.8	335.9	48	2.073	280	45.95	18 000	8 325
5.2	386.6	52	2.394	320	57.33	22 000	10 092
5.6	440.4	56	2.736	360	69.50	26 000	11 834
6.0	497.3	60	3.098	400	82.38	30 000	13 556

by more than one standard deviation. Also there is no definite monotonic trend with particle velocity. The deviations at 5.447 MeV and at 21.21 MeV, however, are too large to be compatible with the measurement errors, and it is believed that the hydrogen-atomic model used by WALSKE for the shell corrections causes C at low velocities to vary too abruplty with particle velo-

city. In fact, by using a constant value of 0.057 for C (corresponding to an effective mean ionization potential of 350 eV), one obtains a virtually perfect fit to the experimental data in the interval 5 to 40 MeV.

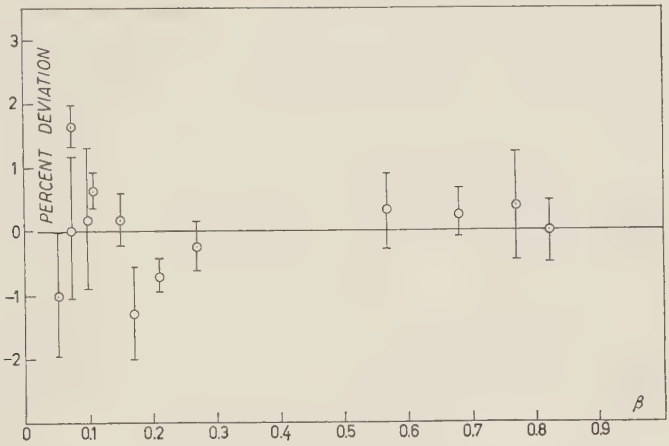

Fig. 3. – The deviation of the measured ranges from the purely theoretical range curve. βc is the particle velocity.

7. – The range-energy relation.

At all high velocities the theoretical range curve is the best available, but below about 40 MeV the calculated shell corrections are imperfect and a semi-empirical determination of the range-energy relation is preferred. Adjusting the Geiger-Bohr relation to emulsion of standard density, we use $\lambda = 0.00006 + 0.00138\tau^{\frac{3}{2}}$ for the initial part of the curve. VIGNERON [16] has utilized the best of the old data including those from ROTBLAT [6] and CÜER and JUNG [7] to prepare his range table. The data for proton energies up to about 5 MeV were derived from thin layers of evacuated Ilford emulsion. The appropriate density was certainly near 4.02 g³cm³, and we have assumed this density in adjusting the empirical data compiled by VIGNERON to standard conditions. Between 1 and 5 MeV this curve is in excellent agreement with our measurements, and one may reasonably adopt it as a standard range-energy relation. Above 5 MeV the data quoted by VIGNERON correspond to progressively lower emulsion densities, and one cannot make a simple density adjustment. One can, however, assume that the ratios of our measured ranges to those computed from the uncorrected Bethe-Bloch theory define a slowly varying

[16] L. VIGNERON: *Journ. Phys. Rad.*, **14**, 145 (1953).

TABLE IV. – *The range-energy relation for standard emulsion.*

The best results in use of this table are obtained if the range measurement techniques and the corrections are the same as those applied in the experimental part of this work.

τ (MeV)	λ (cm)	τ (MeV)	λ (cm)	τ (MeV)	λ (cm)	τ (MeV)	λ (cm)
0.2	$1.8 \cdot 10^{-1}$	20.0	$1\,858 \cdot 10^{-4}$	300	$20.14 \cdot 10^{0}$	1 000	$124.2 \cdot 10^{0}$
0.4	4.1	22.5	2 283	320	22.37	1 200	158.7
0.6	7.0	25.0	2 744	340	24.67	1 400	194.1
0.8	10.5	27.5	3 243	360	27.04	1 600	229.9
1.0	14.4	30.0	3 777	380	29.48	1 800	266.1
1.2	18.7	32.5	4 347	400	31.98	2 000	302.4
1.4	23.4	35.0	4 952	420	34.53	2 200	338.8
1.6	28.6	37.5	5 591	440	37.14	2 400	375.3
1.8	34.3	40.0	6 264	460	39.81	2 600	411.7
2.0	40.4	42.5	6 970	480	42.52	2 800	448.0
2.5	57.4	45	7 709	500	45.28	3 000	484.2
3.0	76.7	50	9 275	520	48.08	3 200	520.4
3.5	98.3	55	$1.097 \cdot 10^{0}$	540	50.93	3 400	556.4
4.0	122.3	60	1.278	560	53.81	3 600	592.3
4.5	148.4	65	1.471	580	56.73	3 800	628.1
5.0	176.5	70	1.675	600	59.69	4 000	663.7
5.5	206.5	75	1.891	620	62.68	4 200	699.2
6.0	238.4	80	2.117	640	65.71	4 400	734.6
6.5	272.4	85	2.353	660	68.76	4 600	769.9
7.0	308.2	90	2.600	680	71.84	4 800	805.0
7.5	346.0	100	3.124	700	74.96	5 000	840.0
8.0	385.7	110	3.686	720	78.09	6 000	1 013
8.5	427.2	120	4.286	740	81.26	7 000	1 184
9.0	470.6	130	4.923	760	84.44	8 000	1 352
9.5	515.7	140	5.594	780	87.65	9 000	1 518
10	562.6	150	6.298	800	90.88	10 000	1 682
11	662.8	160	7.034	820	94.13	11 000	1 844
12	769.6	170	7.800	840	97.40	12 000	2 005
13	882.5	180	8.596	860	100.7	13 000	2 164
14	1 002	190	9.421	880	104.0	14 000	2 323
15	1 129	200	10.27	900	107.3	15 000	2 479
16	1 262	220	12.06	920	110.7	20 000	3 249
17	1 402	240	13.95	940	114.0	25 000	4 000
18	1 548	260	15.92	960	117.4	30 000	4 735
19	1 700	280	17.99	980	120.8	35 000	5 459

function of the particle velocity, and thus can obtain a smooth semiempirical range curve. This has been done in the interval 5 MeV $< \tau <$ 40 MeV. Above 40 MeV the range has been determined solely from the theoretical ι. The range calculation has been terminated at 35 000 MeV for a number of reasons, particularly because the particle mass begins to enter ι in an explicit non-negligible way. The compilation of ranges that results from these considerations is given as Table IV and the comparison between the table and the measurements of Part I are given in Table V.

TABLE V. – *The tabulated ranges compared with the measurements.*

τ (MeV)	λ measured (cm)	λ table (cm)
1.295	$20.7 \pm 0.2 \cdot 10^{-4}$	$20.9 \cdot 10^{-4}$
2.421	$53.9 \pm 0.6 \cdot 10^{-4}$	$54.7 \cdot 10^{-4}$
2.45	$55.67 \pm 0.34 \cdot 10^{-4}$	$55.7 \cdot 10^{-4}$
5.00	$175.1 \pm 2.0 \cdot 10^{-4}$	$176.5 \cdot 10^{-4}$
5.477	$204.6 \pm 0.64 \cdot 10^{-4}$	$205.1 \cdot 10^{-4}$
5.477	$205.5 \pm 1.1 \cdot 10^{-4}$	$205.1 \cdot 10^{-4}$
10.00	$562.7 \pm 2.6 \cdot 10^{-4}$	$562.6 \cdot 10^{-4}$
13.96	$988.3 \pm 7.4 \cdot 10^{-4}$	$997.2 \cdot 10^{-4}$
21.21	$2056 \pm 5 \cdot 10^{-4}$	$2064 \cdot 10^{-4}$
36.55	$5345 \pm 22 \cdot 10^{-4}$	$5348 \cdot 10^{-4}$
200	10.31 ± 0.07	10.27
340	24.74 ± 0.10	24.67
540	51.15 ± 0.45	50.93
700	74.97 ± 0.36	74.96

Recent measurements by FRIEDLANDER, KEEFE and MENON [17] at 87.4, 117.9 and 146.5 MeV are in a velocity interval where we have made no measurements. Their ranges are on the average 0.53% lower then those of Table IV. Their energy calibration was made by determining the ranges of the same particle groups in aluminum, the range curve for which was derived from the work of BLOEMBERGEN and VAN HEERDEN [18]. The ratio of emulsion ranges to aluminum ranges must vary smoothly and monotonically in this region, but for the energy points cited their observed ratios are 1,215, 1.178 and 1.183 respectively. Evidently uncertainties of 1% or 2% are present in the measurements by FRIEDLANDER *et al.* The actual ratios of their ranges

[17] M. W. FRIEDLANDER, D. KEEFE and M. G. K. MENON: *Nuovo Cimento*, **5**, 461 (1957).

[18] N. BLOEMBERGEN and P. J. VAN HEERDEN: *Phys. Rev.*, **83**, 561 (1951).

to those derived from Table IV are 1.011, 0.983, 0.990. It is noticeable that these ratios rise and fall with their emulsion/aluminum ratios (*).

* * *

In carrying out the numerical work, Mr. JAMES BAKER and Mr. KENT CURTIS were very helpful. Mr. CURTIS programmed the range calculation for the IBM 650 computer. I wish also to acknowledge the valuable advice received from Dr. WALSKE and Dr. STERNHEIMER on the application of their calculations to emulsion.

(*) *Note added in proof.* – In a private communication M. W. FRIEDLANDER has pointed out that if the median values of their proton ranges in emulsion are used, (17), the ratios of the ranges in aluminum become 1.221, 1.187 and 1.181. These ratios vary monotonically, and the ratios of the median values to those from Table IV then become 1.014, 0.991, and 0.989.

RIASSUNTO (*)

Si impiega la teoria di Bethe-Bloch dell'arresto, comprese le correzioni di shell e quella per l'effetto di densità per calcolare i range teorici per le emulsioni Ilford G.5 standard. Solo il potenziale di ionizzazione medio è un parametro aggiustabile. Correggendo in tutti gli strati K di tutti gli atomi dell'emulsione eccetto l'idrogeno, e anche correggendo per gli strati L dello iodio, dell'argento e del bromo si può ottenere un accordo coi range misurati dei protoni da 1 a 700 MeV. Il potenziale di ionizzazione medio trovato è di (331 ± 6) eV, e I/Z ha in media il valore di (12.1 ± 0.2) eV per tutti gli elementi dell'emulsione eccetto l'idrogeno. A basse velocità il modello idrogenoide usato pei calcoli di correzione di shell sembra esagerare gli effetti di shell. Un miglior accordo coi dati sperimentali per energie protoniche al di sotto di 40 MeV si ottiene semiempiricamente. Si dà una tabella di range per emulsioni di densità standard. Si allega anche una tabella di range per l'acqua, utile per aggiustare i range misurati in condizioni di densità differenti dallo standard.

(*) *Traduzione a cura della Redazione.*

Etude de l'absorption des mésons K^- au repos dans l'émulsion nucléaire.

G. L. Bacchella (*), A. Berthelot (+), A. Bonetti (*), O. Goussu (+), F. Lévy (+), M. René (†), D. Revel (+), J. Sacton (†) (×), L. Scarsi (*), G. Tagliaferri (*) et G. Vanderhaeghe (†) (×)

(†) *Institut de Physique de l'Université, Service de Physique Nucléaire - Bruxelles*

(*) *Istituto di Scienze Fisiche dell'Università - Milano*

et

Istituto Nazionale di Fisica Nucleare - Sezione di Milano

(+) *Centre d'Etudes Nucléaires - Saclay*

(ricevuto il 28 Agosto 1957 **)

Summary. — The results of the analysis of 391 events of K^- absorption at rest in a large emulsion stack exposed to the Berkeley Bevatron are reported. Scanning « along the track » was used, in order to obtain unbiassed frequencies for the various types of particles. A detailed discussion of the identification of charged hyperons is presented. The findings of previous workers on the features of the observed $\Sigma^{\pm}\pi^{\mp}$ pairs, and their respective rates of observation, are confirmed. Three absorptions on free protons were observed. Several examples of fast Σ-hyperons unaccompanied by charged π's provide direct evidence for two-nucleon absorptions: they account for $\sim 2.5\%$ of the total number of events. Direct production of Λ^0-hyperons is inferred from the observation of fast π-mesons; in addition, hyperfragments associated with 3% of the events indicate production of Λ^0's either directly or via decay or interaction of Σ's. Among the pions whose sign was recognized (40% of the total), the negative ones were found to be more frequent than the positive by a factor of about 3. Evidence for the nuclear reabsorption of hyperons and pions is provided by the study of the visible energy release associated with the absorptions. Some 60% of the events do not contain charged unstable particles: a fair number ($\sim 17\%$) of these events are accompanied by protons of kinetic energy greater than 60 MeV, a fact which suggests the intervention of two-nucleon reactions.

(×) Chercheur agréé de l'I.I.S.N. (Belgique).

(**) Licenziato, in forma emendata, dagli Autori il 10 Marzo 1958. (*N. d. R.*)

1. – Introduction.

L'étude expérimentale de l'interaction des mésons K^- avec les nucléons a été abordée jusqu'à présent par deux techniques: la chambre à hydrogèen liquide [1] et les émulsions nucléaires [2,3]. Si la première donne des informations directes sur l'interaction des mésons K^- avec des protons libres, la deuxième permet l'observation de l'absorption des mésons K^- par des noyaux complexes et permet donc, en principe, l'étude de leur interaction non seulement avec les protons mais aussi avec les neutrons ou avec plusieurs nucléons. Cette étude est toutefois rendue difficile par l'intervention, d'une part, de plusieurs réactions primaires et, d'autre part, de diverses interactions secondaires que peuvent subir les particules émises au cours de ces réactions (absorption, scattering élastique ou inélastique avec ou sans échange de charge). De plus, on peut s'attendre à ce que les fréquences des différentes réactions primaires dépendent de la nature du noyau par lequel le méson K^- est absorbé. C'est pourquoi, l'interprétation des phénomènes observés dans l'émulsion nucléaire nécessitera l'accumulation de données statistiques recueillies dans des conditions expérimentales homogènes.

Dans le présent travail, nous nous proposons d'apporter quelques précisions sur la phénoménologie générale de l'absorption des mésons K^- au repos dans l'émulsion nucléaire, sur la base de l'analyse de près de 400 événements.

2. – Réactions fondamentales.

Les interactions conservant la charge, le nombre de baryons et l'étrangeté, sur lesquelles il est généralement admis de baser l'interprétation de l'absorption

(1) L. W. Alvarez, H. Bradner, P. Falk-Vairant, J. D. Gow, A. H. Rosenfeld, F. T. Solmitz et R. D. Tripp: *Nuovo Cimento*, **5**, 1026 (1957).

(2) W. Chupp, G. Goldhaber, S. Goldhaber et F. H. Webb: *Phys. Rev.*, **100**, 959 (1955); W. F. Fry, J. Schneps, G. A. Snow et M. S. Swami: *Phys. Rev.*, **100**, 950, 1449 (1955); E. P. George, A. J. Herz, J. H. Noon et N. Solntseff: *Nuovo Cimento*, **3**, 94 (1956); J. Hornbostel et E. O. Salant: *Phys. Rev.*, **102**, 502 (1956); D. M. Fournet et M. Widgoff: *Phys. Rev.*, **102**, 929 (1956); D. M. Haskin, T. Bowen et M. Schein: *Phys. Rev.*, **103**, 1512 (1956); W. H. Barkas, W. F. Dudziak, P. C. Giles, H. H. Heckman, W. F. Inman, C. J. Mason, N. A. Nickols et F. M. Smith: *Phys. Rev.*, **105**, 1417 (1957).

N. B. - La bibliographie relative aux articles antérieurs peut être trouvée dans les articles mentionnés ci-dessus.

(3) K^- *interactions at rest*, Rapport présenté par C. Dilworth sur des résultats préliminaires de la « K^--Stack Collaboration », du « N.R.L. Washington group » et de la présente collaboration; *Proceedings of the Seventh Annual Rochester Conference* (New York, 1957).

des mésons K^- sont:

$$K^- + N \to Y + \pi + Q$$

et

$$K^- + N + N \to Y + N + Q' .$$

Détaillons les valeurs de l'énergie libérée au cours de ces interactions, supposant qu'elles ont lieu avec un ou deux nucléons libres et au repos, et utilisant les valeurs des masses adoptées à la septième Conférence de Rochester (4).

a) Pour les interactions avec un seul nucléon:

$$K^- + p \begin{cases} \Sigma^+ + \pi^- + 103.3 \text{ MeV} & (1) \\ \Sigma^- + \pi^+ + 96.1 \text{ MeV} & (2) \\ \Sigma^0 + \pi^0 + 108.7 \text{ MeV} & (3) \\ \Lambda^0 + \pi^0 + 182.2 \text{ MeV} & (4) \end{cases}$$

$$K^- + n \begin{cases} \Sigma^- + \pi^0 + 102.0 \text{ MeV} & (5) \\ \Sigma^0 + \pi^- + 105.4 \text{ MeV} & (6) \\ \Lambda^0 + \pi^- + 178.9 \text{ MeV} & (7) \end{cases}$$

b) Pour les interactions avec deux nucléons:

$$K^- + p + p \begin{cases} \Sigma^+ + n + 241.6 \text{ MeV} & (8) \\ \Sigma^0 + p + 243.7 \text{ MeV} & (9) \\ \Lambda^0 + p + 317.2 \text{ MeV} & (10) \end{cases}$$

$$K^- + p + n \begin{cases} \Sigma^- + p + 237.0 \text{ MeV} & (11) \\ \Sigma^0 + n + 243.7 \text{ MeV} & (12) \\ \Lambda^0 + n + 317.2 \text{ MeV} & (13) \end{cases}$$

$$K^- + n + n \to \Sigma^- + n + 237.0 \text{ MeV} \qquad (14)$$

Sauf dans le cas où le méson K^- est absorbé par un noyau d'hydrogène, les interactions ont lieu avec des nucléons liés et l'énergie de liaison de ceux-ci

(4) L. W. ALVAREZ: *Proceedings of the Seventh Annual Rochester Conference* (New York, 1957).

doit être soustraite des énergies mentionnées ci-dessus. La répartition de l'énergie disponible entre les deux particules produites dépend de l'énergie de Fermi des nucléons. De plus, ces particules étant soumises à l'intérieur des noyaux à des potentiels nucléaires et coulombiens, leurs énergies cinétiques à l'extérieur des noyaux se trouvent encore modifiées ([5]). Enfin, les particules produites peuvent subir divers types d'interactions avec les nucléons du noyau: absorptions, diffusions élastiques ou inélastiques avec ou sans échange de charge.

3. – Matériel expérimental.

3·1. *Exposition.* – Un stack de 300 feuilles d'émulsion Ilford G-5 de 15 cm $\times$25 cm $\times$600 μm, réalisant un volume total de 6.75 litres, a été exposé à un faisceau de mésons K$^-$ produits au Bevatron de Berkeley par des protons de 6 GeV envoyés sur une cible de Cu. Ce faisceau a été extrait à 90° du faisceau de protons et a été analysé magnétiquement de manière à recueillir dans le stack les mésons K$^-$ ayant une quantité de mouvement comprise entre 405 et 275 MeV/c, ce qui correspond à des parcours respectifs de 9.5 cm dans les premières feuilles du stack et 2.8 cm dans les dernières. Le faisceau contenait un méson K$^-$ pour environ 2000 mésons π^-. La distance entre la cible et le stack était de $\sim$ 8 m.

3·2. *Traitement du stack.* – Le stack a été développé suivant la technique classique à cycle de température (*). Des précautions ont été prises au cours du développement pour limiter les gradients de densité de grains (imprégnations à 2 °C et température uniforme à $\pm$ 0.2 °C sur toute la surface des cuves). Cependant, cela n'a pas permis d'éviter, dans certains groupes de plaques, un gradient en fonction de la profondeur donnant lieu à des écarts extrêmes de l'ordre de 10% le long d'une même trace. Ce gradient peut être dû à un effacement local résultant d'un séchage trop lent des émulsions et à une température trop élevée après leur collage sur verre.

La densité de lacunes des traces au plateau d'ionisation varie, d'un groupe de plaques à l'autre, entre 16 et 18 lacunes par 100 μm. Il en résulte de nombreuses lacunes longues, dont la présence entraîne des difficultés de suivage, tant dans une même plaque que d'une plaque à l'autre, et peut être une cause de perte de particules peu ionisantes.

([5]) F. C. GILBERT, C. E. VIOLET et R. S. WHITE: *Phys. Rev.*, **107**, 228 (1957).

(*) Le développement a été effectué au Laboratoire du Service de Physique Nucléaire de l'Université de Bruxelles.

3·3. *Dépouillement et mesures.* – Les laboratoires participant à la présente collaboration ont eu à leur disposition deux portions du stack, exposées dans des régions du faisceau de mésons K^- correspondant respectivement à des quantités de mouvement comprises entre 275 et 320 MeV/c (100 plaques) et entre 375 et 405 MeV/c (68 plaques).

Le dépouillement des plaques a été effectué suivant la méthode dite « par suivage de traces ». Les traces à suivre ont été sélectionnées sur la base d'une mesure d'ionisation parmi les traces faisant un angle inférieur à 10° avec la direction du faisceau. Cette mesure a été faite à une distance du bord des plaques telle que la densité de lacunes des traces de mésons K^- est environ 1.5 fois supérieure à celles des traces de mésons π^- du faisceau. Sur 7 traces ainsi sélectionnées, on a trouvé en moyenne 1 méson K^-, 3 protons et 3 mésons π.

L'énergie des particules chargées résultant de l'absorption des mésons K^- et s'arrêtant dans l'émulsion a été déduite de leur parcours au moyen de la courbe parcours-énergie établie par W. H. Barkas *et coll.* [6]. L'énergie des particules sortant du stack ou disparaissant en vol dans l'émulsion a été déterminée par des mesures d'ionisation, complétées par des mesures de scattering chaque fois que les conditions géométriques et le parcours disponible le permettaient.

Le repérage des événements et le suivage des traces ont été facilités par l'utilisation de quadrillages numérotés, imprimés directement sur le dos des feuilles d'émulsion ou imprimés sur des films minces ($\sim 15\ \mu$m), collés sur le verre ou sur l'émulsion après le traitement du stack.

4. – Résultats expérimentaux.

4·1. *Détermination du nombre de branches.* – Cette détermination présente deux difficultés: l'identification des événements K_ρ^- et l'observation des traces de faible ionisation; elles ont été traitées de la manière suivante:

1) Evénements K_ρ^-. Parmi les traces suivies, nous avons retenu comme K_ρ^- possibles les traces d'allure protonique qui se terminaient dans la région d'arrêt des K_σ^-. La discrimination entre K_ρ^- et protons a ensuite été effectuée par des mesures d'ionisation en fonction du parcours résiduel, complétées dans les cas douteux par des mesures de scattering à flèche constante. Etant donné la dispersion des mesures d'ionisation et de scattering et compte tenu de ce qu'il y a environ 15 protons pour 1 K_ρ^-, on peut s'attendre à une surestimation du nombre de ceux-ci.

(6) W. H. Barkas, P. H. Barret, P. Cüer, H. H. Heckman, F. M. Smith et H. K. Ticho: *Phys. Rev.*, **102**, 583 (1956).

2) Traces de faible ionisation. Nous avons appelé *particules peu ionisantes* celles dont la trace comporte moins de 26 lacunes par 100 μm, ce qui correspond, en principe, à des mésons π d'énergie cinétique supérieure à 35 MeV ou à des baryons d'énergie cinétique supérieure à 240 MeV. Nous avons considéré toutes les particules peu ionisantes non suivies jusqu'au bout comme mésons π. Toutefois, étant donné que le comptage des lacunes sur les traces très inclinées conduit à une sous-estimation de leur ionisation, il faut considérer que parmi les traces de particules peu ionisantes très inclinées qui n'ont pu être suivies suffisamment pour être identifiées, il pourrait y avoir un certain nombre de baryons d'énergie inférieure à 240 MeV.

L'observation de traces de particules peu ionisantes peut être rendue difficile, soit par des conditions géométriques défavorables, soit par des anomalies dans la distribution des grains. Pour cette raison, un examen attentif de chaque événement a été effectué par différents observateurs et les événements situés à moins de 10 μm du verre ou de la surface de l'émulsion on été écartés de la statistique. La distribution des traces de particules peu ionisantes d'après leur angle d'inclinaison ne présente aucun signe de perte systématique suivant certains angles d'observation (Fig. 1). Le nombre d'événements est trop petit pour que l'examen de la distribution en profondeur des étoiles comportant une trace de particule peu ionisante permette une estimation de la perte éventuelle de celles-ci dans les couches extrêmes de l'émulsion. Notons que nous avons observé trois mésons π disparaissant en vol dans l'émulsion pour une seule interaction en vol donnant lieu à une étoile visible. Il est possible que certaines de ces disparitions en vol soient dues à des lacunes importantes dans les traces et de telles lacunes pourraient également se présenter à l'origine des traces. Dans ces conditions, nous considérons que le nombre de particules peu ionisantes pourrait être sousestimé.

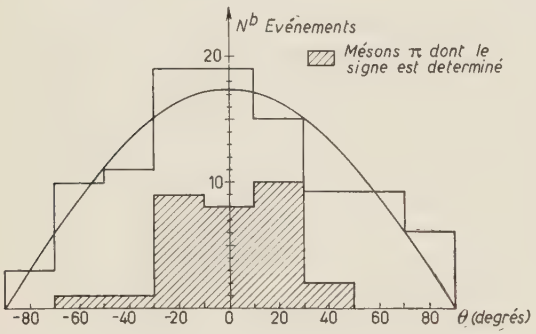

Fig. 1. – Distribution des angles d'inclinaison des traces peu ionisantes. La courbe continue correspond à la distribution isotrope, normalisée au même nombre de traces.

4·2. *Classification des événements d'après le nombre de branches, la nature et l'énergie des particules émises.* – La distribution d'après le nombre de branches des 391 événements au repos retenus dans la statistique est donné dans le

TABLEAU I. – *Distribution des événements suivant le nombre de branches.*

Nombre de branches	0	1	2	3	4	5	6	7	8
Nombre d'événements	72	76	100	66	41	23	8	3	2
% (*)	18.4 ± 2.2	19.4 ± 2.2	25.6 ± 2.6	16.9 ± 2.1	10.5 ± 1.6	5.9 ± 1.2	2.0 ± 0.7	0.8 ± 0.4	0.5 ± 0.4

(*) Les erreurs indiquées sont les erreurs statistiques standard.

Tableau I et par la Fig. 2. Par convention, nous avons appelé *branche* toute trace de longueur supérieure à 5 μm non attribuable à un électron lent. Les traces attribuables à des électrons lents ont été considérées comme traces d'*électrons Auger* (*A*). Les traces noires et droites de longueur inférieure à 5 μm ont été appelées *reculs* (*R*). Nous avons considéré comme *blob* (*B*) tout amas de grains pouvant être dû soit à un électron de très basse énergie, soit à un recul très court. Le nombre moyen de branches est 2.1 ± 0.1.

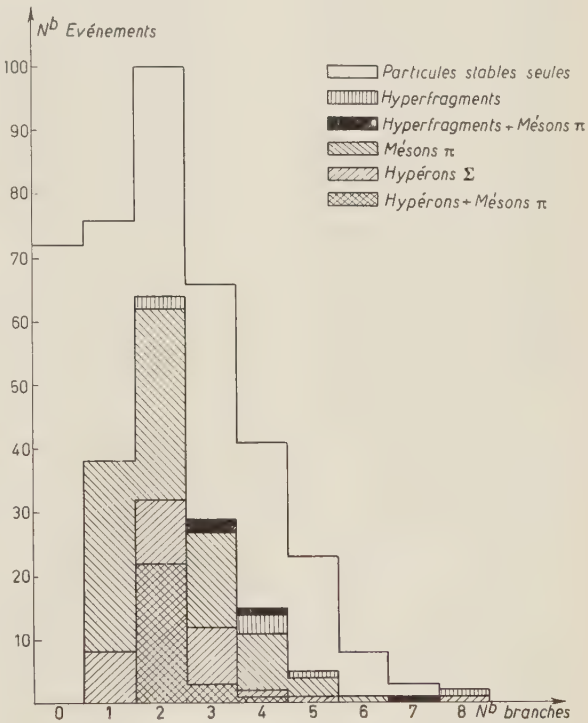

Fig. 2. – Distribution des événements d'après le nombre de branches.

Le diagramme de la Fig. 3 présente sous une forme suggestive l'ensemble des événements K^-_σ. Chaque événement est figuré par une colonne verticale, dont la hauteur totale représente la masse au repos du méson K^- diminuée de 94 MeV pour raison de commodité, soit 400 MeV. Chaque particule chargée émise est représentée par une portion de colonne, dont la couleur indique la nature (voir légende) et dont la hauteur représente l'énergie totale (moins 938 MeV pour les hypérons) dans le cas des particules instables et l'énergie cinétique dans le cas des particules stables. Toutes les

particules stables sont considérées comme protons et leur énergie de liaison (prise égale à 8 MeV) est représentée sur la figure. Les protons sont indiqués de manières distinctes selon que leur énergie cinétique est inférieure ou supérieure à 35 MeV. Les lignes horizontales tracées dans le diagramme indiquent les masses au repos des mésons π, comptées à partir du haut, et les masses au repos des hypérons, diminuées de 938 MeV, comptées à partir du bas.

Les événements sont classés sur une base purement phénoménologique, d'après la nature des particules émises. Les nombres d'événements figurant dans les différentes catégories sont repris dans le Tableau II. Celui-ci permet de faire un certain nombre de constatations qui seront examinées dans les paragraphes suivants.

4·3. *Identification et classification des hypérons chargés.* – Nous avons identifié 56 hypérons chargés d'après les caractéristiques de leur désintégration ou de leur interaction; ils ont été classés dans le Tableau III.

Remarquons qu'à côté de 701 traces de particules de masse protonique suivies jusqu'au bout, parmi lesquelles les 56 hypérons ont été identifiés, il y a 10 traces dont l'identification n'a pas été possible, soit parce qu'elles sortent du stack, soit en raison de difficultés particulières de suivage. Elles ont été classées comme protons, bien qu'un petit nombre d'hypérons pourraient encore se trouver parmi elles.

Les difficultés d'identification et les causes de perte dans chacune des catégories du Tableau III sont examinées dans les commentaires qui suivent le Tableau. Nous ne donnons pas ici une estimation des facteurs de perte, étant donné le nombre limité d'événements dans chaque catégorie.

Fig. 3 (*ici, à droite*). – Représentation des événements d'après la nature et l'énergie des particules émises. *a*) Rouge: Hypérons. L'énergie cinétique des hypérons $\Sigma^{\pm}$ est représentée par la partie de la colonne située au dessus de la ligne horizontale qui représente la masse de l'hypéron. Quand le signe de l'hypéron n'est pas connu, l'énergie cinétique est prise à partir de la valeur moyenne entre les masses de l'hypéron positif et négatif. L'énergie de liaison du nucléon qui intervient dans la réaction de production de l'hypéron n'a pas été représentée. *b*) Rouge hachuré: Hyperfragments. L'énergie cinétique des hyperfragments étant, dans la plupart des cas, impossible à déterminer, elle n'est pas indiquée. *c*) Bleu: mésons π. L'énergie cinétique des mésons $\pi^{\pm}$ est représentée par la partie de la colonne située au dessous de la ligne horizontale qui représente la masse du méson chargé. *d*) Noir: Somme des énergies cinétiques des particules stables (considérées comme protons) d'énergie inférieure à 35 MeV. *e*) Noir hachuré: Protons ayant une énergie cinétique supérieure à 35 MeV. Lorsque deux protons rapides sont émis dans le même événement, la partie correspondante de la colonne est divisée par un trait horizontal. *f*) Blanc: Somme des énergies de liaison des particules stables (considérées comme protons). La valeur de 8 MeV par particule a été adoptée. Une flèche au bout d'une colonne indique que seulement la limite inférieure de l'énergie de la particule a pu être déterminée.

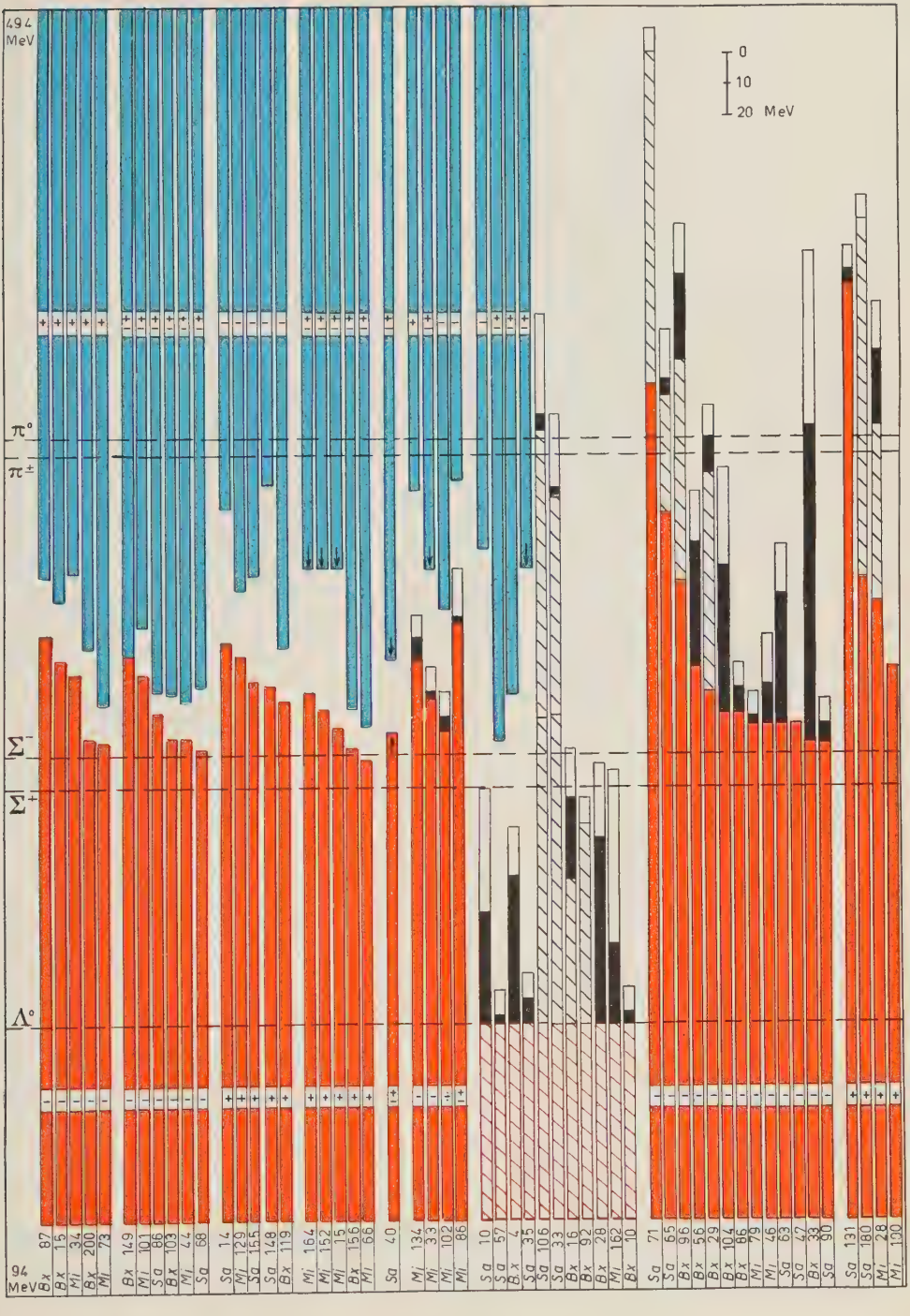
494 MeV
0
10
20 MeV
π°
π±
Σ⁻
Σ±
Λ°
94 MeV
Bx 87
Bx 15
Mi 34
Bx 200
Mi 73
Bx 149
Mi 101
Sa 66
Bx 103
Mi 44
Sa 68
Sa 14
Mi 129
Sa 155
Sa 148
Bx 119
Mi 164
Mi 152
Mi 15
Bx 156
Mi 66
Sa 40
Mi 134
Mi 33
Mi 102
Mi 86
Sa 10
Sa 57
Bx 4
Sa 35
Sa 106
Sa 33
Bx 16
Bx 92
Bx 28
Mi 162
Bx 10
Sa 71
Sa 65
Bx 96
Bx 56
Bx 29
Bx 104
Bx 86
Mi 79
Mi 46
Sa 63
Sa 42
Bx 38
Sa 90
Sa 131
Sa 180
Mi 28
Mi 100

Fig. 3 *a*).

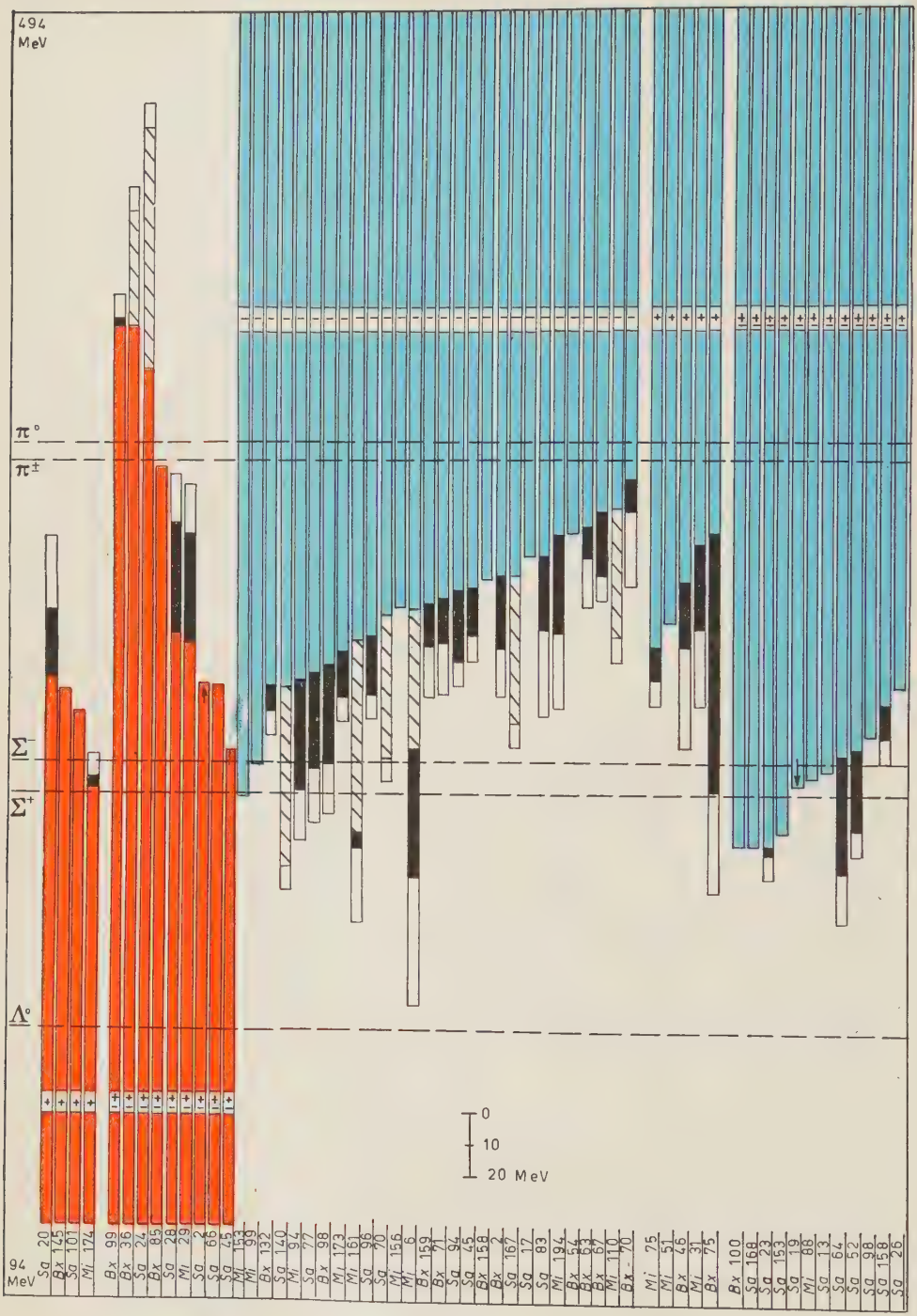

Fig. 3 *b*).

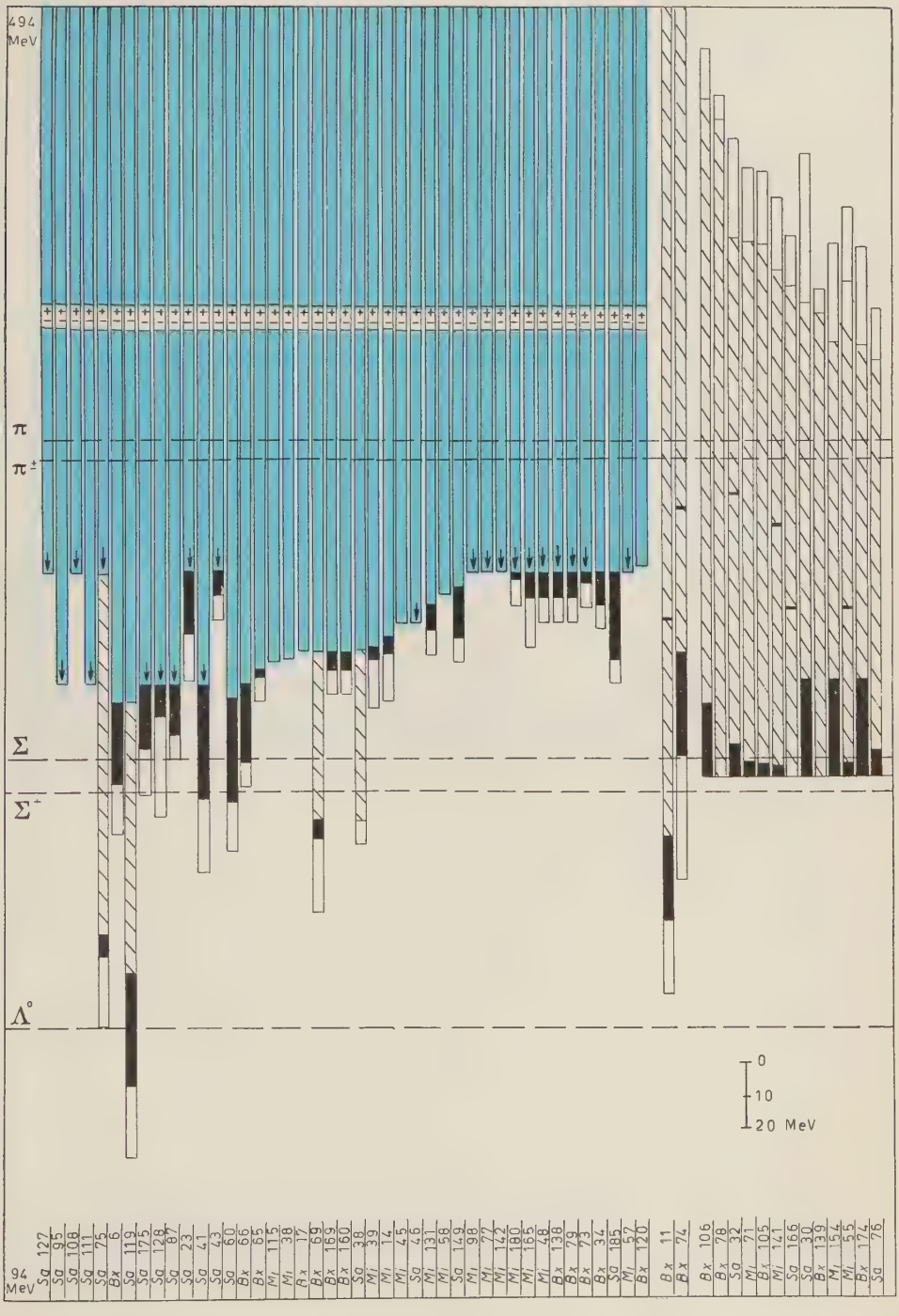
494 MeV
π
π±
Σ
Σ±
Λ°
0
10
20 MeV
94 MeV
Sa 127
Sa 95
Sa 108
Sa 111
Sa 75
Bx 6
Sa 119
Sa 175
Sa 128
Sa 87
Sa 23
Sa 41
Sa 43
Sa 60
Bx 66
Bx 65
Mi 115
Mi 38
Bx 17
Bx 69
Bx 169
Bx 160
Sa 38
Mi 39
Mi 14
Mi 45
Sa 46
Mi 131
Mi 158
Sa 149
Mi 98
Mi 77
Mi 142
Mi 180
Mi 165
Mi 48
Bx 138
Bx 79
Bx 73
Bx 34
Sa 185
Mi 152
Bx 120
Bx 11
Bx 74
Bx 106
Bx 78
Sa 32
Mi 71
Bx 105
Mi 141
Sa 166
Sa 30
Bx 139
Mi 154
Mi 55
Bx 174
Sa 76

Fig. 3 *c*).

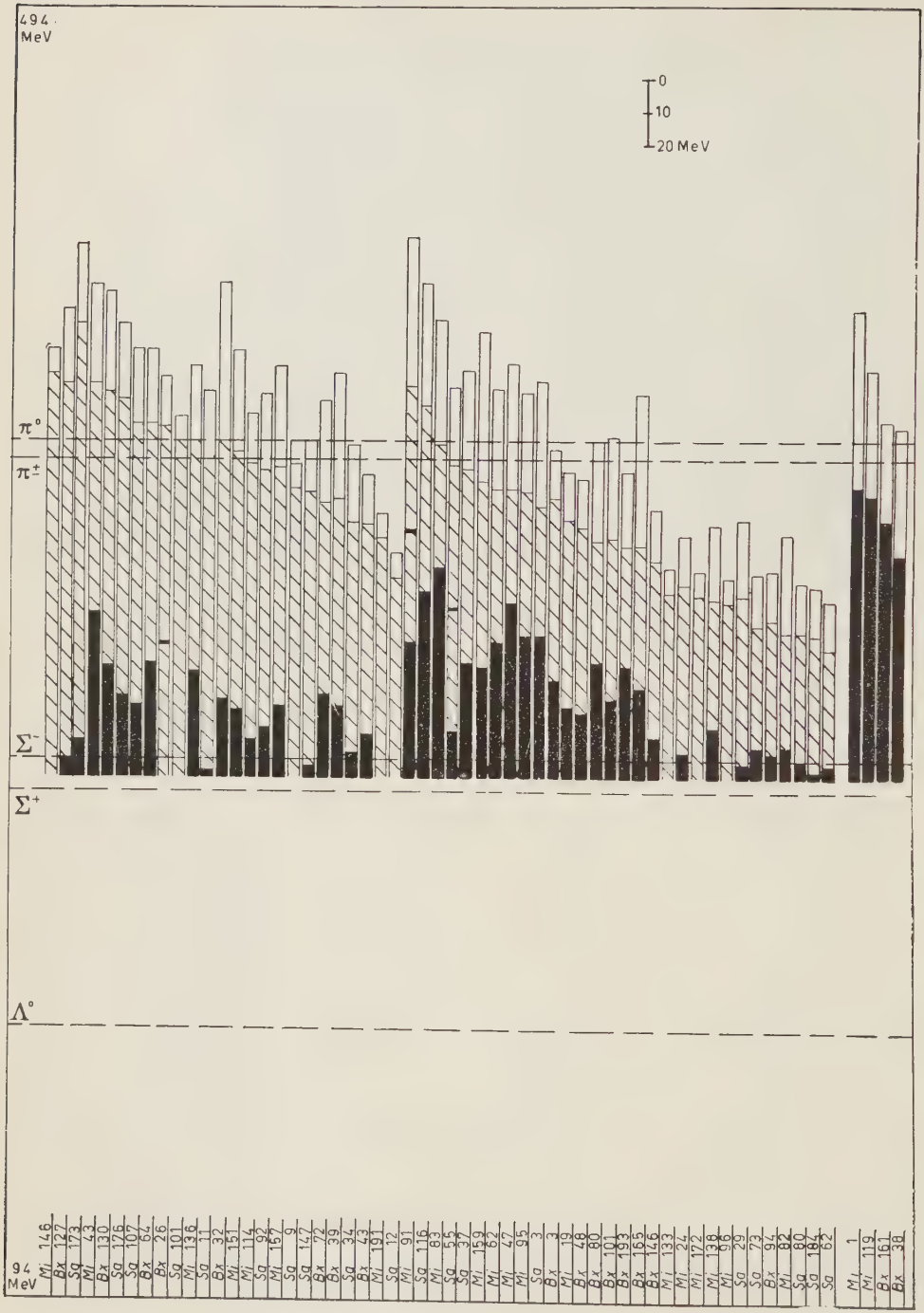

Fig. 3 *d*).

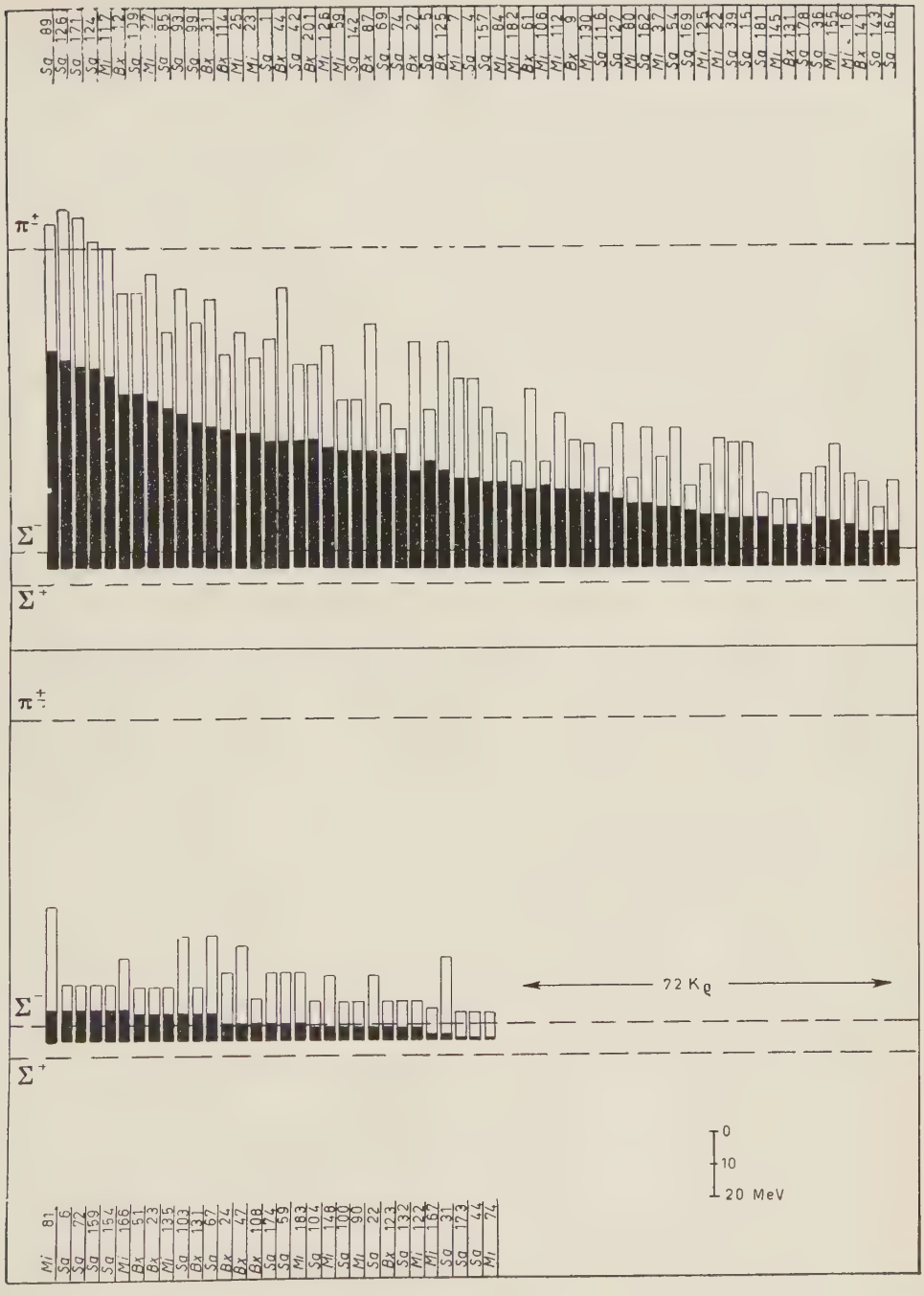

Fig. 3 *e*).

TABLEAU II. – *Répartition des différents types d'événements.*

Type d'événement	Nombre d'événements	Nombre d'événements comportant des protons de $T > 35$ MeV ($T > 60$ MeV)	% par rapport au nombre total de K^-_σ	% par rapport au nombre total d'absorptions ($319K^-_\sigma + 72K^-_\rho$)
$\Sigma^\pm\pi^\mp$ { colinéaires	3	—	1.0 ± 0.6	0.8 ± 0.5
$\Sigma^\pm\pi^\mp$ { non colinéaires	23	—	7.2 ± 1.6	5.9 ± 1.1
$\Sigma^\pm$ (sans $\pi^\pm$) { $T_\Sigma < 50$ MeV	20	1 (1)	6.3 ± 1.2	5.1 ± 0.9
$\Sigma^\pm$ (sans $\pi^\pm$) { $T_\Sigma > 50$ MeV	10	7 (4)	3.1 ± 0.6	2.6 ± 0.5
Total des événements avec $\Sigma^\pm$	**56**		**17.6 ± 2.3**	**14.3 ± 1.9**
$\pi^\pm$ (sans $\Sigma^\pm$ ou HF)	88	10 (3)	27.5 ± 2.9	22.5 ± 2.4
$\pi^\pm$ HF	4	—	1.3 ± 0.7	1.0 ± 0.6
Total des événements avec $\pi^\pm$	**118**		**37.0 ± 3.4**	**30.1 ± 2.8**
HF (sans $\pi^\pm$)	7	4 (3)	2.2 ± 0.9	1.8 ± 0.7
Total des événements avec HF	**11**		**3.4 ± 0.5**	**2.8 ± 0.4**
Evénements sans particule instable chargée mais avec protons de $T > 35$ MeV (ou > 60 MeV)	70 (40)	70 (40)	21.9 ± 2.6 (12.5 ± 2.0)	17.9 ± 2.1 (10.2 ± 1.6)
Evénements ne comportant que des particules stables de $T < 35$ MeV	94	=	29.5 ± 3.1	24.0 ± 2.5
Total des événements K^-_σ sans particule instable chargée	**164**		**51.4 ± 4.0**	**41.9 ± 3.3**
Nombre total des K^-_σ	**319**		**100**	**81.6 ± 4.6**

Les erreurs indiquées sont les erreurs statistiques standard.

TABLEAU III. – *Classification des hypérons chargés.*

	Σ^+		Σ^-				$\Sigma^\pm$	
	$\to \pi^+$	$\to$ p	$\to \pi^-$	σ	$\varrho(A, R; B)$	ϱ	$\to \pi^\pm$	interaction
	1	2	3	4	5	6	7	8
au repos	9 (*a*)	6 (*b*)	—	7 (*c*)	11 (A, R) (*d*) 3 (B)	2 (*e*)	—	—
en vol	1	3 (*f*)	1	—	—	2 (*g*)	10 (*a*)	1 (*f*)

Le type de désintégration ou d'interaction est indiqué dans chaque colonne. Pour les renvois (petites lettres), voir les commentaires.

COMMENTAIRES.

a) L'identification des hypérons Σ^+ qui se désintègrent au repos en donnant lieu à l'émission d'un méson π^+ présente deux difficultés:

D'une part, la trace peu ionisante du méson peut échapper à l'observation (cfr. Sect. 4·1, 2°); nous avons adopté ici les mêmes précautions que dans la recherche des particules peu ionisantes émises dans les absorptions de mésons K^-.

D'autre part, il est difficile et souvent impossible (faible vitesse de la particule primaire, grand angle d'inclinaison de la trace) d'estimer si la particule primaire est à la fin de son parcours ou possède encore une certaine énergie résiduelle. Il devient alors difficile de distinguer entre la désintégration au repos d'un Σ^- et la désintégration en vol d'un $\Sigma^\pm$ (colonne 7 du Tableau). Etant donné le petit nombre d'événements faisant partie de ces catégories, nous nous sommes bornés à estimer visuellement si la particule primaire était au repos ou non.

Pour la perte de secondaires peu ionisants dans les désintégrations en vol, voir (*g*).

b) Dans ces 6 cas, l'énergie du proton secondaire correspond à la désintégration au repos $\Sigma^+ \to p + \pi^0$; nous avons négligé la possibilité que l'absorption d'un hypéron Σ donne lieu à l'émission d'un proton de cette même énergie. Suivant nos critères d'identification, nous trouvons pour le rapport d'embranchement $(\Sigma^+ \to n + \pi^+)/(\Sigma^+ \to p + \pi^0)$ la valeur 9/6 (la valeur connue de ce rapport est voisine de l'unité [1]).

c) Nous avons considéré comme étoiles d'absorption d'hypérons Σ^-, les étoiles associées à la fin de traces d'allure protonique et comportant au moins deux branches ou celles comportant une seule branche dont l'ionisation et le parcours permettaient d'écarter l'hypothèse d'un scattering de proton. Notons que les hypérons Σ^- que nous avons identifiés par leur étoile d'absorption ont tous un parcours supérieur à 70 μm, ce qui rend peu probable toute confusion avec des mésons π^- lents ou des hyperfragments. Dans six événements, une branche courte qui se termine par une étoile et dont l'identification est impossible a été classée comme hyperfragment mais il est possible que certaines d'entre elles soient des hypérons Σ de très faible énergie. En effet, l'hypéron Σ^- de plus basse énergie que nous ayons identifié possède une énergie cinétique de 3 MeV, alors que nous avons observé un hypéron Σ^+ qui se désintègre au repos en un méson π de 1.3 MeV.

d) La présence à la fin d'une trace d'allure protonique d'un électron lent (*A*), d'un blob (*B*) ou d'un recul (*R*) a déjà été signalée comme critère d'identification des Σ^-_ρ au repos [2]. Cependant, l'utilisation d'un tel critère nécessite l'estimation de la fréquence des coïncidences de ces caractéristiques avec la fin de traces de protons dans le même stack. Un tel contrôle a été effectué sur 430 traces de protons; 4 coïncidences ont été relevées: une avec un électron lent et trois avec un blob. Aucun cas de scattering en fin de parcours, simulant un recul, n'a été observé. D'autre part, un dénombrement d'électrons lents isolés dans le *background* de l'émulsion nous permet d'estimer à moins de 0.1% leur probabilité de coïncidence avec la fin d'une trace d'allure protonique, tandis que la probabilité de coïncidence d'un blob (quoique difficile à évaluer par un test de ce type) semble être beaucoup plus élevée. Dans ces conditions, nous n'avons retenu comme traces d'hypérons Σ^-_ρ que celles dont la fin est associée à un électron lent ou à un recul. Toutefois, 3 traces terminées par un blob proviennent d'une étoile comportant une trace de méson π^+ (Bx 87) ou $\pi^\pm$ (Sa 68 et Sa 86) et présentent des caractéristiques analogues à celles des événements $\Sigma\pi$ iden-

tifiés avec certitude (cfr. Sect. 4·4.1 et Tableau IV). C'est pourquoi, nous avons attribué ces trois traces à des hypérons Σ^- et inclu les trois événements dans la catégorie $\Sigma\pi$ (voir aussi (*e*)).

e) Bien que ne répondant pas aux critères d'identification des hypérons Σ_ρ^- décrits ci-dessus, 2 traces (Bx 103, Mi 44) ont été considérées comme telles parce qu'elles appartiennent à des événements qui peuvent être attribués à des absorptions de méson K^- par des noyaux d'hydrogène (voir Sect. 4·4, 1)). De l'existence de telles traces on peut déduire qu'un certain nombre d'hypérons Σ_ρ^- ont dû être confondus avec des protons.

f) Nous avons observé 5 cas dans lesquels une particule d'allure protonique donne naissance en vol à un proton. Dans 4 de ces cas, l'ionisation du proton est inférieure à celle de la particule primaire; le bilan énergétique de ces événements, effectué dans le système du centre de masse de la particule primaire, montre que 3 d'entre eux (Mi 15, Mi 164 et Sa 20) sont compatibles avec le schéma de désintégration $\Sigma^+ \to p + \pi^0$; le quatrième (Bx 30), incompatible avec ce schéma, a été classé comme interaction en vol d'un hypéron Σ^+. Dans le cinquième cas, l'ionisation du proton est supérieure à celle de la particule primaire et l'événement, incompatible avec la désintégration d'un hypéron Σ^+, a été classé comme scattering inélastique d'un proton.

g) Nous avons observé 4 événements dans lesquels une particule d'allure protonique disparaît en vol dans l'émulsion sans donner lieu à l'émission de particule chargée. Ces événements peuvent s'interpréter comme échanges de charge de protons ou d'hypérons, ou encore comme désintégrations d'hypérons en mésons π rapides qui auraient échappé à l'observation. Etant donné que dans les cas observés le point d'arrêt des traces se trouve loin de la surface de l'émulsion ou du verre, nous avons écarté cette dernière possibilité.

Dans un cas (Bx 11), la trace disparaît après un parcours de 9 cm; compte tenu de l'énergie visible dans l'étoile d'absorption du méson K^- et de la durée de vie des hypérons, on peut admettre qu'il s'agit vraisemblablement d'un proton. Dans les trois autres cas (Mi 34, Sa 71, Bx 105), la disparition de la trace se produit après des parcours respectivement égaux à 0.4, 1.5 et 2.5 cm. On peut tenter de donner de ces cas une interprétation basée sur les caractéristiques de l'étoile primaire. Le cas Mi 34 a été classé comme échange de charge d'un hypéron Σ^-, celui-ci étant associé à un méson π^+, l'énergie et la quantité de mouvement résiduelles de l'événement étant comparables à celles des couples $\Sigma\pi$; le cas Sa 71 a été également classé comme échange de charge d'un hypéron Σ^-, celui-ci et le proton auquel il est associé ayant tous deux une énergie cinétique supérieure à 100 MeV, ce qui correspond très probablement à une interaction à deux nucléons avec production d'un hypéron Σ^-; quant au cas Bx 105, dans le doute, il a été classé comme proton subissant un échange de charge.

4·4. *Etude des différentes catégories d'événements.*

1) Evénements $\Sigma\pi$. Nous avons identifié 26 étoiles comportant l'émission simultanée d'un hypéron et d'un méson π chargés; dans 4 cas seulement les particules instables sont accompagnées d'une évaporation nucléaire, d'ailleurs faible. Leurs caractéristiques sont résumées dans le Tableau IV.

Trois événements (Bx 103, Mi 44 et Sa 40) ont été interprétés comme résultant de l'absorption d'un méson K^- par un noyau d'hydrogène, donnant

TABLEAU IV. — *Caractéristiques des événements* $\Sigma\pi$.

No. du K	Caractéristiques de l'hypéron: Signe	Caractéristiques de la désintégration ou de l'interaction	Repos ou Vol	T (MeV)	Caractéristiques du méson: Signe	T (MeV)	Angle d'inclinaison θ (degrés)	Etoile primaire: Angle $\widehat{\Sigma\pi}$ α (degrés)	P résiduelle (MeV/c)	E résiduelle (MeV)	T Br. stables
1	2	3	4	5	6	7	8	9	10	11	12
Bx 103	—	colinéaire avec le méson	r	12.4	±	75±15	— 39	180	9±20	9±15	
Mi 44	—	»	r	11.6	±	77± 3	— 23	180	2± 4	7± 3	—
Sa 40	±	»	v	>11.8	±	> 63	+ 3	180	< 24	< 21	—
Sa 14	+	p	r	43	—	16.5	+ 59	136	276	43	—
Mi 129	+	π^+	r	39.4	—	41.5	+ 24	118	274	22	—
Sa 155	+	π^+	r	31	—	38.0	+ 6	110	257	34	—
Sa 148	+	π^+	r	30.1	—	10.6	+ 1	61	300	62	—
Bx 119	+	p	r	25.5	—	60.5	— 19	155	137	17	—
Mi 164	+	p	v	47±8 *	±	> 35	+ 66	88	—	< 20	—
Mi 152	+	π^+	r	22.5	±	> 35	+ 63	55	—	< 45	—
Mi 15	+	p	v	17.4±2	±	> 35	— 63	94	—	< 51	—
Bx 156	+	p	r	10.4	±	79±8	+ 8	119	165	14	—
Mi 66	+	π^+	r	6.9	±	84±3	— 14	128	139	12	—
Bx 87	—	B	r	38	+	38.0	+ 30	168	195	20	—
Bx 15	—	A+B	r	29.4	+	47.4	— 6	161	154	19	—
Bx 200	—	A	r	5.4	+	60.0	+ 8	67	213	31	—
Mi 73	—	σ_2	r	4.5	+	77.5	— 25	99	183	14	—
Bx 149	—	σ_2	r	33	±	80±20	— 32	154	158	— 17	—
Mi 101	—	A	r	24.8	±	53± 7	— 57	135	177	18	—
Sa 86	—	B	r	12.9	±	73±10	— 32	163	52	10	—
Sa 68	—	B	r	3.9	±	72±8	+ 36	144	94	20	—
Mi 34	—	disparition	v	26±5	+	37.5±1.5	— 27	164	28	32	—
Mi 102	+	p	r	16	—	48	— 14	96	—	39	3.7
Mi 134	—	R	r	30.7	+	10.8	+ 7	67	—	54	6.8
Mi 33	—	A+B	r	17.8	±	> 35	— 60	68	—	< 43	< 0.5
Mi 86	±	$\pi^\pm$	v	45±10	—	8.2	+ 40	57	—	50	< 0.5 < 0.5

Pour les particules suivies jusqu'à leur arrêt dans l'émulsion, l'erreur affectant la mesure de l'énergie cinétique est due essentiellement au straggling (~1% pour les hypérons et 2% pour les mésons π).

* Dans les figg. 3, 4, 5, 6*a*, 7, l'énergie cinétique de l'hypéron Σ^+ de l'événement Mi 164 a été indiquée par erreur comme étant égale à 27 MeV au lieu de 47 MeV. (*Note ajoutée aux épreuves.*)

lieu à l'émission d'un hypéron Σ et d'un méson π chargés. Dans les deux premiers cas, la particule opposée au méson π ne peut pas être identifiée directement comme hypéron Σ^-, parce que la trace se termine dans l'émulsion sans donner lieu à aucun produit visible. Cependant, les traces des deux particules émises sont colinéaires, le parcours du baryon est celui d'un hypéron Σ^- qui résulterait de la réaction $K^- + p \to \Sigma^- + \pi^+$ et l'énergie cinétique du méson π, estimée d'après l'ionisation, est compatible avec cette réaction. Dans le troisième cas, les traces des deux particules émises sont également colinéaires, l'hypéron $\Sigma^\pm$ se désintègre en vol en un méson $\pi^\mp$ et les énergies cinétiques des deux particules sont compatibles avec les réactions $K^- + p \to \Sigma^\pm + \pi^\mp$.

Les 23 couples $\Sigma\pi$ non colinéaires ont été attribués à l'interaction de mésons K^- avec des nucléons liés. Dans 12 cas , les deux particules instables ont été suivies jusqu'à la fin de leur parcours; leurs signes ont toujours été trouvés opposés. Si nous faisons l'hypothèse que les échanges de charge de l'hypéron et du méson π sont négligeables, tous ces événements doivent être attribués à l'une ou à l'autre des réactions (1) et (2); par conséquent, chaque fois que le signe d'une seulement des deux particules instables a pu être déterminé, le signe de l'autre peut en être déduit. Le fait qu'aucun événement $\Sigma^-\pi^-$ ou $\Sigma^+\pi^+$ n'ait été signalé par d'autres auteurs ni observé dans le présent travail vient à l'appui de cette hypothèse, sans constituer toutefois un argument contraignant. Dans ces conditions et en excluant les 4 couples $\Sigma\pi$ avec évaporation, le rapport des fréquences observées des réactions (2) et (1) est égal à

$$\frac{\Sigma^-\pi^+}{\Sigma^+\pi^-} = \frac{9}{10} = 0.9 \pm 0.5 .$$

Si nous incluons les 4 événements $\Sigma\pi$ avec évaporation, la valeur de ce rapport (11/12) reste inchangée. Cette valeur pourrait toutefois être faussée, en raison des difficultés d'identification des événements Σ_ρ^- (voir note (*d*) des commentaires du Tableau III). C'est pourquoi, nous avons appliqué à notre statistique l'argumentation développée par F. C. Gilbert et coll. ([5]), basée sur l'étude des absorptions de mésons K^- donnant lieu à des étoiles à deux branches non colinéaires, dont l'une est attribuée à un méson π et l'autre, soit à un hypéron Σ^+ ou à un hypéron Σ^- identifié avec certitude (Σ_σ), soit à un baryon non identifié (proton ou hypéron Σ_ρ^-), désigné par le symbole H_ρ. Les 49 absorptions de mésons K^- de ce type ont été distribuées dans le Tableau V.

Tableau V. – *Classification des événements* $\Sigma^\pm\pi^\mp$ *et* $H_\rho\pi^\pm$.

Type d'événement	$\Sigma^+\pi^-$	$\Sigma^-\pi^+$	$H_\rho\pi^+$	$H_\rho\pi^\pm$	$H_\rho\pi^-$
Nombre d'événements	10	2	5	22	10

(L'événement Mi 34 a été classé parmi les $H_\rho\pi^+$).

Nous avons aussi représenté dans la Fig. 4, pour tous ces événements, la quantité $\varepsilon = Q - (T_H + T_\pi)$, où Q est l'énergie libérée dans la réaction d'absorption, T_H l'énergie cinétique du baryon et T_- l'énergie cinétique du méson π.

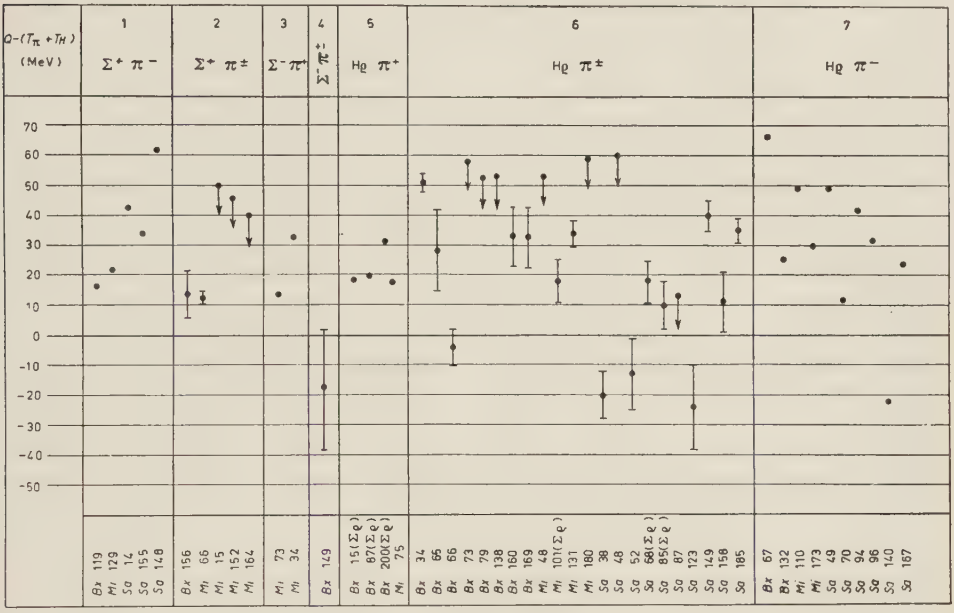

Fig. 4. – Energie résiduelle $\varepsilon = Q - (T_H + T_\pi)$ des événements $\Sigma\pi$ et $H_\varrho\pi$. ↓ indique que l'on a pu déterminer seulement la limite inférieure de l'énergie du méson π.

ε est indiquée comme *énergie résiduelle* dans la colonne 11 du Tableau IV. On voit que l'énergie résiduelle est comprise entre 0 et 60 MeV pour tous les événements dans lesquels l'hypéron est reconnu avec certitude (Fig. 4, colonnes 1, 2, 3, 4); sa valeur moyenne est 25 MeV et sa valeur la plus probable est environ 20 MeV, ce qui est en bon accord avec les observations de GILBERT et coll. ([5]). En prenant les mêmes limites pour l'énergie résiduelle des événements $H_\varrho\pi$, on déduit que tous les événements $H_\varrho\pi^+$ (Fig. 4, colonne 5) peuvent être interprétés comme $\Sigma^-\pi^+$. Par conséquent, au plus 7 des 19 événements $H_\varrho\pi^\pm$ (Fig. 4, colonne 6) ayant une énergie résiduelle comprise entre les limites choisies peuvent être considérés comme couples $\Sigma^-\pi^+$. On obtient ainsi un total de 14 couples $\Sigma^-\pi^+$, ce qui donne pour le rapport des fréquences observées des réactions (2) et (1) la valeur

$$\frac{\Sigma^-\pi^+}{\Sigma^+\pi^-} = \frac{14}{10} = 1.4 \pm 0.6 .$$

Les deux valeurs de ce rapport que nous avons obtenues sont affectées d'erreurs statistiques importantes; dans ces limites, elles sont en accord aver la valeur 0.83 ± 0.25 obtenue pac GILBERT et coll. (5).

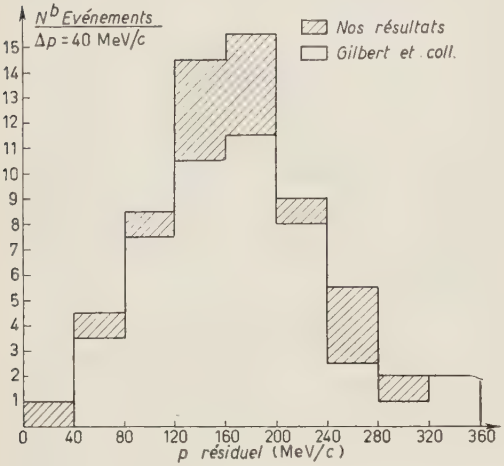

Fig. 5. - Distribution de la quantité de mouvement résiduelle des événements $\Sigma\pi$.

La quantité de mouvement résiduelle des couples $\Sigma\pi$ (à l'exclusion des événements avec évaporation) est indiquée dans le Tableau IV, colonne 10; sa valeur moyenne est 175 MeV/c, ses valeurs extrêmes sont 28 et 300 MeV/c. Ces résultats sont représentés aussi dans la Fig. 5, où ils sont comparés avec ceux de GILBERT *et coll.*.

Les spectres énergétiques des hypérons et des mésons émis dans les événements $\Sigma\pi$ ont été représentés dans la Fig. 6, *a* et *b*. L'énergie cinétique moyenne des hypérons Σ^- est 20.6 MeV et celle des hypérons Σ^+ est 26.3 MeV. Réserve faite pour les incertitudes qui affectent les mesures dans certains cas (désintégrations en vol), l'énergie cinétique maximum observée ne dépasse pas

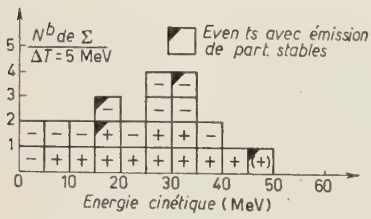

Fig. 6*a*. – Distribution des énergies cinétiques et des signes des Σ dans les événements $\Sigma\pi$ non colinéaires.

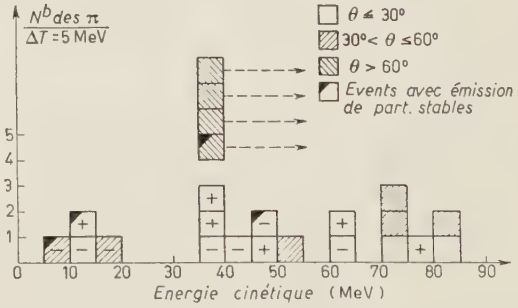

Fig. 6*b*. – Distribution des énergies cinétiques et des signes des π dans les événements $\Sigma\pi$ non colinéaires. ϑ est l'angle d'inclinaison par rapport à la surface de l'émulsion.

50 MeV. L'énergie cinétique des mésons π est dans tous les cas inférieure à 90 MeV, avec une valeur moyenne d'environ 50 MeV. Tous ces résultats sont en accord avec les observations de GILBERT *et coll.* (5). Remarquons que pour les 4 couples $\Sigma\pi$ accompagnés d'une évaporation nucléaire visible

l'énergie moyenne des hypérons est 27.5 MeV, ce qui est en accord avec les autres événements $\Sigma\pi$, tandis que l'énergie moyenne des mésons π est inférieure à 30 MeV. D'autre part, l'énergie résiduelle (qui dans ces cas comprend la faible énergie évaporative visible) est en moyenne voisine de 45 MeV, au lieu des 25 MeV observés dans les autres événements $\Sigma\pi$. Ces observations suggèrent que dans ces cas le méson π a interagi à l'intérieur du noyau.

2) Evénements Σ. Nous avons identifié 30 étoiles sans méson π chargé mais comportant un hypéron chargé, accompagné ou non de particules stables. Les caractéristiques de ces événements sont données dans le Tableau VI. Le spectre d'énergie cinétique des hypérons est représenté dans la Fig. 7, où on a mis en évidence l'association des hypérons avec des protons d'énergie supérieure à 35 MeV (appelés par la suite *protons rapides*). On voit qu'un tiers des hypérons non accompagnés de mésons π chargés possèdent une énergie supérieure à 50 MeV et sont en majorité associés à des protons rapides (voir aussi le Tableau II), tandis qu'un seul hypéron d'énergie inférieure présente cette association.

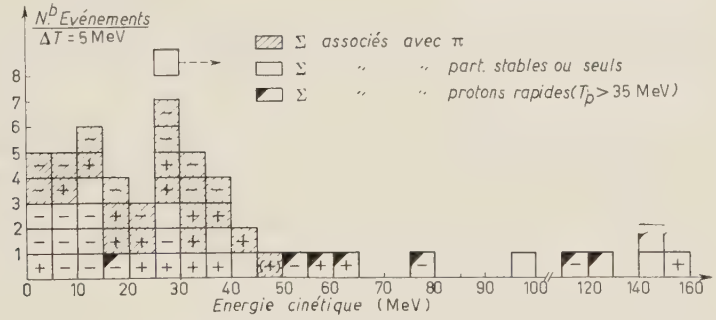

Fig. 7. – Spectre d'énergie des hypérons des événements Σ.

a) Evénements dans lesquels $T_\Sigma > 50$ MeV. Dans 5 de ces événements, l'hypéron a une énergie supérieure à 100 MeV; ils ne peuvent être attribués qu'à des réactions à deux nucléons des types (8), (11) et (14). Dans trois d'entre eux, l'hypéron est associé à un proton rapide.

Les autres événements peuvent résulter de l'absorption de mésons K^- par un ou par deux nucléons. On peut essayer de reconnaître parmi ces événements une partie des réactions à deux nucléons, en utilisant deux critères: l'énergie des hypérons et la présence de protons rapides. A cet effet, rappelons que la limite supérieure expérimentale des énergies cinétiques des hypérons chargés accompagnés de mésons π chargés est environ 50 MeV. Si l'on admet que cette limite est valable pour tous les hypérons chargés provenant des réactions à un nucléon, nous pouvons considérer que les cinq événements comprenant un hypéron d'énergie cinétique comprise entre 50 et 100 MeV peuvent être

TABLEAU VI. – *Caractéristiques des événements* Σ.

No. du K⁻	Caractéristiques de l'hypéron: Signe	Caractéristiques de la désintégration ou de l'interaction	Repos ou Vol	T (MeV)	Particules stables: Nombre de branches $T \leqslant 35$ (MeV)	Particules stables: Nombre de branches $T > 35$ (MeV)	Particules stables: Energie cinétique (MeV)
Sa 180	+	π^+	r	63	0	1	110
Mi 28	+	π^+	r	56	1	1	77.5
Mi 100	+	π^+	r	37	0		—
Mi 174	+	π^+	r	1.3	1		< 0.5
Sa 131	+	π^+	v	155 ± 3.4	1		14
Bx 145	+	p	r	29.6	0		—
Sa 101	+	p	r	23.4	0		—
Sa 20	+	p	v	34.5 ± 0.3	3		20.5
Bx 96	—	σ_1	r	54.5	1	1	95.5
Bx 29	—	σ_3	r	19.7	1	1	75
Bx 104	—	σ_4	r	11.3	4		45
Mi 79	—	σ_1	r	10.1	1		< 1
Sa 90	—	σ_3	r	3.1	1		8
Bx 56	—	A	r	28	2		40
Bx 86	—	A	r	11.2	1		8
Mi 46	—	R	r	9.8	2		12
Sa 47	—	2R	r	9.6	0		—
Sa 63	—	R	r	9.5	2		38.5
Bx 33	—	A	r	4.4	7		99
Sa 65	—	π^-	v	76 ± 2.5	1	1	40
Sa 71	—	disparition	v	~ 115	0	1	105
Bx 99	±	$\pi^\pm$	v	140 ± 20	1		1
Sa 24	±	$\pi^\pm$	v	126 ± 15	0	1	74
Bx 85	±	$\pi^\pm$	v	97 ± 10	0		—
Sa 58	±	$\pi^\pm$	v	44	2		35
Mi 29	±	$\pi^\pm$	v	35 ± 5	2		34
Sa 2	±	$\pi^\pm$	v	> 28	0		—
Sa 66	±	$\pi^\pm$	v	27 ± 0.6	0		—
Sa 45	±	$\pi^\pm$	v	~ 10	0		—
Bx 30	±	interaction	v	140 ± 10	0	1	35

Pour les hypérons s'arrêtant dans l'émulsion l'erreur affectant la mesure de l'énergie cinétique est due au straggling (~1%).

attribués à des réactions à deux nucléons; dans 4 de ces 5 cas, l'hypéron est associé à un proton rapide, ce qui, sans être décisif, est en faveur de cette attribution.

Les 10 événements attribués à des réactions à deux nucléons présentent les caractéristiques suivantes:

— un hypéron Σ^+ (Sa 131), accompagné seulement d'évaporation, attribuable à la réaction (8);

— deux hypérons Σ^+ (Sa 180, Mi 28), accompagnés d'un proton rapide, provenant, si on néglige la possibilité de deux échanges de charge, soit de la réaction (8) suivie d'un échange de charge: $n+p \rightarrow p+n$, soit de la réaction (9) suivie d'un échange de charge de l'hypéron neutre;

— trois hypérons Σ^-, dont deux (Sa 71 et Bx 96), accompagnés de protons de plus de 60 MeV, pouvant être interprétés directement par la réaction (11); le troisième (Sa 65) pouvant provenir des réactions (11) ou (14);

— enfin 4 hypérons de signe indéterminé (Bx 30, Bx 99, Sa 24, Bx 85), pouvant provenir d'une quelconque des réactions à deux nucléons, à l'exclusion de (10) et (13).

b) Evénements dans lesquels $T_\Sigma \leqslant 50$ MeV. Les 20 hypérons d'énergie cinétique inférieure à 50 MeV ont été attribués à des réactions à un seul nucléon, bien qu'un certain nombre d'entre eux pourraient aussi provenir de réactions à deux nucléons.

L'examen de l'évaporation nucléaire qui accompagne ces 20 événements permet la remarque suivante. Dans 2 cas (Mi 119, Bx 33), le bilan de l'énergie visible libérée lors de l'interaction exclut la possibilité de l'émission d'un méson π et dans 6 autres cas (voir Tableau IV, et Fig. 3), l'énergie d'évaporation est nettement supérieure à celle qui accompagne les événements $\Sigma\pi$. Cette constatation impose dans les 2 premiers cas et suggère fortement dans les autres que le méson π, chargé ou non, associé à l'hypéron a été réabsorbé. Le fait que l'énergie moyenne d'évaporation associée aux hypérons Σ^- identifiés avec certitude (32 MeV) ou identifiés sur la base du critère *électron Auger* ou *recul* (33 MeV) est supérieure à celle associée aux hypérons Σ^+ (4 MeV) ne va pas à l'encontre de cette conclusion, l'énergie moyenne d'évaporation qui accompagne l'absorption des mésons π^+ étant supérieure à celle qui accompagne l'absorption des mésons π^- ([7]). Il est toutefois impossible de préciser l'importance de ces phénomènes sur la base de la présente statistique. On peut remarquer, en effet, que la petite valeur de l'énergie d'évaporation associée aux hypérons Σ^+ est due au fait que dans 3 cas sur 5 l'hypéron est seul. Ce fait pourrait être expliqué non seulement par la réabsorption ou l'échange de charge des mésons π^-, mais encore par l'intervention de la réaction à deux nucléons (8).

3) Evénements π. Cette catégorie comprend les événements qui comportent un méson π comme seule particule chargée instable. Nous avons observé

([7]) G. Ferrari, L. Ferretti, R. Gessaroli, E. Manaresi, E. Pedretti, G. Puppi, G. Quareni, A. Ranzi, A. Stanghellini et S. Stantic: *Suppl. Nuovo Cimento*, **4**, 914 (1956).

88 événements de ce type, dont 30 dans lesquels le méson π est la seule particule chargée émise et 58 dans lesquels il est accompagné de particules stables; dans 10 (3) de ceux-ci, un proton de plus de 35 (60) MeV est émis. Ces événements peuvent provenir soit des réactions (6) et (7) donnant lieu à l'émission d'un méson π^-, suivies ou non de la réabsorption de l'hypéron neutre, soit des réactions (1) et (2) donnant lieu à l'émission d'un méson $\pi^\pm$, suivies

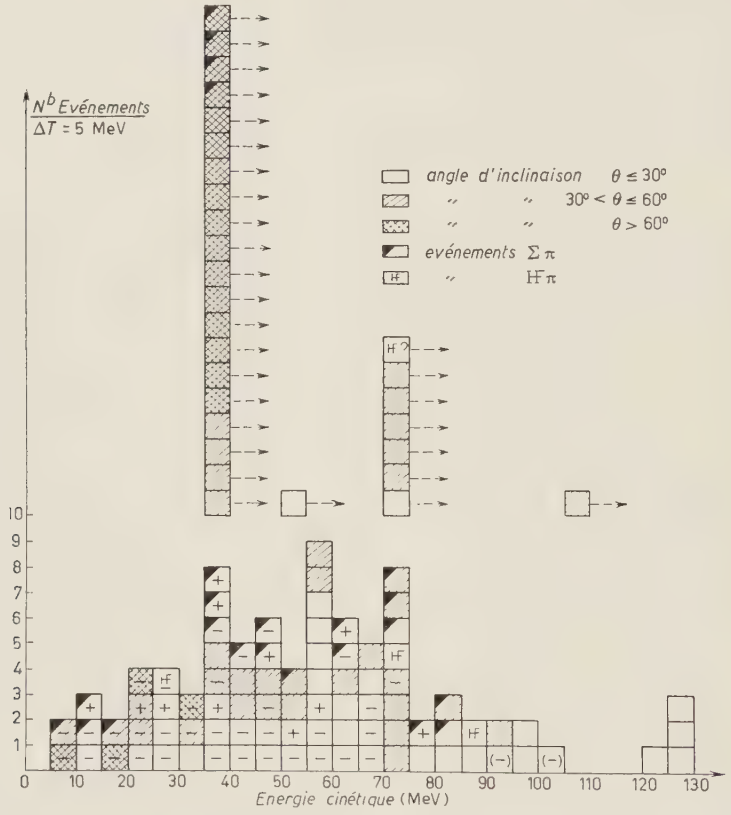

Fig. 8. – Spectre d'énergie et signes des mésons π (à l'exclusion de ceux des événements $\Sigma\pi$ colinéaires). La flèche à côté de certaines cases indique que seulement une limite inférieure de l'énergie du méson π a pu être determinée. (–) représente une trace de méson π s'arrêtant en vol dans l'émulsion, ce qui est en faveur de l'attribution du signe moins.

de la réabsorption de l'hypéron Σ^-. Si on tient compte, en outre, de la possibilité d'échange de charge des mésons π^0, les réactions (3), (4) et (5) peuvent être aussi responsables d'une partie des événements π.

La Fig. 8 représente le spectre d'énergie cinétique de l'ensemble des mésons π chargés (88 événements π, 23 événements $\Sigma\pi$ non colinéaires et 4 évé-

nements HFπ). Nous y avons distingué trois catégories:

— mésons dont la trace a une inclinaison inférieure à 30° et dont l'énergie a été déterminée avec une erreur inférieure à 15%, soit par la mesure de leur parcours, soit par des mesures conjuguées d'ionisation et de scattering, soit par des mesures d'ionisation effectuées en plusieurs endroits du parcours;

— mésons d'inclinaison supérieure à 30° dont l'énergie a été déterminée avec une erreur comprise entre 15 et 25% par des mesures d'ionisation;

— mésons d'inclinaison supérieure à 30° pour lesquels nous avons pu seulement déterminer une limite inférieure de l'énergie par une mesure d'ionisation à l'origine de la trace.

Si on considère la première catégorie, qui constitue un échantillonnage sans biais géométrique, on constate que le spectre est pratiquement continu de 5 à 125 MeV. Les 4 mésons dont l'énergie est voisine de 125 MeV proviennent vraisemblablement de la réaction (7) donnant lieu à l'émission directe d'un hypéron Λ^0; ceci nous donne une limite inférieure d'environ 1% pour la fréquence relative de cette réaction.

La partie du spectre comprise entre 5 et 105 MeV résulte essentiellement de la superposition des spectres d'énergie des mésons π provenant, d'une part, des réactions (1), (2) et (6) et, d'autre part, de la réaction (7), dont nous ne connaissons pas les fréquences relatives. L'énergie moyenne des mésons π des événements π est environ 60 MeV, énergie quelque peu supérieure à celle des mésons π associés à un hypéron Σ chargé. Cette différence pourrait être attribuée soit à la contribution de la réaction (7), soit au fait que l'hypéron Σ peut être absorbé dans des états liés, ce qui a pour effet d'augmenter l'énergie du méson π associé (*).

Parmi les 88 événements π, nous avons pu identifier 26 mésons π^- et 5 mésons π^+, soit environ 5 fois plus de mésons négatifs que de mésons positifs. Si nous considérons en outre les événements $\Sigma\pi$ et HFπ, nous avons pu identifier au total 34 mésons π^- et 11 mésons π^+, soit environ 3 fois plus de mésons négatifs que de mésons positifs. On pourrait se baser sur ce rapport pour déterminer les fréquences des différentes réactions à un nucléon. Cependant, il est encore difficile d'arriver à quelque conclusion sur ce point. Il a déjà été signalé [3] que la valeur expérimentale de ce rapport est plus élevée que celle à laquelle on pourrait s'attendre si les probabilités de réabsorption des mésons π^- et π^+ dans le noyau de production étaient égales. Pour atteindre le but proposé, il serait donc nécessaire de mieux connaître les probabilités respectives d'absorption des mésons π^- et π^+ et d'établir, sur une statistique plus élevée, comment ce rapport varie en fonction de l'énergie des mésons π.

(*) F. C. Gilbert et R. S. White: *UCRL* 4966 (1957). (*Note ajoutée aux épreuves*).

TABLEAU VII. –

N° du K^-	Hyperfragment			Particules chargées
	Longueur	Nature	Composition de l'étoile secondaire	mésons π
Bx 4	3.5 μm	HF, Σ^-	α, 10.4 MeV p, 10.8 MeV	$\pi^\pm$, 75 MeV
Bx 16	18 μm	HF	α, (6 μm) p, (6 μm) π^-, 32 MeV	—
Bx 10	4.5 μm	HF	p, 7,5 MeV π^-, 17 MeV	—
Bx 28	3 μm	HF, Σ^-, π^-	F β-actif ? (80 μm) p, 12.5 MeV p, 7.8 MeV	—
Bx 92	7.5 μm	HF, Σ^-	π^-, 27 MeV	—
Mi 162	2 μm	HF, Σ^-, π^-	recul p, 121 MeV	—
Sa 10	2 μm	HF, Σ^-, π^-	recul p, (d, t, α) 3.8 MeV p, 5.3 MeV	π^-, 28.5 MeV
Sa 33	11.5 μm	HF, Σ^-, π^-	p, (d, t, α, F) (7 μm) p, 3.2 MeV	—
Sa 35	< 2 μm	HF, Λ^0, Σ^+	p, (d, t, α) 7.4 MeV π^-, 41.3 MeV	$\pi^\pm$, > 70 MeV
Sa 57	4 μm	HF, Σ^-, π^-	p, 13.4 MeV p, (d, t, α) 0.5 MeV p, (d, t, α) 3.8 MeV α, 10.5 MeV	$\pi^\pm$, 90 MeV
Sa 106	5 μm	HF, Σ^-, π^-	p, (d, t, α) 1.6 MeV p, (d, t, α) 2 MeV	—

Evénements HF.

associées à l'HF		Remarques
protons rapides ($T_p \geqslant 35$ MeV)	autres particules	
—	2p, 46 MeV	—
1p, 45 MeV	1p, 1α } 25 MeV	Désintégration mésique ($^5He_\Lambda$)
—	1α, 8.7 MeV	Désintégration mésique
—	3p, 60 MeV	—
1p, 62 MeV	—	Désintégration mésique
—	7p, 30 MeV	Désintégration avec p rapide
—	5p, 34 MeV	—
2p { 95 MeV, 68.5 MeV	1p, 3.1 MeV	S'il s'agit d'un Σ^-, l'événement pourrait être expliqué par la réabsorption d'un méson π^+, donnant lieu à l'émission de 2 protons rapides.
—	—	L'événement peut être interprété: *a*) Désintégration mésique d'un HF de parcours très petit ou cryptofragment; *b*) Désintégration d'un Λ^0 de ~ 12 MeV au voisinage de l'étoile d'absorption du K^-; *c*) Evénement $\pi^-\Sigma^+$, avec Σ^+ très court.
—	1α, 3.5 MeV	—
2p { 94 MeV, 90 MeV	1p, 5.5 MeV	Voir Sa 33.

L'examen de l'énergie cinétique des particules stables accompagnant les mésons π chargés fournit quelques indications sur le comportement des hypérons initialement créés. La réabsorption de l'hypéron est prouvée dans deux cas (Sa 52 et Sa 119) où l'énergie visible est telle que l'émission d'un hypéron est impossible. Dans 18 autres cas, l'émission d'un hypéron Σ est impossible mais l'énergie disponible permet l'émission d'un hypéron Λ^0.

La réabsorption de l'hypéron pourrait toutefois être plus fréquente que ne l'indique le petit nombre de cas où elle est certaine et pourrait rendre compte du fait que dans 58 événements π (soit 66 %) le méson est accompagné de particules stables, alors que parmi les événements $\Sigma\pi$ seulement 4 sur 24 (soit 17 %) sont accompagnés d'évaporation. (Ce dernier pourcentage est en accord avec un résultat préliminaire de la « K-Stack Collaboration », basé sur 119 événements $\Sigma\pi$, qui a été communiqué à Rochester ([3])). La comparaison de ces pourcentages permet, moyennant des hypothèses simplificatrices, de faire une estimation globale de la fréquence de réabsorption des hypérons chargés et neutres. Supposons, en effet, que l'évaporation associée aux événements π dans lesquels un hypéron neutre est émis soit en moyenne comparable à celle associée aux événements $\Sigma\pi$ (ce qui n'est vraisemblable que si l'émission d'hypérons Λ^0 n'est pas prépondérante) et supposons que dans les 30 événements π ne comprenant pas de particule stable il y ait émission d'un hypéron neutre. On peut alors admettre qu'un hypéron neutre a également été émis dans environ 6 événements π (17 %) comportant une évaporation, tandis que dans les 52 autres événements π comportant des particules stables, l'hypéron, chargé ou neutre, a été réabsorbé. Ces 52 événements représentent 45 % de l'ensemble des 115 événements comprenant un méson π chargé. Ce pourcentage est entaché d'erreurs, d'une part, parce qu'on n'a pas tenu compte de ce que des hypérons peuvent être réabsorbés sans donner lieu à l'émission de particules stables chargées (en particulier les hypérons Σ^-) et, d'autre part, de ce que l'énergie libérée dans la réaction (7) donnant naissance à un hypéron Λ^0 est nettement plus élevée que dans les réactions donnant naissance à un hypéron Σ.

Suivant FRIEDLANDER *et coll.* ([8]), l'interaction secondaire de l'hypéron dans le noyau où il a été créé peut donner lieu à une étoile qui se superpose à l'étoile d'absorption du méson K^-. On a proposé le nom de *cryptofragment* ([3]) pour de tels événements, qui comprennent aussi des hyperfragments de parcours trop petit pour être décelé. L'événement Sa 35, dans lequel deux mésons π sont émis (voir Tableau VII) peut être considéré comme un exemple de cryptofragment subissant une désintégration mésique (*).

([8]) M. W. FRIEDLANDER, Y. FUJIMOTO, D. KEEFE et M. G. K. MENON: *Nuovo Cimento*, **2**, 90 (1955).

(*) Deux autres événements de ce type ont été signalés par la « K Stack Collaboration » à la Conférence de Padoue-Venise (Septembre 1957). (*Note ajoutée aux épreuves.*)

4) Evénements HF. Nous avons classé dans cette catégorie 11 événements dont les caractéristiques sont données dans le Tableau VII; ils constituent $(3\pm1)\%$ de l'ensemble des événements.

Certaines des étoiles secondaires pourraient être dues à l'absorption d'un hypéron Σ^- ou d'un méson π^- de parcours très petit. Quelques interprétations possibles d'événements particuliers sont données dans la colonne « Remarques » du Tableau VII.

La présence des hyperfragments indique la production d'hypérons Λ^0, soit directement suivant une des réactions fondamentales (4), (7), (10) ou (13), soit par la réaction secondaire $\Sigma + N \rightarrow \Lambda^0 + N$.

5) Evénements ne comportant pas de particule instable chargée. Comme l'indiquent les Tableaux I et II, 60% des absorptions de mésons K^- dans l'émulsion nucléaire ne donnent lieu à aucune particule instable chargée: sur les 391 événements que nous avons observés, il y a 72 K_ε (18.4%) et 164 étoiles ne comportant que des particules stables (41.9%).

La proportion des réactions à un ou à deux nucléons responsables de ces événements est difficile à estimer. On peut toutefois souligner qu'il existe un pourcentage élevé d'événements (40 sur 236, soit 17%) comportant un ou deux protons de plus de 60 MeV. Si ces protons provenaient de la réabsorption de mésons π ou d'hypérons résultant de réactions à un nucléon, on pourrait s'attendre à observer l'émission de tels protons avec une fréquence comparable dans les événements π ou les événements Σ à un nucléon (voir Sect. 4, 2), *b*)). Or, cette fréquence est de 3/88 (3.4%) dans les événements π et de 1/20 (5%) dans les événements Σ à un nucléon. Par contre, dans les événements Σ à deux nucléons, cette fréquence est de 4/10 (40%).

TABLEAU VIII. – *Fréquences relatives des événements avec protons rapides.*

Type d'événement	Protons d'énergie cinétique $T > 35$ MeV	Protons d'énergie cinétique $T > 60$ MeV
Evénements π (seuls)	10/88 = 11%	3/88 = 3.4%
Evénements Σ avec $T_\Sigma \leq 50$ MeV . .	1/20 = 5%	1/20 = 5%
Evénements Σ avec $T_\Sigma > 50$ MeV . .	7/10 = 70%	4/10 = 40%
Evénements HF (seuls)	(4/7 = 57%) (*)	(3/7 = 43%) (*)
Evénements sans particule instable chargée	70/236 = 30%	40/236 = 17%

*) Pour l'interprétation de ces événements voir le Tableau VII.

Les fréquences relatives des événements qui contiennent des protons d'énergie cinétique supérieure à 35 ou à 60 MeV sont données dans le Tableau VIII.

Quoique ces fréquences soient basées sur une statistique faible, leur comparaison suggère une contribution non négligeable des réactions à deux nucléons dans les événements ne comportant pas de particule instable visible.

5. – Conclusions.

De l'examen systématique des étoiles d'absorption de mésons K^- au repos, nous retenons les conclusions suivantes:

1) *Evénements* $\Sigma\pi$. Nous avons observé trois cas d'absorption d'un méson K^- par un noyau d'hydrogène (interaction avec un proton libre), ce qui représente $(0.8 \pm 0.5)\%$ de l'ensemble des événements.

Les événements non colinéaires $\Sigma^-\pi^+$ et $\Sigma^+\pi^-$ ont été observés avec des fréquences à peu près égales. Dans la moitié des événements $\Sigma\pi$ non colinéaires, les signes des deux particules ont été identifiés; ils sont opposés dans tous les cas, ce qui permet de supposer que la grande majorité des événements $\Sigma\pi$ peuvent être attribués aux réactions (1) et (2) avec un proton lié. La valeur maximum observée de l'énergie cinétique des hypérons est (47 ± 8) MeV. $(17 \pm 8)\%$ des événements $\Sigma\pi$ sont accompagnés d'une faible évaporation visible. Tous ces résultats sont en accord avec ceux publiés antérieurement ([2,3,5]).

2) *Evénements* Σ. Cinq hypérons chargés dont l'énergie cinétique dépasse 100 MeV confirment l'existence de réactions à deux nucléons ([2]). En outre, cinq hypérons chargés dont l'énergie cinétique est comprise entre 50 et 100 MeV peuvent être également attribués à ces réactions, en se basant sur l'énergie cinétique maximum observée des hypérons émis dans les événements $\Sigma\pi$.

L'examen de l'évaporation qui accompagne les hypérons Σ dont l'énergie cinétique ne dépasse pas 50 MeV, suggère, dans l'hypothèse d'une réaction à un nucléon, que dans certains cas le méson π a été réabsorbé par le noyau dans lequel il a été produit.

3) *Evénements* π. Nous avons constaté, dans l'ensemble des événements qui comportent un méson π chargé, un excès de mésons négatifs par rapport aux mésons positifs; si cet excès n'est pas dû uniquement à une différence des sections efficaces d'interaction des mésons π^- et π^+ à l'intérieur du noyau, il constitue une indication de l'existence de réactions d'absorption du méson K^- par un neutron. Une confirmation expérimentale de la réaction (7) est fournie par l'observation de mésons π de plus de 100 MeV ([2,3]).

L'examen des bilans énergétiques individuels des événements π comprenant des particules stables permet de conclure, dans quelques cas, à la réabsorption de l'hypéron dans le noyau où il a été créé. La comparaison du pourcentage de ces événements avec celui des événements $\Sigma\pi$ accompagnés d'évaporation conduit, moyennant des hypothèses simplificatrices, à estimer que la fréquence de réabsorption des hypérons chargés et neutres pourrait être de l'ordre de 45%.

4) *Evénements ne comportant pas de particule instable chargée.* Les événements qui ne comportent aucune particule instable chargée constituent 60% de l'ensemble des absorptions. La justification du pourcentage élevé de ces événements ne peut être basée uniquement sur les réactions comportant l'émission de particules instables neutres, mais nécessite l'hypothèse qu'un nombre élevé parmi les particules instables chargées subissent des interactions secondaires (absorption ou échange de charge) dans le noyau où elles ont été produites. Nous avons déjà souligné l'importance de telles interactions dans les paragraphes consacrés aux événements Σ et aux événements π; nous ne pouvons toutefois donner une estimation quantitative de la fréquence de ces interactions.

La comparaison des pourcentages de protons rapides ($T > 60$ MeV) associés aux événements qui ne comportent pas de particule instable chargée, d'une part, et aux événements qui comportent une particule instable chargée provenant d'une réaction à un nucléon, d'autre part, font penser que la contribution des réactions à deux nucléons au premier groupe d'événements pourrait être importante. La contribution totale des réactions à deux nucléons est encore difficile à estimer sur la base de la présente statistique mais elle pourrait être sensiblement supérieure aux 2.5% d'événements identifiés individuellement d'aprés l'énergie cinétique des hypérons chargés ($T_\Sigma > 50$ MeV).

Les réactions mises en jeu dans l'absorption des mésons K^- ne sont identifiables que dans moins de 10% des événements observés. La détermination des fréquences des différentes réactions fondamentales énumérées à la Sect. 2 ou, plus simplement, des réactions avec un proton, avec un neutron ou avec deux nucléons nécessitera une meilleure connaissance des processus d'interaction des hypérons et des mésons π créés dans ces réactions et une augmentation notable du matériel expérimental, ce qui permettrait une analyse statistique plus raffinée.

* * *

Nous remercions très vivement le groupe du Bevatron de Berkeley et, en particulier, le Professeur E. J. LOFGREN, pour l'exposition du stack.

Nous sommes heureux d'exprimer notre gratitude au Professeur G. Oc-

CHIALINI qui a été l'initiateur de la collaboration entre les trois laboratoires et qui a dirigé le travail des groupes de Bruxelles et de Milan.

Nous sommes reconnaissants envers les Professeurs J. GÉHÉNIAU et J. MESSIAH pour de très utiles discussions, ainsi qu'envers le Professeur C. DILWORTH pour son aide et ses précieuses critiques. Nous remercions vivement aussi le Professeur J. PLAINEVAUX pour ses suggestions pendant le développement du stack et son aide dans l'élimination des bactéries.

Nous tenons enfin à remercier les microscopistes des trois laboratoires pour leur collaboration dévouée.

RIASSUNTO

Vengono studiati in emulsione fotografica 391 assorbimenti a riposo di mesoni K^- prodotti con il Bevatrone di Berkeley. Gli assorbimenti sono stati individuati seguendo la traccia di ciascun mesone K^- sino alla sua fine nell'emulsione. L'esame degli eventi così trovati ha permesso di determinare le frequenze di emissione dagli assorbimenti dei vari tipi di particelle instabili e stabili. Vengono confermati i risultati di precedenti autori sulle caratteristiche delle coppie $\Sigma^{\pm}\pi^{\mp}$, e sulle loro rispettive frequenze di osservazione. Parecchi esempi di iperoni Σ veloci, non accompagnati da pioni carichi, forniscono una prova diretta dell'esistenza di catture da due nucleoni: il loro numero è $\sim 2.5\%$ del numero totale degli assorbimenti. L'osservazione di pioni di energia superiore a 100 MeV permette di dedurre la produzione diretta di iperoni Λ^0. Lo studio dell'energia visibile liberata negli assorbimenti indica che gli iperoni e i pioni possono essere riassorbiti nei nuclei nei quali sono stati prodotti. Fra i pioni il cui segno è stato riconosciuto, i negativi sono risultati più frequenti che i positivi per un fattore ~ 3. Il 60% circa degli assorbimenti non hanno particelle instabili cariche: tuttavia, un considerevole numero ($\sim 17\%$) di questi eventi sono accompagnati da protoni di energia cinetica maggiore di 60 MeV; questo fatto suggerisce che il contributo delle catture da due nucleoni potrebbe essere importante.

Sulla forza di reazione del campo sulla sorgente in forma relativistica (*).

E. Bellomo

Istituto di Fisica Teorica dell'Università - Genova

(ricevuto il 15 Ottobre 1957)

Riassunto. — Si ricava una formula che permette di ottenere la forza di reazione per campi generici soddisfacenti l'equazione $\Box h^A = 0$. Come applicazione si ottengono i risultati noti per il caso elettromagnetico e per il caso scalare « attrattivo », per il quale la dinamica della sorgente è del tutto simile a quella della particella con carica elettrica, comprese le soluzioni « fuggenti » quando la sorgente è troppo piccola. In altri casi la forza di reazione potrebbe far variare la massa di riposo della sorgente. I calcoli sono riportati nei dettagli.

Introduzione.

Il problema che ci si pone è quello dell'emissione classica della radiazione e della forza di reazione sulle sorgenti per campi lineari di componenti h^A soddisfacenti nel vuoto l'equazione $\Box h^A = 0$. L'indice maiuscolo sta per ogni insieme di indici, anche non di varianza tensoriale.

Mediante la formula (9) del testo è semplice il calcolo della forza di reazione in forma relativistica per sorgenti non puntiformi a simmetria sferica. Questo rende possibile, con passaggio al limite, anche la scrittura delle equazioni relativistiche del moto per sorgenti puntiformi (analoghe a quelle di Dirac [1]) per il campo elettromagnetico), però la sorgente estesa offre dei vantaggi per

(*) Presentato al *Congresso Internazionale sui mesoni e sulle particelle recentemente scoperte*, Padova-Venezia, 1957.

(1) P. A. M. Dirac: *Proc. Roy. Soc.*, A **167**, 148 (1938).

ottenere dettagli circa l'emissione della radiazione. Inoltre le caratteristiche soluzioni singolari ([2,3]) esistono anche per sorgenti estese ([4-6]).

La loro origine è nota e può essere chiarita dalle seguenti considerazioni non relativistiche.

Se un sistema è composto di due masse, di cui una, la minore, negativa, accoppiate in modo non rigido, le forze di azione e reazione generano accelerazioni nello stesso verso, ma diverse come valore. Si può avere un moto divergente o meno a seconda delle modalità di accoppiamento.

Ad esempio, se si tratta di una forza crescente con la distanza e diretta secondo la congiungente delle due masse, si possono avere soluzioni rettilinee « fuggenti » del sistema, la massa negativa precedendo la positiva con aumento progressivo della distanza reciproca, e quindi in questo caso dell'accelerazione.

Se la forza di interazione fosse come la precedente, eccetto per il segno, si avrebbero soluzioni rettilinee oscillanti.

Come altro esempio supponiamo che una delle due masse « segua » l'altra, cioè assuma quelle accelerazioni che l'altra ha già avuto ad un tempo precedente l'attuale di un certo valore δ.

La forza di reazione deve essere fissata da questa accelerazione.

Consideriamo due casi:

1) La massa positiva segue la negativa. In questo caso, essendo sempre minore l'accelerazione della massa maggiore, l'accelerazione della massa negativa (e quindi del sistema) aumenta, e si hanno soluzioni rettilinee fuggenti.

2) La massa negativa segue la positiva. In questo caso non si hanno soluzioni rettilinee fuggenti. Però si può facilmente constatare che se la massa maggiore è sottoposta ad una forza esterna di tipo « centripeto », cioè con centro di azione dalla stessa parte del centro di curvatura della traiettoria, l'effetto netto sul sistema della reazione della massa negativa ritardata è quello di aggiungere una forza longitudinale nel senso del moto. Viceversa nel caso « centrifugo ». Nel caso di forza esterna ortogonale alla traiettoria della prima particella, la velocità del sistema aumenta dunque, se le condizioni iniziali del sistema non sono eccezionali.

Per portare queste considerazioni sul piano relativistico, bisogna ripeterle nel sistema in cui la prima particella è in riposo e non trascurare le componenti temporali delle forze.

([2]) C. J. Eliezer: *Rev. Mod. Phys.*, **19**, 147 (1947).
([3]) G. Zin: *Nuovo Cimento*, **6**, 1 (1949).
([4]) D. Bohm e M. Weinstein: *Phys. Rev.*, **74**, 305 (1949).
([5]) K. Wildermuth: *Zeits. f. Naturf.*, **10***a*, 450 (1955).
([6]) E. Bellomo: *Nuovo Cimento*, **2**, 456 (1955).

L'autore divide la forza di reazione del campo in due contributi:

— quello dovuto all'emissione di radiazione, e

— quello attribuibile all'inerzia del campo accompagnante la sorgente.

L'inerzia del campo è ritardata rispetto a quella della massa meccanica e quindi si differenzia da essa dal punto di vista dinamico.

Il segno del tensore energetico del campo, fissate per quest'ultimo le equazioni in presenza di sorgenti, dipende dal segno usato nella legge della forza; infatti quest'ultima è la divergenza del primo cambiata di segno.

A causa del legame esistente tra il segno della densità di energia ed il segno della forza, un dato tipo di campo, per avere densità di energia positiva (almeno nel caso statico perchè non è detto che l'energia sia una forma quadratica definita) non può essere che attrattivo o repulsivo.

Per esempio, consideriamo il caso del campo elettromagnetico. Mantenendo invariate le equazioni inomogenee di Maxwell, ma cambiando il segno della forza di Lorentz, la densità di energia si dovrebbe scrive $-(E^2+H^2)/8\pi$, e così per tutte le componenti del tensore energetico.

Anche la forza di reazione sarebbe cambiata di segno.

Si avrebbero allora soluzioni singolari, ad esempio, per una carica inizialmente moventesi di moto uniforme che venisse a trovarsi in un campo magnetico, per quanto già spiegato. Nel caso fittizio considerato verrebbe anche emessa energia negativa (in questo caso l'energia è una forma quadratica definita) e l'energia iniziale della particella è già positiva e non può quindi che aumentare ([7]). Tutto questo non dipenderebbe dalle dimensioni della sorgente, contrariamente a quanto accade per le soluzioni autoaccelerate (rettilinee) nel caso ordinario.

Un criterio immediato per controllare il segno della densità di energia del campo è quello di considerare una sorgente che sia allontanata lentamente da un'altra uguale, in modo che non venga emessa radiazione. Ricordando che la quarta componente della forza del campo, cambiata di segno, dà l'*aumento* dell'energia del campo nell'unità di tempo (proprio), e osservando che il modulo di questa energia è alla fine più piccolo che al principio del processo, si ricava appunto per il caso precedente (Fig. 1*a*) che questa energia è negativa (e la sua variazione è compensata dal lavoro fatto dalle forze esterne, che supponiamo ortogonali alle linee di universo delle sorgenti).

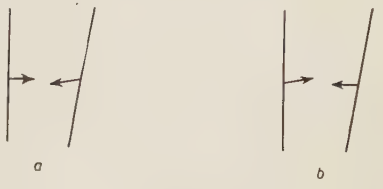

Fig. 1.

Per il caso del campo scalare attrattivo (Fig. 1*b*) il criterio esposto ci dice che la densità di energia è positiva. Si ha una diminuzione dell'energia del campo,

([7]) Dato che la massa non varia. Cfr. lavori citati in note ([2]) e ([3]).

sempre pari al lavoro esterno compiuto, che non viene quindi compensato. Ma si deve assumere una variabilità della massa di riposo delle sorgenti, dato che le forze del campo non sono ortogonali alle loro linee di universo. Si può verificare che ciascuna delle due masse aumenta di una quantità pari al lavoro esterno compiuto.

Per questo campo, benchè attrattivo, la forza di reazione a parte un fattore $\frac{1}{2}$ è identica anche per il segno a quella del campo elettromagnetico (repulsivo). Questo è in accordo con quanto è stato detto per il segno della densità di energia del campo.

Per campi generanti forze non ortogonali alle linee di universo delle sorgenti, a priori la forza di reazione potrebbe anche causare una variazione della massa durante l'emissione. Questo non avviene per il campo scalare, come abbiamo ricordato e come ritroveremo nella Sez. **4** ([8]).

1. – Ci limitiamo a sorgenti non puntiformi « rigide » relativisticamente ([9]), cioè tali che vi sia sempre un sistema di riferimento in cui la particella possa vedersi in quiete, intendendo con ciò che la distribuzione della sorgente in tutte queste sezioni spaziali risulti la stessa, e che inoltre considerando le linee connettenti punti corrispondenti della distribuzione nei diversi istanti, queste risultino ortogonali alle corrispondenti sezioni spaziali. Prendendo una di queste linee come linea fondamentale assumeremo in ognuna di queste sezioni che la sorgente abbia simmetria sferica intorno al punto corrispondente di detta linea. Indicheremo con $\boldsymbol{x}_0(s)$ le coordinate spazio-temporali dei punti della linea base in funzione del loro tempo proprio s, che sarà preso come tempo proprio di riferimento per tutta la sorgente, mentre indicheremo con s_x o s_z il tempo proprio della linea passante per $\boldsymbol{x}$ o per $\boldsymbol{z}$.

Per una tale sorgente si assume che valga l'equazione

$$\frac{\mathrm{d}}{\mathrm{d}s}\left(m_{\text{mecc.}}\frac{\mathrm{d}x_0^\mu}{\mathrm{d}s}\right) = -\int_\sigma T^{\mu\alpha}{}_{,\alpha}\frac{\mathrm{d}x^\omega}{\mathrm{d}s}\,\mathrm{d}\sigma_\omega\,, \tag{1}$$

dove $T^{\mu\nu}$ è il tensore energetico del campo, $\mathrm{d}\sigma_\omega$ è l'elemento di volume spaziale su $\sigma(s)$, lo spazio ortogonale a $\mathrm{d}x_0^\mu/\mathrm{d}s$ passante per $\boldsymbol{x}_0(s)$ e il vettore $\mathrm{d}x^\mu/\mathrm{d}s$, funzione di $\boldsymbol{x}$ su σ, può essere considerato parallelo a $\mathrm{d}x_0^\omega/\mathrm{d}s$ e uguale a $(\mathrm{d}x_0^\omega/\mathrm{d}s)(1-(\boldsymbol{x}-\boldsymbol{x}_0)\cdot\mathrm{d}^2\boldsymbol{x}_0/\mathrm{d}s^2)$. Si assume inoltre $(\boldsymbol{x}-\boldsymbol{x}_0)\cdot\mathrm{d}^2\boldsymbol{x}_0/\mathrm{d}s^2 \ll 1$, cioè che l'intersezione degli spazi σ non avvenga nell'interno della sorgente, ipotesi che può essere considerata senz'altro verificata. Non è necessario che $\mathrm{d}^2\boldsymbol{x}_0/\mathrm{d}s^2$ sia funzione continua di s. Ove $\mathrm{d}^2\boldsymbol{x}_0/\mathrm{d}s^2$, cioè $\dot{\boldsymbol{v}}(s)$, non esista, potremmo supporre l'esistenza dei valori derivati $\dot{\boldsymbol{v}}_-(s)$ e $\dot{\boldsymbol{v}}_+(s)$.

([8]) Sulla presenza delle soluzioni singolari nella teoria quantistica dei campi si veda K. Wildermuth e K. Baumann: *Nuclear Physics*, **3**, 612 (1957) e A. Loinger: *Nuovo Cimento*, **2**, 511 (1955).

([9]) Cfr. M. Born: *Ann. der Phys.*, **30**, 1 (1909).

La metrica è positiva per vettori temporali.

Il secondo membro della (1) rappresenta la forza del campo sulla sorgente, cioè una eventuale forza esterna più la forza di reazione.

Dalla (1), per calcolo diretto del secondo membro si può ricavare nel caso elettromagnetico, la formula

$$(2) \qquad \frac{\mathrm{d}}{\mathrm{d}s}\,(m_0 \boldsymbol{v}(s)) + \frac{4}{3}\iint \frac{\delta\varrho\,\delta\varrho'}{2\xi}\,\dot{\boldsymbol{v}}(s-\xi)^* = \boldsymbol{F}_{\text{est.}}(s)\,,$$

come riotterremo nella Sez. **4**.

È $m_0 = m_{\text{mecc.}} - \frac{1}{3}\iint \delta e\,\delta e'/2\xi = m_{\text{mecc.}} - \frac{1}{3}m_{\text{e.m.}}$ e $\dot{\boldsymbol{v}}(s-\xi)^*$ è il trasformato di $\dot{\boldsymbol{v}}(s-\xi)$ con la trasformazione di Lorentz che fa passare da $\boldsymbol{v}(s-\xi)$ a $\boldsymbol{v}(s)$. ξ è la distanza spaziale ad ogni tempo s tra i due elementi di carica δe e $\delta e'$.

Dalla (2), scindendo $\dot{\boldsymbol{v}}(s-\xi)^*$ in

$$(3) \qquad \dot{\boldsymbol{v}}(s-\xi) - \boldsymbol{v}(s)\big(\dot{\boldsymbol{v}}(s-\xi)\cdot\boldsymbol{v}(s)\big) \approx \dot{\boldsymbol{v}}(s-\xi) - \xi\boldsymbol{v}(s)\big(\dot{\boldsymbol{v}}(s-\xi)\cdot\bar{\dot{\boldsymbol{v}}}\big)\,,$$

dove $\bar{\dot{\boldsymbol{v}}} = (1/\xi)\int_{s-\xi}^{s} \dot{\boldsymbol{v}}(\eta)\,\mathrm{d}\eta$, si ottiene una formula di cui la seguente è una forma approssimata

$$(4) \qquad \frac{\mathrm{d}}{\mathrm{d}s}\left(m_{\text{mecc.}}\boldsymbol{v}(s) - \frac{1}{3}\,m_{\text{e.m.}}\boldsymbol{v}(s) + \frac{4}{3}\,m_{\text{e.m.}}\boldsymbol{v}(s-\varrho)\right) - \frac{2}{3}\,e^2\boldsymbol{v}(s)\big(\dot{\boldsymbol{v}}(s)\cdot\dot{\boldsymbol{v}}(s)\big) = \boldsymbol{F}_{\text{est.}}\,.$$

$\frac{2}{3}e^2\,\boldsymbol{v}(s)\dot{\boldsymbol{v}}\big((s)\cdot\dot{\boldsymbol{v}}(s)\big)$ è la reazione della radiazione di componente temporale sempre negativa, e ϱ è una costante dell'ordine delle dimensioni della sorgente e tale che $2m_{\text{e.m.}}\varrho \approx e^2$, così che la precedente equazione diventa

$$(5) \qquad \frac{\mathrm{d}}{\mathrm{d}s}\left(m\boldsymbol{v}(s) - \frac{2}{3}\,e^2\,\frac{\boldsymbol{v}(s)-\boldsymbol{v}(s-\varrho)}{\varrho}\right) - \frac{2}{3}\,e^2\boldsymbol{v}(s)\big(\dot{\boldsymbol{v}}(s)\cdot\dot{\boldsymbol{v}}(s)\big) = \boldsymbol{F}_{\text{est.}}\,,$$

con $m = m_{\text{mecc.}} + m_{\text{e.m.}}$ massa totale sperimentale.

$-\frac{2}{3}e^2\,\dot{\boldsymbol{v}}(s)$ è la cosidetta energia (e quantità di moto) di accelerazione [10]. Dalla (5) si ottiene al limite per ϱ tendente a zero l'equazione di Dirac.

La forza di reazione del campo dunque è ortogonale alle linee di universo della sorgente; tale è infatti $\frac{2}{3}e^2[\ddot{\boldsymbol{v}}(s) + \boldsymbol{v}(s)(\dot{\boldsymbol{v}}(s)\cdot\dot{\boldsymbol{v}}(s))]$ come era logicamente attendibile dall'ortogonalità della forza di Lorentz alla linea di universo di ogni elemento della sorgente. $m_{\text{mecc.}}$ rimane così costante, come pure m.

2. – Vogliamo ora ottenere una equazione simile alla (2) per ogni campo h^A soddisfacente nel vuoto l'equazione $\Box h^A = 0$.

---

[10] G. A. Schott: *Phil. Mag.*, **29**, 49 (1915).

Indichiamo con $\delta S^B(\boldsymbol{x})$ gli elementi di sorgente su cui il campo agisce e con $\delta S'^A(\boldsymbol{z})$ quelli che generano il campo.

Occorre conoscere l'espressione della forza, cioè $-T^{\mu\,x}{}_{,\lambda}$. Assumiamo che sia una funzione lineare di δS^B e delle derivate di h^A: $\delta f_\mu = \delta S^B \; \Phi^\beta_{\mu BA} \; h^A{}_{,\beta}$.

Per h^A, la soluzione coi potenziali ritardati si scrive:

$$h^A(x) = \int \frac{\delta S'^A(\boldsymbol{z})}{(\dot{\boldsymbol{z}},\, \boldsymbol{x}-\boldsymbol{z})} = \int \delta h^A(\boldsymbol{x}, \boldsymbol{z})\,, \tag{6}$$

l'integrale essendo esteso al cono del passato con vertice in $\boldsymbol{x}$; $\dot{\boldsymbol{z}}$ è la derivata rispetto al tempo proprio delle coordinate dell'elemento di sorgente. Seguendo Dirac [1], $h^A{}_{,\nu}$ è allora ottenuto integrando la formula

$$\delta h^A{}_{,k} = \frac{1}{(\dot{\boldsymbol{z}},\, \boldsymbol{x}-\boldsymbol{z})^2} \frac{\mathrm{d}}{\mathrm{d}s_z} \frac{\delta S'^A(x_k - z\,)}{(\dot{\boldsymbol{z}},\, \boldsymbol{x}-\boldsymbol{z})}\,, \tag{7}$$

cioè

$$\delta h^A{}_{,k} = \delta S'^A(\boldsymbol{z}) \left\{ \frac{-\dot{z}_k}{(\dot{\boldsymbol{z}},\, \boldsymbol{x}-\boldsymbol{z})^2} - \frac{(x_k - z_k)}{(\dot{\boldsymbol{z}},\, \boldsymbol{x}-\boldsymbol{z})^3} [(\ddot{\boldsymbol{z}},\, \boldsymbol{x}-\boldsymbol{z}) - 1] \right\} + \tag{8}$$

$$+ \frac{\mathrm{d}(\delta S'^A(\boldsymbol{z}))}{\mathrm{d}s_z} \frac{x_k - z_k}{(\dot{\boldsymbol{z}},\, \boldsymbol{x}-\boldsymbol{z})^2}\,.$$

Mostreremo nella sezione seguente che nel caso di sorgenti a simmetria sferica è sufficiente usare, al posto delle derivate $\delta h^A{}_{,\nu}$ le espressioni

$$\delta \underset{\sim}{h}{}^A{}_{,\nu} = \delta S'^A(s) \left\{ \frac{1}{6} \frac{\dot{v}_\nu(s)}{\xi} + \frac{1}{3} \frac{\dot{v}_\nu(s-\xi)^*}{\xi} \right\} + \overline{\frac{\mathrm{d}}{\mathrm{d}s} \delta S'^A(s-\xi)} \frac{v_\nu(s-\xi)}{\xi}\,, \tag{9}$$

dove ξ è sempre la distanza a riposo tra gli elementi di sorgente influenzante ed influenzata e le medie del terzo termine sono opportune, prese in un intorno di $s-\xi$, e possono essere sostituire dal valore calcolato in $s-\xi$, se $\dot{\boldsymbol{v}}(s)$ è ivi derivabile.

La formula precedente deve essere integrata senza prima moltiplicare per il fattore $(1 - (\boldsymbol{x}-\boldsymbol{x}_0)\cdot\dot{\boldsymbol{v}}(s))$, già in essa contenuto.

3. – Si ponga per la coordinata generica di un punto della sorgente

$$\boldsymbol{x} = \boldsymbol{x}_0(s) + \boldsymbol{\gamma}_1 \quad \text{e} \quad \boldsymbol{z} = \boldsymbol{x}_0(s') + \boldsymbol{\gamma}_2 \quad \text{con} \quad \boldsymbol{\gamma}_1 \cdot \boldsymbol{v}(s) = \boldsymbol{\gamma}_2 \cdot \boldsymbol{v}(s') = 0\,.$$

Useremo anche per brevità $\boldsymbol{x}_0$ per $\boldsymbol{x}_0(s)$, $\boldsymbol{x}_0'$ per $\boldsymbol{x}_0(s')$ ed analogamente $\boldsymbol{v}$ e $\boldsymbol{v}'$ per $\boldsymbol{v}(s)$ e $\boldsymbol{v}(s')$.

Se $\delta S^B(\boldsymbol{x})$ è ora l'elemento di sorgente situato in $\boldsymbol{x} = \boldsymbol{x}_0(s) + \boldsymbol{\gamma}_1$ (vedi fig. 2), supporremo che ogni sua componente sia funzione del solo $|\boldsymbol{\gamma}_1|$. Queste dipendenze radiali possono essere diverse per componenti diverse eccettuato il caso che si tratti di componenti di uno stesso tensore. Poichè questo tensore lo assumiamo formato tramite i tensori $g^{\mu\nu}$ e v^μ, la stessa dipendenza radiale è richiesta per tutte le sue componenti. Naturalmente le componenti di $\mathrm{d}S^B/\mathrm{d}s$ hanno le stesse dipendenze radiali di quelle di S^B.

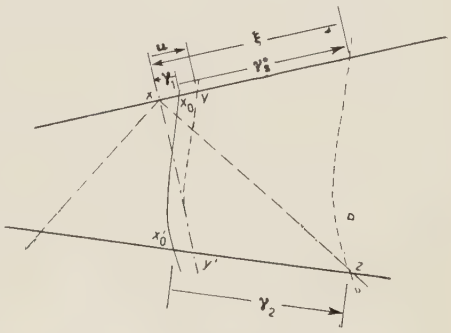

Fig. 2.

L'espressione della densità di forza è lineare negli elementi influenzante ed influenzato, ed in generale c'è diversità tra la sua espressione e quella che si ottiene scambiando la posizione dei due elementi di sorgente, appunto per la diversa possibile dipendenza radiale delle componenti. Questo può dare origine a dei contributi non figuranti nella formula (9), che saranno meglio specificati durante il calcolo.

Inoltre s' è determinato da s per mezzo della relazione $(\boldsymbol{x} - \boldsymbol{z}) \cdot (\boldsymbol{x} - \boldsymbol{z}) = 0$ contenente $\boldsymbol{\gamma}_2$; ne viene che $\delta S'^A(\boldsymbol{x}')$ e $\mathrm{d}\delta S'^A/\mathrm{d}s'$ non dipendono da $\boldsymbol{\gamma}_2$ solo attraverso il modulo, fissato s.

Su $\delta S^B(\boldsymbol{x})$ possono dunque agire i campi emessi in tempi precedenti dagli altri elementi di sorgente, situati in $\boldsymbol{x}_0(s') + \boldsymbol{\gamma}_2$. Indicando con $\boldsymbol{\gamma}_2^*$ il trasformato di $\boldsymbol{\gamma}_2$ con la trasformazione di Lorentz che fa passare da $\boldsymbol{v}(s')$ a $\boldsymbol{v}(s)$ e con $\boldsymbol{y}'$ il piede della normale (di lunghezza t) condotta da $\boldsymbol{x}$ sullo spazio relativo a s', e con le altre notazioni della Fig. 2, tra cui $\boldsymbol{u} = \boldsymbol{y} - \boldsymbol{x}$:

$$t = \boldsymbol{v}' \cdot (\boldsymbol{x}_0 - \boldsymbol{x}_0' + \boldsymbol{\gamma}_1) = |\boldsymbol{\gamma}_1 + \boldsymbol{u} - \boldsymbol{\gamma}_2^*| , \tag{10a}$$

$$\boldsymbol{y}' = \boldsymbol{x}_0 + \boldsymbol{\gamma}_1 - \boldsymbol{v}'[\boldsymbol{v}' \cdot (\boldsymbol{x}_0 + \boldsymbol{\gamma}_1 - \boldsymbol{x}_0')] , \tag{10b}$$

come si potrebbe ricavare dal sistema

$$\begin{cases} \boldsymbol{y}' = \boldsymbol{x}_0 + \boldsymbol{\gamma}_1 - \boldsymbol{v}' t , \\ (\boldsymbol{y}' - \boldsymbol{x}_0') \cdot \boldsymbol{v}' = 0 . \end{cases}$$

Possiamo dunque scrivere la (8), raggruppando il primo ed il terzo termine

$$\delta h^A{}_{,k} = \delta S'^A \left\{ - \frac{(\boldsymbol{\gamma}_2 - \boldsymbol{y}' + \boldsymbol{x}_0')_k}{|\boldsymbol{u} + \boldsymbol{\gamma}_1 - \boldsymbol{\gamma}_2^*|^3} - \right. \tag{11}$$

$$\left. - \frac{(\boldsymbol{v}' t - \boldsymbol{\gamma}_2 + \boldsymbol{y}' - \boldsymbol{x}_0)_k}{|\boldsymbol{u} + \boldsymbol{\gamma}_1 - \boldsymbol{\gamma}_2^*|^3} \frac{[(\boldsymbol{u} + \boldsymbol{\gamma}_1 - \boldsymbol{\gamma}_2^*) \cdot \dot{\boldsymbol{v}}'^*]}{[1 - \boldsymbol{\gamma}_2^* \cdot \dot{\boldsymbol{v}}'^*]} \right\} + \frac{\mathrm{d}\delta S'^A}{\mathrm{d}s_z} \frac{(\boldsymbol{v}' t - \boldsymbol{\gamma}_2 + \boldsymbol{y}' - \boldsymbol{x}_0')_k}{|\boldsymbol{u} + \boldsymbol{\gamma}_1 - \boldsymbol{\gamma}_2^*|^2} .$$

Si può ottenere la forza agente in $\boldsymbol{x}$ integrando sull'elemento di sorgente in $\boldsymbol{z}$; occorre poi integrare nuovamente su tutta la sorgente stessa premettendo il fattore $(1-\boldsymbol{\gamma}_1\cdot\dot{\boldsymbol{v}}(s))$.

Indichiamo per semplicità $\boldsymbol{\gamma}_1-\boldsymbol{\gamma}_2^*$ e $|\boldsymbol{\gamma}_1-\boldsymbol{\gamma}_2^*|$ rispettivamente con $\boldsymbol{\xi}$ e ξ.

Le seguenti espressioni sono ancora necessarie:

al terzo ordine

$$|\boldsymbol{u}+\boldsymbol{\xi}| = \xi\left(1, -\frac{2\boldsymbol{u}\cdot\boldsymbol{\xi}}{\xi^2}, -\frac{\boldsymbol{u}\cdot\boldsymbol{u}}{\xi^2}\right)^{\frac{1}{2}}, \tag{12a}$$

$$\frac{1}{|\boldsymbol{u}+\boldsymbol{\xi}|^3} = \frac{1}{\xi^3}\left[1, +\frac{3\boldsymbol{u}\cdot\boldsymbol{\xi}}{\xi^2}, +\frac{3}{2}\frac{\boldsymbol{u}\cdot\boldsymbol{u}}{\xi^2} + \frac{3\cdot 5}{2}\left(\frac{\boldsymbol{u}\cdot\boldsymbol{\xi}}{\xi^2}\right)^2\right], \tag{12b}$$

al secondo ordine

$$\frac{1}{|\boldsymbol{u}+\boldsymbol{\xi}|} = \frac{1}{\xi}\left(1, +\frac{\boldsymbol{u}\cdot\boldsymbol{\xi}}{\xi^2}\right), \tag{12c}$$

$$\frac{1}{|\boldsymbol{u}+\boldsymbol{\xi}|^2} = \frac{1}{\xi^2}\left(1, +2\frac{\boldsymbol{u}\cdot\boldsymbol{\xi}}{\xi^2}\right), \tag{12d}$$

essendo a priori il terzo ordine necessario per $\boldsymbol{u}$ nei termini sottolineati.

A meno di infinitesimi del terzo ordine:

$$s-s' = \boldsymbol{v}'\cdot(\boldsymbol{x}_0-\boldsymbol{x}_0') = |\boldsymbol{u}+\boldsymbol{\xi}|-\boldsymbol{\gamma}_1\cdot\boldsymbol{v}' = \xi - \frac{\boldsymbol{u}\cdot\boldsymbol{\xi}}{\xi} - \boldsymbol{\gamma}_1\cdot\boldsymbol{v}' = \tag{13}$$

$$= (s-s_1)+(s_1-s''),$$

con

$$s-s_1 = \xi \quad \text{e} \quad s_1-s'' \approx -\tfrac{1}{2}\xi(\boldsymbol{\xi}\cdot\dot{\boldsymbol{v}}_-(s)), \qquad \text{(cfr. (17))}.$$

Se $s-s'$ è piccolo, si può esprimere al terzo ordine $-(\boldsymbol{x}_0'+\boldsymbol{\gamma}_2-\boldsymbol{y}')$ tramite $(\boldsymbol{u}+\boldsymbol{\gamma}_1-\boldsymbol{\gamma}_2^*) = (\boldsymbol{u}+\boldsymbol{\xi})$:

$$-(\boldsymbol{x}_0'+\boldsymbol{\gamma}_2-\boldsymbol{y}') = (\boldsymbol{u}+\boldsymbol{\xi}) + \boldsymbol{v}(s)\left[(\boldsymbol{u}+\boldsymbol{\xi})\cdot\int_{s_1}^{s}\dot{\boldsymbol{v}}(\eta)\,\mathrm{d}\eta\right] + \frac{1}{2}\frac{[\boldsymbol{\xi}\cdot\int_{s_1}^{s}\dot{\boldsymbol{v}}(\eta)\,\mathrm{d}\eta]^2}{\xi^2}\boldsymbol{\xi}_a, \tag{14}$$

con $\boldsymbol{\xi}_a$ si intende la proiezione di $\boldsymbol{\xi}$ sul piano $(\boldsymbol{x}, \boldsymbol{y}, \boldsymbol{y}')$.

È

$$\begin{cases} \boldsymbol{u} = (\boldsymbol{y}-\boldsymbol{x}) = (\boldsymbol{y}-\boldsymbol{x}_0+(\boldsymbol{x}_0-\boldsymbol{x})), \\ \dfrac{\mathrm{d}\boldsymbol{u}}{\mathrm{d}s'} = \dfrac{\mathrm{d}}{\mathrm{d}s'}(\boldsymbol{y}-\boldsymbol{x}_0) \simeq \dfrac{\mathrm{d}}{\mathrm{d}s'}(\boldsymbol{y}'-\boldsymbol{x}_0')^*. \end{cases}$$

Ma si noti che $(\boldsymbol{y}'-\boldsymbol{x}_0')^*$ varia al variare di s' solo in quanto varia la

direzione della normale condotta da $\boldsymbol{x}$ allo spazio relativo a s', cioè la direzione di $\boldsymbol{v}'t$. Si ha dunque

$$\frac{\mathrm{d}\boldsymbol{u}}{\mathrm{d}s'} = -\dot{\boldsymbol{v}}'^{*}t = -(\boldsymbol{v}'\cdot(\boldsymbol{x}_0 - \boldsymbol{x}_0') + \boldsymbol{v}'\cdot\boldsymbol{\gamma}_1)\dot{\boldsymbol{v}}'^{*},$$

ed a meno di quantità del terzo ordine

$$\frac{\mathrm{d}\boldsymbol{u}}{\mathrm{d}s'} = -((s - s') + \boldsymbol{v}'\cdot\boldsymbol{\gamma}_1)\dot{\boldsymbol{v}}'^{*}. \tag{15}$$

Integrando il primo dei due termini si ottiene un contributo ad $\boldsymbol{u}$ che è funzione di s e s' soltanto, e la cui parte principale è contenuta nella espressione che si ottiene sostituendo s_1 a s' e che si scrive

$$\boldsymbol{u}(s, s_1) = \tfrac{1}{2}(s - s_1)^2\,\dot{\boldsymbol{v}}(s, s_1), \tag{16}$$

dove $\dot{\boldsymbol{v}}(s, s_1)$ è ortogonale a $\boldsymbol{v}(s)$ e tende a $\dot{\boldsymbol{v}}_-(s)$ quando s_1 tende a s. Osserviamo che

$$\frac{\boldsymbol{u}\cdot\boldsymbol{\xi}}{\xi} + \boldsymbol{\gamma}_1\cdot\boldsymbol{v}' \approx -\frac{1}{2}\xi((\boldsymbol{\gamma}_1 + \boldsymbol{\gamma}_2^{*})\cdot\dot{\boldsymbol{v}}_-(s)), \tag{17}$$

quindi i termini del terzo ordine sopra trascurati valgono

$$\left(\frac{\mathrm{d}\boldsymbol{u}}{\mathrm{d}s'}\right)_{s'=s_1}(s' - s_1) = \frac{1}{2}\,\xi^2\,\overline{\dot{\boldsymbol{v}}'^{*}}(s_1)((\boldsymbol{\gamma}_1 + \boldsymbol{\gamma}_2^{*})\cdot\dot{\boldsymbol{v}}_-(s)).$$

Anche il contributo proveniente dal secondo termine della (15) cambia di segno cambiando il segno dei $\boldsymbol{\gamma}$.

Calcoliamo ora la (11), termine per termine, col fattore $(1 - \boldsymbol{\gamma}_1\cdot\dot{\boldsymbol{v}}(s))$.

Cominciamo con il primo termine, per il quale è necessario il più alto ordine di approssimazione.

$$(1 - \boldsymbol{\gamma}_1\cdot\dot{\boldsymbol{v}}(s))\,\frac{\boldsymbol{\gamma}_2 - \boldsymbol{y}' + \boldsymbol{x}_0'}{|\boldsymbol{u} + \boldsymbol{\xi}|^3}\,\delta S'^{A}(s) = \tag{18}$$

$$= \frac{-(\boldsymbol{\gamma}_2 - \boldsymbol{y}' + \boldsymbol{x}_0')}{|\boldsymbol{u} + \boldsymbol{\xi}|^3}\left[\delta S'^{A}(s_1) - \left(\frac{\mathrm{d}\delta S'^{A}}{\mathrm{d}s}\right)_{s=s_1}(s_1 - s')\right] - (\boldsymbol{\gamma}_1\cdot\dot{\boldsymbol{v}}(s))\,\frac{-(\boldsymbol{\gamma}_2 - \boldsymbol{y}' + \boldsymbol{x}_0')}{|\boldsymbol{u} + \boldsymbol{\xi}|^3}\,\delta S'^{A}(s_1).$$

La prima parte si scrive, per le (10) e (14)

$$\delta S'^{A}(s_1)\,\frac{-(\boldsymbol{\gamma}_2 - \boldsymbol{y}' + \boldsymbol{x}_0')}{|\boldsymbol{u} + \boldsymbol{\xi}|^3} = \delta S'^{A}(s_1)\left\{\frac{\boldsymbol{\xi}}{\xi^2}\left[1, + \frac{3\boldsymbol{u}\cdot\boldsymbol{\xi}}{\xi^2} + \frac{3}{2}\,\frac{\boldsymbol{u}\cdot\boldsymbol{u}}{\xi^2} + \frac{3\cdot 5}{2}\left(\frac{\boldsymbol{u}\cdot\boldsymbol{\xi}}{\xi^2}\right)^2\right] + \right. \tag{19}$$

$$+ \frac{\boldsymbol{u}}{\xi^3}\left(1 + \frac{3\boldsymbol{u}\cdot\boldsymbol{\xi}}{\xi^2}\right) + \boldsymbol{v}(s)\,\frac{\boldsymbol{\xi}\cdot\left[\int_{s_1}^{s}\dot{\boldsymbol{v}}(\eta)\,\mathrm{d}\eta - \dot{\boldsymbol{v}}(s_1)((\xi/2)(\boldsymbol{\gamma}_1 + \boldsymbol{\gamma}_2^{*})\cdot\dot{\boldsymbol{v}}_-(s))\right]}{\xi^3}\cdot\left(1 + \frac{3\boldsymbol{u}\cdot\boldsymbol{\xi}}{\xi^2}\right) +$$

$$\left. + \boldsymbol{v}(s)\,\frac{\boldsymbol{u}\cdot\int_{s_1}^{s}\dot{\boldsymbol{v}}(\eta)\,\mathrm{d}\eta}{\xi^3} + \frac{1}{2}\,\frac{\left[\boldsymbol{\xi}\cdot\int_{s_1}^{s}\dot{\boldsymbol{v}}(\eta)\,\mathrm{d}\eta\right]^2}{\xi^5}\,\boldsymbol{\xi}_a\right\}.$$

Questi termini danno nella forza contributi che o restano invariati o cambiano di segno cambiando di segno γ_1 e γ_2. I termini che non cambiano di segno sono

$$(20)\qquad \delta S'^{A}(s_1)\left\{\frac{\boldsymbol{\xi}}{\xi^3}\,\frac{3\boldsymbol{u}\cdot\boldsymbol{\xi}}{\xi^2}+\frac{\boldsymbol{u}}{\xi^3}+\boldsymbol{v}(s)\,\frac{\boldsymbol{u}\cdot\int_{s_1}^{s}\dot{\boldsymbol{v}}(\eta)\,\mathrm{d}\eta}{\xi^3}+\right.$$

$$\left.+\frac{\boldsymbol{v}(s)}{\xi^3}\,\boldsymbol{\xi}\cdot\left[\int_{s_1}^{s}\dot{\boldsymbol{v}}(\eta)\,\mathrm{d}\eta\,\frac{3\boldsymbol{u}\cdot\boldsymbol{\xi}}{\xi^2}-\frac{\xi}{2}\,\dot{\boldsymbol{v}}(s_1)((\gamma_1+\gamma_2^*)\cdot\dot{\boldsymbol{v}}_-(s))\right]\right\},$$

dove $\boldsymbol{u}$ è considerato solo al secondo ordine, cioè è dato dalla (16).

A parte l'ultimo termine, per la simmetria sferica, integrando con $|\gamma_1|$, $|\gamma_2|$ e ξ costanti, i termini precedenti sono equivalenti a

$$\delta S'^{A}(s_1)\left\{-\frac{\boldsymbol{u}}{\xi^3}+\frac{\boldsymbol{u}}{\xi^3}+\frac{\boldsymbol{v}(s)}{\xi^3}\left(\int_{s_1}^{s}\dot{\boldsymbol{v}}(\eta)\,\mathrm{d}\eta\cdot\boldsymbol{u}\right)-\frac{\boldsymbol{v}(s)}{\xi^3}\left(\int_{s_1}^{s}\dot{\boldsymbol{v}}(\eta)\,\mathrm{d}\eta\cdot\boldsymbol{u}\right)\right\}$$

e danno quindi contributo nullo.

L'ultimo termine invece, per integrazione con $|\gamma_1|$, $|\gamma_2|$ e $(\gamma_1+\gamma_2^*)$ costanti equivale a

$$(21)\qquad \delta S'^{A}(s_1)\,\frac{1}{2}\,\frac{\boldsymbol{v}(s)}{\xi^2}\,[\boldsymbol{\xi}\cdot(\gamma_1+\gamma_2^*)]\,\frac{(\gamma_1+\gamma_2)\cdot\dot{\boldsymbol{v}}(s_1)}{|\gamma_1+\gamma_2^*|^2}\,[(\gamma_1+\gamma_2^*)\cdot\dot{\boldsymbol{v}}_-(s)],$$

che integrando ancora con $|\gamma_1|$, $|\gamma_2|$, ξ (e $|\gamma_1+\gamma_2^*|$) costanti equivale a

$$(22)\qquad \delta S'^{A}(s_1)\,\frac{1}{6}\,\boldsymbol{v}(s)\,\frac{|\gamma_1|^2-|\gamma_2|^2}{\xi^2}\,(\dot{\boldsymbol{v}}(s_1)^*\cdot\dot{\boldsymbol{v}}_-(s))\quad (11).$$

Esso può dare un contributo nella forza di reazione se la dipendenza radiale delle diverse componenti della sorgente non è la stessa.

Termini come questo non sono stati considerati nella formula (9) del testo.

Per la seconda parte della (18) si ottiene similmente:

$$(23)\qquad -\left(\frac{\mathrm{d}\delta S'^{A}}{\mathrm{d}s}\right)_{s=s_1}\frac{-(\gamma_2-\boldsymbol{y}'+\boldsymbol{x}_0')}{|\boldsymbol{u}+\boldsymbol{\xi}|^3}\,(s_1-s')\simeq\frac{1}{2}\,\frac{\boldsymbol{\xi}}{\xi^2}\,((\gamma_1+\gamma_2^*)\cdot\dot{\boldsymbol{v}}_-(s))\left(\frac{\mathrm{d}\delta S'^{A}}{\mathrm{d}s}\right)_{s=s_1},$$

equivalente a

$$-\frac{1}{6}\,\dot{\boldsymbol{v}}_-(s)\,\frac{|\gamma_1|^2-|\gamma_2|^2}{\xi^2}\left(\frac{\mathrm{d}\delta S'^{A}}{\mathrm{d}s}\right)_{s=s_1}.$$

(11) Con maggior precisione si otterrebbe $(\dot{\boldsymbol{v}}_+(s_1)+\dot{\boldsymbol{v}}_-(s_1))/2$ al posto di $\dot{\boldsymbol{v}}(s_1)$.

Terza parte:

$$(24)\qquad -(\boldsymbol{\gamma}_1\cdot\dot{\boldsymbol{v}}(s))\frac{-(\boldsymbol{\gamma}_1-\boldsymbol{y}'+\boldsymbol{x}_0')}{|\boldsymbol{u}+\boldsymbol{\xi}|^3}\,\delta S'^{A}(s_1)=$$

$$=-\delta S'^{A}(s_1)(\boldsymbol{\gamma}_1\cdot\dot{\boldsymbol{v}}(s))\left[\frac{(\boldsymbol{u}+\boldsymbol{\xi})}{\xi^3}\left(1+\frac{3\boldsymbol{u}\cdot\boldsymbol{\xi}}{\xi^2}\right)+\boldsymbol{v}(s)\frac{\boldsymbol{\xi}\cdot\int_{s_1}^{s}\dot{\boldsymbol{v}}(\eta)\,\mathrm{d}\eta}{\xi^3}\right]=$$

$$=-\delta S'^{A}(s_1)(\boldsymbol{\gamma}_1\cdot\dot{\boldsymbol{v}}(s))\left[\frac{\boldsymbol{\xi}}{\xi^3}\left(1+\frac{3\boldsymbol{u}\cdot\boldsymbol{\xi}}{\xi^2}\right)+\frac{\boldsymbol{u}}{\xi^3}+\boldsymbol{v}(s)\frac{\boldsymbol{\xi}\cdot\int_{s_1}^{s}\dot{\boldsymbol{v}}(\eta)\,\mathrm{d}\eta}{\xi^3}\right].$$

I soli termini che danno un contributo sono

$$(25)\qquad -\delta S'^{A}(s_1)\,\frac{1}{2}[\boldsymbol{\xi}\cdot\dot{\boldsymbol{v}}(s)+(\boldsymbol{\gamma}_1+\boldsymbol{\gamma}_2^*)\cdot\dot{\boldsymbol{v}}(s)]\left[\frac{\boldsymbol{\xi}}{\xi^3}+\boldsymbol{v}(s)\frac{\boldsymbol{\xi}\cdot\int_{s_1}^{s}\dot{\boldsymbol{v}}(\eta)\,\mathrm{d}\eta}{\xi^3}\right].$$

I termini non contenuti $(\boldsymbol{\gamma}_1+\boldsymbol{\gamma}_2^*)$ sono equivalenti per la simmetria sferica a

$$(26)\qquad \delta S'^{A}(s_1)\left\{\frac{1}{6}\,\frac{\dot{\boldsymbol{v}}(s)}{\xi}+\frac{1}{6}\,\boldsymbol{v}(s)\left(\frac{\dot{\boldsymbol{v}}(s)\cdot\int_{s_1}^{s}\dot{\boldsymbol{v}}(\eta)\,\mathrm{d}\eta}{\xi}\right)\right\},$$

mentre i rimanenti equivalgono a

$$-\frac{1}{6}\,\dot{\boldsymbol{v}}(s)\,\frac{|\boldsymbol{\gamma}_1|^2-|\boldsymbol{\gamma}_2|^2}{\xi^3}\delta S'^{A}(s_1)\quad\text{e}\quad\frac{1}{6}\,\boldsymbol{v}(s)\,\frac{|\boldsymbol{\gamma}_1|^2-|\boldsymbol{\gamma}_2|^2}{\xi^3}\left(\dot{\boldsymbol{v}}(s)\cdot\int_{s_1}^{s}\dot{\boldsymbol{v}}(\eta)\,\mathrm{d}\eta\right)\delta S'^{A}(s_1).$$

Tutti questi termini sono termini istantanei in quanto contenenti come fattore l'accelerazione al tempo s.

Dopo il primo termine consideriamo ora il terzo termine della formula (11)

$$(27)\qquad \left(\frac{\mathrm{d}\delta S'^{A}}{\mathrm{d}s_z}\right)\frac{\boldsymbol{v}'t-\boldsymbol{\gamma}_2+\boldsymbol{y}'-\boldsymbol{x}_0'}{|\boldsymbol{u}+\boldsymbol{\xi}|^2}((1-\boldsymbol{\gamma}_1\cdot\dot{\boldsymbol{v}}(s))=$$

$$=\left(\frac{\mathrm{d}\delta S'^{A}}{\mathrm{d}s}\right)_{s=s'}\frac{\boldsymbol{v}'t-\boldsymbol{\gamma}_2+\boldsymbol{y}'-\boldsymbol{x}_0'}{|\boldsymbol{u}+\boldsymbol{\xi}|^2}\,\frac{1-\boldsymbol{\gamma}_1\cdot\dot{\boldsymbol{v}}(s)}{1-\boldsymbol{\gamma}_2\cdot\dot{\boldsymbol{v}}(s')}=\left(\frac{\mathrm{d}\delta S'^{A}}{\mathrm{d}s}\right)_{s=s'}\left\{\left(\frac{\boldsymbol{v}(s')}{|\boldsymbol{u}+\boldsymbol{\xi}|}+\frac{\boldsymbol{u}+\boldsymbol{\xi}}{|\boldsymbol{u}+\boldsymbol{\xi}|^2}\right)\cdot\right.$$

$$\left.\cdot((1-\boldsymbol{\gamma}_1\cdot\dot{\boldsymbol{v}}(s)+\boldsymbol{\gamma}_2\cdot\dot{\boldsymbol{v}}(s'))+\boldsymbol{v}(s)\frac{\boldsymbol{\xi}\cdot\int_{s_1}^{s}\dot{\boldsymbol{v}}(\eta)\,\mathrm{d}\eta}{\xi^2}\right\}\simeq\left(\frac{\mathrm{d}\delta S'^{A}}{\mathrm{d}s}\right)_{s=s'}\left\{\frac{\boldsymbol{v}(s_1)}{\xi}\left(1+\frac{\boldsymbol{u}\cdot\boldsymbol{\xi}}{\xi^2}\right)+\right.$$

$$\left.+\frac{\boldsymbol{\xi}}{\xi^2}\left(1+2\,\frac{\boldsymbol{u}\cdot\boldsymbol{\xi}}{\xi^2}\right)+\frac{\boldsymbol{u}}{\xi^2}-\left(\frac{\boldsymbol{v}(s_1)}{\xi}+\frac{\boldsymbol{\xi}}{\xi^2}\right)((\boldsymbol{\gamma}_1\cdot\dot{\boldsymbol{v}}(s)-\boldsymbol{\gamma}_2\cdot\dot{\boldsymbol{v}}(s'))+\boldsymbol{v}(s)\frac{\boldsymbol{\xi}\cdot\int_{s_1}^{s}\dot{\boldsymbol{v}}(\eta)\mathrm{d}\eta}{\xi^2}\right\}.$$

Qui bisogna tener presente che $(\mathrm{d}\delta S'^{A}/\mathrm{d}s)_{s=s'}$ non resta invariato cambiando di segno γ_1 e γ_2^* in quanto cambia s', secondo la (13). Se $\mathrm{d}\delta S'^{A}/\mathrm{d}s$ fosse ulteriormente derivabile in s_1, per la (13) essa potrebbe senz'altro venir sostituita con $(\mathrm{d}\delta S'^{A}/\mathrm{d}s)_{s=s_1}$. Altrimenti occorrerebbe ricorrere a delle medie opportune per i vari termini [12].

I termini che possono dare un contributo sono

$$(28)\qquad \left(\frac{\mathrm{d}\delta S'^{A}}{\mathrm{d}s}\right)_{s=s_1}\left\{\frac{\boldsymbol{v}(s_1)}{\xi}+\frac{\boldsymbol{u}}{\xi^2}+\frac{2\boldsymbol{\xi}}{\xi^4}(\boldsymbol{u}\cdot\boldsymbol{\xi})-\frac{\boldsymbol{\xi}}{\xi^2}\left[\boldsymbol{\xi}\cdot\frac{\dot{\boldsymbol{v}}(s)+\dot{\boldsymbol{v}}(s')}{2}\right]-\right.$$
$$\left.-\frac{\boldsymbol{\xi}}{\xi^2}\left[(\boldsymbol{\gamma}_1+\boldsymbol{\gamma}_2^*)\cdot\frac{\dot{\boldsymbol{v}}(s)-\dot{\boldsymbol{v}}(s')}{2}\right]\right\},$$

e, a parte l'ultimo che tralasciamo per le solite ragioni, sono equivalenti a

$$(29)\qquad \left(\frac{\delta\mathrm{d}S'^{A}}{\mathrm{d}s}\right)_{s=s_1}\left\{\frac{\boldsymbol{v}(s)}{\xi}+\frac{1}{2}\dot{\boldsymbol{v}}(s,s_1)-\frac{1}{3}\dot{\boldsymbol{v}}(s,s_1)+\frac{1}{6}(\dot{\boldsymbol{v}}(s)+\dot{\boldsymbol{v}}^*(s_1))\right\}.$$

Rimane ora il secondo termine della (11)

$$(30)\qquad -\frac{1-\boldsymbol{\gamma}_1\cdot\dot{\boldsymbol{v}}(s)}{1-\boldsymbol{\gamma}_2^*\cdot\dot{\boldsymbol{v}}(s')^*}\,\delta S'^{A}(s')\,\frac{\boldsymbol{v}'t-(\boldsymbol{z}-\boldsymbol{y}')}{|\boldsymbol{u}+\boldsymbol{\xi}|^3}[(\boldsymbol{u}+\boldsymbol{\xi})\cdot\dot{\boldsymbol{v}}']=$$

$$=-\frac{1-\boldsymbol{\gamma}_1\cdot\dot{\boldsymbol{v}}(s)}{1-\boldsymbol{\gamma}_2^*\cdot\dot{\boldsymbol{v}}(s')^*}\,\delta S'^{A}(s')\left[\frac{\boldsymbol{v}'}{|\boldsymbol{u}+\boldsymbol{\xi}|^2}+\frac{(\boldsymbol{u}+\boldsymbol{\xi})+\boldsymbol{v}(s)[(\boldsymbol{u}+\boldsymbol{\xi})\cdot\int_{s_1}^{s}\boldsymbol{v}(\eta)\mathrm{d}\eta]}{|\boldsymbol{u}+\boldsymbol{\xi}|^3}\right]\cdot$$

$$\cdot[(\boldsymbol{u}+\boldsymbol{\xi})\cdot\dot{\boldsymbol{v}}'^*]=-\left[1-\frac{\boldsymbol{\xi}\cdot(\dot{\boldsymbol{v}}(s)+\dot{\boldsymbol{v}}(s'))}{2}+\frac{(\boldsymbol{\gamma}_1+\boldsymbol{\gamma}_2^*)\cdot(\dot{\boldsymbol{v}}(s)-\dot{\boldsymbol{v}}(s'))}{2}\right]\delta S'^{A}(s_1)\cdot$$

$$\cdot\left\{\frac{\boldsymbol{v}'}{\xi^2}\left(1+2\frac{\boldsymbol{u}\cdot\boldsymbol{\xi}}{\xi^2}\right)+\frac{\boldsymbol{\xi}}{\xi^3}\left(1+3\frac{\boldsymbol{u}\cdot\boldsymbol{\xi}}{\xi^2}+\frac{\boldsymbol{u}}{\xi^3}+\boldsymbol{v}(s)\,\frac{\boldsymbol{\xi}\cdot\int_{s_1}^{s}\dot{\boldsymbol{v}}(\eta)\mathrm{d}\eta}{\xi^3}\right)\right\}[(\boldsymbol{u}+\boldsymbol{\xi})\cdot\dot{\boldsymbol{v}}'^*].$$

---

[12] Per esempio il termine $(\mathrm{d}\delta S'^{A}/\mathrm{d}s)_{s=s'}(\boldsymbol{\xi}/\xi^2)$ si potrebbe scrivere

$$\frac{|\boldsymbol{\gamma}_1|^2-|\boldsymbol{\gamma}_2|^2}{|\boldsymbol{\gamma}_1+\boldsymbol{\gamma}_2^*|^2}\,\frac{1}{\xi^2}\overline{\left((\boldsymbol{\gamma}_1+\boldsymbol{\gamma}_2^*)\left(\frac{\mathrm{d}\delta S'^{A}}{\mathrm{d}s}\right)_{s=s'}\right)}$$

dove la media è quella che si ottiene per integrazione con $|\boldsymbol{\gamma}_1|$, $|\boldsymbol{\gamma}_2|$, e $|\boldsymbol{\gamma}_1+\boldsymbol{\gamma}_2|$ (e quindi ξ) costanti. Essa è del terzo ordine, se $\mathrm{d}\delta S'^{A}/\mathrm{d}s$ è continua, come si sarebbe del resto ricavato usando la formula (13).

I termini restanti sono

$$(31)\qquad -\delta S'^{A}(s_1)\left[\frac{\boldsymbol{v}(s_1)}{\xi^2}+2\boldsymbol{v}(s_1)\frac{\boldsymbol{u}\cdot\boldsymbol{\xi}}{\xi^4}+\frac{\boldsymbol{\xi}}{\xi^3}+\boldsymbol{v}(s)\frac{\boldsymbol{\xi}\cdot\int_{s_1}^{s}\dot{\boldsymbol{v}}(\eta)\,\mathrm{d}\eta}{\xi^3}\right][(\boldsymbol{u}+\boldsymbol{\xi})\cdot\dot{\boldsymbol{v}}'^{*}]+$$

$$+\frac{\boldsymbol{\xi}\cdot(\dot{\boldsymbol{v}}(s)+\dot{\boldsymbol{v}}(s'))}{2}\,\delta S'^{A}(s_1)\frac{\boldsymbol{v}(s_1)}{\xi^2}[\boldsymbol{\xi}\cdot\dot{\boldsymbol{v}}'^{*}],$$

equivalenti a

$$(32)\qquad -\delta S'^{A}(s_1)\left\{\frac{1}{2}\boldsymbol{v}(s_1)(\dot{\boldsymbol{v}}(s,s_1)\cdot\dot{\boldsymbol{v}}'^{*})-\frac{1}{3}\boldsymbol{v}(s_1)(\boldsymbol{v}(s,s_1)\cdot\dot{\boldsymbol{v}}'^{*})-\frac{1}{3}\frac{\dot{\boldsymbol{v}}'^{*}}{\xi}-\right.$$

$$\left.-\frac{1}{3}\boldsymbol{v}(s)\frac{(\int_{s_1}^{s}\dot{\boldsymbol{v}}(\eta)\,\mathrm{d}\eta\cdot\dot{\boldsymbol{v}}'^{*})}{\xi}\right\}-\frac{1}{3}\,\delta S'^{A}(s_1)\,\boldsymbol{v}(s_1)\frac{(\dot{\boldsymbol{v}}(s)+\dot{\boldsymbol{v}}(s')^{*})\cdot\dot{\boldsymbol{v}}'^{*}}{2}.$$

Sommando insieme tutti i contributi della (11) si ottiene

$$(33)\qquad \delta S'^{A}(s_1)\left\{\frac{1}{6}\frac{\dot{\boldsymbol{v}}(s)}{\xi}+\frac{1}{6}\boldsymbol{v}(s)\left(\frac{\dot{\boldsymbol{v}}(s)\cdot\int_{s_1}^{s}\dot{\boldsymbol{v}}\,(\eta)\,\mathrm{d}\eta}{\xi}\right)\right\}+\left(\frac{\mathrm{d}\delta S'^{A}}{\mathrm{d}s}\right)_{s=s_1}\cdot$$

$$\cdot\left\{\frac{\boldsymbol{v}(s_1)}{\xi}+\frac{1}{6}\dot{\boldsymbol{v}}(s,s_1)+\frac{1}{6}\dot{\boldsymbol{v}}(s)+\frac{1}{6}\dot{\boldsymbol{v}}^{*}(s_1)\right\}+\delta S'^{A}(s_1)\left\{-\frac{1}{6}\boldsymbol{v}(s_1)(\dot{\boldsymbol{v}}(s,s_1)\cdot\dot{\boldsymbol{v}}'^{*})+\right.$$

$$\left.+\frac{1}{3}\frac{\dot{\boldsymbol{v}}'^{*}}{\xi}+\frac{1}{3}\boldsymbol{v}(s)\frac{\int_{s_1}^{s}\dot{\boldsymbol{v}}(\eta)\mathrm{d}\eta\cdot\dot{\boldsymbol{v}}'^{*}}{\xi}-\frac{1}{6}\boldsymbol{v}(s_1)(\dot{\boldsymbol{v}}(s)\cdot\dot{\boldsymbol{v}}'^{*})-\frac{1}{6}\boldsymbol{v}(s_1)(\dot{\boldsymbol{v}}'^{*}\cdot\dot{\boldsymbol{v}}'^{*})\right\}.$$

e quindi la (9).

4. – Come applicazione consideriamo dapprima il caso del campo elettromagnetico.

L'espressione della forza ora è

$$(34)\qquad \delta f_\mu=\delta S^{\nu}(h_{\nu,\mu}-h_{\mu,\nu})=\delta S^{\gamma}(\delta_\mu^{\beta}\delta_\gamma^{\alpha}-\delta_\mu^{\nu}\delta_\gamma^{\beta})h_{\alpha,\beta},$$

con $\delta S^{\gamma}=\delta e\,v^{\gamma}$ e, nell'espressione di $h_{\alpha,\beta}$, $\delta S'^{\alpha}(s)=\delta e\,v^{\alpha}$, $\mathrm{d}\,\delta S'^{\alpha}/\mathrm{d}s=\delta e\,\dot{v}'^{\alpha}$.

Per la (9) si ottiene

$$f_\mu=\int\delta e(\delta_\mu^{\beta}v^{\alpha}-\delta_\mu^{\alpha}v^{\beta})\int\delta e'\left\{v_\alpha\left[\frac{1}{6}\frac{\dot{v}_\beta(s)}{\xi}+\frac{1}{3}\frac{\dot{v}_\beta(s-\xi)^{*}}{\xi}\right]+\dot{v}'_\alpha v'_\beta\frac{1}{\xi}\right\}=$$

$$=\iint\delta e\,\delta e'\left\{\frac{1}{6}\frac{\dot{v}_\mu(s)}{\xi}+\frac{1}{3}\frac{\dot{v}_\mu(s-\xi)^{*}}{\xi}+v'_\mu\frac{(\dot{\boldsymbol{v}}'\cdot\boldsymbol{v})}{\xi}\right\}-\iint\delta e\,\delta e'\frac{\dot{v}_\mu(s-\xi)}{\xi}=$$

$$=\iint\delta e\,\delta e'\left\{\frac{1}{6}\frac{\dot{v}_\mu(s)}{\xi}+\frac{1}{3}\frac{\dot{v}_\mu(s-\xi)^{*}}{\xi}\right\}+\iint\delta e\,\delta e'\left\{v'_\mu\left(\frac{1}{\xi}\dot{\boldsymbol{v}}'\cdot\int_{s-\xi}^{s}\dot{\boldsymbol{v}}(\eta)\,\mathrm{d}\eta\right)-\frac{\dot{v}_\mu(s-\xi)}{\xi}\right\},$$

da cui la (2), ricordando la (3).

* * *

Consideriamo ora il campo scalare.
L'espressione della forza è

$$\delta f_\mu = -\,\delta g\, h_{,\mu} \quad \text{con} \quad \delta S' = \delta g' \quad \text{e} \quad \frac{\mathrm{d}\delta S'}{\mathrm{d}s} = 0\,. \tag{35}$$

$$f_\mu = -\int \delta g \int \delta g' \left(\frac{1}{6}\frac{\dot v_\mu(s)}{\xi} + \frac{1}{3}\frac{\dot v_\mu(s-\xi)^*}{\xi}\right) =$$

$$= -\frac{1}{3}\,\dot v_\mu(s)\iint \frac{\delta g\,\delta g'}{2\xi} - \frac{2}{3}\iint \frac{\delta g\,\delta g'}{2\xi}\,\dot v_\mu(s-\xi)^*,$$

quindi l'equazione del moto è

$$\left(m_{\text{mecc}} + \frac{1}{3}\,m_{\text{se}}\right)\dot{\boldsymbol v}(s) = -\frac{2}{3}\iint \frac{\delta g\,\delta g'}{2\xi}\,\dot{\boldsymbol v}(s-\xi)^* \tag{36}$$

o anche

$$\left(m_0\dot{\boldsymbol v}(s) + \frac{2}{3}\iint \frac{\delta g\,\delta g'}{2\xi}\,\dot{\boldsymbol v}(s-\xi)\right) - \frac{1}{3}\,g^2\boldsymbol v(s)\,(\bar{\dot{\boldsymbol v}}\cdot\dot{\boldsymbol v}') = 0 \tag{37}$$

per la (3) ([13]).

Poichè la forza totale di reazione del campo risulta ortogonale alla linea di universo, anche in questo caso la massa della sorgente non cambia. Inoltre il segno dell'ultimo termine della (37) che dà la reazione della radiazione, ed il segno del coefficiente di inerzia dovuto al campo confermano che la densità di energia di quest'ultimo è positiva.

Così il campo scalare « attrattivo » si comporta, per quanto riguarda la dinamica delle sorgenti, esattamente come il campo elettromagnetico (repulsivo). Si incontrano anche le stesse difficoltà (soluzioni rettilinee autoaccelerate) quando la sorgente è sufficientemente piccola.

([13]) L'equazione per la sorgente puntiforme è dunque

$$m\dot{\boldsymbol v}(s) - \frac{1}{3}\,g^2[\ddot{\boldsymbol v}(s) + \boldsymbol v(s)(\dot{\boldsymbol v}(s)\cdot\dot{\boldsymbol v}(s))] = \boldsymbol F_{\text{est.}}\,.$$

Cfr. inoltre per il campo *mesonico*: P. Havas: *Phys. Rev.*, **93**, 882 (1954); F. R. Crownfield e P. Havas: *Phys. Rev.*, **94**, 471 (1954); H. J. Bhabha: *Proc. Roy. Soc.*, A **172**, 384 (1939); Haris-Chandra: *Proc. Roy. Soc.*, A **185**, 269 (1946); Majumdar, S. Gupta e S. K. Trehan: *Prog. Theor. Phys.*, **12**, 31 (1954).

* * *

Applichiamo ora la formula (9) al caso generale di campi lineari per i quali l'espressione della forza sia

$$\delta f_\mu = K^{AB}_{\ \ -}\,\delta S_A h_{B,\mu} \qquad (K^{BA} = K^{AB}) \tag{38}$$

caratteristica delle conservazioni corrispondenti all'invarianza della lagrangiana per traslazioni spaziali e temporali.

Gli indici A e B stanno ancora per un gruppo di indici, in alto o in basso e non sono necessariamente indici di varianza tensoriale. Non assumeremo la costanza col tempo degli elementi δS, quindi in $h_{B,\mu}$ $(\mathrm{d}\,\delta S'_B/\mathrm{d}s) \neq 0$ in generale.

Si ottiene

$$\begin{aligned} f_\mu = K^{AB}\int \delta S_A \int \delta S'_B \left[\frac{1}{6}\frac{\dot v_\mu(s)}{\xi} + \frac{1}{3}\frac{\dot v_\mu(s-\xi)^*}{\xi}\right] + K^{AB}\int \delta S_A \int \frac{\mathrm{d}\delta S'_B}{\mathrm{d}s}\frac{v_\mu(s-\xi)}{\xi} = \\ = \frac{1}{3}\dot v_\mu(s)\iint \frac{K^{AB}\,\delta S_A\,\delta S'_B}{2\xi} + \frac{2}{3}\iint \frac{K^{AB}\,\delta S_A\,\delta S'_B}{2\xi}\,\dot v_\mu(s-\xi)^* + \\ + \iint K^{AB}\,\delta S_A \frac{\mathrm{d}\delta S'_B}{\mathrm{d}s}\,\frac{v_\mu(s-\xi)}{\xi}\,. \end{aligned} \tag{39}$$

Se l'ultimo termine non è nullo si ha dunque un cambiamento della massa propria della sorgente.

Esso può scriversi, all'ordine considerato,

$$\begin{aligned} \iint K^{AB} v_\mu(s-\xi)\frac{\mathrm{d}}{\mathrm{d}s}\,\frac{\delta S_A(s-\xi)\,\delta S'_B(s-\xi)}{2\xi} + \\ + \iint K^{AB} v_\mu(s-\xi)\,\frac{\mathrm{d}\delta S_A(s-\xi)}{\mathrm{d}s}\,\frac{\mathrm{d}\delta S'_B(s-\xi)}{\mathrm{d}s}\,. \end{aligned} \tag{40}$$

Il calcolo diretto della potenza irradiata fatto in maniera relativistica a grande distanza dalla sorgente, assunta puntiforme, dà come risultato (vedi Appendice)

$$\frac{\mathrm{d}P^\mu}{\mathrm{d}s} = v^\mu(s)\left[(K^{AB}S_A S'_B)\,\frac{(\dot{\boldsymbol v}(s)\cdot\dot{\boldsymbol v}(s))}{3} - \left(K^{AB}\frac{\mathrm{d}S_A}{\mathrm{d}s}\frac{\mathrm{d}S'_B}{\mathrm{d}s}\right)\right] - \frac{\dot v^\mu(s)}{3}\frac{\mathrm{d}}{\mathrm{d}s}(K^{AB}S_A S_B)\,, \tag{41}$$

e la parte della formula (39) corrispondente all'inerzia ritardata del campo si dovrebbe scrivere, sommando la (41) alla (39)

$$\begin{aligned} \frac{1}{3}\,\dot{\boldsymbol v}(s)\iint \frac{K^{AB}\,\delta S_A\,\delta S'_B}{2\xi} + \frac{2}{3}\iint \frac{K^{AB}\,\delta S_A\,\delta S'_B}{2\xi}\,\dot{\boldsymbol v}(s-\xi) - \frac{\dot{\boldsymbol v}(s)}{3}\frac{\mathrm{d}}{\mathrm{d}s}(K^{AB}S_A S_B) + \\ - \boldsymbol v(s)\left(K^{AB}\frac{\mathrm{d}S_A}{\mathrm{d}s}\frac{\mathrm{d}S_B}{\mathrm{d}s}\right) + \iint K^{AB}\,\delta S_A \frac{\mathrm{d}\delta S'_B}{\mathrm{d}s}\frac{\boldsymbol v(s-\xi)}{\xi}\,, \end{aligned} \tag{42}$$

che si potrebbe scrivere

$$(43)\qquad \frac{1}{3}\dot{\boldsymbol{v}}(s)\iint\frac{K^{AB}\delta S_A(s)\,\delta S'_B(s)}{2\xi}+\frac{2}{3}\iint\frac{K^{AB}\delta S_A(s-\xi)\,\delta S'_B(s-\xi)}{2\xi}\,\dot{\boldsymbol{v}}(s-\xi)+$$
$$+\iint\boldsymbol{v}(s-\xi)\,\frac{\mathrm{d}}{\mathrm{d}s}\,\frac{\delta S_A(s-\xi)\,\delta S'^{B}(s-\xi)}{2\xi}\,.$$

Se

$$K^{AB}\,\frac{\mathrm{d}}{\mathrm{d}s}\,\frac{\delta S_A(s-\xi)\,\delta S'_B(s-\xi)}{2\xi}=0\,,$$

il contributo longitudinale proviene solo dal secondo termine, ed il segno è quello legato alla densità di energia totale del campo statico, che è dello stesso segno e proporzionale (vedi Appendice) a $-K^{AB}S_AS_B$, forma quadratica che non è necessariamente definita.

Per quanto riguarda il termine longitudinale della forza di reazione totale, responsabile di una eventuale forzata variabilità della massa, se $K^{AB}S_AS_B$ è costante, l'unico contributo proviene dal secondo termine della (40) che è proporzionale a $K^{AB}(\mathrm{d}S_A/\mathrm{d}s)(\mathrm{d}S_B/\mathrm{d}s)$. Se $S_A(s)$ dipende da $\boldsymbol{v}(s)$, K^{AB} contiene il tensore metrico (pseudoeuclideo), e $\mathrm{d}S_A(s)/\mathrm{d}s$ contiene $\dot{\boldsymbol{v}}(s)$. Il contributo di questo termine nella (11) può essere così di segno opposto a quello proporzionale a $K^{AB}S_AS_B$, e può anche cambiare il segno dell'energia irradiata.

5. – Nel contributo alla reazione del campo vi sono termini «istantanei» provenienti dal primo termine della (9) e che sono stati nelle (2) e (37) conglobati in m_0 insieme a $m_{\text{mecc.}}$. Il loro segno è diverso a seconda se il campo è attrattivo o repulsivo, in quanto connessi con i flussi di impulso del campo, diversi nei due casi.

Si sa [14] che integrando il campo di una sorgente in moto per ottenerne l'energia si trova anche il contributo di quelli che erano i flussi di impulso nel sistema a riposo con la sorgente. Questi sono compensati se si ruota lo spazio di integrazione fino a riportarlo ortogonale alla linea di universo della sorgente. Se ora si accelera una sorgente ferma, ruotando contemporaneamente lo spazio di integrazione in modo che resti ortogonale alla sua linea di universo, il contributo proveniente da questa rotazione è istantaneo e corrisponde al primo termine della (9), mentre il contributo del flusso di impulso segue nel tempo come tutto il riassettamento della parte coulombiana, e si ritrova incluso nel secondo termine della (9).

---

[14] Cfr. R. Becker: *Teoria dell'elettricità* (Firenze, 1950), formule (66.4) e (66.1).

Così per il campo elettromagnetico (repulsivo) compare il coefficiente $\frac{4}{3} = 1 + \frac{1}{3}$, mentre per il campo scalare (attrattivo) il coefficiente è $\frac{2}{3} = 1 - \frac{1}{3}$.

D'altra parte se si considera il tensore energetico totale, a divergenza nulla, l'energia totale non può essere alterata per una semplice rotazione dello spazio di integrazione; questo secondo l'autore è un motivo per considerare la parte istantanea dell'inerzia del campo insieme alla parte « meccanica » della massa.

Appendice

Per calcolare l'energia e la quantità di moto irradiate durante il tempo proprio ds, conviene integrare il loro flusso uscente a grandi distanze su una striscia di superficie spazio-temporale che unisca i due coni del futuro aventi vertice rispettivamente in s e $s+ds$.

L'energia e la quantità di moto uscenti da un elemento di superficie di modulo $\Delta\sigma$ e di normale esterna η^μ vale

$$\Delta P^\mu = - T^{\mu\alpha}\eta_\alpha \Delta\sigma \,. \tag{1A}$$

Assumendo come superficie il luogo dei punti $\boldsymbol{x}$ soddisfacenti le condizioni

$$(\dot{\boldsymbol{z}}(s),\ \boldsymbol{x} - \boldsymbol{z}) = C\,, \qquad (\boldsymbol{x} - \boldsymbol{z},\ \boldsymbol{x} - \boldsymbol{z}) = 0$$

per qualche valore di s, e dove $\boldsymbol{z}$ sono le coordinate della sorgente e C è una costante positiva, e ancora ponendo $\boldsymbol{v} = \dot{\boldsymbol{z}}(s)$ e $\boldsymbol{z} = \boldsymbol{x} - \boldsymbol{z}$, si può scrivere

$$\eta^\nu \Delta\sigma = (\boldsymbol{v}\cdot\boldsymbol{r})^2 \,\mathrm{d}\omega\,\mathrm{d}s \left(\frac{1 - (\boldsymbol{r}\cdot\dot{\boldsymbol{v}})}{(\boldsymbol{r}\cdot\boldsymbol{v})}\, r^\nu - v^\nu \right), \tag{2A}$$

essendo $d\omega$ l'angolo solido spaziale sotto cui è visto il precedente elemento di superficie nel sistema legato alla sorgente al tempo s.

Nel caso in cui l'espressione della forza sia

$$f_\mu = K_{\alpha\beta} S^\alpha h^\beta{}_{,\mu} \qquad (K_{\alpha\beta} = K_{\beta\alpha})$$

il tensore energetico si scrive

$$T^{\mu\nu} = -\frac{1}{4\pi}\left(g^{\mu m} g^{\nu n} K_{\alpha\beta} \frac{\partial h^\alpha}{\partial x^m} \frac{\partial h^\beta}{\partial x^n} - \frac{1}{2}\, g^{\mu\nu} g^{mn} K_{\alpha\beta} \frac{\partial h^\alpha}{\partial x^n} \frac{\partial h^\beta}{\partial x^n} \right). \tag{3A}$$

Usando la formula (8) si ottiene, integrando su tutto l'angolo solido e tra-

scurando quindi i termini che svaniscono a grandi distanze:

$$\frac{\mathrm{d}P^{\mu}}{\mathrm{d}s} = \boldsymbol{v}(s)\left[(K_{\alpha\beta}S^{\alpha}S^{\beta})\frac{(\dot{\boldsymbol{v}}\dot{\boldsymbol{v}})}{3} - \left(K_{\alpha\beta}\frac{\mathrm{d}S^{\alpha}}{\mathrm{d}s}\frac{\mathrm{d}S^{\beta}}{\mathrm{d}s}\right)\right] - \frac{\mathrm{d}}{\mathrm{d}s}(K_{\alpha\beta}S^{\alpha}S^{\beta})\frac{\dot{\boldsymbol{v}}(s)}{3}\,. \tag{4A}$$

Per il campo statico il tensore energetico si riduce a

$$T^{\mu\nu} = -\frac{1}{4\pi}\frac{1}{(\boldsymbol{r}\cdot\boldsymbol{v})^{6}}K_{\alpha\beta}S^{\alpha}S^{\beta}[(\boldsymbol{x}-\boldsymbol{z})^{\mu}_{\perp v}(\boldsymbol{x}-\boldsymbol{z})^{\nu}_{\perp v} + g^{\mu\nu}(\boldsymbol{r}\cdot\boldsymbol{v})^{2}]\,. \tag{5A}$$

SUMMARY

One gets a formula (eq. (9)), by which one can calculate the self-force for a source of a field h^{A} satisfying the equation $\Box h^{A}=0$. One can so obtain the known results for the electromagnetic field, and for the scalar attractive field, which behaves just like the former. For some other fields, during the emission, the mass of the source must vary.

On Time-Irreversible Nucleon-Nucleon Scattering.

R. J. N. Phillips

Atomic Energy Research Establishment - Harwell, Berks. - England

(ricevuto il 23 Dicembre 1957)

Summary. — The S-matrix for time-irreversible nucleon-nucleon scattering is parametrized by a simple extension of the phase-shift method.

1. – Introduction.

Until the present time, there has been no direct evidence that nuclear forces are invariant under Wigner time-reversal (*), (henceforth denoted by T), although this is commonly assumed. However, a scattering experiment to test this assumption is being carreid out at Uppsala (+), and experiments are being considered at other laboratories.

This note suggests a way to parametrize the nucleon-nucleon S-matrix when T-invariance is not assumed; besides the usual phase shifts and mixing parameters, one additional real parameter is needed for each two-channel (coupled triplet) process. It provides a framework in which to discuss scattering experiments, and to analyse any deviations from T-invariance they may reveal.

It is assumed throughout that nuclear forces conserve parity: experimental evidence to support this has been found [3,4].

(*) For a discussion of T, see for example, refs. [1] and [2].

(+) Private communication from P. Hillman.

[1] J. M. Blatt and V. F. Weisskopf: *Theoretical Nuclear Physics* (New York, 1952).

[2] R. G. Sachs: *Nuclear Theory* (Cambridge, Mass., 1953).

[3] N. Tanner: *Phys. Rev.*, **107**, 1203 (1957).

[4] D. H. Wilkinson: *Phys. Rev.* (in the press).

2. – S-matrix parameters.

The present work is confined to energies below the threshold for meson production; the nucleon-nucleon S-matrix is therefore unitary. It also has spherical symmetry. If S is written in the (L, S, J, M) representation, with the usual convention ([5]), it can be shown that T-invariance ([×]) implies the single further condition that S is symmetric.

The single-channel scattering processes in this representation are each described by a single real phase shift; the S-matrix is diagonal with respect to these processes, and T-invariance adds nothing to our knowledge of them. However, T-invariance is not trivial for the two-channel processes (in the coupled triplet states $L=J\pm 1$); for such a process, S is a (2×2) matrix.

The most general unitary (2×2) matrix has the form

$$(1) \qquad \begin{pmatrix} \cos\alpha \exp[i\beta_{11}], & \sin\alpha \exp[i\beta_{12}] \\ \sin\alpha \exp[i\beta_{21}], & \cos\alpha \exp[i\beta_{22}] \end{pmatrix},$$

where $\beta_{11}+\beta_{22}=\beta_{12}+\beta_{22}-\pi$, ($\alpha$, β_{ij} all real), and thus contains four independent real parameters. When this matrix is symmetric, however, the independent parameters reduce to three. For the case of interest, in which the first and second row (and column) refer to the triplet states $|L=J-1)$ and $|L=J+1)$ respectively, the S-matrix can be written ([6])

$$(2) \qquad S = U^{-1}\Delta U ,$$

$$(3) \qquad U = \begin{pmatrix} \cos\varepsilon^J, & \sin\varepsilon^J \\ -\sin\varepsilon^J, & \cos\varepsilon^J \end{pmatrix},$$

$$(4) \qquad \Delta = \begin{pmatrix} \exp[2i\delta_\alpha^J], & 0 \\ 0, & \exp[2i\delta_\beta^J] \end{pmatrix}.$$

This form, originally due to SCHWINGER, represents S in terms of its eigenvalues. U describes the composition of the eigenstates in terms of the states

---

([5]) E. U. CONDON and G. H. SHORTLEY: *Theory of Atomic Spectra* (Cambridge, 1935).

([×]) To be precise, « reciprocity » is used here: it is implied by T-invariance and unitarity. See ref. ([1]).

([6]) J. M. BLATT and L. C. BIEDENHARN: *Phys. Rev.*, **86**, 399 (1952); *Rev. Mod. Phys.*, **24**, 258 (1952).

$|L = J \pm 1)$, while δ_α^J and δ_β^J are the eigenstate phase-shifts (often conventionally written $\delta_{J\ 1}^J$ and δ_{J+1}^J). The two-channel scattering process is thus decomposed into two single-channel processes; the nature of this decomposition depends on the details of the nucleon-nucleon interaction, of course, and may be expected to vary with the energy.

When S is not symmetric, a parametrization very similar to Equations (2)-(4) can be achieved by altering (3) to the form

$$(3') \qquad U = \begin{pmatrix} \cos \varepsilon^J & , & \sin \varepsilon^J \exp [2i\lambda^J] \\ -\sin \varepsilon^J \exp [-2i\lambda^J] , & & \cos \varepsilon^J \end{pmatrix}.$$

This has the effect of introducing factors $\exp [\pm 2i\lambda^J]$ into the off-diagonal matrix elements of S: it can readily be seen that this parametrization represents the most general case. The eigenstates are now made up from the states $|L = J \pm 1)$ with complex coefficients, and the decomposition into single-channel processes is no longer T-invariant.

Stapp ([7,8]) has suggested an alternative parametrization of S for the symmetric case, which has decided advantages when Coulomb effects have to be included. When T-invariance is relaxed, factors $\exp [\pm 2i\lambda^J]$ can again be inserted in the off-diagonal elements of S. The relation ([8]) between Stapp's parameters and the Blatt-Biedenharn parameters remains unchanged.

It is evident that a complete parametrization of the S-matrix for time-irreversible scattering can be achieved by adding in this way a single real parameter for each J-value (except $J = 0$, for which there is no two-channel process). When $\lambda^J = 0$, this reduces to the usual parametrization.

3. – Illustration: p-p scattering with $L \leqslant 3$.

In this case there is only one coupled triplet state, that with $J = 2$, and deviations from T-invariance are described by a single real parameter.

For analysing experiments it is convenient to use the scattering matrix M of Wolfenstein and Ashkin ([9]) and Dalitz ([10]), a matrix in the two-particle composite spin space which describes the scattered wave in terms of the incident plane wave. Using symmetry and time-reversal arguments, these authors

([7]) H. P. Stapp: *University of California thesis*, UCRL-3098 (1955).
([8]) H. P. Stapp, T. Ypsilantis and N. Metropolis: *Phys. Rev.*, **105**, 302 (1957).
([9]) L. Wolfenstein and J. Ashkin: *Phys. Rev.*, **85**, 947 (1952).
([10]) R. H. Dalitz: *Proc. Phys. Soc.*, A **65**, 175 (1952).

showed that it has the general form

$$M = a + c(\sigma_N^{(1)} + \sigma_N^{(2)}) + m\sigma_N^{(1)}\sigma_N^{(2)} + (g + h)\sigma_P^{(1)}\sigma_P^{(2)} + (g - h)\sigma_K^{(1)}\sigma_K^{(2)} . \tag{5}$$

The coefficients a, c etc., are functions of energy and scattering angle θ. The notation follows STAPP ([7]). $\boldsymbol{N}$, $\boldsymbol{P}$ and $\boldsymbol{K}$ are unit vectors in the directions $\boldsymbol{K}_i \times \boldsymbol{K}_f$, $\boldsymbol{K}_i + \boldsymbol{K}_f$ and $\boldsymbol{K}_f - \boldsymbol{K}_i$ respectively, where $\hbar\boldsymbol{K}_i$ and $\hbar\boldsymbol{K}_f$ are the initial and final relative momenta. Lower suffixes in (5) denote scalar products.

Without T-invariance, M can contain one more term (*)

$$t(\sigma_K^{(1)}\sigma_P^{(2)} + \sigma_P^{(1)}\sigma_K^{(2)}) . \tag{6}$$

Taking a suitable trace in the combined spin space, one finds

$$t(\theta) = \frac{1}{8}\,\mathrm{Tr}\; M(\sigma_K^{(1)}\sigma_P^{(2)} + \sigma_P^{(1)}\sigma_K^{(2)}) = \tag{7}$$

$$= \frac{\sin\theta}{4}(M_{00} - M_{11} + M_{1\,-1}) + \frac{\cos\theta}{2\sqrt{2}}(M_{01} + M_{10}) .$$

The M_{ij} are the usual triplet matrix elements, with azimuthal dependence suppressed. The vanishing of t gives a familiar identity for T-invariant scattering ([9]).

In general, $t(\theta)$ can be any complex function of θ (+). However, M can be expressed in terms of the S-matrix parameters, and in the present case (7) becomes

$$t(\theta) = \frac{5\sqrt{6}}{16k}\sin 2\theta \sin 2\varepsilon^{(2)} \sin 2\lambda^{(2)} (\exp[2i\delta_3^2] - \exp[2i\delta_1^2]) . \tag{8}$$

θ is the scattering angle, and k the wave number of each particle, in the center-of-mass system. The generalized Blatt-Biedenharn parameters have been used, and Coulomb effects have been ignored. This gives an upper bound for $t(\theta)$, as well as its θ-dependence.

A simple way to test T-invariance is to compare the polarization $P(\theta)$ produced in the collision of unpolarized protons, with the asymmetry $\varepsilon = P_1\mathscr{A}(\theta)$ in the cross-section for scattering protons of polarization P_1 from unpolarized protons. With suitable conventions and choice of scattering planes, $P(\theta) = \mathscr{A}(\theta)$ for time-reversible scattering ([9,10]).

(*) With charge-symmetry, a similar result holds for n-p scattering. See refs. ([9,10]).

(+) F. MANDL (to be published) has studied the case where t, a, c, etc. are arbitrary complex functions of θ.

There can be time-irreversible scattering in which this equality holds. However, if one takes the energy to be 140 MeV, neglects partial waves with $L > 3$, and assumes that all the S-matrix parameters other than $\lambda^{(2)}$ have the values given by the potential model of Gammel and Thaler ([11]) (very similar results are found with the Signell-Marshak potential ([12])), then at 45° c.m.

$$(9) \qquad I_0(P - \mathscr{A}) = \sin \lambda^{(2)} \cos \lambda^{(2)} [5.0 - 1.0 \sin^2 \lambda^{(2)}] \text{ mb/sr} .$$

I_0 is the differential cross-section: at this energy and angle, $I_0 P$ is about 0.9 mb/sr. The greatest possible departure from S-matrix symmetry occurs when $\lambda^{(2)} = \pm 45°$, and in a sense this is the maximum violation of T-invariance. However, even for $\lambda^{(2)}$ as small as 5°, $I_0(P - \mathscr{A})$ is 0.4 mb/sr, which represents a large effect. The assumptions that have been made are not safe, but the result suggests that a measurement of P—$\mathscr{A}$ at this energy might be a sensitive test of T-invariance.

4. – Discussion.

For a rigorous investigation of T-invariance, the parameters λ^J would have to be included in a complete phase-shift analysis. Although this adds to the number of parameters to be determined, the number of distinct experiments is also increased.

There are several other identities, beside $P = \mathscr{A}$, which depend on time-reversal arguments. These include a relationship between the triple-scattering quantities A, R, A' and R' ([13]), and three relations connecting the correlation parameters C_{PK}, C_{PP} and C_{KK} ([7]) to the cross-sections for scattering a polarized beam from a polarized target. The experiments needed to check these identities are extremely difficult, however.

The new parameters λ^J do not appear in the total cross-section. Blatt and Biedenharn ([6]) showed for the T-invariant case that only the eigenphase shifts appear; their proof depends on the unitarity of U, and applies also to the present case. There are some novel features to the scattering, however. A somewhat academic example is provided by triplet scattering in a single eigenstate (e.g. δ_0^1, $\varepsilon^{(1)}$, $\lambda^{(1)} \neq 0$; all other triplet parameters $= 0$): ordinarily no polarization or asymmetry can be set up, but in time-irreversible scattering both can occur.

([11]) J. L. Gammel and R. M. Thaler: *Phys. Rev.*, **107**, 291 (1957).
([12]) P. S. Signell and R. E. Marshak: *Phys. Rev.*, **106**, 832 (1957).
([13]) L. Wolfenstein: *Phys. Rev.*, **96**, 1654 (1954); *Ann. Rev. Nucl. Sci.*, **6**, 43 (1956).

* * *

The author would like to thank Dr. J. S. Bell and Dr. F. Mandl for their helpful comments.

RIASSUNTO (*)

Per mezzo di una semplice estensione del metodo dello spostamento di fase si parametrizza la matrice S per lo scattering nucleone-nucleone irreversibile nel tempo.

(*) *Traduzione a cura della Redazione.*

On the Magnetic Behaviour of Ferrous Fluosilicate.

D. Palumbo (*)

H. H. Wills Physics Laboratory - University of Bristol

(ricevuto il 29 Dicembre 1957)

Summary. — In this work the magnetic behaviour of $FeSiF_6 \cdot 6H_2O$ is investigated. A calculation based on third order perturbation leads to results in accord with available experimental data. The possibility of covalent bonds and weak trigonal crystal field has been considered.

1. – Introduction.

Ferrous fluosilicate hexahydrate (1), in common with many hexahydrated fluosilicates, has a structure like CsCl. The place of Cs in the crystal is occupied by the paramagnetic ion surrounded by an almost regular octahedron of water molecules. The crystal has rhombohedral symmetry; in the unit cell there is a single molecule ($FeSiF_6 \cdot 6H_2O$). The (111) axis of the water molecule octahedron is the axis of the crystal. The salt appears light green. The temperature dependence of its magnetic susceptibilities over a range from 1.57 °K to room temperature has recently been investigated experimentally at Bristol by Jackson (2). Its main features (3) are as follows: the susceptibility along the crystal axis, $\chi_{\parallel}$, is very small at low temperatures; rises with temperature T; has a single maximum, afterwards decreases and at room temperature it obeys the Curie-Weiss law. The susceptibility perpendicular to the crystal axis $\chi_{\perp}$ decreases monotonically as T increases and also obeys the Curie-Weiss law at room temperature and the product $(T\chi_{\perp})$ has a single maximum.

(*) On leave from Istituto di Fisica, Università di Palermo.

(1) R. W. G. Wyckoff: *Crystal Structures*, (New York), Chapt. 7, p. 33.

(2) L. C. Jackson: private communication.

(3) M. H. L. Pryce: *Lezioni di Varenna*, in *Suppl. Nuovo Cimento*, **6**, 817 (1957).

2. – Levels of Fe^{++} ion.

The Fe^{++} ion is a $3d^6\ ^5D$ state. As is well known ([4,5]), the five-fold orbital degeneracy is partially removed by a crystal electric field of cubic symmetry which leaves a $d\varepsilon$ triplet and a $d\gamma$ doublet. As in the case of the $3d^1\ ^2D$ ions, the $d\varepsilon$ triplet is energetically lower than the $d\gamma$ doublet. The distance Δ between these levels, determined by optical absorption measurement, is $10\,000\ cm^{-1}$ and is probably responsible for the green colour of the salt.

On account of the spin ($S = 2$) we should have in the ground level a 5×3-fold degeneracy, partially removed by spin-orbit coupling. In these conditions we should expect an isotropic susceptibility obeying Curie's law even at low temperatures. This result does not agree with experimental data. In fact there is a slight distortion about the (111) axis of the water molecule octahedron surrounding the ferrous ion which reduces the symmetry from cubic to trigonal. Thus the crystal field has a trigonal component, which we suppose smaller than the cubic one. It introduces into the Hamiltonian a term of the form:

$$T = a' r^2 Y_2^0 + b' r^4 Y_4^0 \tag{1}$$

(here and in the rest of this paper the z-axis is taken to be along the crystal axis).

This field by itself would split the $d\varepsilon$ triplet into a doublet and a singlet. The distance between the two levels is expressed as

$$\delta = -4.5a - 10b\,, \tag{1'}$$

where

$$a = \frac{a'}{21}\sqrt{\frac{5}{\pi}}\langle r^2\rangle\,; \qquad b = \frac{b'}{21\sqrt{\pi}}\langle r^4\rangle\,.$$

The orbital singlet will be lower if $\delta > 0$. Let f_0, $f_{\pm 1}$ represent the orbital wave function of these levels and $f_{\pm 2}$ those of upper levels. (The labels do not represent L_z).

As Professor Pryce has pointed out to me, an analysis of available spectroscopic data ([6]) shows that, in the case of the free ferrous ion, the whole perturbation from spin-orbit and spin-spin interaction can be introduced into

---

([4]) A. Abragam and M. H. L. Pryce: *Proc. Roy. Soc.*, A **205**, 135 (1951).
([5]) B. Bleaney and K. W. H. Stevens: *Rep. on Prog. in Phys.*, **16**, 107 (1953).
([6]) C. H. Moore: *Atomic En. Lev., U. S. Nat. B. of St.*, Circular 467.

the Hamiltonian as an operator

$$\lambda(\boldsymbol{L}\cdot\boldsymbol{S}) - \varrho'(\boldsymbol{L}\cdot\boldsymbol{S})^2 - \varrho''(\boldsymbol{L}\cdot\boldsymbol{S})^3 , \tag{2}$$

where

$$\lambda = -104 \text{ cm}^{-1} ; \quad \varrho' = 1.125 \text{ cm}^{-1} ; \quad \varrho'' = 0.0355 \text{ cm}^{-1} .$$

Possible deviations from (2) or from the above numerical values will be examined in Sect. **4**.

As the same splitting between the lower levels and much the same magnetic behaviour are to be expected irrespective of whether T is much greater than (2) or of the same order, it is convenient to carry out the calculations without assuming a specific value for T.

The representation of T with the $d\varepsilon$ orbital triplet as basis is diagonal, but in the D five dimensional manifold the representation of T has off diagonal elements whose effect will be considered next. With $T = \lambda\tau$, the $\lambda(\tau + \boldsymbol{L}\cdot\boldsymbol{S})$ operator commutes with $S_z + L_z$ in the 5×3 manifold. Hence it is possible to classify the states by a fictitious m ($m = -3, -2, ..., 3$) and the fifteenth-degree secular equation factorizes into a chain of lower degree equations one for each value of m. These equations are:

$$\begin{cases} x^3 + (7-\tau)x^2 + (10-4\tau)x - 4\tau = 0 ; \\ y^3 + (7-\tau)y^2 + (10-4\tau)y - 3\tau = 0 ; \\ z^2 + (7-\tau)z + 2(10-4\tau) = 0 ; \quad u + 5 = 0 . \end{cases} \tag{3}$$

Owing to the negative sign of λ the lower levels belong to the larger roots. Let us take the roots in descending order. The roots, x, x'' belong to the $m = 0$ singlets whose wave functions are $\sqrt{3}\, f_{-1}s_1 + (x+2)f_0 s_0 + \sqrt{3}\, f_1 s_{-1}$ and the root $x' = 1$ belongs, irrespective of its τ value, to the $m = 0$ singlet, whose wave function is $f_{-1}s_1 - f_1 s_{-1}$. The $m = \pm 1$ doublets belonging to y (and y', y'') have the wave function $\sqrt{2}(y+3)f_{-1}s_2 + (y+1)(y+3)f_0 s_1 + \sqrt{3}(y+1)f_1 s_0$ (and similarly for $m = -1$). The wave function of the $m = \pm 2$ doublets belonging to the z, z' roots is $(z+4)f_0 s_2 + \sqrt{2} f_1 s_1$ (and similarly for $m = -2$). Here s indicates the spin and we shall indicate by N_0, N_0', ..., N_2' the normalization factors. By inspection of (3), if $\tau > 0$, the ground state is the $m = 0$ singlet belonging to x; above this the y doublet and then the levels belonging to z, $x = 1$, y', z', x'', y'', u. On the other hand, if $\tau < 0$, the ground state is the $m = \pm 1$ doublet. Since, in the low temperature region, only the ground state is populated, then if this is the $m = 0$, one expects χ to be very small. The reverse is true if the $m = \pm 1$ is lower. Therefore to accord with Jackson's experimental results, τ must be positive.

The $-\varrho'(\boldsymbol{L}\cdot\boldsymbol{S})^2$ operator produces on the x, y, z, levels the energy shifts ε':

$$(4)\qquad \begin{cases} 6N_0^2(2x+9)\varrho'\,; \quad 3\varrho'+8N_1^2(y^3+8y^2+15y+9)\varrho'\,; \\ 12\varrho'+N_2^2(4z+26)\varrho'\,. \end{cases}$$

There are non-vanishing off diagonal elements between states with the same m value and with m values $(0, \pm 3)$, $(\pm 1, \pm 2)$. Irrespective of the value of τ they produce very small energy shifts (of the order of 0.01 cm^{-1}) and their effect on magnetic behaviour is negligible. If $\tau \gg 1$ then (4) becomes (eliminating constants):

$$(4')\qquad 0\,; \quad 3\varrho'\,; \quad 12\varrho'\,.$$

No account has been taken here of the small ϱ'' term.

The upper $d\gamma$ doublet, because of the non-diagonal elements of T in the D orbital representation and spin-orbit coupling, produces a further energy shift ε'' of the 0, ± 1 lower levels where:

$$(5)\qquad \varepsilon'' = \gamma^2\delta[N_0^2(x+2)^2 - N_1^2(y+3)^2(y+1)^2] + \\ + \frac{\lambda^2}{\Delta}[6N_0^2(x+2)^2 - 4N_1^2(y+3)^2(y^2+2y+2)]\,,$$

where

$$(5')\qquad \gamma = \frac{\delta}{\Delta\sqrt{2}}\cdot\frac{5b-3a}{10b+4.5a}\,.$$

Both (4) and (5) would vanish in a field of pure cubic symmetry. Actually they are of the order of 1 cm^{-1}. Thus, in a trigonal field, the $m=0$, $m=\pm 1$ lower levels are separated energetically by an amount ε where:

$$(6)\qquad \varepsilon = \lambda(y-x) + \varepsilon' + \varepsilon''$$

and x, y, ε', ε'' are functions of τ. For all values of τ, the $(y-x)$ term is largest and it has a maximum value of about $0.17\,|\lambda|$ when $\tau \simeq 6$. For large values of τ it decreases as $1/\tau$. The next level, $m=2$, which belongs to the root z, is $2|\lambda|$ above the ground state (in a cubic field). This separation decreases monotonically as τ increases and approaches 4ε. The other levels lie successively above the previous pair with mutual separations of the order of $\lambda|$. If τ is small in the crystal, then in the low temperature region only the 0, ± 1 levels should be populated.

2·1. – If $\tau \gg 1$ (i.e. $\delta \gg |\lambda|$) the ± 1, ± 2 levels are both fairly close to the ground state. All the other levels lie at energies of order of δ above these.

This is shown in Fig. 1. In this case, only the first three levels will be populated at room temperature. The mathematical procedure in this case is well known (4). The trigonal field leaves an orbital singlet f_0; by virtue of the

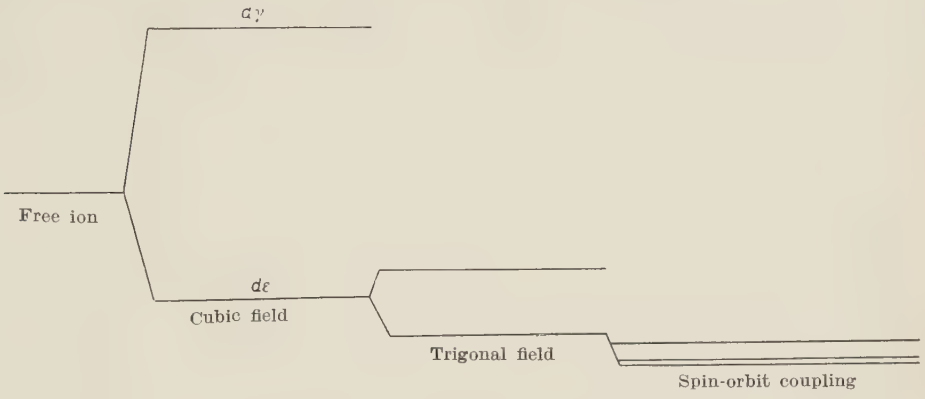

Fig. 1.

non-diagonal elements of T the orbital wave functions of the other states become:

$$F_{\pm 1} = f_{\pm 1} - \gamma f_{\mp 2}\,; \qquad F_{\pm 2} = f_{\pm 2} + \gamma f_{\mp 1}$$

(γ is still given by (5′)).

The $F_{\pm 1}$, $F_{\pm 2}$ are respectively δ and Δ above f_0. In the (f_0, $F_{\pm 1}$) orbital triplet it is still possible to define an L operator. The non-vanishing elements of $1/\sqrt{2}\cdot L^{\pm}$ have the value $A' = 1 - \sqrt{2}\,\gamma$; those of L_z, $A = 1 + 2\sqrt{2}\,\gamma$. With the same notation as (4) we find that the non-vanishing elements of the Λ tensor are:

$$\Lambda_{xx} = \Lambda_{yy} = \left(\frac{A'^2}{\delta} + \frac{2B^2}{\Delta}\right)\lambda^2,$$

where $B = \frac{1}{2}\langle 0|L^{\pm}|\mp 2\rangle = 1 + \gamma/\sqrt{2}$.

In the 5-fold spin multiplet, arising from (4′), the $-\varrho'(\boldsymbol{L}\cdot\boldsymbol{S})^2$ operator is represented by $3\varrho' S_z^2$. We are able to arrive at this result directly by noting that in the f_0 orbital ground state $L_xL_y = \ldots = L_z^2 = 0$; $L_x^2 = L_y^2 = 3$. It also follows that there are not off diagonal non-vanishing matrix elements. The effect of $-\varrho''(\boldsymbol{L}\cdot\boldsymbol{S})^3$ is easily calculated by observing that, in the orbital ground state, we have

$L_z = 0$; $L^{+3} = L^{-2}L^- = L^+L^-L^+ = 0$ (and similarly for L^- by interchanging L^+, L^-); $L^-L_zL^+ = -L^+L_zL^- = 6$; thus we find $(\boldsymbol{L}\cdot\boldsymbol{S})^3 = \frac{3}{2}(S^+S_zS^- - S^-S_zS^+)$,

and from the commutation rules:

$$(\boldsymbol{L}\cdot\boldsymbol{S})^3 = 6S_z^2 - 18\,.$$

Finally, omitting constant terms, the energy contribution coming from ϱ', ϱ'' is

$$3\varrho S_z^2 \qquad \text{where} \qquad \varrho = \varrho' - 2\varrho''\,. \tag{7}$$

3. – Paramagnetic behaviour.

If δ is of the order of $|\lambda|$, at sufficiently low temperature, $(kT < |\lambda|)$, so that only the $m = 0$, $m = \pm 1$ lower levels are populated, we are able to define a spin-Hamiltonian (with a fictitious spin $S = 1$):

$$H_s = \varepsilon S_z^2 + g_{\parallel}\beta H_z S_z + g_{\perp}\beta(H_x S_x + H_y S_y) + H^2 \text{ term} \tag{8}$$

(ε is given by (6)). Omitting terms of order of λ/Δ (which are calculated numerically a posteriori and whose expression is somewhat complicated) and the $0.0023\,g$ correction we find:

$$\begin{cases} g_{\parallel} = 2 + 3N_1^2(15 + 6y - y^2); \\ g_{\perp} = \sqrt{3}\,N_0 N_1[y^2 + 14y + 21 + (x+2)(2y+7)(y+1)]\,. \end{cases} \tag{9}$$

Both reduce to 3.5 in a cubic field. By using the partition function in the normal way we find

$$\chi_{\parallel} = C\,\frac{t}{e^t + 2} + \chi_{\parallel}^0; \qquad \chi_{\perp} = C'\,\frac{e^t - 1}{e^t + 2} + \chi_{\perp}^0\,, \tag{10}$$

where

$$C = \frac{2N\beta^2}{kT'}\,g_{\parallel}^2; \qquad C' = \frac{2N\beta^2}{kT'}\,g_{\perp}^2; \qquad kT' = \varepsilon; \qquad t = \frac{T'}{T}\,, \tag{10'}$$

and the $\chi_{\parallel}^0$, $\chi_{\perp}^0$ terms come from the H^2 terms of the spin-Hamiltonian.

3·1. – If $\delta \gg |\lambda|$ it is convenient to adopt the approximation of **2·1**. The spin-Hamiltonian keeps the form (8), but now $S = 2$. Its coefficients, obtained by a second order perturbation technique are determined by the Δ

tensor and by (4′). Now, to arrive at a better agreement with experimental data, we can include the third order terms without changing the form of the spin-Hamiltonian. We keep only the relevant terms in λ^3/δ^2, $\beta\lambda^2/\delta^2$. The third order contributions to the spin-Hamiltonian from the operator $\lambda \boldsymbol{L}\cdot\boldsymbol{S}+$ $+(\boldsymbol{L}+2\boldsymbol{S})\cdot\boldsymbol{H}$ are found by the same procedure as that in 2·1. For the term in λ^3/δ^2 we find:

$$-A'^2A\,\frac{\lambda^3}{\delta^2}\,(S^+S_zS^- - S^-S_zS^+)\,.$$

Omitting constants and corrections of the order of γ^2, the latter becomes $-2(\lambda^3/\delta^2)S_z^2$. Similarly, for the term in $\beta\lambda^2/\delta^2$ we find

$$-(2+A)\,\frac{A'^2}{2}\,\frac{\beta\lambda^2}{\delta^2}\cdot H_zS_z\,.$$

Hence, in the spin-Hamiltonian, the coefficients become:

$$\varepsilon = \lambda^2\left(\frac{A'^2}{\delta}+\frac{2B^2}{\Delta}\right)+3\varrho-2\,\frac{\lambda^3}{\delta^2}\,, \tag{11}$$

$$g_\parallel - 2.0023 = -(2+A)A'^2\,\frac{\lambda^2}{\delta^2}; \qquad g_\perp - 2.0023 = -2\lambda\left(\frac{A'^2}{\delta}+\frac{2B^2}{\Delta}\right),$$

from which we obtain:

$$g_\perp - 2.0023 = -2\left(\frac{\varepsilon-3\varrho}{\lambda}+2\,\frac{\lambda^2}{\delta^2}\right). \tag{11′}$$

Finally:

$$\begin{cases} \chi_\parallel = \dfrac{c}{T}\cdot\dfrac{\exp[-t]+4\exp[-4t]}{1+2\exp[-t]+2\exp[-4t]}+\dfrac{1}{10T''}; \\ \chi_\perp = \dfrac{c'}{T'}\cdot\dfrac{9-7\exp[-t]-2\exp[-4t]}{1+2\exp[-t]+2\exp[-4t]}+\dfrac{1}{4T''}\,, \end{cases} \tag{12}$$

where

$$c=\frac{2N\beta^2}{k}\,g_\parallel^2; \qquad c'=\frac{2N\beta^2}{3k}\,g_\perp^2\,; \qquad kT'=\varepsilon; \qquad t=\frac{T'}{T}; \qquad kT''=\delta\,. \tag{12′}$$

In both cases (10) and (12) the behaviour has the form predicted by Pryce and is in qualitative agreement with the experimental data of Jackson. At room temperature the expressions (12) agree with the Curie-Weiss law.

4. – Effect of covalent bonds.

When the ion is in the crystal it is probable that the matrix elements and coefficients of the operator (2) are modified. This occurs for two main reasons:

a) The electric field is no longer a central field but may be considered as a predominantly central field plus a field of lower symmetry (cubic or trigonal).

b) The orbital wave functions are no longer $3d$ orbital wave functions as in a paramagnetic ion but are the orbital wave functions of the $Fe(H_2O)_6^{++}$ complex.

Because of *a*) the spin-orbit coupling can no longer be represented by an operator of the form $\sum \zeta \boldsymbol{l}\cdot\boldsymbol{s}$ (the $\sum$ is extended over the electrons or electron holes which constitute the configuration), but will be a more general expression whose form may be determined by symmetry considerations ([7]). It may be convenient to express this operator as the sum of two, the first having the free ion form and the second the form indicated by STEVENS ([7]). The effect of *b*) can be studied by the method of molecular orbitals ([8]), which involves representing the wave function as a linear combination of the ionic $3d$ orbital and the atomic orbitals of the ligands. Following OWEN ([9]) we consider only the σ bonds related to the $d\gamma$ orbitals; no consideration will be given to the π bonds related to the $d\varepsilon$ orbitals. Hence the $d\varepsilon$ wave functions will still be f_0, $f_{\pm 1}$ (we will not consider here the effect of the off diagonal elements of T), but the $d\gamma$ normalized wave functions become:

$$f'_{\pm 2} = \alpha f_{\pm 2} + \psi_{\pm 2}\,, \tag{13}$$

the ψ's being suitable linear combinations of oxygen wave functions (see [8,9]) for their expressions referred to tetragonal axes). α is supposed to be close to unity. Since the experimental data are not sufficient for a numerical determination of all the parameters we limit ourselves to a qualitative analysis. Let us consider the Fe^{++} configuration as 4 electron holes. The wave functions are the antisymmetrical products of 4 individual wave functions, i.e. $\{f_1 f_{-1} f'_2 f'_{-2}\}$ for the orbital ground state: $\{f_1 f_{-1} f'_2 f'_{-2}\}$, ..., for other $d\varepsilon$ states and $\{f_1 f_{-1} f_0 f'_{-2}\}$,... for $d\gamma$ states. Since the major contribution to the λ term in operator (2) comes from that part of space where the electric field is strong, that is close to the

---

([7]) R. W. H. STEVENS: *Proc. Roy. Soc.*, A **219**, 542 (1953).
([8]) J. H. VAN VLECK: *Journ. Chem. Phys.*, **3**, 807 (1935).
([9]) J. OWEN: *Proc. Roy. Soc.*, A **227**, 183 (1955).

Fe nucleus, we will neglect correction a). Hence it appears that the matrix elements of the $\boldsymbol{l}$ operators between $d\varepsilon$ states are unaffected, while those between the ground state and the $d\gamma$ states are multiplied by α. For the same reason when we are dealing with the electric field strength, the numerical value of ζ should not change much. To this approximation the effect of the bonds can be represented by a reduction of some matrix elements, or more precisely by substituting αB for B in (11). If we suppose, rather arbitrarily, that the term ϱ behaves in the same way, we must substitute $1+2\alpha^2$ for 3 in (11). In the absence of more precise information about the value of α^2 we may say that it must be near that found for the $++$ ions, i.e. between 0.8 and 0.9.

5. – Conclusion and comparison with experimental data.

Expressions (10) and (12), corresponding respectively to δ small or δ large, show similar behaviour. As we show below, the latter hypothesis is in very good agreement with the experimental data, while with the former the agreement is not so good. In both cases $(kT'/2N\beta^2 g_\parallel^2)\chi_\parallel$, $(3kT/2N\beta^2 g_\perp^2)\chi_\perp$ are functions of t without any parameter. These functions have a single maximum. For the expressions (10) these maxima are respectively 0.236 and 0.364; they occur for t values close to 1.5 and 1.1. For the expressions (12) the corresponding values are 0.249 and 1.217. They occur for t values near to 1 and 0.72. The maximum value of $\chi_\perp$, (say $\overline{\chi}_\perp$) is proportional to $g_\parallel^2/\varepsilon$, and is, apart from its dependence on α, which is difficult to determine and is in any case unimportant, a function of δ only. We can deduce from (6) and (9) that this function has a minimum which occurs when δ is about $5|\lambda|$. Hence, in general, for a given experimental value of $\overline{\chi}_\perp$ we can determine two values for δ. In the same way $\overline{T\chi}_\perp$ the maximum value of $T\chi_\perp$, expressed as a function of δ shows a maximum which occurs when δ is about $4|\lambda|$. Now that we know δ we can determine T in terms of t and hence compare the experimental curve $\chi_\parallel(T)$, $\chi_\perp(T)$ with the theoretical curves (10) and (12). In fact for (10), the calculation of $\chi_\parallel^0$, $\chi_\perp^0$ and the minor corrections are given a posteriori. In the present case, using Jackson's experimental data, $\overline{\chi}_\perp = 0.0463$, $\overline{T\chi}_\perp = 4.123$, we found, by application of (10) and related formula, $\delta = 2|\lambda|$. But the agreement with the experimental behaviour is not very good mainly because of the large values of $\chi_\parallel^0$, $\chi_\perp^0$.

A very close agreement, however, is obtained with (12) and related formulae. Despite the high number of unknown parameters (δ, γ, α) the equation (11′) is a fairly restrictive condition because it is little influenced by any variation of the parameters such that their values remain physically reasonable. In effect g and ε may be deduced from the experimental values of $\overline{T\chi}_\perp$ and $\overline{\chi}_\perp$ or T'. Now (11′) is satisfied well by the experimental values

$\varepsilon = 10.9\ \text{cm}^{-1}$ ($T' = 15.7\ ^\circ\text{K}$), $g_\perp = 2.12$ when reasonable values are assigned to the other parameters. Thus, if we put $\alpha^2 = 0.9$ we find $\delta = 1\,200\ \text{cm}^{-1}$, $A' = 0.75$. The δ value is little influenced by the choice of α^2, but these values are not very exact. Very good agreement is obtained between equation (12) and the experimental $\chi_\perp(T)$. The agreement between theory and experiment for $\chi_\parallel(T)$ is satisfactory.

TABLE I.

t	$1/t$	$T'\chi_\perp/c'$	$T'\chi_\parallel/c$
0.05	20	0.155	0.046 5
0.1	10	0.319	0.086 5
0.15	6.67	0.491	0.120
0.2	5	0.607	0.148
0.3	3.33	1.042	0.189
0.4	2.5	1.422	0.215
0.5	2	1.805	0.231
0.6	1.66	2.184	0.240
0.7	1.43	2.554	0.243 5
0.8	1.25	2.915	0.247
0.9	1.11	3.266	0.248
1	1	3.604	0.249
1.2	0.833	4.247	0.248
1.6	0.625	5.389	0.237
2	0.5	6.333	0.215
2.5	0.4	7.236	0.176
3	0.333	7.868	0.136
3.5	0.286	8.288	0.099 7
4	0.25	8.560	0.070 6
5	0.2	8.833	0.033 3
6	0.167	8.938	0.014 8
8	0.125	8.992	0.002 7
10	0.1	8.999	0.000 45

Table I gives the calculated values of $T'\chi_\parallel/c$ and $T'\chi_\perp/c'$, without the contributions from the temperature independent terms. These have been calculated from (12), which implicitly assumes that the second energy level is at exactly 4ε. Numerical calculation has verified that this is so nearly true that negligible change results in χ when the correct energy is used.

* * *

I am deeply indebted to Professor M. H. L. PRYCE, who suggested this work to me, for much help, many suggestions and much useful discussion, and to Dr. L. C. JACKSON for giving me access to his unpublished experimental data.

I wish to thank my wife for help in the numerical calculations and Dr. R. Englman and Dr. S. Koide for discussion of some points in the present work.

I wish to express my gratitude to the Italian C.N.R. for the gift of a Scholarship and to the H. H. Wills Physics Laboratory for the hospitality and facilities given to me.

RIASSUNTO

In questo lavoro viene studiato il comportamento magnetico del fluosilicato ferroso esaidrato utilizzando i dati sperimentali ottenuti da Jackson. Poichè, come mostrano i risultati, comportamenti non molto diversi a bassa temperatura si ottengono sia nell'ipotesi che l'effetto del campo trigonale prevalga su quello dell'accoppiamento spin-orbita, sia in quella che i due effetti abbiano lo stesso ordine di grandezza, i calcoli sono stati svolti in entrambi i casi. Nel primo caso, (per il quale si ha il migliore accordo con i dati sperimentali), viene mostrata l'opportunità di introdurre nell'hamiltoniana di spin (la cui forma tuttavia rimane invariata) i termini di III ordine. È anche preso in esame l'effetto di eventuali legami covalenti. L'accordo con i dati sperimentali è molto buono.

On the Bloch Integral Equation at Low Temperatures.

B. JAKŠIĆ

Institute «Ruđer Bošković» and The University of Zagreb - Zagreb, Yugoslavia

(ricevuto il 2 Gennaio 1958)

Summary. — It is shown that the Bloch integral equation for the factor of conductivity of metals is equivalent in the first approximation at low temperatures to a differential equation on the Fermi surface $E = \zeta$. In the special case $w \ll 1$, the second approximation can also be obtained from a single differential equation. The method is of interest for metals with anisotropic Fermi surfaces.

In a recent paper by Prof. SUPEK (1) it has been shown that the simplified Bloch integral equation can be reduced, at low temperatures, to a differential equation on the Fermi surface $E = \zeta$.

We should like to show in this note that such reduction is possible also in the most general case. At the same time the proof will be greatly simplified by using Kohler's variation principle (2) for the Bloch equation.

The notation used here will be the same as in the previous papers (3,4). The electron spin variable $\sigma = \pm 1$, and the phonon polarization variable $s = 1, 2, 3$ will not be written down explicitely, so that the integrals

$$\int \ldots \mathrm{d}^3k \qquad \text{and} \qquad \int \ldots \mathrm{d}^3q \,,$$

over the wave vectors $\boldsymbol{k}$ and $\boldsymbol{q}$ will always mean

$$\sum_{\sigma} \int \ldots \mathrm{d}^3k \qquad \text{and} \qquad \sum_{s} \int \ldots \mathrm{d}^3q \,,$$

respectively.

(1) I. SUPEK: *Zeits. f. Phys.*, **149**, 324 (1957).
(2) M. KOHLER: *Zeits. f. Phys.*, **124**, 772 (1948); **125**, 679 (1949).
(3) V. GLASER and B. JAKŠIĆ: *Nuovo Cimento*, **7**, 259 (1958).
(4) V. GLASER and B. JAKŠIĆ: *Glasnik*, **12**, 257 (1957).

The function $\Phi(\boldsymbol{k})$ is defined as usual by

$$f(\boldsymbol{k}) = f_0(E) - \frac{\mathrm{d}f_0}{\mathrm{d}E}\Phi(\boldsymbol{k}) . \tag{1}$$

Here Φ is a linear function of the electric field $\boldsymbol{F}$: $\Phi = \Phi_{\alpha} F_{\alpha}$. The integral [illegible] condition is expressed through the Bloch integral equation

$$\int [K(\boldsymbol{k}, \boldsymbol{q}; \boldsymbol{k}) - K(\boldsymbol{k}, \boldsymbol{q}; \boldsymbol{k})] \Phi(\boldsymbol{k}) \, \mathrm{d}\Omega_{\boldsymbol{k}} = -\frac{\partial \Phi}{\partial E} , \tag{2}$$

which can be derived from the variation principle:

$$\delta L[\Phi] = 0 , \tag{3}$$

with

$$L[\Phi] = -\frac{1}{2}\int K(\boldsymbol{k}, \boldsymbol{q}; \boldsymbol{k}')[\Phi(\boldsymbol{k}) - \Phi(\boldsymbol{k}')]^2 \mathrm{d}^3k \mathrm{d}^3k' \mathrm{d}^3q - \\ - \frac{e}{(2\pi)^3}\int \frac{\mathrm{d}f_0}{\mathrm{d}E} F \Phi(\boldsymbol{k}) \mathrm{d}^3k . \tag{4}$$

The kernel $K(\boldsymbol{k}, \boldsymbol{q}; \boldsymbol{k}')$ [illegible] The Umklapp-processes are neglected in the Bloch theory.

The physically interesting quantity is the conductivity tensor $\sigma_{\alpha\beta}$ defined by

$$\sigma_{\alpha\beta} = -\frac{e}{(2\pi)^3}\int \frac{\mathrm{d}f_0}{\mathrm{d}E} v_{\alpha} \Phi_{\beta}(\boldsymbol{k}) \mathrm{d}^3k . \tag{5}$$

The last step in solving the problem will be to introduce the new variables $u = u(\varepsilon, \zeta)$, k, the coordinates of being surface harmonics defined on the energy surfaces $E(\boldsymbol{k}) = E$. Then we can develop Φ in powers of $\varepsilon = (E - \zeta)/kT$

$$\Phi = \sum_{n=1}^{\infty} \Phi_n(u) \varepsilon^n . \tag{6}$$

and use (6) as a [illegible] with unknown functions $\Phi_n(u)$. Inserting (6) into (4) and defining the quantities

$$\Gamma_{nn'}(u, u') = \int K_{\alpha}(\boldsymbol{k}, \boldsymbol{q}, \boldsymbol{k}') \varepsilon^{n} \frac{\partial g}{\partial E} \mathrm{d}E \frac{\partial g}{\partial E'} \mathrm{d}E' \mathrm{d}^3q . \tag{7a}$$

$$\tilde{\Gamma}_{nn'}(u, u') = \int K_{\alpha}(\boldsymbol{k}, \boldsymbol{q}, \boldsymbol{k}') \varepsilon^{n} (\varepsilon'^{n'} - \varepsilon^{n}) \frac{\partial g}{\partial E} \mathrm{d}E \frac{\partial g}{\partial E'} \mathrm{d}E' \mathrm{d}^3q . \tag{7b}$$

$$(7c) \qquad \Gamma_{m,n}(u, u') = \int K_s(\boldsymbol{k}, \boldsymbol{q}, \boldsymbol{k}')(\varepsilon'^m - \varepsilon'^m)(\varepsilon'^n - \varepsilon^n) \cdot \frac{\sqrt{g'}}{|\nabla E'|\sqrt{g'(\zeta)}}\,\mathrm{d}E' \,\frac{\sqrt{g}}{|\nabla E|\sqrt{g(\zeta)}}\,\mathrm{d}E\,\mathrm{d}^3q\,,$$

$$(7d) \qquad \varrho_m(u) = -\frac{e}{(2\pi)^3}\int \frac{\mathrm{d}f_0}{\mathrm{d}E}\, n\varepsilon^m \sqrt{\frac{g}{g(\zeta)}}\,\mathrm{d}E\,,$$

where n_i is the normal to the energy surface E, and

$$K_s(\boldsymbol{k}, \boldsymbol{q}, \boldsymbol{k}') = \tfrac{1}{2}[K(\boldsymbol{k}, \boldsymbol{q}; \boldsymbol{k}') + K(\boldsymbol{k}', -\boldsymbol{q}; \boldsymbol{k})]\,,$$

$$g = \mathrm{Det}\,(g_{\alpha\beta})\,, \qquad g' = g(u', E')\,, \qquad g'(\zeta) = g(u', \zeta)\,,$$

$$\varepsilon' = \varepsilon(\boldsymbol{k}') = \varepsilon(u', E')\,, \qquad \nabla E' = \nabla E(\boldsymbol{k}') = \nabla E(u', E')\,,$$

we can write $L[\Phi]$ in the following form

$$(8) \qquad L = \int \mathcal{L}(u, u')\,\mathrm{d}S\,\mathrm{d}S', \qquad \mathrm{d}S = \sqrt{g(\zeta)}\,\mathrm{d}u^1\,\mathrm{d}u^2\,.$$

Here the integration includes the summation over the electron spin σ, and

$$(8a) \qquad \mathcal{L}(u, u') = -\tfrac{1}{2}\sum_{m,n}[\Gamma_{m+n}(u, u')(\Phi_m(u') - \Phi_m(u))(\Phi_n(u') - \Phi_n(u)) +$$

$$+ 2\,\tilde{\Gamma}_{m,n}(u, u')(\Phi_m(u') - \Phi_m(u))\,\Phi_n(u) + \Gamma_{m,n}(u, u')\,\Phi_m(u)\,\Phi_n(u)] + \sum_m \varrho_m \Phi_m\,.$$

In this way the problem is reduced to a two-dimensional one, but the number of unknown functions is now infinite.

In (8a) $\Phi_m(u')$ appears only in the combination $\Phi_m(u') - \Phi_m(u)$ which can be developed in the Taylor series

$$(9) \qquad \Phi_m(u') - \Phi_m(u) = \sum_{r=1}^{\infty} \frac{1}{r!}\,\partial_{\alpha_1} \ldots \partial_{\alpha_r}\Phi_m(u)\,\Delta u^{\alpha_1} \ldots \Delta u^{\alpha_r}\,.$$

At low temperatures this series will rapidly converge. After the integration over dS', we obtain

$$(10) \qquad L = \int \mathcal{L}(u)\,\mathrm{d}S\,,$$

where

$$(10a)\qquad \mathcal{L}(u) = -\frac{1}{2}\sum_{m,n}\Big|\sum_{r,s}\frac{1}{r!\,s!}\,\Gamma^{\lambda_1\dots\lambda_{r+s}}_{m,n}(u)\big(\partial_{\lambda_1}\dots\partial_{\lambda_r}\Phi_m(u)\big)\big(\partial_{\lambda_{r+1}}\dots\partial_{\lambda_{r+s}}\Phi_n(u)\big) +$$

$$+\,2\sum_{r}\frac{1}{r!}\,\tilde{\Gamma}^{\lambda_1\dots\lambda_r}_{m,n}(u)\big(\partial_{\lambda_1}\dots\partial_{\lambda_r}\Phi_m(u)\big)\Phi_n(u) + \Gamma_{m,n}(u)\Phi_m(u)\Phi_n(u)\Big| + \sum_m \varrho_m(u)\Phi_m(u)\,.$$

The new quantities $\Gamma^{\lambda_1\dots\lambda_r}_{m}(u)$, $\tilde{\Gamma}^{\lambda_1\dots\lambda_r}_{m,n}(u)$ and $\Gamma_{m,n}(u)$ are obtained from the old ones (7*a*, *b*, *c*) by integration over $\Delta u^{\lambda_1}\dots\Delta u^{\lambda_r}\,\mathrm{d}S'$, i.e.

$$(11a)\qquad \Gamma^{\lambda_1\dots\lambda_r}_{m}(u) = \int K_s(\boldsymbol{k},\boldsymbol{q},\boldsymbol{k}')\,\Delta u^{\lambda_1}\dots\Delta u^{\lambda_r}\varepsilon'^m\,\mathrm{d}^3k'\,\mathrm{d}^3q\,\frac{\sqrt{g}}{|\nabla E|\sqrt{g(\zeta)}}\,\mathrm{d}E\,,$$

$$(11b)\qquad \tilde{\Gamma}^{\lambda_1\dots\lambda_r}_{m,n}(u) = \int K_s(\boldsymbol{k},\boldsymbol{q},\boldsymbol{k}')\,\Delta u^{\lambda_1}\dots\Delta u^{\lambda_r}\varepsilon'^m(\varepsilon'^n-\varepsilon^n)\,\mathrm{d}^3k'\,\mathrm{d}^3q\,\frac{\sqrt{g}}{|\nabla E|\sqrt{g(\zeta)}}\,\mathrm{d}E\,,$$

$$(11c)\qquad \Gamma_{m,n}(u) = \int K_s(\boldsymbol{k},\boldsymbol{q},\boldsymbol{k}')(\varepsilon'^m-\varepsilon^m)(\varepsilon'^n-\varepsilon^n)\,\mathrm{d}\,k'\,\mathrm{d}^3q\,\frac{\sqrt{g}}{|\nabla E|\sqrt{g(\zeta)}}\,\mathrm{d}E\,.$$

Since the Umklapp-processes are not taken into account in the Bloch equation, we have to consider only those cases where they are really negligible. This will be the case for Fermi surfaces $E=\zeta$ which do not come too close to the boundary of the first Brillouin zone. Such surfaces are simply closed, and the variation principle gives us the following system of differential equations for $\Phi_n(u)$

$$(12)\qquad \sum_n\Big[\sum_{r,s}\frac{(-1)^{r+1}}{r!\,s!}\,\frac{1}{\sqrt{g(\zeta)}}\,\partial_{\lambda_1}\dots\partial_{\lambda_r}\sqrt{g(\zeta)}\,\Gamma^{\lambda_1\dots\lambda_{r+s}}_{m,n}(u)\,\partial_{\lambda_{r+1}}\dots\partial_{\lambda_{r+s}}\Phi_n(u) -$$

$$-\sum_r\frac{1}{r!}\,\tilde{\Gamma}^{\lambda_1\dots\lambda_r}_{n,m}(u)\,\partial_{\lambda_1}\dots\partial_{\lambda_r}\Phi_n(u) +$$

$$+\sum_r\frac{(-1)^{r+1}}{r!}\,\frac{1}{\sqrt{g(\zeta)}}\,\partial_{\lambda_1}\dots\partial_{\lambda_r}\sqrt{g(\zeta)}\,\tilde{\Gamma}^{\lambda_1\dots\lambda_r}_{m,n}(u)\Phi_n(u) - \Gamma_{m,n}(u)\Phi_n(u)\Big| = -\varrho_m(u)\,.$$

In this way the Bloch integral equation is transformed into an equivalent infinite system of differential equations. To analyse this system at low temperatures it is necessary to estimate the temperature dependence of the Γ's. This can be done without any assumption about the matrix element or the vibrational spectrum of the lattice. The only assumption that we shall make is that $w = u/|\boldsymbol{v}| < 1$, i.e. that the velocity of phonons is smaller than the velocity of electrons. The leading term at low temperatures will be of an

order not lower than

$$(13a)\qquad \Gamma_{n}^{\nu_1\dots\nu_r}(u)\sim\begin{cases} T^{r+3}, & r+n \text{ even}\\ T^{r+4}, & r+n \text{ odd}\end{cases}$$

$$(13b)\qquad \tilde{\Gamma}_{m,n}^{\nu_1\dots\nu_r}(u)\sim\left.\begin{cases} T^{r+3}, & r+m+n \text{ even}\\ T^{r+4}, & r+m+n \text{ odd}\end{cases}\right\} m\neq 0$$

$$\tilde{\Gamma}_{m,0}^{\nu_1\dots\nu_r}(u) = 0\,,$$

$$(13c)\qquad \Gamma_{m,n}(u)\sim\left.\begin{cases} T^{3}, & m+n \text{ even}\\ T^{4}, & m+n \text{ odd}\end{cases}\right\} n,\, m\neq 0$$

$$\Gamma_{m,0}(u) = 0\,,$$

$$(13d)\qquad \varrho_m(u)\sim\begin{cases} 1 & m \text{ even}\\ T & m \text{ odd}\end{cases}$$

Using these estimates we can obtain from (12) the behaviour of Φ_n at low temperatures. The singularity at $T=0$ will not be worse than

$$(13e)\qquad \Phi_0\sim\frac{1}{T}\,,\quad \Phi_{2n+1}\sim\frac{1}{T^4}\,,\quad \Phi_{2n}\sim\frac{1}{T^3}\,.$$

Knowing the behaviour of all quantities at low temperatures, it is easy to write down the leading term in $\mathcal{L}(u)$

$$(14)\qquad \mathcal{L}(u) = -\tfrac{1}{2}[\Gamma_0^{\nu\beta}(u)\big(\partial_\nu\Phi_0(u)\big)\big(\partial_\beta\Phi_0(u)\big) + 2\sum_{n=0}^{\infty}\tilde{\Gamma}^{\nu}_{0,2n+1}(u)\big(\partial_\nu\Phi_0(u)\big)\Phi_{2n+1}(u) + \\ + \sum_{m,n=0}^{\infty}\Gamma_{2m+1,2n+1}(u)\Phi_{2m+1}(u)\Phi_{2n+1}(u)] + \varrho_0(u)\Phi_0(u).$$

The Γ's and ϱ_0 are taken here in the lowest approximation. The corresponding equations are

$$(15)\qquad \begin{cases} \dfrac{1}{\sqrt{g(\zeta)}}\,\partial_\nu\sqrt{g(\zeta)}\Gamma_0^{\alpha\beta}(u)\,\partial_\beta\Phi_0(u) + \displaystyle\sum_{n=0}^{\infty}\frac{1}{\sqrt{g(\zeta)}}\,\partial_\nu\sqrt{g(\zeta)}\tilde{\Gamma}^{\alpha}_{0,2n+1}(u)\Phi_{2n+1}(u) = \\ \qquad\qquad -\dfrac{e}{(2\pi)^3\hbar}\,n(\zeta)\,, \\ \displaystyle\sum_{n=0}^{\infty}\Gamma_{2m+1,2n+1}(u)\Phi_{2n+1}(u) = -\tilde{\Gamma}^{\alpha}_{0,2m+1}(u)\,\partial_\nu\Phi_0(u)\,. \end{cases}$$

Let us cut-off the second system of equations at $n = N$. Then this is an ordinary non-homogeneous system of $(N+1)$ linear equations for $(N+1)$ variables Φ_{2n+1} $(n = 0, 1, ..., N)$ which can be solved immediately (for physical reasons we assume the determinant of the system to be non-singular). In this way we can eliminate Φ_{2n+1} in the first equation, so that

$$\sum_{n=0}^{N} \tilde{\Gamma}^{\lambda}_{0,2n+1} \Phi_{2n+1} = -\sum_{m,n=0}^{N} \tilde{\Gamma}^{\lambda}_{0,2n+1} \Gamma^{-1}_{2n+1,2m+1} \tilde{\Gamma}^{\beta}_{0,2m+1} \partial_\beta \Phi_0 = -\tilde{\Gamma}^{\alpha} \Gamma^{-1} \tilde{\Gamma}^{\beta} \partial_\beta \Phi_0 .$$

Here Γ^{-1} is the inverse of the matrix $(\Gamma_{2m+1,2n+1})$. We now let $N \to \infty$ and, for physical reasons, assume the convergence of the quantity $\tilde{\Gamma}^{\lambda} \Gamma^{-1} \tilde{\Gamma}^{\beta}$. So, after the elimination of Φ_{2n+1}, we obtain the differential equation

$$\frac{1}{\sqrt{g(\zeta)}} \partial_\alpha \sqrt{g(\zeta)} \Gamma^{\alpha\beta}(u) \partial_\beta \Phi_0(u) = -\frac{e}{(2\pi)^3 \hbar} n(\zeta) , \tag{16}$$

where

$$\Gamma^{\alpha\beta} = \Gamma^{\beta\alpha} = \Gamma_0^{\alpha\beta} - \tilde{\Gamma}^{\lambda} \Gamma^{-1} \tilde{\Gamma}^{\beta} . \tag{16a}$$

This equation follows from the variation principle with

$$L = -\frac{1}{2} \int \Gamma^{\alpha\beta}(u) (\partial_\alpha \Phi_0(u)) (\partial_\beta \Phi_0(u)) \, \mathrm{d}S + \frac{e}{(2\pi)^3 \hbar} \int n \Phi_0(u) \, \mathrm{d}S , \tag{16b}$$

where the integration extends over the simply closed Fermi surface $E = \zeta$, and includes the summation over the electron spin σ. From the solution Φ_0 we obtain the leading term of the conductivity tensor at low temperatures:

$$\sigma_{ij} = \frac{e}{(2\pi)^3 \hbar} \int n_i \Phi_{0,j}(u) \, \mathrm{d}S \sim \frac{1}{T^5} . \tag{17}$$

In this way we have shown that the leading term of the conductivity at low temperatures can be obtained from a differential equation for a single function, defined on the Fermi surface $E = \zeta$. The method also allows the calculation of higher order terms. Here one must bear in mind that $T = 0$ is an essential singularity of the differential equations (12). Namely, the Γ's are not polynomials in T, but of the form

$$\sum_{n=n_0}^{\infty} a_n(T) T^n , \qquad a_n(T) = a_n(0) + \sum_m p_{n,m}(T) \exp\left[-\frac{c_{n,m}}{T}\right] ,$$

i.e. they have an essential singularity at $T = 0$ due to the exponentials. For

that reason Φ_n will be of the form

$$\sum_{m \leqslant m_n} b_{n,m}(T)\, T^{-m} ,$$

where $b_{n,m}(T)$ is similar to $a_n(T)$.

Our method of successive approximations consists in calculating, step by step, the functions $b_{n,m}(T)$. In general, higher order terms will be determined by an infinite system of differential equations and not simply by a single differential equation.

In case $w \ll 1$, it is sufficient to retain only the lowest power of w. This means that the variation with energy of all quantities, except the Fermi function, can be neglected, so that $\Gamma^{\alpha_1 \ldots \alpha_r}_{n+m}(u)$, $\tilde{\Gamma}^{\alpha_1 \ldots \alpha_r}_{n,m}(u)$, $\Gamma_{n,m}(u)$ will vanish, if $n+m$ is odd, and $\varrho_n(u)$, if n is odd. Now it is easy to see that $\Phi_{2n+1} = 0$, so that the first approximation follows from the differential equation (16), with $\Gamma^{\alpha\beta} = \Gamma^{\alpha\beta}_0$. It is interesting that the second approximation in this case can also be reduced to a single differential equation, because the elimination of Φ_{2n}, $n \neq 0$, consists in solving a linear algebraic system of equations, like that one in (15).

In the case of the Debye isotropic model and the usual approximation of the matrix element, we can calculate the lowest approximation for the tensor $\Gamma^{\alpha\beta}$ in the differential equation (16). First of all, in this approximation $\Gamma^{\alpha\beta} = \Gamma^{\alpha\beta}_0$, where $\Gamma^{\alpha\beta}_0$ can be calculated from the definition (11a). After integration over $\boldsymbol{k}'$, we approximate the energy surface, at the point $\boldsymbol{k}$, by the tangential plane, i.e. we put

$$E(\boldsymbol{k} + \boldsymbol{q}) \approx E(\boldsymbol{k}) + \boldsymbol{q} \cdot \nabla E ,$$

so that we can write

$$\delta[E(\boldsymbol{k}) \pm \hbar\omega(\boldsymbol{q}, 0) - E(\boldsymbol{k} + \boldsymbol{q})] \approx \frac{1}{q\,|\nabla E|}\, \delta(\cos\theta + w) .$$

Here we have introduced a local polar system with ∇E as the polar axis and w is equal to $u_0/|\boldsymbol{v}|$. The integration over $\boldsymbol{q}$ can now be easily performed. The integration over θ will give us the factor $\Theta_+(1 - w)$, with $\Theta_+(x) = +1$ for $x > 0$, and $\Theta_+(x) = 0$ for $x < 0$, and the integration over φ will be reduced, because of the assumed elastic isotropy of the crystal, to calculating the mean value

$$\Delta u^\alpha \Delta u^\beta = \frac{1}{2\pi} \int_0^{2\pi} \Delta u^\alpha \Delta u^\beta \, \mathrm{d}\varphi .$$

This quantity is a symmetric tensor which in our approximation and for

$w < 1$ can be equal only to $\alpha g^{\alpha\beta}$, where α is a constant that can be easily determined by multiplication with $g_{\alpha\beta}$. The result is

$$\Delta u^{\alpha} \Delta u^{\beta} = \frac{q^2}{2} (1 - w^2) g^{\alpha\beta} .$$

In our approximation ∇E and $g^{\alpha\beta}$ ought to be taken on the surface $E = \zeta$. Then the integration over E and q can easily be performed. The value of $I^{\alpha\beta}$ obtained in this way for $w < 1$, will be

$$I^{\alpha\beta} = \varrho g^{\alpha\beta} , \tag{18}$$

where

$$\varrho = \lambda w^2 (1 - w^2) , \tag{18a}$$

$$\lambda = \frac{\Omega_0 \hbar q_m^8 I_5 C^2}{9 (2\pi)^4 M (k\Theta)^3} \left(\frac{T}{\Theta} \right)^5 , \tag{18b}$$

with the usual definitions

$$I_5 = \int_0^{\Theta/T} \frac{x^5}{(e^x - 1)(1 - e^{-x})} \, \mathrm{d}x , \qquad \hbar u_0 q_m = k\Theta . \tag{18c}$$

In case $w \ll 1$, this partial differential equation is identical to the one found by Prof. SUPEK (1).

If $w > 1$ in some region of the Fermi surface $E = \zeta$, the conductivity will depend exponentially on the temperature. We shall not discuss this case here.

For surfaces with an axis of symmetry it is easy to find the exact solution of the differential equation (16). Unfortunately, such surfaces are not of great physical interest. In practice we shall always restrict the number of trial functions $\Phi_n(u)$ to a finite number, let us say to $n = 0, \ldots, N$. In this way we shall obtain a finite system of differential equations for these functions. Such system can always be solved by using an electronic computer and the eigenvalues of the conductivity tensor σ_{ij}, obtained in this approximation, will not exceed the exact values. This result follows from Kohler's variation principle.

—

RIASSUNTO (*)

Si dimostra che l'equazione integrale di Bloch nella teoria della conduttività dei metalli è equivalente, in prima approssimazione, alle basse temperature a un'equazione differenziale sulla superficie di Fermi $E = \xi$. Nel caso speciale $w \ll 1$, si può ottenere anche la seconda approssimazione ricorrendo ad un'unica equazione differenziale. Il metodo presenta interesse per metalli con superfici di Fermi anisotrope.

(*) *Traduzione a cura della Redazione.*

Starting Potential for the Coaxial Cylinder Coronas in Hydrogen Under Low Frequency Silent Electric Discharge.

D. P. Jatar

Department of Physics - University of Saugar

(ricevuto il 3 Gennaio 1958)

Summary. — The starting potential for the low frequency silent electric discharge between coaxial glass cylinders has been measured over a range of pressure from 3 to 700 mm Hg. It is suggested that the starting potential is analogous to the intermittent pre-onset burst pulse corona. The other onset potentials have been evaluated from the current-potential characteristics and agree closely with those evaluated from the variation of the Joshi effect.

1. – Introduction.

From studies [1] of a number of physico-chemical reactions under electrical discharge, especially in Siemens type glass ozonizers, Joshi [2] found that, to start the reaction, a minimum critical potential, V_m, has to be exceeded. This V_m was indicated by a sudden rise in the current flowing through, and the power dissipated in the system. The importance of V_m for the Joshi effect was also pointed out by Joshi [2-3] who first observed the non-occurrence of Joshi effect below V_m in spite of a wide change in the operative conditions such as the intensity and frequency of light [4], the frequency of a.c. supply [5]

[1] S. S. Joshi: *Trans. Farad. Soc.*, **25**, 108, 118, 143 (1929).
[2] S. S. Joshi: *Curr. Sci.*, **8**, 548 (1939).
[3] S. S. Joshi: *Curr. Sci.*, **22**, 389 (1945); **15**, 281 (1946).
[4] S. S. Joshi and P. G. Deo: *Curr. Sci.*, **11**, 306 (1943).
[5] S. S. Joshi and K. Z. Lad: *Proc. Ind. Acad. Sci.*, **22**, 293 (1945).

and the current detectors (6). This has been confirmed by subsequent studies of a number of workers. In spite of the original suggestion of JOSHI (2), however, that for simple gases this V_m may be identified with, or simply related to, the corresponding Paschen potential, no attempt appears to have been made to identify this threshold potential with one of the starting potentials for d.c. corona.

Under d.c. excitation extensive studies using point-to plane, coaxial cylinder and other coronas have been made by a number of workers. (7). These studies have shown that in such gaps with two electrodes of different size, breakdown takes place in two steps. Due to the local concentration of electrical field, breakdown first proceeds at the electrodes, one or both; and ultimately the gap as a whole breaks down and a spark passes. The peculiar forms of these localized and partial breakdowns are characterized by different visual forms, different thresholds, slightly different mechanisms and different names depending on their visual appearance. The present studies were undertaken with a view to investigate if similar corona regimes are obtained under the silent electric discharge also.

2. – Experimental method.

The general experimental arrangement was essentially similar to that used by earlier workers (8). The hydrogen used was preapred by electrolysis of barium hydroxide solution and finally dried over P_2O_5. The discharge tube was an all glass ozonizer of the Siemens type with an outer glass cylinder of inner diameter 1.70 cm and the inner glass cylinder of outer diameter 1.06 cm, the thickness of the glass walls being 0.135 cm each. It was filled with hydrogen in the range of pressure from 3 to 715 mm Hg, and was excited by an H.T. transformer using 50 Hz a.c. The potential applied to the discharge tube was measured by a procedure similar to that of THORNTON (9), and in the present case is accurate to $\pm$ 0.03 kV for potentials up to 3.0 kV and to $\pm$ 0.05 kV for potentials beyond 3.0 kV. The current flowing through the system was measured by a galvanometer in the plate circuit of the detector, RCA 30, connected to the L.T. line across a transformer. To observe the current waveform, the potential drop across a serial resistance of 1.2 MΩ in the L.T. line was fed to the vertical input of the cathode ray oscillograph, Dumont 274 A.

(6) S. S. JOSHI: *Proc. Ind. Acad. Sci.*, **22**, 225 (1945).
(7) L. B. LOEB: *Fundamental processes of electrical discharge in gases* (New York, 1939).
(8) P. G. DEO: *Ind. Journ. Phys.*, **18**, 84 (1944).
(9) W. M. THORNTON: *Phil. Mag.*, **28**, 666 (1939).

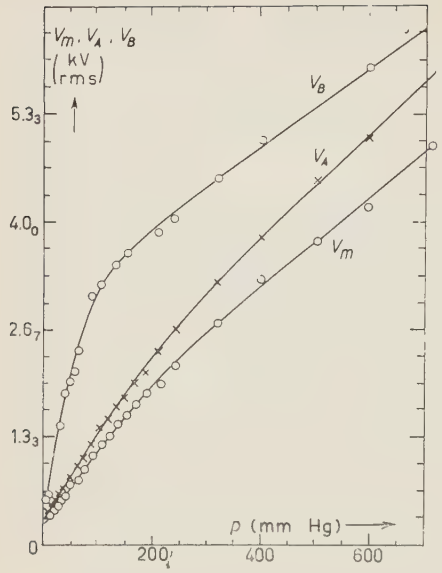

Fig. 1. – Variation of Corona thresholds, V_m, V_A, and V_B with the pressure of the gas.

3. – Results.

Corresponding to each pressure, no current was registered in the galvanometer below a certain critical value of the potential applied to the tube. At this critical potential, V_m, the galvanometer suddenly registered a current. This was accompanied by the initiation of an intermittent glow in the discharge tube characteristic of the gas and also the appearance of pulses on the sinusoidal current waveform. Values of V_m observed directly as above, are reported in Table I and are also shown in Fig. 1.

Beyond V_m, the potential applied to the tube was increased gradually and the current was registered both when the tube was in dark, i_D and when it was under the light of a 200 W bulb, i_L. Out of a large number of pressures investigated, typical current potential curves, when the tube was in dark, for a few pressures are shown in Fig. 2. It is seen that these current-potential characteristics show three distinct regions: (i) the initial region of rapid rise near V_m, up to the potential V_A, (ii) the intermediate sag corresponding to a low rise in the conductivity, up to V_B, followed by (iii) a fast rise in the conductivity. The transition from the initial fast rise to the sag region is well marked whereas that from the sag region to the subsequent fast rise is not so sharp. While these will be discussed in detail elsewhere, it is suggested here that these two transitions

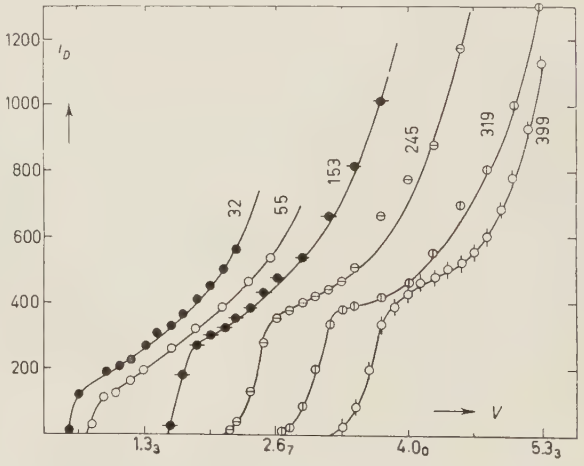

Fig. 2. – Typical current-potential characteristics for hydrogen. Current in arbitrary units. Potential in kV (r.m.s.). Numbers on curves indicate pressure of hydrogen in mm Hg.

TABLE I. – *Influence of gas pressure on the threshold potentials in hydrogen.*

p in mm Hg	V_m in kV		V_A (*) in kV	V_B (*) in kV
	direct	computed (*)		
3.5	0.29	0.29		
7	0.32	0.31	0.40	0.53
12	0.35	0.32	0.40	0.60
18	0.45	0.37	0.45	—
24	0.50	0.47	0.53	—
27	0.53	0.48	0.60	—
32	0.57	0.53	0.67	1.47
41	0.67	0.62	0.85	1.87
49	0.71	0.69	0.80	2.00
57	0.77	0.74	0.93	2.13
65	0.80	0.76	1.00	2.40
76	0.96	0.90	1.07	—
91	1.09	1.07	1.25	3.07
106	1.27	1.23	1.47	3.20
120	1.33	1.33	1.60	3.47
137	1.47	1.44	1.73	3.47
153	1.60	1.57	1.85	3.60
170	1.73	1.70	2.00	—
190	1.87	1.80	2.13	—
212	2.00	1.98	2.40	3.85
245	2.20	2.19	2.67	4.00
319	2.73	2.78	3.20	4.53
399	3.33	3.39	3.80	5.00

(*) Computed from current characteristics.

correspond to transitions from one to the other corona regime. The two transition potentials, V_A and V_B, can be computed from the current-potential characteristics, in addition to the threshold potential V_m, which can also be computed from the initial fast rise. Fig. 1 shows the variation

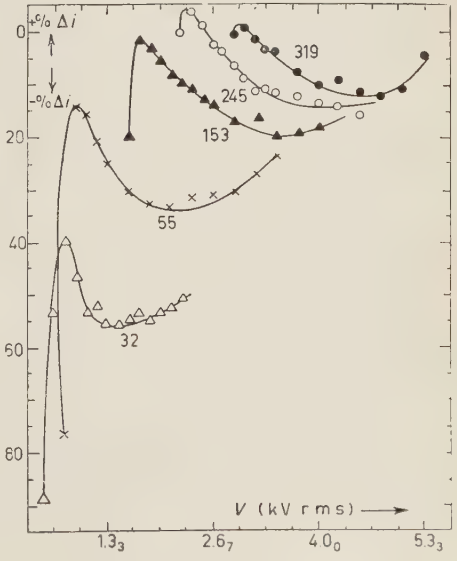

Fig. 3. – Typical relative Joshi effect, % Δi-potential characteristics for hydrogen. Potential in kV (r.m.s.). Numbers on curves indicate the pressure of hydrogen in mm Hg.

of such computed V_A and V_B which together with the computed V_m are recorded in Table I.

The variation of the relative Joshi effect, $\% \Delta i = ((i_L - i_D)/i_D) \cdot 100$, with the applied potential is shown in Fig. 3 for a few typical pressures. The three regions corresponding to the three regions of the current characteristics are clearly seen and V_A and V_B may also be computed from the minimum and the subsequent maximum in the relative Joshi effect. These computed values are in close agreement with those obtained from the current characteristics, though in some cases a slight difference amounting to approximately 100 V has also been observed, the values computed from the Joshi effect being higher.

4. – Discussion.

The important role of the threshold potential, V_m, in reactions under electrical discharge and also in the Δi phenomena has been emphasized by JOSHI ([2,3]), who suggested that the gas breaks down as a dielectric at V_m which also corresponds to the energy of activation. This V_m in the present work is indicated by a sudden rise in the current flowing through the system, the initiation of a glow characteristic of the gas and the appearance of high frequency pulses on the current waveform. In a point-to-plane corona in air, LOEB ([10]) states essentially similar criteria for V_0, the threshold of the intermittent pre-onset burst pulse corona initiating the Geiger counter regime. Detailed studies ([11]) of TRICHEL, KIP, WEISSLER, ENGLISH and others have shown that in such a corona, the streamer onset starts at a potential slightly above V_0 (50 to 150 V), while the onset of a steady burst pulse corona lies some 100 to 500 V higher. The observation of three distinct regions in the current-potential characteristic strongly suggests that V_m may be analogous to V_0, the transition from one corona regime to the other giving rise to the observed changes in the current-potential characteristic. This is supported by the recent studies in low pressure corona discharges by CRAGGS and MEEK ([12]) who observed a great variety of intermittent discharges in hydrogen between the initial breakdown and the full establishment of a glow discharge.

Since the onset is dependent on the parameter X/p, where X is the field strength and p the gas pressure, it is to be expected that, with a constant gap, the corona thresholds, V_m, V_A and V_B would vary linearly with pressure. From the data available in literature, however, it is seen that the onset po-

([10]) L. B. LOEB: *Phys. Rev.*, **73**, 798 (1948).

([11]) W. N. ENGLISH: *Phys. Rev.*, **71**, 638 (1947); **74**, 170 (1948); A. F. KIP: *Phys. Rev.*, **54**, 139 (1938); **55**, 549 (1939); G. W. TRICHEL: *Phys. Rev.*, **54**, 1078 (1938); **55**, 382 (1939); G. L. WEISSLER: *Phys. Rev.*, **63**, 96 (1943).

([12]) J. D. CRAGGS and J. M. MEEK: *Proc. Phys. Soc. London*, **60**, 327 (1948).

tential is not a linear function of the gas pressure in the case of corona discharges. Corona studies in hydrogen have been made by a number of workers, BRUCE [13], WERNER [14], SLOANE [15], WEISSLER [11], CRAGGS and MEEK [12], and JONES and DAVIES [15]. In all these studies, in spite of a much smaller pressure range than that investigated in the present work, the curves for the onset potential as a function of pressure exhibit a definite curvature, the curves being concave towards the pressure axis as in the present case. (Though no mention of this has been made by the various authors referred to, this conclusion is drawn from the curves reported in the respective papers). The theory of these corona thresholds has been worked out by LOEB [16] and his relations indicate that variation with pressure in electron emission by positive ion bombardment at the cathode and photon absorption in the gas play such a role that the curves need not be linear.

While details regarding the $i_D - V$ and the $\% \Delta i - V$ characteristics will be published elsewhere, it may be pointed out that the observation that the current characteristic is almost vertical for potentials below V_A, indicates that here the space charges have no influence as pointed out by DRUYVESTEYN and PENNING [17]. The threshold V_A marks the transition from a space charge free to a space charge limited corona regime, with a sudden increase in the corona gap resistance as indicated by the slope of the characteristic. Assuming the modified Townsend-Werner relation, $V - V_m = iR$, to hold in the present case, the slope of the current characteristic is a measure of the corona gap resistance, R, which diminishes again at the next threshold, V_B, corresponding to a final fast rise of the current characteristic. Essentially similar results are obtained with a.c. corona using Maze counters, to be published elsewhere.

[13] J. H. BRUCE: *Phil. Mag.*, **10**, 476 (1930).
[14] S. WERNER: *Zeits. f. Phys.*, **90**, 354 (1934); **92**, 705 (1934).
[15] F. L. JONES and D. E. DAVIES: *Proc. Phys. Soc. London*, B **64**, 397, 519 (1951); R. H. SLOANE: *Phil. Mag.*, **23**. 534 (1937).
[16] L. B. LOEB: *Journ. Appl. Phys.*, **19**, 882 (1948 *b*).
[17] M. J. DRUYVESTEYN and F. M. PENNING: *Rev. Mod. Phys.*, **12**, 387 (1940).

RIASSUNTO (*)

Si sono misurati in un intervallo di pressione da 3 a 700 mm Hg i potenziali d'innesco per scarica elettrica di bassa frequenza fra cilindri di vetro coassiali. Si ritiene che il potenziale d'innesco sia analogo a quello della scarica intermittente a corona. Gli altri potenziali d'innesco sono stati valutati in base alle caratteristiche corrente-potenziale e sono in stretto accordo con quelli valutati in base alla variazione dell'effetto Joshi.

(*) *Traduzione a cura della Redazione.*

Observation of Production, Decay, and Interaction of Strange Particles (*).

H. Blumenfeld (+), W. Chinowsky (−) and L. M. Lederman

Columbia University and Brookhaven National Laboratories

(ricevuto l'11 Gennaio 1958)

Summary. — The operation of the Columbia 36 in. magnet cloud chamber at the Cosmotron is described. The production of unstable particles by 1.9 GeV π^- pions in lead and carbon is studied. The yields are interpreted in terms of nuclear interactions of Λ^0 and θ^0 particles in the nucleus of production. A large cross section for the reaction $\Sigma \to \Lambda^0$ is deduced from this and other data. The disappearance of θ^0's is observed in lead relative to carbon, and possible mechanisms are discussed. The Λ^0 lifetime is redetermined to be $(2.75^{+0.45}_{-0.40}) \cdot 10^{-10}$ s; that of the θ^0 is found to be $(1.15^{+0.40}_{-0.25}) \cdot 10^{-10}$ s. Associated production is discussed and an upper limit for the fraction of Λ^0's associated with unknown particles is found to be 0.40. Correlation angles in Λ^0 decay are observed to favor «front-to-back» asymmetry. Some anomalous events are described.

1. – Introduction.

This investigation was begun in the summer of 1954 in order to study the process of unstable particle production using a controlled source: 1.9 GeV negative pions from the Brookhaven Cosmotron. The technique employs a large cloud chamber in a 10 000 gauss magnetic field. Unstable particles are produced by an incoming beam of negative π-mesons in thin lead and carbon plates, the actual thickness being a compromise between yield and the desire

(*) This research is supported by the Office of Naval Research and the Atomic Energy Commission.

(+) Submitted in partial fulfilment of the requirements for the degree of Doctor of Philosophy in the Faculty of Pure Science, Columbia University.

(−) Brookhaven National Laboratories.

to minimize the « dead-time », i.e. the time spent by the unstable particle within the plate. The vast accumulation of data since 1954 has provided strong evidence for the hypothesis of associated production as advanced by A. Pais [1], by Gell-Mann [2] and by Nakamo and Nishijima [3].

The data obtained in this experiment, consisting of 189 unstable particle disintegrations, provide information on lifetimes, relative production yields, branching ratios, correlation effects in production and decay, production energy spectra, angular distributions and nuclear interactions of the unstable particles.

2. – Description of experimental equipment.

The detector is a pressure controlled expansion type cloud chamber, with an inside diameter of 36 in. and an illuminated depth of 8 in. It is provided with a magnetic field of 10 kG uniform to $\pm 2\%$ over the illuminated region of the chamber. Except for size, the chamber design, employing a rubber diaphragm and pop valve mechanism, is entirely conventional [4]. The gas used in the chamber was argon, saturated with a 70–30 ethyl alcohol water vapor mixture, operating slightly above atmospheric pressure. A black velvet baffle above the diaphragm serves also to store alcohol and act as the fiduciary plane for the optical system.

The chamber contained three carbon plates, each of thickness 2 g/cm^2 and two lead plates 7 g/cm^2 thick. In the beam direction the arrangement was C–Pb–C–Pb–C. The corresponding distances between plates were 4 in., 6 in., 4 in. (Fig. 1). The lead plates were at ground potential. The carbon plates established a sweeping field of 50 V/cm in each of the six chamber regions. In addition, a clearing electrode was placed below the velvet in order to reduce the fog formed in this region. This electrode was found to be quite helpful, especially under conditions of heavy ionization [5].

The chamber was illuminated by four G.E.F.T. 422 flash tubes with reflectors milled out of aluminum blocks. The reflectors were designed to correct for the finite source size (9 mm) and were intermediate between parabolic and circular in cross-section [6]. Each lamp received the discharge of 600 μF condensers at 2000 V.

[1] A. Pais: *Physica*, **19**, 869 (1953).
[2] M. Gell-Mann: *Phys. Rev.*, **92**, 833 (1953).
[3] T. Nakamo and K. Nishijima: *Progr. Theor. Phys.*, **10**, 581 (1953).
[4] C. T. R. Wilson: *Phil. Trans.*, **189**, 265 (1897).
[5] H. Blumenfeld, E. T. Booth and L. M. Lederman: *Rev. Sci. Instr.*, **25**, 1120 (1954).
[6] The suggestion of this design is due to Prof. J. Rainwater.

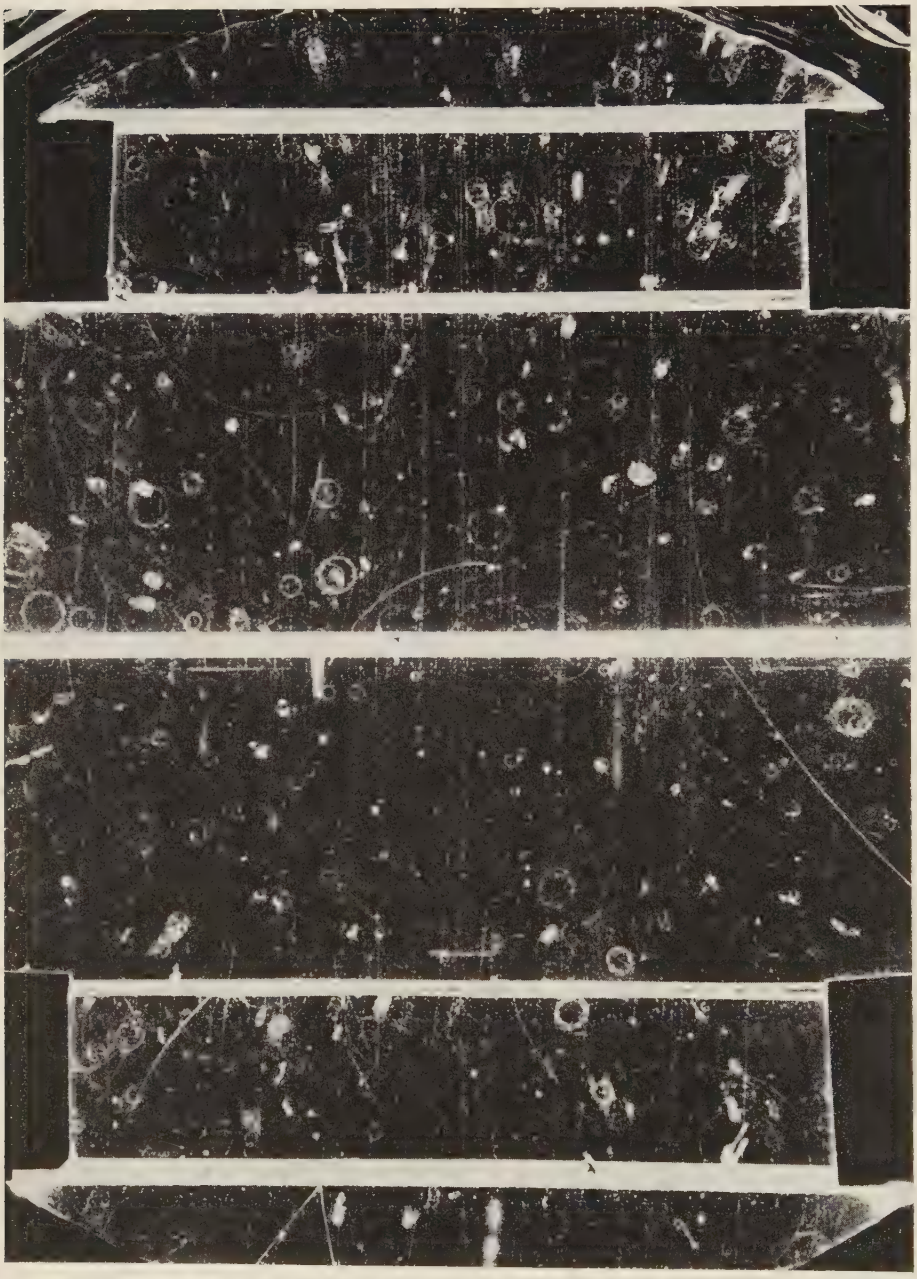

Fig. 1. – 36 in. cloud chamber photograph in 2 GeV pion beam. The plates (from top to bottom) are carbon, lead, carbon, lead, carbon. A production event yielding $K \to \mu \to e$ occurs in the first lead plate.

Pictures were taken with three cameras on 70 mm linograph ortho film. The three 150 mm Tessar lenses were located at an optical distance of 276 cm above the velvet, the lens axis being perpendicular both to the plane of the film and to the velvet. The line joining the lenses was at right angles to the direction of the incoming π-meson beam. The distance between adjacent lenses was 38.1 cm.

The magnet is essentially a Helmholtz coil with a three inch thick iron return path (7). The magnet was pulsed to 10 kG every 90 s, for a duration of 7 s at a peak value of 3 400 A at 200 V. Cooling water flow of 10 $\sim$ gpm limited the temperature rise to ~ 10 °C. The chamber was thermally shielded from the magnet by a copper jacket whose temperature was regulated by circulating water from a large temperature controlled barrel. Several cooling coils were also used to regulate the chamber temperature and to maintain an appropriate gradient. Thermistors, at various locations, permitted a periodic check on the temperatures. The establishment of thermal equilibrium was found to be crucial in order to minimize turbulent distortion of particle tracks.

The combination of plates inside the chamber, pulsed magnetic field, and the exigencies of accelerator schedules created a unique situation relative to the establishment of thermal equilibrium. The pulsed field induces eddy currents which can easily generate hundreds of watts in the brass structure of the cloud chamber, These were dealt with where possible by strategic laminations and cooling pads. The plates tend to warm the gas and prevent the establishment of uniform saturation. This made the expansion ratio critical. The establishment of equilibrium required continuous operation of the equipment for many hours, which often conflicted with accelerator running schedules. All of these considerations resulted in far more variable performance in so far as track distortions are concerned, relative to a cosmic ray chamber, operating continuously in a d-c magnetic field. Whereas the latter may achieve maximum determinable momenta of $\sim (10 \div 50)$ GeV/c, our best results were of the order of several GeV/c. The situation is somewhat relieved by the much lower average momenta of interesting particles combined with longer average track length. Each photograph contains twenty to thirty 1.9 GeV/c pions which serve as a convenient measure of the effect of turbulence near each event of interest. On the average, momentum uncertainties were of the order of $(10 \div 20\%)$. However, in the majority of cases, the condition of coplanarity and transverse momentum balance (as well as Q-value for obvious Λ^0 decays) supplemented the direct measurements of momentum, resulting in better knowledge of time of flight, correlation angles, kinetic energy. The obvious

(7) J. Kessler and L. M. Lederman: *Phys. Rev.*, **94**, 689 (1954). This paper describes the Nevis 20 in. magnet which is identical in design with a linear scale factor of $\sim \frac{1}{2}$.

difficulty is that the measurement errors may well have masked some interesting anomalous processes.

As a measure of the average results, the mean « raw » Q-values for Λ^0 and θ^0 values were found to be:

$$Q_{\Lambda^0} = (\ 36.2 \pm\ 0.6)\ \text{MeV} \qquad (106\ \text{events}),$$

$$Q_{\theta^0} = (222 \quad \pm 20\ )\ \text{MeV} \qquad (\ 34\ \text{events}).$$

The agreement with the literature ([8]) is taken as a measure of the systematic errors in momentum and angle determination.

3. – Operation with the cosmotron.

A plan view of the arrangement is given in Fig. 2. The 1.9 GeV π^- beam is generated by the collisions of 3.0 GeV protons with a beryllium target which is inserted into the east straight section of the Cosmotron every 90 s by a pneumatic ram. The mesons emitted at about 0° to the proton beam are deflected by the Cosmotron magnetic field into a channel through the concrete shield. At the exit of this shield, they are deflected through 6° by a steering magnet into the lead collimator directly in front of the cloud chamber.

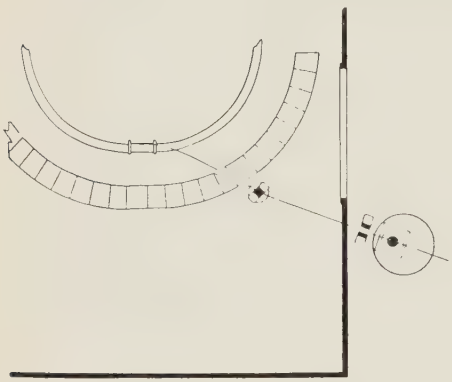

Fig. 2. – Plan view of arrangement showing the deflection of the Cosmotron π^- pion beam into the cloud chamber.

The 90 s cycle included the following automatic operations: at $t = 0$, a pulse from the cosmotron timing circuit starts a synchronous-motor driven timer. The cloud chamber magnet is energized and when near peak field, a second cosmotron pulse triggers the expansion so that full sensitivity is reached 10 ms before ejection of the meson burst. The chamber lights are flashed 70 ms later. The chamber is then reset, overcompressed, slow expanded, recompressed rapidly to equilibrium, the film is transported, flash condensers recharged, and the system waits for the following cosmotron lock-in pulse. In this manner a total of 8 000 usable photographs were obtained in the course of about 10 running periods distributed over the interval September 1954 to October 1955.

([8]) R. THOMPSON: *Progress in Cosmic Ray Physics*, **3** (1955), quotes values of $Q_\Lambda = 36.9 \pm .4$ and $Q_\theta = 214 \pm 5$.

4. – Analysis of pictures.

A representative picture is shown in Fig. 1. The pictures were analyzed by separately projecting the three views to half scale, on a horizontal stationary rear projection screen. The correct scale was obtained from fiduciary marks sewn on the velvet. Measurements were made directly on the linearly reprojected magnified images. All conical effects were accounted for by the series expansion method (expansion parameter is tangent of dip angle divided by object to lens distance) described by SARGENT *et al.* [9]. The long object distance insured rapid convergence of the series. The pictures were first « rough scanned » to find events of interest. These consisted of neutral V events (V^0), and charged V events ($V^\pm$). A V^0 event is defined by a clear vertex from which emerge two oppositely curved tracks. The vertex represents the point of decay of an unstable neutral particle. The vector resultant of the momenta of the positive and negative secondary gives the direction of flight and should point towards the origin of the V^0, generally a collision of an incident pion with a lead or carbon nucleus.

A $V^\pm$ appears as a charged primary decaying into a lighter particle of the same charge, which differs markedly in direction or in ionization from the primary. The primary data on each V^0 consisted on the following measurements:

1) The momenta $\boldsymbol{p}^+$ and $\boldsymbol{p}^-$ of the decay products;

2) The space angles φ^+ and φ^- between the V^0 direction and the decay tracks;

3) The included angle θ. The condition $\theta = \varphi^+ + \varphi^-$ is a check on coplanarity, which is computed directly from $\boldsymbol{p}^0 \cdot \boldsymbol{p}^+ \times \boldsymbol{p}^-$;

4) The angle β_0 between the V^0 line and the direction of the incident pion;

5) Ionization estimates of the decay tracks by comparison with nearby beam tracks (defined as minimum ionizing) and with proton tracks from nearby star prongs.

In cases of short tracks, the conditions of transverse momentum balance and coplanarity were used to deduce the unknown momentum. The Q value was next computed. i.e. the mass of the V^0 minus mass of the secondaries, mass assignments being suggested by the ionization estimates. Whenever the Q value agreed, within the estimated errors, with Q_{Λ^0} or Q_{0^0}, the known Q values

[9] C. P. SARGENT, M. RINEHART, L. M. LEDERMAN and K. C. ROGERS: *Phys. Rev.*, **99**, 885 (1955).

(36.9 MeV for Λ^0, 214 MeV for θ^0) were used to improve the knowledge of p^-, p^+, q^+, q^- in relation to the errors. Finally, the kinetic energy, momentum p_T, time of flight and various correlation angles (Sect. **10**) were computed from the corrected measurements. Although this procedure may have forced some anomalous decay events into the Λ^0 and θ^0 group (where the raw Q value errors were quite large), these are not numerous enough to distort the statistical significance of the results.

For charged V's, considerably less information is obtained as the problem is generally underdetermined and no cross-checks are available. The measurements for $V^\pm$ yielded p^*, the momentum of the charged secondary in the center of mass of the V. Often, only lower limits on p^* were obtained.

In addition, the star prongs emitted in all interactions which provided V's were examined, the momenta and ionization determined. These interactions were classified as: *a*) no prongs, *b*) protons or heavier tracks only, *c*) possible K-mesons, *d*) others, i.e. mesons and protons.

5. – Efficiencies.

5·1. *Observational.* – Rescanning provided the only check on the efficiency for finding events of all categories. Thus, the absolute yields are not very well known. In addition, decays yielding minimum tracks, e.g. fast θ^0's, are harder to find than slow Λ^0's. We can only estimate the efficiency for finding fast θ^0's or fast Λ^0's yielding near minimum protons. This is probably higher than 75%. However, we are equally efficient for observing any given type of event originating in any plate in the chamber. Modifications in the observed results due to nuclear interactions of the strange particles in the plates (except for interactions in the nucleus in which they were produced) are negligible.

5·2. *Geometrical.* – By this we mean the fraction of events which are lost by decay inside the plate of origin or outside of the chamber. This can be deduced if the lifetime and velocity of the particle are known. We have weighted each Λ^0 and θ^0 event by the inverse of the probability that it would decay inside the visible region of the chamber, using the mean life obtained from our data. For the charged events, both our uncertain identification and the uncertain mean life made it unprofitable to apply this correction. We also determined the overall geometrical efficiency for Λ^0 and θ^0 for each separate plate in the chamber (see Table I), using the mean life $3.0 \cdot 10^{-10}$ for Λ^0, $1.0 \cdot 10^{-10}$ for θ^0, and assuming a reasonably velocity and angular distribution compatible with our data. It should be noted from the table that, in spite of the small plate thicknesses, approximately 40% of all V^0's decay inside the plates.

TABLE I. – *Geometrical losses due to lifetime.*

	$Pb_{1.2}$	$C_{1.2}$	C_3
Λ^0 percent lost in plate	36%	32%	32%
Λ^0 percent outside illuminated region	2%	2%	12%
θ^0 percent lost in plate	42%	48%	48%
θ^0 percent outside illuminated region	2%	2%	5%

The chamber was relatively efficient for the detection of unstable particles which decayed into charged secondaries and had a lifetime ranging from $5 \cdot 10^{-11}$ to $2 \cdot 10^{-9}$ s.

One of the aims of the selected plate geometry was the possibility of converting π^0 photons from alternate decay modes and photons from presumed $\Sigma^0 \to \Lambda^0$ process. However, the presence of a high back-ground of photons from the Cosmotron seriously decreased our effective efficiency for alternate mode detection. The efficiency for converting Σ^0 photons from lead production plates is of the order of $\sim 40\%$. An observed pair could, of course, have originated from a π^0 born in the same production act. Three pairs were observed in association at production, one with a Λ^0 and two with θ^0's made in lead.

6. – Results. Nuclear interactions.

Table II lists all the events found in the chamber during the course of the experiment. An event is classified by the measurements on the decay products only when the unstable particle can be associated with an incoming pion which stops in a plate. Anomalous Q values, outside of estimated errors, were found in 5 events included in the Λ^0 group and five events included in the θ^0 group. However, the quality of most of these events is not sufficient to establish the existence of abnormal V^0 groups. These will be further dis-

TABLE II. – *Unstable particle yields.*

	Λ^0	θ^0	Ch^+	Ch^-	V^0	Total
Pb	76	18	9	9	3	115
C	34	22	6	8	1	71
Total	110	40	15	17	4	186

cussed in Sect. **12**. Listed in the table are four V^0 events which could either be Λ^0 or θ^0. Included in the charged particle decays are two negative tracks which could represent the decays of K-particles coming with the beam from outside the chamber. The yield represents an absolute cross-section which is estimated to be about $(2.5 \pm 1.0)\%$ geometric for both carbon and lead.

Table III presents the fractions of Λ^0 and θ^0 particles corrected for lifetime and given per g/cm² of target material. The uncertainty in absolute scanning efficiency makes it necessary to use the data in a form which is relatively

TABLE III. – *Yields corrected for lifetimes in events per* g/cm².

	Λ^0	θ^0
Pb	8.90 ± 1.02	2.30 ± 0.54
C	9.93 ± 1.70	8.10 ± 1.72

free from possible bias. Since observations of disintegrations are independent of the production plate (after geometrical corrections) we treat as significant the ratios of yields per nucleon from lead to yields from carbon,

$$R_{\Lambda^0} = \frac{(\Lambda^0)_{\mathrm{Pb}}}{(\Lambda^0)_{\mathrm{C}}} = 0.90 \pm 0.18 \,, \tag{1}$$

$$R_{\theta^0} = \frac{(\theta^0)_{\mathrm{Pb}}}{(\theta^0)_{\mathrm{C}}} = 0.28 \pm 0.07 \,. \tag{2}$$

As an orientation, if one assumes the production cross-section to vary as $A^{\frac{2}{3}}$ the expected ratio would be

$$R = \left(\frac{207}{12}\right)^{-\frac{1}{3}} = 0.39 \,. \tag{3}$$

The situation would obtain, for example, if the incoming pions had an infinitesimal mean free path in nuclear matter so that all production occurred at the surface. At the other extreme, the production cross-section varies as the volume of the nucleus and the expected ratio would be unity.

The actual pion interaction in hydrogen has been measured by COOL *et al.* [10]. They find $\sigma(\pi^- + \mathrm{p}) = \sigma(\pi^+ + \mathrm{p}) = 30$ mb at 1.8 GeV. This corresponds to a mean free path in nuclear matter of $\sim 4 \cdot 10^{-13}$ cm. Using the optical model, we obtain $\sigma_{\mathrm{Pb}}/\sigma_{\mathrm{C}} \sim 10$ and the above ratio becomes

$$R_{\mathrm{opt}} = 10 \cdot \frac{12}{207} = 0.54 \,. \tag{4}$$

[10] R. COOL, O. PICCIONI and D. CLARK: *Phys. Rev.*, **103**, 1082 (1956).

This latter value represents more closely, the effect of pion interactions in the lead to carbon ratio. Presumably any difference in the observed yields represents mainly the effect of nuclear interactions of the emitted secondaries. Thus it appears as if there were present an excess of Λ^0's in lead and a disappearance of θ^0's in lead, with the latter effect the more pronounced, statistically. More significant is the difference in the Λ/θ ratio in lead and carbon since this is essentially independent of the pion interaction effect:

$$\frac{(\Lambda^0/\theta^0)_{\mathrm{Pb}}}{(\Lambda^0/\theta^0)_{\mathrm{C}}} = 3.17 \pm 1.2 \,. \tag{5}$$

The observed deviation from unity presumably represents secondary interactions, i.e. either the generation of additional Λ^0's in lead over carbon or the additional disappearance of θ^0's in lead or both. Any effect of the neutron excess in lead would tend to yield more θ^0's relative to Λ^0's. These effects are reduced by the possibility, at these energies, for production of additional pions.

A possible mechanism for the Λ^0 excess is the production of Σ^- in lead (and carbon) with the subsequent nuclear interaction of Σ^-:

$$\Sigma^- + \mathrm{p} \rightarrow \Lambda^0 + \mathrm{n} \,.$$

The $\Sigma \rightarrow \Lambda$ exchange reaction on a bound nucleon could strongly favor the lead nucleus for reasonable mean free paths. It also has the attractive property of providing a source of very low velocity Λ^0's as are observed in this experiment, in the cosmic rays ([11]), and in the formation of hyperfragments. Quantitative support for the hypothesis of a large $\Sigma^- \rightarrow \Lambda^0$ conversion cross-section comes from a comparison of the K^- absroption data in hydrogen ([12]) and in nuclear emulsion ([13]). The Berkeley data and charge independence ((to give $K^- + n$) provide the information on the elementary absorption act, i. e. total production of Σ^- that is assumed to take place in the emulsion nuclei. Comparing this with the Σ^- yield observed in emulsion gives 0.5 for the probability of a Σ^- particle to escape from the average emulsion nucleus ([11]). This

([11]) G. James and R. Salmaron: *Phil. Mag.*, **46**, 571 (1955); G. T. Reynolds: *Nuovo Cimento*, **4**, 933 (1956).

([12]) W. Alvarez, H. Bradner, P. Falk-Vairant, J. D. Gow, A. H. Rosenfeld, F. T. Solmitz and R. D. Tripp: *Nuovo Cimento*, **5**, 1026 (1957).

([13]) G. Snow: private communication of the results of the Wisconsin group of Fry, Snow and Schneps.

([14]) We are indebted to Dr. S. Goldhaber for communicating the results of her independent analysis, based on the Berkeley emulsion data. She obtains 0.44 as the fraction of $\Sigma^\pm$ which escape from the average emulsion nucleus, but points out that the Z-law for capture does not hold in emulsion. This effect would make the $\Sigma \rightarrow \Lambda$ mean free path even shorter than $4 \cdot 10^{-13}$ cm.

corresponds to a mean free path in the nuclear matter of $4 \cdot 10^{-13}$ cm. Thus, for equal numbers of Σ's produced, 80% will have converted in lead whereas only 40% will have converted in carbon. If we correct the Λ^0-numbers of Table II on the basis of this efficiency and the geometrically corrected V^- yields (assuming these are mostly Σ particles), we obtain for the ratio at production $R \sim 0.5$ in agreement with (4). The resulting Σ^- yield at production is also not inconsistent with (4).

It should be noted also that if K-pair production is important at this energy ([15]), then K^-'s may interact in lead to give Λ^0's. Not enough is known about cross-sections to evaluate this contribution.

There are three mechanisms for the disappearance of θ^0 within the Gell-Mann scheme: 1) charge exchange scattering into the long-lived K^+ state; 2) nuclear scattering followed by capture into a hyperfragment ([16]); 3) interaction to give Λ^0 by virtue of the θ^0 amplitude which is generated in the (short) flight path through the production plate ([17]). 1) and 2) cannot be estimated since the relevant cross-sections are unknown at the mean θ^0 energy in this experiment (~ 500 MeV). At lower energies, the K^+ exchange scattering cross-section is known to be small ([18]). In the case of (1) one would have to say that $K^+ \to \theta^0$ conversion does not proceed with equal rate because of a difference in production spectra. 3) may be calculated. The θ^0 amplitude generated by the ~ 0.5 cm flight path is found to be negligible. (See note added in proof). Evidence for a significant scattering of θ^0's is also presented in Sect. **11**.

7. – Lifetimes of unstable particles.

7'1. *Lifetime of the* Λ^0. – The technique and preliminary results on the determination of Λ^0 and θ^0 lifetimes have been reported previously ([19]). The maximum likelihood analysis is employed for those Λ^0 events which satisfy the criteria of 1) normal Q value, 2) positive prong ionization $> 2 \times$ minimum.

([15]) M. SCHEIN, D. M. HASKIN and R. G. GLASSER: *Nuovo Cimento*, **3**, 131 (1956).

([16]) W. F. FRY, J. SCHNEPS and M. S. SWAMI: *Phys. Rev.*, **101**, 1526 (1956); R. SERBER and A. PAIS: *Phys. Rev.*, **99**. 1551 (1955).

([17]) See, for example, A. PAIS and O. PICCIONI: *Phys. Rev.*, **100**, 1487 (1955).

([18]) J. E. LANNUTTI, W. W. CHUPP, S. GOLDHABER, G. GOLDHABER, E. HELMY, E. L. ILOFF, A. PEVSNER and D. RITSON: *Phys. Rev.*, **101**, 1617 (1956). Also, preprint of S. BISWAS, L. CECCARELLI-FABBRICHESI, M. CECCARELLI, K. GOTTSTEIN, N. VARSHNEYA and P. WALOSCHEK (Göttingen). More recent data (G. GOLDHABER: private communication) indicate a definite increase of K^+ exchange scattering with energy See PIPPI: *Seventh Annual Rochester Conference Report.*

([19]) H. BLUMENFELD, E. T. BOOTH, L. M. LEDERMAN and W. CHINOWSKY: *Phys. Rev.*, **102**, 1184 (1956).

For this group $Q_{av} = 36.4$ MeV. Maximum likelihood procedure on 74 such events yields the result:

$$\tau_{\Lambda^0} = (2.75^{+0.40}_{-0.38}) \cdot 10^{-10} \text{ s} .$$

The mean potential path length is $\sim 12 \cdot 10^{-10}$ s, which represents a 20% correction to the « raw » average lifetime. The error includes the uncertainty due to momentum errors as well as statistics.

7·2. θ^0 *Lifetime.* – Maximum likelihood analysis of 39 events classified as θ^0 decays yields.

$$\tau_{\theta^0} = (1.15^{+0.45}_{-0.25}) \cdot 10^{-10} \text{ s} .$$

The deletion of 7 events with poor Q values reduces this result by less than the stated errors. Both Λ^0 and θ^0 lifetimes are in agreement with those previously reported on the basis of 63 Λ^0 and 27 θ^0 events ([19]). The θ^0 lifetime is in good agreement with cosmic ray determinations ([20]); the Λ^0 result somewhat lower.

7·3. *Charged* V *lifetime.* – Since the $V^{\pm}$ events are not well identified and may be mixtures of several particles, a determination of lifetime is not regarded as very significant. However, it seems plausible that most of the negatives, V^-, are actually Σ^- made in reactions like $\pi^- + p \to \Sigma^- + K^+$. There will, of course, be some contamination of K^-. The Bartlett procedure applied to all V^- events which are not identified K^-'s yields

$$(\tau(V^-) \ = 1.2^{+0.5}_{-0.3}) \cdot 10^{-10} \text{ s} .$$

This is in good agreement with recent Σ^- lifetime determinations ([21]) and serves as a consistency check on the interpretation of the data.

8. – Charged V-events.

Seventeen negative and twelve positive charged V events were observed to be produced in lead and carbon. Identification of primary mass was possible for one K^- event, one K^+ event (which subsequently underwent $K^+ \to$

([20]) D. I. Page and J. A. Newth: *Phil. Mag.*, **45**, 44 (1954). More recently, Λ^0 and θ^0 lifetimes have been determined by the Columbia bubble chamber group. They find $\tau_{\Lambda^0} = (2.8 \pm .2) \cdot 10^{-10}$ s and $\tau_{\theta^0} = (.95 \pm .08) \cdot 10^{-10}$ s. See: M. Schwartz: *Proceedings of the Seventh Annual Rochester Conference.*

([21]) R. Budde, M. Chretien, J. Leitner, N. P. Samios, M. Schwartz and J. Steinberger: *Phys. Rev.*, **103**, 1827 (1956).

$\rightarrow\mu^+\rightarrow e^+$ in the gas, Fig. 1), and one Σ^+ (proton secondary) associated with a θ^0. In view of the very limited measurements, one can only conclude that the data is consistent with many of the V^- being Σ^- (Sect. 7·3), the V^+ being K^+ (note in Table IV that four accompany Λ^0) and Σ^+ in unknown ratio. We

TABLE IV. – *Associated events.*

	$\Lambda\theta$	Λ_{ch^+}	0_{ch^-}	$\theta\Sigma^+$	$\Lambda\Lambda$
Pb	7	4	2	1	1
C	5	0	0	0	0

only note here that the four associated V^+'s have a mean ratio of flight path to potential path of $\sim\frac{1}{2}$. In view of the low efficiency for observing K^+ and the large absorption of Σ , the data are in agreement with bubble chamber results, which indicate that Σ^-K^+ production is relatively important in π^--nucleus collisions.

9. – Correlation angles.

Anisotropies in the angular distribution of the decay products of Λ^0 and θ^0 particles may result from 1) spin greater than $\frac{1}{2}$ ([22]), (2) non-conservation of parity in the decay processes ([23]) and 3) interference between opposite parity states of the particle ([24]). Fig. 3 shows the co-ordinate system used in the description of the decay process. The Z-axis is along the direction of flight of the decaying primary particle; the incoming π^- meson is in the X-Z plane (production plane). Events are then specified by the polar co-ordinates (θ_L, Σ) of the positive decay product in the center of mass system of the primary (P^+_{CM}).

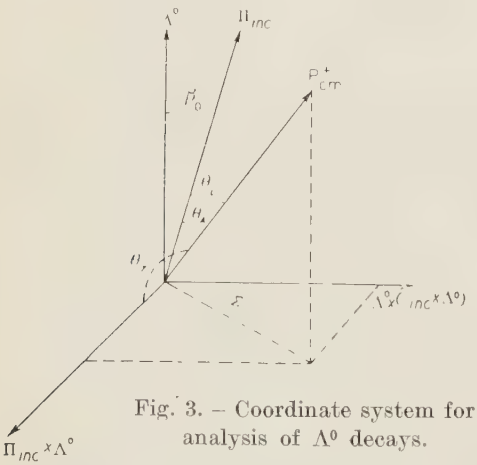

Fig. 3. – Coordinate system for analysis of Λ^0 decays.

([22]) S. B. TREIMAN and H. W. WYLD: *Phys. Rev.*, **100**, 1039 (1955); R. ADAIR: *Phys. Rev.*, **100**, 1540 (1955).

([23]) T. D. LEE and C. N. YANG: *Phys. Rev.*, **104**, 254 (1956).

([24]) T. D. LEE and C. N. YANG: *Phys. Rev.*, **104**, 822 (1956).

The distribution of the following angles have been examined:

1) The dihedral angle, Σ, between the planes of production and decay;

2) The cosine of the angle, $\cos\theta_L$, between P_{CM} and the line of flight of the primary;

3) The cosine of the angle, $\cos\theta_A$, between P_{CM} and the direction of the incoming π^- meson;

4) The cosine of the angle, $\cos\theta_\gamma$, between P_{CM} and the perpendicular to the plane of production.

Non-uniformity of the above distributions, when folded about 90°, would be attributed to spin greater than $\frac{1}{2}$. Asymmetry about 90° in the distribution 2 would result from the interference between the parity doublets Λ_1^0, Λ_2^0, and asymmetry about 90° in the distribution 4 would be attributed to failure of parity conservation. Such asymmetries will appear only if the Λ^0 is polarized, and further will vary with production angle. Our events were produced in carbon and lead nuclei, and polarization present at production may be destroyed is subsequent interaction in the nucleus. Isotropic distributions in the pertinent angles do not yield any positive information.

The dihedral angle distribution is observed to be uniform. The number

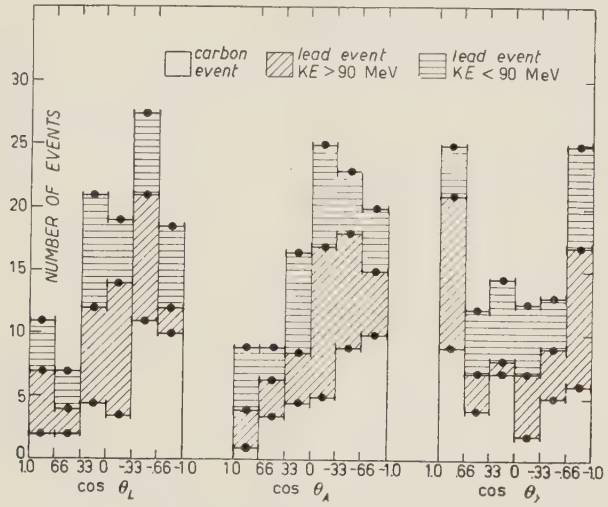

Fig. 4. – Histograms of angular distributions.

of Λ^0 events from carbon where $\Sigma > 45° = 16.5$, the number of Λ^0 events from carbon where $\Sigma < 45° = 16.5$. For lead the respective numbers are 32.5 and 36.5. The asymmetries that we observe are illustrated in Fig. 4. At first sight they appear striking. However, all three distributions may arise from

one effect: the absence of events in which the decay proton makes a small angle with the Λ^0 direction. This is most directly seen in the θ_L distribution. A tendency for protons to be emitted backwards in the Λ^0 rest system has also been observed by FOWLER ([25]), ARMSTRONG ([26]), FRETTER ([27]), ARMENTEROS ([28]), GUPTA ([29]) and BRIDGE ([30]). Events in hydrogen ([21]) do not show this effect. We have considered the possibility of observational bias influencing these distributions ([31]). Two kinds of bias may enter: 1) observational favoring of heavily ionizing Λ^0 protons could tend to select backward ejected protons in the Λ^0 center of mass; 2) systematic tendency to underestimate the momentum of « almost-straight » tracks. Also, errors in angle measurements tend to project Λ^0's backward. We find that it is difficult to exclude these possibilities rigorously. However, neither can we say that bias effects can easily account for these asymmetries. To eliminate rigorously this type of bias in our pictures would require an additional scanning effort of two or three times that already expended. At the present time, these distributions are offered (inconclusively) as suggesting asymmetry, which violates parity conservation in production. This is interesting in view of recent results ([32]) which make it extremely tempting to discard as unnecessary, the parity conjugation hypothesis of LEE and YANG ([24]) (*).

10. – Kinetic energy and angular distributions.

In Fig. 5, 6, 7 and 8 are plotted the K.E. and angular distribution for the θ^0 and Λ^0 events observed. In each case the event was divised by the probability for observing its decay in the visible region of the chamber. The distributions are similar to those obtained with cosmic rays ([33-35]). Although the

([25]) W. B. FOWLER, R. P. SHUTT, A. M. THORNDIKE and W. L. WHITTEMORE: *Phys. Rev.*, **98**, 121 (1955).

([26]) B. ARMSTRONG: UCRL Report 3470, unpublished.

([27]) W. FRETTER and M. NAKATA: *Phys. Rev.*, **89**, 168 (1953).

([28]) R. ARMENTEROS: *Proceedings of Conference Bagnères de Bigorre* (1953).

([29]) I. C. GUPTA, W. Y. CHANG and A. L. SNYDER: *Phys. Rev.*, **106**, 141 (1957).

([30]) H. BRIDGE: *Phys. Rev.*, **91**, 362 (1953).

([31]) The Ecole Polytechnique analysis removes all events subject to criteria designed to eliminate bias from the overall sample. This group then finds no significant asymmetry. B. GREGORY: private communication.

([32]) C. S. WU, E. AMBLER, R. W. HAYWARD, D. D. HOPPES and R. P. HUDSON: *Phys. Rev.*, **105**, 1413 (1957); R. L. GARWIN, L. M. LEDERMAN and M. WEINRICH: *Phys. Rev.*, **105**, 1415 (1957).

(*) See however R. GATTO: *Phys. Rev.* (in press) for a possible explanation.

([33]) D. GAYTHER and C. C. BUTLER: *Phil. Mag.*

([34]) G. JAMES and R. SALMERON: *Phil. Mag.*, **46**, 511 (1955).

([35]) B. GREGORY *et al.*: *Nuovo Cimento*, **11**, 292 (1954).

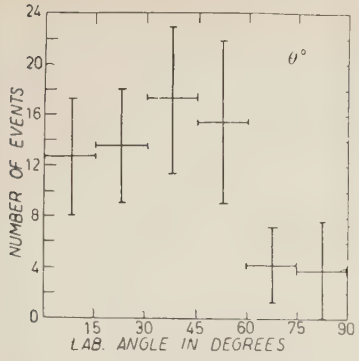

Fig. 5. – Angular distribution of observed θ^0 events.

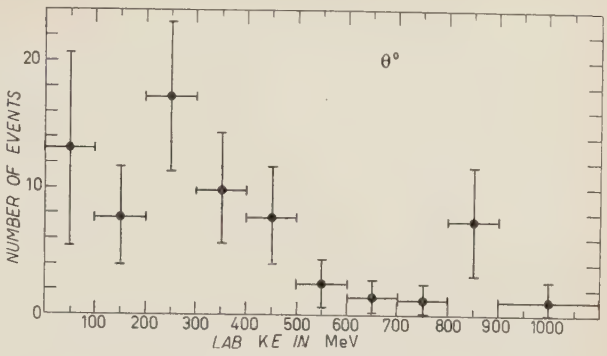

Fig. 6. – Kinetic energy distribution of observed θ^0 events.

essential features of the distributions are very probably correct, the high energy component of the Λ^0 and θ^0 distributions may be too low, due to the bias effects discussed above.

One noticeable feature is the preponderance of low energy Λ^0's from lead.

$$\frac{\Lambda^0\,[\text{K.E.} < 100\ \text{MeV from Pb}]\ \text{per nucleon}}{\Lambda^0\,[\text{K.E.} > 100\ \text{MeV from C }]\ \text{per nucleon}} = 2.3\,,$$

$$\frac{\Lambda^0\,[\text{K.E.} > 100\ \text{MeV Pb}]\ \text{per nucleon}}{\Lambda^0\,[\text{K.E.} > 100\ \text{MeV C }]\ \text{per nucleon}} = 0.39\,.$$

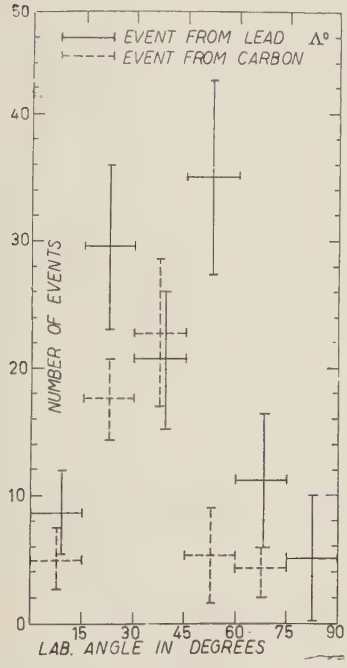

Fig. 7. – Angular distribution of observed Λ^0 events.

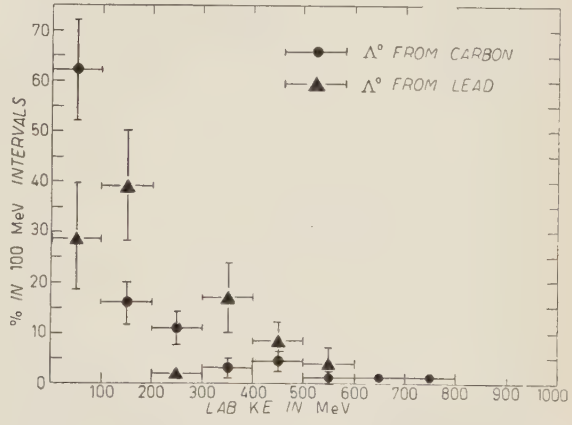

Fig. 8. – Kinetic energy distribution of observed Λ^0 events.

This effect is just what would be expected from exchange scattering such as $\Sigma^- + p \to n + \Lambda^0$ or $\Lambda^0 + n \to n + \Lambda^0$. The sum for the mean K.E. of Λ^0 pro-

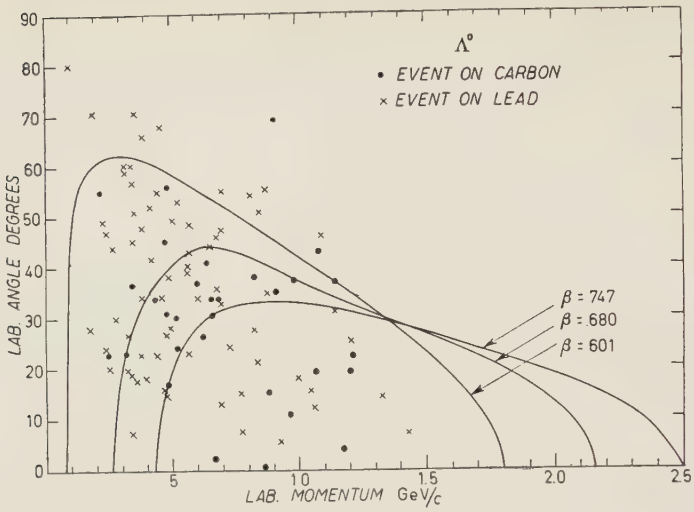

Fig. 9. – Kinematical analysis of Λ^0 production, assuming a pion-nucleon collision in the « center-of-mass ». The center of mass velocities are determined from a 25 MeV Fermi energy, and motions toward, away from, and at rest, relative to the incoming pion.

duced in associated events is (600 MeV). If the mechanism for production were $\pi^- + p \to \Lambda^0 + \theta^0$ with a 1.9 GeV π^- and no further interaction, the average K.E. for Λ^0 would be 1200 MeV.

We tried to analyze our events by transforming the kinematics to the center of mass of a $\pi^- + p$ system, allowing for the Fermi momentum of the proton. Fig. 9 and 10 show the degree to which our data conform to this model. Here again, strong nuclear scattering is required in order to understand the laboratory distributions.

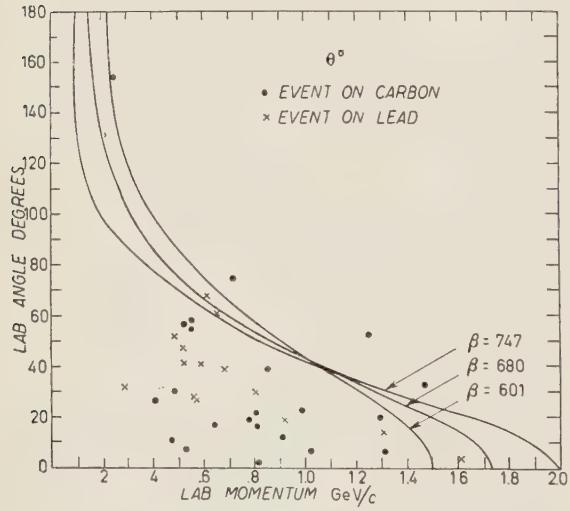

Fig. 10. – Kinematical analysis of θ^0 production.

11. – Anomalous events.

We observed five Λ^0 events whose Q values seemed to differ measurably from the normal Q value 36.9. Their Q values were: (11.4 ± 3), (17.2 ± 3), (17.5 ± 8), (27 ± 2), (68 ± 8) Gev.

Two θ^0 seemed to show appreciable deviation from $Q = 214$ MeV, namely: 140 ± 25, 140 ± 15.

One event produced two Λ^0's, which most probably originated from the

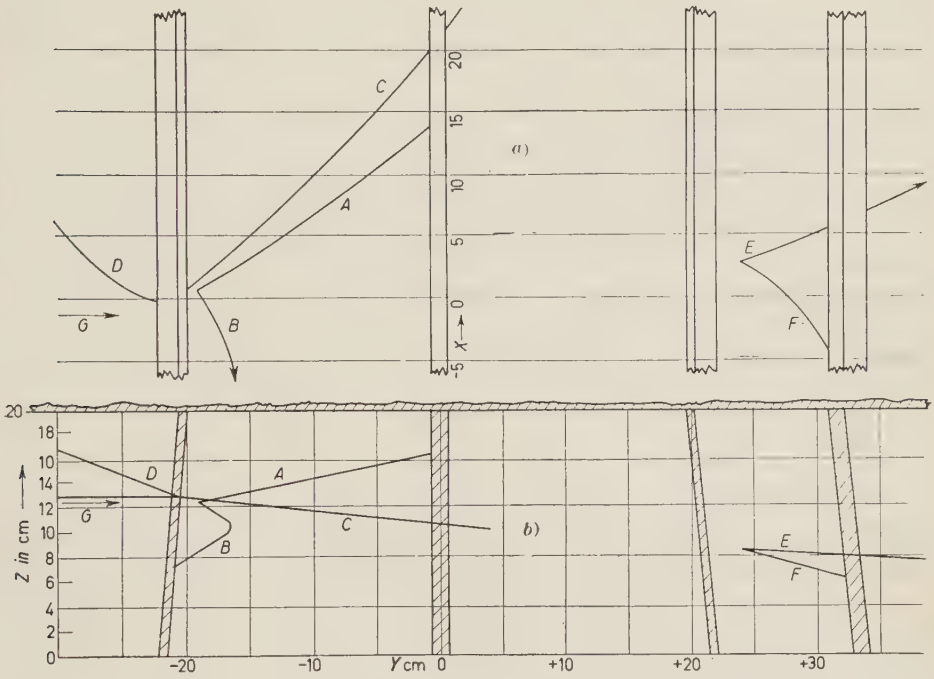

Fig. 11. – Double Λ-θ production in lead. *a*) is horizontal projection; *b*) is elevation. Track G is incoming meson, D is outgoing 12 MeV, π^-, C is proton. A and B are secondaries of a Λ^0 ($Q = 36 \pm 2$ MeV). E and F are secondaries of a Λ^0 ($Q = (37 \pm 4)$ MeV). No beam tracks are observed to stop in the intervening two plates. The line of flight of Λ_{EF} intersects the origin defined by G,D,C and Λ_{AB} to within 1.2 cm².

same incoming π^- meson interaction, see Fig. 11. The second Λ^0 decays six mean lifetimes away from the origin. The most plausible explanation is that the event consists of the production of a Λ^0 plus a θ_2^0 where the θ_2^0 interacts by virtue of its $\bar{\theta}^{-0}$ component in the second lead plate to produce another Λ^0, according to the scheme of Gell-Mann ([2]). A peculiar feature is that the second Λ^0 points to the origin of the event within a very small error.

In one event the positive decay product of a V^0 appears to be definitely heavier than a proton. The momentum of the positive track is $p^+ = (616 \pm 112)$ MeV/c, the ionization $(6 \div 12) \times$ minimum; the momentum of the negative track is $p^- = (345 \pm 22)$ MeV/c, the ionization $1 \times$ minimum. The opening angle is $\theta = (29 \pm 1)°$. The event is too near the origin, as defined by a stopping π^- incoming meson, and a 600 MeV/c proton coming out of the

interaction, to give usable measurements on coplanarity and transverse momentum. As suming a two body decay into a deuteron and a π^- meson ([36]), the Q value obtained is (136 ± 17) MeV.

12. – Conclusions.

We summarize the main conclusions of this study as follows:

1) Λ^0, θ^0, Σ^-, K^+ particles are observed with good yields ($\sim 3\%$ of geometric cross-section) where 1.9 GeV pions bombard carbon and lead.

2) Evidence is presented for the strong reaction $\Sigma^- \to \Lambda^0$ within the production nucleus. Evidence is also presented for the scattering and some disappearance of θ^0 mesons when production takes place in a heavy nucleus. It is possible to understand this qualitatively if the θ^0 scattering cross-section increases with energy from 100 MeV to 500 MeV.

3) The lifetimes of the Λ^0 $(2.75^{+0.45}_{-0.40})\cdot 10^{-10}$ s) and the θ^0 $(1.15^{+0.40}_{-0.25})\cdot 10^{-10}$ s) have been redetermined.

4) The hypothesis of associated production and the charge conjugation doubling enable us to establish a firm upper limit on invisible K-particles associated with Σ^0's. Thus, less than 64% of the observed Λ^0's are accompanied by invisible K-particles, e.g. $\theta^0 \to 2\pi^0$. We recall here, that since charge conjugation is now known not to be conserved ([25]), it is no longer necessary to assume equal production of θ_1^0 and θ_2^0 (by « 1 » and « 2 » we now mean short and long-lived) ([37]). However, because of the observed difference in lifetime, the ratio of θ_1^0 to θ_2^0 is still approximately one. Using this fact, the upper limit for association with unknown neutral particles becomes 40%.

5) The problem of front-to-back Λ^0 decay asymmetry is presented from this and older cosmic ray data.

Note added in proof.

The small number of double Λ^0 events can be used (S. Weinberg: private communication) to investigate the possibility of very large mass shift between θ_1^0 and θ_2^0. Such a shift generates a rapid oscillation between θ^0 and $\bar{\theta}^0$. If the θ^0 interaction to yield Λ^0, Σ^- is geometric, several events apparently violating strangeness conservation should have been observed. More sensitive tests of this point are forthcoming from Princeton and M.I.T. cosmotron data (private communications from G. Reynolds and D. Caldwell).

([36]) Fridiender and Bercha: *Doklady*, **1**, 162 (1956). These authors find a Q for a similar event of (56 ± 10) MeV.

([37]) T. D. Lee, R. Oehme and C. N. Yang: Nevis 36.

* * *

This work was throughout a co-operative effort between Columbia University and the Brookhaven National Laboratory. We would like to express our thanks to Dr. GEORGE COLLINS, Dr. WILLIAM MORE, Mr. EDWARD DEXTER, and the Cosmotron Staff for absolutely essential assistance. Mr. G. IMPEDUGLIA directed the scanning staff and assisted in the measurements. Mr. KENNETH LANDE contributed valuable assistance in taking the pictures and Dr. MORTON FUCHS assisted with the computations.

It is a great pleasure to thank Professor E. T. BOOTH who collaborated in the taking of the photographs and in the early analysis of the data.

RIASSUNTO (*)

Si descrive il funzionamento della camera a nebbia da 36 in. annessa al cosmotrone. Si studia la produzione di particelle instabili dovuta all'azione di mesoni π^- di 1.9 GeV su piombo e carbonio. Le rese sono interpretate in termini di interazioni nucleari di particelle Λ^0 e θ^0 nel nucleo di produzione. Da questi e altri dati si deduce una grande sezione d'urto per la reazione $\Sigma \to \Lambda^0$. Si osserva che nel piombo si hanno meno θ^0 che nel carbonio e si discutono i possibili meccanismi del fenomeno. Si ridetermina la vita media del Λ^0 trovando $(2.75^{+0.45}_{-0.40}) \cdot 10^{-10}$ s; la vita media del θ^0 risulta $(1.15^{+0.40}_{-0.25}) \cdot 10^{-10}$ s. Si discute la produzione associata e si trova per la frazione di Λ^0 associati con particelle ignote il valore 0.40. Si osserva che gli angoli di correlazione nel decadimento del Λ^0 favoriscono l'asimmetria « dall'avanti all'indietra. Si descrivono alcuni eventi anomali.

(*) *Traduzione a cura della Redazione.*

On the Solution of Certain Singular Integral Equations of Quantum Field Theory.

R. Omnès (*)

CERN - Geneva

(ricevuto il 19 Gennaio 1958)

Summary. — In the study of complex phenomena involving π-mesons (e.g. simple and double photoproduction, radiative scattering, double production, etc.) one encounters singular integral equations linking the matrix elements and phase-shifts. We give here a general method of resolution of these equations which furnishes the following results: *a*) the simplest type is integrable by quadratures; *b*) the general type is reducible to a Fredholm equation. We give also the solution of a system of coupled integral equations and of the particular one which occurs in the double production problem. This last case may be integrated by quadratures.

1. – Introduction.

We want to study singular integral equations of the following type

$$\varphi(x) = f(x) + \frac{1}{\pi}\int_1^\infty \frac{h^*(x')\varphi(x')}{x' - x - i\varepsilon}\,\mathrm{d}x' + \int K(x'x)\varphi(x')\,\mathrm{d}x', \tag{1.1}$$

where $h(x)$ has the form $e^{i\delta}\sin\delta$ (real δ) and $K(xx')$ is a regular kernel.

This type of equation frequently occurs in the static theory of Chew-Low-Wick ([1,2]) for instance when one studies processes initiated or ending by a π-nucleon system. Such equations are thus fundamental in the problems of simple ([1]) and double photoproduction, radiative scattering ([3]), production of

(*) On leave of absence from CEA, Saclay, France.

([1]) G. F. Chew and F. E. Low: *Phys. Rev.*, **101**, 1579 (1956).

([2]) C. G. Wick: *Rev. Mod. Phys.*, **27**, 339 (1955).

([3]) B. Bosco: *Nuovo Cimento*, **5**, 1361 (1957).

mesons by meson ([4,6]). However, we suppose that the interest of such a problem is not completely restricted to the static approximation.

Equation (1.1) is not of Fredholm type although analogous in form and, for instance, classical results such as Fredholm alternative are not applicable. Moreover, due to the kernel singularity, these equations do not lend themselves simply to approximation methods and numerical integration. This point does not seem to have been clearly stressed in literature and errors in the choice of approximation methods have been made concurrently (cf. ref. ([6])). As the mathematical problem seemingly will keep its importance, we want to give to it in this article a form upon which the classical methods of approximation and the general theorems will be applicable. By the way, we shall be able to show in particular cases the existence of a solution and its non-uniqueness, and shall determine what conditions of a physical nature allow complete uniqueness. In fact the method can be generalized to a quite wide variety of problems which we shall indicate.

In Sect. 2 we give the general solution of the simplest equation of type (1.1). We study the uniqueness problem when certain conditions of physical nature are imposed. Sect. 3 deals with the reduction of a quite general case to Fredholm's one; the problem of the equivalence between these two forms is not treated. Sect. 4 generalizes this reduction to systems of coupled integral equations. Finally, we treat in Sect. 5 a particular system of coupled equations which is encountered in the problem of π-meson production by mesons ([4,6]). This last case is seen to reduce to simple quadratures, just as the problem of Sect. 2.

2. – Fundamental equation.

The simplest equation of type (1.1) is

$$\varphi(x) = f(x) + \frac{1}{\pi}\int_1^\infty \frac{h^*(x')\varphi(x')}{x' - x - i\varepsilon}\,\mathrm{d}x', \tag{2.1}$$

here $f(x)$ is a given function which we suppose bounded between 1 and ∞. $h(x)$ is a given function of the form $\exp[i\delta]\sin\delta$, where $\delta(x)$ is bounded. Whe choose arbitrarily the determination of δ which tends to 0 at infinity (supposing this choice possible) and $\delta(1) = k\pi$. δ tends to zero at least as quickly as x^{-1} when x tends to infinity. $\varphi(x)$ is the unknown function. In order to solve (2.1) we shall use a method which is a generalization of the

([4]) J. Fukuda and J. S. Kovacs: *Phys. Rev.*, **104**, 1784 (1956).
([5]) L. S. Rodberg: *Phys. Rev.*, **106**, 1090 (1957).
([6]) R. Omnès: *Nuovo Cimento*, **6**, 780 (1957).

method introduced by N. I. MUSKHELISHVILI ([7]) for the solution of Hilbert problem in elasticity, the essential difference being that here the kernel contains $h(x)$ and is not a simple Cauchy kernel. We shall have to introduce functions of a variable z defined in a complex plane cut along the interval $(1, \infty)$ and shall call $G(x+)$ (resp. $G(x-)$) the limit of a function $G(z)$ when z tends to x upon (resp. under) the cut. In the following, the cut will be called L.

Let us define the function

$$F(z) = \frac{1}{2\pi i}\int_L \frac{h^*(x')\varphi(x')}{x'-z}\,\mathrm{d}x', \tag{2.2}$$

which implies

$$\frac{1}{\pi}\int_L \frac{h^*(x')\varphi(x')}{x'-x-i\varepsilon}\,\mathrm{d}x' = 2iF(x+)\,, \tag{2.3a}$$

$$\varphi(x) = h^{*-1}_{(x)}\left[F(x+)-F(x-)\right]. \tag{2.3b}$$

Equation (2.1) takes now the form

$$\exp\left[-2i\delta\right]F(x+)-F(x-) = f(x)h^*(x)\,, \tag{2.4}$$

where we have used $1-2ih^* = \exp\left[-2i\delta\right]$. Let us now put

$$F(z) = \Phi(z)\Omega(z)\,, \tag{2.5}$$

where the function $\Omega(z)$ is defined by the condition

$$\exp\left[-2i\delta\right]\Omega(x+)-\Omega(x-) = 0\,. \tag{2.6}$$

This last equation admits a solution (which is found by taking the logarithm of (2.6))

$$\Omega(z) = \exp\left[u(z)\right]$$

with

$$u(z) = \frac{1}{\pi}\int_L \frac{\delta(\zeta)}{\zeta-z}\,\mathrm{d}\zeta\,,$$

if we define

$$\varrho(x) = \frac{1}{\pi}\,P\int_1^\infty \frac{\delta(\zeta)}{\zeta-x}\,\mathrm{d}\zeta\,, \tag{2.7}$$

([7]) MUSKHELISHVILI: *Trud. Tbil. Mat. Inst.*, **10**, 1 (1941), cited in S. G. MIKHLIN: *Integral Equations* (London, 1957), p. 126 ff.

we have

$$\Omega(x+) = \exp[\varrho + i\delta]; \quad \Omega(x-) = \exp[\varrho - i\delta]. \tag{2.8}$$

Equation (2.4) may now be transformed in a relation for $\Phi(z)$ which is of the Hilbert type

$$\Phi(x+) - \Phi(x-) = f(x)h^*(x)\Omega^{-1}(x-) = f(x)\sin\delta(x)\exp[-\varrho(x)], \tag{2.9}$$

which has a solution

$$\Phi(z) = \frac{1}{2\pi i}\int_L \frac{f(\zeta)\sin\delta(\zeta)\exp[-\varrho(\zeta)]}{\zeta - z}\,\mathrm{d}\zeta: \tag{2.10}$$

one may now derive $\varphi(x)$ by (2.1) or (2.3*b*) which give evidently the same result

$$\varphi(x) = \Big[f(x)\cos\delta(x) + \frac{1}{\pi}\exp[\varrho(x)]\cdot \cdot P\int_1^\infty \frac{f(\zeta)\sin\delta(\zeta)\exp[-\varrho(\zeta)]}{\zeta - x}\,\mathrm{d}\zeta\Big]\exp[i\,\delta(x)]. \tag{2.11}$$

It is an easy task to verify that every step of this method is correct, provided the written integrals converge and that (2.11) is truly a solution of (2.1).

It is important to point out that (2.11) is not the only solution of (2.1) for one may add to it any solution of the homogeneous equation

$$\varphi_0(x) = \frac{1}{\pi}\int_L \frac{h^*(x')\varphi(x')}{x' - x - i\varepsilon}\,\mathrm{d}x', \tag{2.12}$$

such a solution of (2.12) may yet be defined by (2.3) and a relation analogous to (2.5)

$$F_0(z) = \Phi_0(z)\Omega(z), \tag{2.13}$$

where $\Phi_0(z)$ must now verify

$$\Phi_0(x+) - \Phi_0(x-) = 0. \tag{2.14}$$

This last relation shows that $\Phi_0(z)$ is an analytic function in the whole complex plane except eventually at the points 1 and ∞ where it may have singularities. If we exclude essential singularities, the general solution of (2.1)

appears as

$$\text{(2.15)} \qquad \begin{cases} \varphi'(x) = \varphi(x) + L(x) \exp\left[\varrho(x) + i\,\delta(x)\right], \\ L(x) = \dfrac{P(x)}{(x-1)^n}, \end{cases}$$

where $P(x)$ and n are arbitrary polynomial and integer. Generally a solution will be completely determined by its asymptotic behaviour in the neighbourhood of 1 and ∞ for this behaviour by (2.11) and (2.15) determines n and $P(x)$. Particularly, for

$a)$ $\qquad k = 0 \qquad$ or $\qquad \delta(1) = 0\,,$

$b)$ $\qquad k = -1 \qquad$ or $\qquad \delta(1) = -\pi; \quad |\delta(\varepsilon) + \pi| \sim \varepsilon^{\beta} \qquad \beta > 1\,,$

(2.11) is the only solution of (2.1) regular in the neighbourhood of 1 and which tends to 0 at infinity (see appendix). These cases are precisely the more interesting in practical use since, in the context of Chew and Low model, case $a)$ may be adopted for the small phase-shifts and case $b)$ for δ_3 with $\beta = \frac{3}{2}$. Let us recall here that we have taken the determination of 2δ which is 0 at infinity. The choice $k = -1$ is equivalent to suppose only one resonance for the $(\frac{3}{2}\,\frac{3}{2})$ pion-nucleon state. Let us stress that hypotheses $a)$ and $b)$ simplify happily the calculations but are absolutely not essential to the success of this approach. If, effectively, $a)$ and $b)$ are not verified by δ, it is an easy task to determine the singularities of the integrals appearing in (2.7) and (2.11) using the first terms of the Taylor expansion of δ near 1, and to choose in a unique fashion an integer n and a polynomial $P(x)$ in (2.15) in order to have a regular solution in the neighbourhood of 1 and ∞. We shall consider this solution as the interesting one although we do not want to enter here in the difficult problem of the choice of physical criteria for a solution (see ref. [8-10]).

Let us now remark that, for $f(x)$ real, the phase of $\varphi(x)$ is δ which is intimately connected with a theorem by Fubini, Nambu and Wataghin [11].

Finally, in the more general case where h has not the form $e^{i\delta}\sin\delta$ our method is yet applicable in principle, the essential condition being now that $|1 - 2ih^*|$ must not be zero on L. One may yet write $1 - 2ih^* = \exp[-2i\gamma]$, where γ is now complex. The method used by Muskhelishvili [7] in the resolution of Hilbert's problem is apparently a particular case (*).

---

[8] L. Castillejo, R. H. Dalitz and F. J. Dyson: *Phys. Rev.*, **101**, 453 (1956).

[9] F. J. Dyson: *Phys. Rev.*, **106**, 157 (1957).

[10] R. Haag: *Nuovo Cimento*, **5**, 203 (1957).

[11] S. Fubini, Y. Nambu and V. Wataghin: to be published.

(*) *Note added in proof:* This general case was known to Muskhelishvili and treated in his book "*Singular Integral Equations*", Groningen, 1953; this was kindly pointed out to us by J. Lascoux.

3. – Equation reducible to Fredholm's type.

Let us consider the equation

$$\varphi(x) = f(x) + \frac{1}{\pi}\int_1^\infty \left[\frac{h^*(x')}{x' - x - i\varepsilon} + K(x'x)\right]\varphi(x')\,\mathrm{d}x', \tag{3.1}$$

where the kernel $K(xx')$ is regular. Including $\int K\varphi$ in the inhomogeneous part, one finds a solution analogous to (2.11) where $f(x)$ is now replaced by

$$f(x) + \frac{1}{\pi}\int K(x'x)\varphi(x')\,\mathrm{d}x',$$

if we suppose $\varphi(x)$ bounded and continuous and that $K(xx')$ verifies $K(xx') \to 0$ when $x \to \infty$, and is submitted to a Lipshitz condition, one may invert the order of integrations in

$$\begin{cases} P\int \frac{\lambda(\zeta)}{\zeta - x}\int K(x'x)\varphi(x')\,\mathrm{d}x', \\ \lambda(\zeta) = \sin\delta(\zeta)\exp[-\varrho(\zeta)]\,, \end{cases} \tag{3.2}$$

which leads to

$$\varphi(x) = \mu(x) + \frac{1}{\pi}\int_1^\infty N(x'x)\varphi(x')\,\mathrm{d}x', \tag{3.3}$$

where

$$\mu(x) = \left[f(x)\cos\delta(x) + \frac{1}{\pi}\exp[\varrho(x)]P\int_1^\infty \frac{f(\zeta)\lambda(\zeta)}{\zeta - x}\,\mathrm{d}\zeta\right]\exp[i\delta(x)]\,, \tag{3.4}$$

$$N(x'x) = \left[K(x'x)\cos\delta(x) + \exp[\varrho(x)]P\int \frac{K(x'\zeta)\lambda(\zeta)}{\zeta - x}\,\mathrm{d}\zeta\right]\exp[i\delta(x)]\,. \tag{3.5}$$

Here we shall not try to determine in detail what are necessary conditions for K and h in order that equation (3.3) be of Fredholm type: we think it to be a matter of interest only in each particular case. The solution we have obtained must evidently be regular at 1 and ∞ and one may repeat here the arguments given in the preceding section.

4. – The case of a system of coupled integral equations.

Let us consider the system

$$\varphi_i(x) = f_i(x) + \frac{1}{\pi}\int_1^\infty \left[\frac{h_i^*(x')\varphi_i(x')}{x' - x - i\varepsilon} + \sum_j K_{ij}(x'x)\varphi_j(x')\right] \mathrm{d}x', \tag{4.1}$$

by the method of the Sect. **3**, this may be put eventually in Fredholm form by

$$\varphi_i(x) = \mu_i(x) + \frac{1}{\pi}\sum_j \int N_{ij}(x'x)\varphi_j(x')\,\mathrm{d}x', \tag{4.2}$$

where

$$\begin{cases} \mu_i(x) = \left[f_i \cos\delta_i + \dfrac{1}{\pi}\exp[\varrho_i]P\displaystyle\int \frac{f_i(x')\lambda_i(x')}{x' - x}\,\mathrm{d}x'\right]\exp[i\,\delta_i(x)], \\ N_{ij}(x'x) = [K_{ij}(x'x)\cos\delta_i(x') + U_{ij}(x'x)]\exp[i\,\delta_i(x)], \end{cases} \tag{4.3}$$

$$U_{ij}(x'x) = \exp[\varrho_i(x)]P\int \frac{K_{ij}(x'\zeta)\lambda_i(\zeta)}{\zeta - x}\,\mathrm{d}\zeta\,. \tag{4.4}$$

5. – Equations for the production of mesons by mesons.

When one studies the reaction nucleon $+\pi \to$ nucleon $+2\pi$ by the methods of Chew-Low-Wick, one obtains equations of the following type for reduced matrix elements (*)

$$\varphi_i(xx_1x_2) = f_i(xx_1x_2) + \frac{1}{\pi}\int_1^\infty \frac{h_i^*(x')\varphi_i(x'x_1x_2)}{x' - x - i\varepsilon}\,\mathrm{d}x' + \tag{5.1}$$

$$+ \sum_{j=1}^{8} A_{ij}C_{ij}(x_1x_2)\,, \qquad (i = 1, \ldots, 8),$$

where A_{ij} are real numbers and

$$C_j(x_1x_2) = \frac{1}{\pi}\int \varphi_j^*(x'x_1x_2)h_j(x')\left[\frac{1}{x' - x_1 - i\varepsilon} + \frac{1}{x' - x_2 - i\varepsilon}\right], \tag{5.2}$$

(*) These equations reproduce equations (5.1) of reference [6] where we have put, in order to save writing $\varphi_i = T_{JL}$ and we have taken into account relation $\overline{T}_{JL} = (-)^{2J}T_{JL}$ which follows by time-reversal invariance.

equation (5.1) is in fact a particular case of (2.1) and its solution is given by

$$\varphi_i(xx_1x_2) = \varphi_i^{(1)}(xx_1x_2) + \varphi_i^{(2)}(xx_1x_2)\,, \tag{5.3}$$

where

$$\varphi_i^{(1)}(xx_1x_2) = \left[f_i(xx_1x_2)\cos\delta_i(x) + \frac{1}{\pi}\exp[\varrho_i(x)]\cdot P\int_1^\infty \frac{f_i(\zeta x_1x_2)\lambda_i(\zeta)}{\zeta - x}\,\mathrm{d}\zeta\right]\exp[i\,\delta_i(x)]\,, \tag{5.4}$$

$$\varphi_i^{(2)}(xx_1x_2) = \sum_j A_{ij}C_j(x_1x_2)u_i(x)\,, \tag{5.5}$$

$$u_i(x) = \left[\cos\delta_i(x) + \frac{1}{\pi}\exp[\varrho_i(x)]P\int\frac{\lambda_i(\zeta)}{\zeta - x}\,\mathrm{d}\zeta\right]\exp[i\,\delta_i(x)]\,, \tag{5.6}$$

if we define the operations $D_i[\psi(xx_1x_2)]$ which transforms a function ψ of (x, x_1, x_2) in a function of x_1 and x_2 only by

$$D_i[\psi] = \int \psi^*(x'x_1x_2)h_i(x')\left[\frac{1}{x' - x_1 - i\varepsilon} + \frac{1}{x' - x_2 - i\varepsilon}\right]\mathrm{d}x'\,, \tag{5.7}$$

$$D_i[\varphi_i] = C_i(x_1x_2) \tag{5.8}$$

and apply it to (5.4), we obtain

$$C_i(x_1x_2) = D_i[\varphi_i^{(1)}] + \sum_j A_{ij}C_j^* D_i[u_i]\,. \tag{5.9}$$

In (5.9) $D_i[\varphi_i^{(1)}]$ and $D_i[u_i]$ may be explicitely calculated and one may easily solve (5.9) for the C_j and bring them in (5.3–6). It is seen that the solution so obtained involves only quadratures, which is indeed an unexpected simple result.

6. – Conclusions.

We have given a method for the resolution of integral equations which present themselves in quantum field theory and, in particular, in the model of Chew-Low and Wick. Following the difficulties involved in the considered

problem, one is led to an explicit solution by quadratures or to non-singular integral equations. The method may be generalized to a quite wide lot of other cases. An explicit and suggesting example is given by the equations for production of mesons.

* * *

The author is happy to thank Professor C. J. Bakker for his hospitality at CERN and Professor B. Ferretti for his constant interest.

Appendix

In this appendix, we want to study the convergence of integrals appearing in equations (2.8) and (2.11). In this respect, let us consider

$$I(x) = P\int_0^\infty \frac{F(\zeta)}{\zeta - x}\,\mathrm{d}\zeta\,. \tag{A.1}$$

Here we have replaced the limit 1 by 0 in order to simplify developments and $F(\zeta)$ is a bounded and derivable function such that

$$F(\zeta) = \frac{A}{\zeta^\alpha} + O\left(\frac{1}{\zeta^\alpha}\right), \qquad \zeta > Z,\ \alpha > 0, \tag{A.2}$$

$$F(\zeta) = k + B\zeta^\beta + O(\zeta^\beta)\,, \qquad \zeta \sim 0,\ \beta > 0. \tag{A.3}$$

Let us study $I(x)$ for x near to 0 and infinitely great.

a) *x great.*

Let us put

$$I = I_1 + I_2\, I_1 = \int_0^z \frac{F(\zeta)}{\zeta - x}\,\mathrm{d}\zeta\,, \tag{A.4}$$

$$I_2 = P\int_z^\infty \frac{F(\zeta)}{\zeta - x}\,\mathrm{d}\zeta,\,,$$

for $x \gg Z\, I_1$ is of order const$/x + O(1/x)$. If we define $\alpha = n + \alpha'$ $(0 \leqslant \alpha' < 1)$

it comes

$$(A.5)\qquad I_2 = A\sum_{p=2}^{n}\frac{(-)^{n-p+1}}{x^{n-p+1}Z^{p+\alpha'-1}(p+\alpha'-1)} + \\ + (-)^{n+1}\frac{A}{x^n}P\int_z^{\infty}\frac{1}{\zeta^{\alpha'}(\zeta-x)}\,\mathrm{d}\zeta + P\int_z^{\infty}\frac{O(1/\zeta^{\alpha})}{\zeta-x}\,\mathrm{d}\zeta\,.$$

By the boundedness of the derivative the last integral is $O(x^{-1})$ and the preceding one is bounded by $Ax^{-n}\log(x-Z)Z^{-\alpha'}\log Z$. The results of Table I follow.

Table I.

ζ, x	Cases	Order of $I(x)$	Order of $\exp[I(x)]$
∞	$\alpha > 1$	x^{-1}	1
	$\alpha = 1$	$x^{-1}\log x$	1
	$\alpha < 1$	?	?
0	$k \neq 0$	$-k\log x$	x^{-k}
	$k = 0$	1	1

b) *x near to 0.*

The method is analogous, one uses (A.3) and separates the parts of I due to k, to ζ^{β} and $O(\zeta^{\beta})$, which gives, term-by-term

$$I(x) = -k\log x + \mathrm{const} + O(x)\,,$$

from which results of Table I follow.

In Table I, we give the asymptotic values of $I(x)$ and $\exp[I(x)]$. Table II

Table II.

ζ, x	Cases	Order of δ	Order of e^{ϱ}	Order of ν	Order of J
∞	$\alpha > 1$	$\zeta^{-\alpha}$	1	$\zeta^{-\alpha}$	1
	$\alpha = 1$		1		1
	$\alpha < 1$		?		?
0	$k \neq 0$ $\beta < -k$	1	x^{-k}	$\zeta^{\beta+k}$	?
	$\beta = -k$	1	x^{-k}		$\log x$
	$\beta > -k$	1	x^{-k}		1
	$k = 0$	ζ^{β}	1		1

is a direct application of the results of Table I to $\delta(\zeta)$ and $\nu(\zeta) = f(\zeta) \sin \delta(\zeta) \cdot \exp[-\varrho(\zeta)]$ where $f(\zeta)$ is bounded, and finally of $J_{(x)} = P\int \nu(\zeta)\, d\zeta/(\zeta - x)$.

One sees, as indicated in the text, that if $\beta > -k$, the integral of (2.11) converges and if $k \leqslant 0$ $\exp[\varrho(x)]$ is everywhere bounded.

RIASSUNTO (*)

Nello studio dei fenomeni complessi interessanti i mesoni π (ad es. fotoproduzione semplice e doppia, scattering radiativo, produzione doppia, ecc) si incontrano equazioni integrali che collegano gli elementi di matrice coi spostamenti di fase. Diamo qui un metodo generale per la soluzione di queste equazioni che conduce ai seguenti risultati: *a*) il tipo più semplice è integrabile per quadrature; *b*) il tipo generale è riducibile a una equazione di Fredholm. Diamo anche la soluzione di un sistema di equazioni integrali accoppiate e di quella particolare equazione che interviene nel problema della produzione doppia. Quest'ultimo caso può essere integrato per quadrature.

(*) *Traduzione a cura della Redazione.*

Meßprozeß und algebraische Eigenschaften der Feldgrößen in einer einfachen Modell-Feldtheorie.

G. Heber

Theoretisch-Physikalisches Institut der Universität - Jena

(ricevuto il 23 Gennaio 1958)

Zusammenfassung. — Es wird versucht, die bei der Ausmessung eines bestimmten Feldes mit realen Probekörpern auftretenden Meßbarkeits-Beschränkungen organisch in den feldtheoretischen Formalismus einzubauen. Hierzu werden aus den Vertauschungsregeln zwischen Ort und Impuls eines Probekörpers Vertauschungsregeln zwischen Feldgrößen und dem Ort, an dem diese Feldgrößen herrschen, abgeleitet und diskutiert.

1. – Einführung.

Angesichts der gegenwärtigen Situation auf dem Gebiete der quantisierten Feldtheorien hält es der Autor für nützlich, sich über die empirischen Grundlagen des Feldbegriffs Klarheit zu verschaffen. Für das elektromagnetische Feld wurde dies in einer früheren Untersuchung des Verf. angestrebt (1). Das wesentliche Resultat jener Arbeit war, daß bei Verwendung von in der Natur wirklich vorkommenden Probekörpern die Feldgrößen des elektromagnetischen Feldes *nicht* beliebig genau ausgemessen werden können.

Für diese Meßbarkeits-Beschränkungen wurden Unschärfe-Relationen abgeleitet. Die in (1) enthaltenen Überlegungen lassen sich unter geringfügigen Änderungen auf alle diejenigen Felder übertragen, deren Feldgrößen in linearer Weise mit Kraftwirkungen zusammenhängen.

Die vorliegende Untersuchung schließt insofern direkt an (1) an, als hier versucht wird, die in (1) abgeleiteten Unbestimmtheitsrelationen durch die Einführung passender Vertauschungsrelationen zwischen den in Frage kom-

(1) G. Heber: *Nuovo Cimento*, **7**, 677 (1958).

menden Größen zu erfüllen. Die erhaltenen Vertauschungsregeln werden dann diskutiert, insbesondere hinsichtlich ihrer physikalischen Bedeutung und ihrer formalen Struktur.

Um möglichst einfache Verhältnisse zu haben, wurde allerdings hier ein anderes Feld untersucht als in [1]. Jedoch lassen sich alle wesentlichen Resultate dieser Untersuchung auf den Fall des elektromagnetischen Feldes übertragen.

2. – Unser Modell-Feld.

Das einfachste Modell einer Feldtheorie, welches sich denken läßt, ist in der klassischen Theorie charakterisiert durch die Gleichung:

$$\Box U(x) = 0 \,, \tag{1}$$

wo $U(x)$ eine skalare, reelle Größe sein soll (*).

Man kann dieses Feld entweder als vereinfachtes Modell der Elektrodynamik oder als spezielles Mesonfeld auffassen. Wir wollen ihm physikalisch keinerlei reale Bedeutung beilegen, sondern studieren es nur seiner Einfachheit wegen. Man findet Bemerkungen über dieses Modell z.B. an verschiedenen Stellen von [2].

Will man dieses Feld $U(x)$ ausmessen, so muß man Probekörper in das Feld setzen, auf die das Feld wirkt, und muß diese Wirkungen des Feldes auf die Probekörper beobachten. Wir wissen, daß auf Quellen des Feldes [1] eine Kraft ausgeübt wird. Diese Kraft wollen wir zur Feldmessung verwenden. Dazu wird ein Probekörper bestimmter räumlicher Ausdehnung der Quelldichte des U-Feldes eine bestimmte (möglichst kurze) Zeit in der Umgebung des Punktes x_μ in das Feld gebracht. Der Probekörper erzeugt dabei eine skalar vorausgesetzte Quelldichte $\varphi(x)$ des U-Feldes, so daß statt (1) zu schreiben wäre:

$$\Box U(x) = \varphi(x) \,. \tag{1a}$$

Aus dem bekannten Energie-Impuls-Tensor des Feldes folgt dann, daß die Dichte k_ν der auf die Quelle φ wirkenden Kraft gegeben ist durch:

$$k_\nu(x) = \varphi(x)\, f_\nu(x) \,, \tag{2}$$

mit

$$f_\nu(x) = -\,\partial_\nu U(x) \qquad \text{(vgl. z.B. [2])}.$$

(*) x ist natürlich als Abkürzung des Koordinaten-Vierervektors x_ν zu verstehen.

[2] F. HUND: *Materie als Feld* (1954).

Direkt meßbar ist also hier nicht U, sondern der Gradient f_ν von U. Deshalb ist es evtl. nützlich, (1a) zu ersetzen durch Gleichungen in f_ν. Diese lauten (vgl. (2)):

$$\partial_\mu f_\nu(x) - \partial_\nu f_\mu(x) = 0\,; \qquad \partial_\mu f^\mu(x) = \varphi(x)\,. \tag{3}$$

Durch Integration von (2) über eine raumartige Hyperfläche erhielte man die Kraft auf den Probekörper; durch weitere Integration über die Zeit ergibt sich der Impuls (*), der vom Feld auf den Probekörper übergegangen ist, während er dem Feld ausgesetzt war:

$$\int f_\nu(x)\varphi(x)\,\mathrm{d}^4x \equiv F_\nu[\varphi] = p_{\nu E} - p_{\nu A}\,; \tag{4}$$

hier ist $F_\nu[\varphi]$ eine Abkürzung für das linksstehende Integral; P_{ν_E}, p_{ν_A} sind die Viererimpulse der Probekörpers zu Ende bzw. Anfang der Messung.

3. – Messungen mit einem Probekörper.

Neben F_ν bzw. p_ν ist für uns von Interesse der Vierervektor ξ_μ des « Schwerpunktes » der Quellverteilung des Probekörpers. Er ist definiert durch:

$$\xi_\mu[\varphi] \equiv \frac{\int x_\mu \varphi(x)\,\mathrm{d}^4x}{\int \varphi(x)\,\mathrm{d}^4x}\,. \tag{5}$$

$\xi_\mu[\varphi]$ ist offensichtlich diejenige Stelle, in deren Umgebung das Feld $f_\nu(x)$ (bzw. $F_\nu[\varphi]$) ausgemessen wird.

Bisher haben wir uns sowohl das Feld als auch den Probekörper als durchaus klassische Gebilde vorgestellt. Jetzt jedoch wollen wir uns überlegen, was geschieht, wenn wir den Probekörper der gewöhnlichen Quantenmechanik unterwerfen, aber noch keine eigentliche Feldquantelung vornehmen (+). Es wird sich zeigen, daß dies zu charakteristischen Begrenzungen der Lokalisierbarkeit des Feldes führt.

Falls also unser Probekörper der Quantenmechanik gehorcht, dann be-

(*) Es sei darauf hingewiesen, daß F_ν natürlich nur dann einer Impulsdifferenz gleich ist, wenn φ, wie oben erklärt, die einem bewegten Teilchen zugeordnete Quelldichte ist.

(+) Man bemerke, daß dies dem Übergang von makroskopischen zu mikroskopischen Probekörpern entspricht. Fragt man nach der Stärke des Feldes an einem bestimmten Raum-Zeit-Punkt oder nach dem Mittelwert des Feldes über ein sehr kleines Raum-Zeit-Gebiet, so kommt man bei Verwendung von in der Natur existierenden Probekörpern notwendig zu diesem Grenzübergang.

friedigen die Vierervektoren seines Impulses p_ν und seins Ortes ξ_μ die bekannten Relationen (*):

$$[p_\nu, \xi_\mu] = -i\hbar\,\delta_{\nu\mu}\,, \tag{6}$$

mit

$$\delta_{\nu\mu} = \begin{pmatrix} -1 & & 0 & \\ & +1 & & \\ & & +1 & \\ 0 & & & +1 \end{pmatrix}.$$

Aus (4) und (6) folgt aber sofort:

$$[F_\nu[\varphi],\ \xi_\mu[\varphi]] = -i\hbar\,\delta_{\nu\mu}\,. \tag{7}$$

Das heißt, $F_\nu[\varphi]$ und $\xi_\mu[\varphi]$ sind gleichzeitig nicht genau meßbar; sie haben keine gemeinsamen Eigenfunktionen. Wenn man also die Impulsdifferenz (4), aus der man auf das Feld (+) schließen könnte, exakt gemessen hat, bleibt ξ (das ist die Stelle, an der das Feld herrscht), völlig unbestimmt. Umgekehrt schließt exakte Kenntnis von ξ_ν jede Kenntnis von F_ν aus. Unser Feld ist also nicht lokalisierbar. Man wird zweckmäßig nur solche Zustände des Feldes betrachten, in denen sowohl ξ als auch F entsprechend unscharf sind.

Selbstverständlich steckt in (7) ein ernster Widerspruch zu jeder lokalen Feldtheorie. Er scheint aber unvermeidlich zu sein. Denn für die möglichst genaue Ausmessung eines Feldes in möglichst kleinen Raum-Zeit-Gebieten stehen uns nur Atome, Atomkerne, Nukleonen usw. zur Verfügung, die gewiß die Regeln (6) befolgen. Im Gedankenexperiment könnte man allerdings mit fiktiven Probekörpern arbeiten, die eine unendlich große Ladung tragen und vielleicht sogar punktförmig sein mögen. Dann könnte man die Ladung in (7) nach rechts werfen und F_ν würde mit ξ_μ tatsächlich kommutieren. Aber entsprechend einem in [1] ausgesprochenen Prinzip wollen wir solche fiktiven Probekörper nicht zulassen, sondern nur mit realen Probekörpern arbeiten.

Wir wollen also (7) ernst nehmen und möchten gern eine konsequente Feldtheorie unter Berücksichtigung von (7) aufbauen. Das heißt, wir möchten die Feldtheorie gern so formulieren, daß sie keine unbeobachtbaren Züge enthält. Von diesem Ziel sind wir allerdings noch weit entfernt. Zunächst müssen wir beachten, daß zur Ermittlung des Feldzustandes natürlich ein Probekörper

(*) Man beachte, daß der Probekörper nur in der Umgebung des Zeitpunktes ξ_0 dem Felde ausgesetzt wird. Zum Zeitpunkt ξ_0 wird also die Energie P_0 mit dem Felde ausgetauscht.

(+) Der Kürze halber nennen wir in Zukunft meist die $F_\nu[\varphi]$ « Feldgrößen ».

nicht ausreicht. Vielmehr muß man unendlich viele Probekörper einsetzen. Bei der Aufstellung von Vertauschungsrelationen zwischen unseren F und ξ genügt es jedoch, das Verhalten von zwei Probekörpern zu studieren.

4. – Messungen mit zwei Probekörpern.

Wird der eine Probekörper durch die Quelldichte $\varphi(x)$, der andere durch $\varphi'(x)$ charakterisiert, so ist eine für das algebraische Verhalten von F und ξ entscheidende Größe:

$$[F_\nu[\varphi], \xi_\mu[\varphi']] = -i\hbar G_{\nu\mu}[\varphi, \varphi'] . \tag{8}$$

Anschaulich mißt $G_{\nu\mu}[\varphi, \varphi']$ die unkontrollierbare Störung, die durch eine Ortsmessung am Probekörper φ' bei der Feldmessung mittels des Probekörpers φ entsteht und umgekehrt. Von $G_{\nu\mu}$ wissen wir bisher nur aus (7):

$$G_{\nu\mu}[\varphi, \varphi] = \delta_{\nu\mu} .$$

Unser Ziel ist es zunächst, das Funktional $G_{\nu\mu}$ etwas genauer kennenzulernen. Dazu müssen wir freilich die in (8) zugelassenen φ stark einschränken.

Die Vorschrift, durch die wir die zugelassenen φ charakterisieren wollen, sei folgende: Alle zugelassenen $\varphi(x)$ lassen sich durch Translationen aus einer willkürlich wählbaren Grundfunktion $\varphi_0(x)$ herstellen. Das heißt wir fordern für ein beliebiges $\varphi(x)$ die Existenz eines Vierervektors y_ν mit der Eigenschaft:

$$\varphi(x) \equiv \varphi_0(x - y) . \tag{9}$$

Man kann die Parameter y_ν zur Kennzeichnung einer bestimmten Struktur-Funktion verwenden und schreiben: $\varphi_y(x) \equiv \varphi_0(x - y)$. $\varphi_0(x)$ muß natürlich die in der Fußnote (*) von S. 329 erwähnte Bedingung erfüllen, ist sonst aber weitgehend willkürluch. Ohne Beschränkung der Allgemeinheit können wir annehmen, daß das Zentrum von $\varphi_0(x)$ der Punkt $x = 0$ ist. Die Quellfunktion $\varphi_y(x)$ bedeutet dann klassich-anschaulich, daß sich ein durch die Quelldichte φ_0 gekennzeichneter Probekörper an der Stelle y befindet (+). Das für alle y gleiche φ_0 heißt, alle Messungen werden nur mit *einer* Sorte von Teilchen, sagen wir mit irgendwelchen «idealen Probekörpern» ausgeführt. Wir werden also in dieser Arbeit nicht das an sich reizvolle Problem der Abhängigkeit von $G_{\nu\mu}$ usw. von φ_0 diskutieren.

(+) In der klassischen Theorie wäre natürlich gemäß (5) $\xi_\mu = y_\mu$. Aber in der Quantentheorie braucht diese Relation nicht notwendig zu gelten. Vgl. hierzu die Ausführungen im nächsten Abschnitt!

Man kann die Frage aufwerfen, welche y man in (9) zulassen sollte. Homogenität und Isotropie des Raumes scheinen zu verlangen, daß y in keiner Weise eingeschränkt werde. Wir wollen in dieser Arbeit auch dementsprechend verfahren.

Trotzdem möchte der Autor an dieser Stelle darauf hinweisen, daß dies vielleicht nicht unbedingt notwendig ist; die y_ν sind ja zunächst nur Parameter; der wirkliche physikalische Raum wird durch die Observablen ξ_μ aufgespannt; nur für die ξ_μ-Eigenwerte sollten streng genommen obige Forderungen erhoben werden (*).

Unter den in obigen Zeilen enthaltenen Voraussetzungen über die zugelassenen φ können wir also schreiben:

$$F_\nu[\varphi_y] \equiv F_\nu(y) \quad (^+); \qquad \xi_\mu[\varphi_{y'}] \equiv \xi_\mu(y)\,; \qquad G_{\nu\mu}[\varphi_y, \varphi_{y'}] \equiv G_{\nu\mu}(y - y')\,.$$

Letzteres muß wegen der Invarianz von (8) gegenüber gemeinsamen Translationen gelten. Die Abhängigkeit dieser Größen von φ_0 unterdrücken wir programmgemäß.

(8) lautet in den neuen Bezeichnungen:

$$(8a) \qquad [F_\nu(y), \xi_\mu(y')] = -i\hbar G_{\nu\mu}(y - y')\,, \qquad \text{mit} \quad G_{\nu\mu}(0) = \delta_{\nu\mu} \quad (^\times).$$

Um über $G_{\nu\mu}$ auch für $y \neq y'$ etwas aussagen zu können, müssen wir uns physikalisch klarzumachen suchen, ob und wie die Messungen $\xi_\mu(y')$ und $F_\nu(y)$ aufeinander einwirken.

Damit die durch die Messungen verursachten Störungen möglichst klein bleiben, wird es zweckmäßig sein, die Probekörper wirklich nur während der Zeitdauer der Messung dem Felde auszusetzen. Die Probekörper sollen also zu Beginn der Messung durch eine geeignete Vorrichtung in das Feld gebracht und am Ende der Messung durch eine passende Apparatur aus dem Felde genommen werden.

Den Prozeß der Injektion eines Teilchens kann man sicher so ausbilden, daß er gleichzeitig als Vorrichtung zur Messung des Vierer-Ortes ξ_μ und des Anfangs-Viererimpulses p_{ν_A} des Probekörpers dient.

Natürlich wäre es unsachgemäß, diese Vorrichtung so zu konstruieren, daß entweder ξ_ν oder p_{ν_A} genau bekannt wird, weil ja die beiden Größen komple-

(*) Auch experimentelle Verfahren der Feldmessung arbeiten ja praktisch nie mit kontinuierlich verteilten Probekörpern!

(+) Wir wollen jedoch nicht vergessen, daß $F_\nu(y)$ nicht etwa das Feld am Orte y ist, sondern der mit Hilfe des dem geometrischen Parameter y zugeordneten Probekörpers gemessene Feld(mittel)wert. Die Observable « Ort des y-Probekörpers » ist $\xi_\mu(y)$.

(×) Diese Beziehung wird übrigens weiter unten eine große Rolle spielen!

mentär zueinander sind. Man muß die Injektion deshalb so vornehmen, daß $\xi_\nu(y)$ irgendwo im Intervall $[(y_\nu - (\Delta\xi_\nu/2)) \ldots (y_\nu + (\Delta\xi_\nu/2))]$ liegt und $p_{\nu A}$ soll sich zweckmäßig im Intervall $[(-\Delta p_\nu/2) \ldots (+\Delta p_\nu/2)]$ befinden. Dabei wird man bei optimaler Konstruktion des Injektions-Apparates für jede Komponente $\Delta\xi_\nu \Delta p_\nu \approx \hbar$ erreichen können. Man bemerke, daß hierdurch 4 freie Parameter in die Theorie kommen, etwa die $\Delta\xi_\nu$. Oft wird es zweckmäßig sein, alle 4 $\Delta\xi_\nu$ einander gleich zu setzen, aber das ist keineswegs notwendig!

Wegen der Unschärfe Δp_ν von $p_{\nu A}(y)$ wird natürlich auch bei noch so genauer Messung von $p_{\nu E}(y)$ die Differenz $p_{\nu E}(y) - p_{\nu A}(y)$ $F_\nu(y)$ um eben die Größe Δp_ν unsicher. Wie aber wird durch die oben skizzierte Methode der Messung von $\xi_\mu(y)$ die Messung von $F_\nu(y')$ für $y' \neq y$ beeinflußt?

Verfasser sieht hierfür 3 Mechanismen:

a) Direkte Wechselwirkung bei Überlappung von Probekörpern;

b) Austauscheffekte;

c) Strahlungswechselwirkung.

Allen 3 Mechanismen ist gemeinsam, daß sie trivialerweise höchstens die ganze bei $y = y'$ auftretende Störung, meist aber weniger vom Probekörper $\varphi_y(x)$ auf $\varphi_{y'}(x)$ übertragen; d.h. es gilt:

$$G_{\nu\mu}(y - y') \leqslant \delta_{\nu\mu} = G_{\nu\mu}(0)\,. \tag{10}$$

Ferner kann man folgendes über dieses 3 Mechanismen sagen:

Zu *a*): Wenn sich φ_y und $\varphi_{y'}$ im x-Raum teilweise überlappen, d.h. wenn die beiden Probekörper teilweise den gleichen Raum erfüllen, werden sie natürlich irgendwie direkt miteinander wechselwirken. Allerdings ist es sehr schwer, ohne genaue Kenntnis der Natur der Probekörper etwas über die Stärke dieser Wechselwirkung zu sagen. Man kann ohne solche besonderen Kenntnisse nur gewiss sein, daß (10) erfüllt ist. Unter geeigneten Voraussetzungen über die Ausdehnung der φ und die Größe der $\Delta\xi_\nu$ wird jedoch dieser Effekt vom Mechanismus *b*) völlig überdeckt. Wir begnügen uns deshalb mit diesen wenigen Bemerkungen.

Zu *b*): Falls die Injektion der beiden identischen Probekörper, die y bzw. y' zugeordnet sind, in solcher Weise erfolgt, daß sich die Spektren von $\xi(y)$ und $\xi(y')$ teilweise überlappen, wird es schwierig sein, die beiden Probekörper voneinander zu unterscheiden. Es treten die aus der Quantenmechanik wohlbekannten Austauscheffekte auf. Dies führt dazu, daß man nach Injektion zweier Probekörper mit überlappenden ξ-Spektren $\xi(y)$ und $\xi(y')$ bei einer F-Messung zunächst nicht weiß, ob man $F(y)$ oder $F(y')$ gemessen hat. Um bei

diesem Sachverhalt nicht in Konflikt mit den Unschärferelationen zu gelangen, möchte man

$$\text{für } (y_\nu - y'_\nu) < (\Delta\xi_\nu(y) + \Delta\xi_\nu(y'))\cdot\tfrac{1}{2} \text{ fordern:}$$

$$[F_\nu(y), \xi_\mu(y')] = [F_\nu(y), \xi_\mu(y)] = -i\hbar\delta_{\nu\mu}\,. \tag{11}$$

Das heißt:

$$G_{\nu\mu}(y - y') = \delta_{\nu\mu} \quad \text{für} \quad (y_\nu - y'_\nu) < \tfrac{1}{2}(\Delta\xi_\nu(y) + \Delta\xi_\nu(y'))\,. \tag{12}$$

Eine solche Relation ist aber unschön und merkwürdig, weil man erwartet, daß die rechte Seite von (8*a*) eine universelle Funktion ist. Das durch (12) definierte G hängt jedoch von den freien Parametern $\Delta\xi_\nu$ ab. Wir wollen deshalb folgendes vereinbaren: Die in (12) auftretenden $\Delta\xi_\nu$ sollen nicht beliebige Unschärfen von ξ_ν sein, sondern die minimal möglichen. Es ist ja zu erwarten, daß der Injektionsapparat niemals so konstruiert werden kann, daß $\Delta\xi_\nu \to 0$ erreichbar wird. Vielmehr hält der Autor für sachgemäß, an dieser Stelle einen «kleinsten Vierervektor» l_ν einzuführen, so daß $\Delta\xi_\nu(y) \geqslant l_\nu$ und

$$G_{\nu\mu}(y - y') = \delta_{\nu\mu} \quad \text{für} \quad (y_\nu - y'_\nu) < l_\nu\,. \tag{12a}$$

l_ν soll durchaus universelle Bedeutung besitzen. In Abständen, die kleiner als l_ν sind, kann man prinzipiell keine gleichartigen Teilchen mehr voneinander unterscheiden (*). Natürlich darf man statt der 4 l_ν eine einzige Größe einführen, die dann die Bedeutung einer «elementaren Länge» besäße und selbstverständlich irgend einen Wert der Größenordnung 10^{-13} cm besitzen sollte (+).

Für $(y_\nu - y'_\nu) > l_\nu$ gibt der gegenwärtig diskutierte Mechanismus keinen Beitrag zu $G_{\nu\mu}(y - y')$.

Die unter *a*) erwähnte Schwierigkeit einer quantitativen Berücksichtigung des Beitrages der direkten Wechselwirkung zu $G_{\nu\mu}$ kann umgangen werden, wenn man die Freiheit in der Wahl der Quellfunktion $\varphi_0(x)$ so ausnützt, daß jede Überlappung zweier Quellen φ_ν und $\varphi_{\nu'}$ für $(y_\nu - y'_\nu) > l_\nu$ unterbleibt. Die Überlappung der φ im Gebiet $(y_\nu - y'_\nu) < l_\nu$ kann dann zu (12*a*) wegen (10) nichts mehr beitragen.

Zu *c*): Beim Prozeß der Ortsmessung $\xi_\nu(y)$ (das heißt bei der entsprechenden Injektion eines Probekörpers $\varphi_\nu(x)$) wird natürlich eine Strahlung, das heißt

(*) Man denke auch an die bei genügend kleinen Abständen einsetzenden starken Wechselwirkungen, die die Individualität der beteiligten Teilchen zerstören.

(+) Es sei erwähnt, daß wir physikalisch recht verwandte Aussagen erhalten, wenn wir nur eine diskrete Mannigfaltigkeit von y_ν zulassen, die aus den Punkten eines Raum-Zeit-Gitters mit Gitterabstand Z_ν besteht. Wegen der damit verbundenen Verletzung der Homogenität und Isotropie des y-Raumes haben wir diesen Weg aber vermieden.

eine Erregung des U-Feldes emittiert. Da wegen der Unschärferelationen (6) für den Probekörper diese Strahlung ebenfalls unscharf ist, kann sie unter Umständen eine spätere Feldmessung $F_\nu(y')$ in unkontrollierbarer Weise stören. Das heißt, falls die Strahlung von y zu y' gelangen kann, hätte man mit $[F_\nu(y'), \xi_\mu(y)] \neq 0$ zu rechnen. Man kann auch sagen: Die Strahlung hat einen Teil des durch die $\xi(y)$-Messung unbestimmten Impulses von φ_y zum Probekörper $\varphi_{y'}$ transportiert.

Weil der reziproke Prozeß, die Beeinflussung der ξ durch die F-Messung entsprechend unseren Vorstellungen über diese Messungen nicht existiert, muß G eine retardierte Funktion sein. Ferner muß, wie oben betont, die Funktion $G_{\nu\mu}(y-y')$ die Eigenschaften (10) besitzen. Sie kann also keine Pole und dergleichen besitzen. Das ist die wichtigste Erkenntnis dieses Abschnittes, die bei unseren weiteren Überlegungen wesentlich sein wird. Die explizite Gestalt von $G_{\nu\mu}$ benötigen wir im Augenblick nicht unbedingt. Doch wollen wir zusammenfassend hervorheben, daß unter vernünftigen Annahmen über φ_0 die Formel (12a) eine brauchbare Näherung sein dürfte.

Bei Messungen mit 2 Probekörpern interessiert natürlich auch, wie sich zwei Ortsmessungen gegenseitig beeinflussen. Das heißt, man fragt nach dem Wert von $[\xi(y), \xi(y')]$. Unseren oben entwickelten Vorstellungen über den ξ-Meßprozeß entspricht es, wenn wir

$$[\xi_\nu(y), \xi_\mu(y')] \equiv 0 \tag{13}$$

setzen. Denn jede Injektion ist ein von der anderen völlig unabhängiger Eingriff von außen und kann für sich beliebig geregelt werden.

Ferner interessiert die Größe $[F(y), F(y')]$. Hier wird in Strenge wegen des durch die Strahlung und andere Prozesse ermöglichten Impulstransportes von φ_y nach $\varphi_{y'}$ im allgemeinen gelten:

$$[F(y), F(y')] \neq 0 .$$

Aber da wir von der klassischen Feldtheorie ausgehen, möchten wir der Einfachheit wegen zunächst probieren, ob man nicht auch mit

$$[F_\nu(y), F_\mu(y')] \equiv 0 \tag{14}$$

sowie (13), (10) und (8a) eine in sich konsequente Feldtheorie aufbauen kann.

Abschließend zu diesem Abschnitt sei ausdrücklich darauf hingewiesen, daß die hier skizzierten Überlegungen natürlich die Form der fraglichen Vertauschungsrelationen nur plausibel machen können. Man kann nämlich prinzipiell eine Quantentheorie aus der korrespondierenden klassischen Theorie nicht streng ableiten. Man kann also nur die plausibel gemachten Vertauschungsregeln und die anderen Grundgleichungen axiomatisch an die Spitze der Theorie stellen und sehen, ob man vernünftige Folgerungen aus der Theorie erhält.

5. – Einige spezielle Fragen.

Der eben genannte Gesichspunkt ist auch wichtig für die Beurteilung der Frage, ob die Gleichungen (1) bis (5) der klassischen Theorie in unsere Quantentheorie als Operatorgleichungen übernommen werden sollen.

Die Korrespondenz zur klassischen Theorie verlangt nur, daß die klassischen Relationen in Beziehungen zwischen den Erwartungswerten der betreffenden Größen übergehen. Operatorgleichungen *können* aus klassischen Gleichungen hervorgehen, das *muß* aber nicht so sein. Wir diskutiren hierzu zwei Beispiele:

a) Offensichtlich können die Differentialgleichungen der klassischen Theorie für die $f_\nu(x)$ bzw. $F_\nu(y)$ nicht als Operatorgleichungen in die Quantentheorie übernommen werden. Denn sonst würden aus (8*a*) entsprechende Feldgleichungen für die $\xi_\mu(y)$ folgen. Die Größen $\xi_\mu(y)$ sind aber gar keine Feldgrößen im konventionellen Sinne (s.o.) und es wäre nach Meinung des Autors unsachgemäß, wollte man sie einer Feldgleichung unterwerfen.

b) Wir wollen im folgenden prüfen, wozu die Übernahme von Gl. (5) in die Quantentheorie führt. Aus (5), (9) und

$$\int x\varphi_0(x)\,\mathrm{d}^4x = 0\,,$$

folgt:

$$\xi_\mu(y) \equiv \frac{\int x_\mu \varphi_\nu(x)\,\mathrm{d}^4x}{\int \varphi_\nu(x)\,\mathrm{d}^4x} = y_\mu\,. \tag{15}$$

Man kann mit Hilfe von (15) die Größen $\xi_\mu(y)$ völlig aus der Theorie eliminieren. Hiermit würde z.B. (8*a*) übergehen in:

$$[F_\nu(y),\, y'_\mu] = -i\hbar G_{\nu\mu}(y - y')\,. \tag{8b}$$

(8*b*) ist eine recht interessante Relation. Zunächst ist klar, daß y jetzt ein Operator geworden ist. Vordem hatten wir y als c-Zahl-Parameter angesehen, der die verschiedenen Probekörper charakterisiert. Aus (8*b*) folgt aber vor allem, daß $F_\nu(y)$ keine Funktion von y allein sein kann. Denn speziell für $y = y'$ lautet ja (8*b*):

$$[F_\nu(y)\,,\, y_\mu] = -i\hbar G_{\nu\mu}(0) = -i\hbar\,\delta_{\nu\mu}\,.$$

Das ist aber nicht verträglich mit der notwendig gültigen Identität: $[y_\nu, y_\mu] = 0$. Vielmehr muß F_ν noch von einer anderen Variablen, sagen wir η_ν, abhängen: $F_\nu = F_i(y, \eta)$, wobei im allgemeinen $[\eta_\nu, y_\mu] \neq 0$ sein sollte. Damit sind wir zu einer Theorie vom bilokalen Typ gelangt (vgl. hierzu etwa [3]).

[3] J. Rayski: *Nuovo Cimento*, **2**, 255 (1955).

Der Autor hat jedoch einige gewichtige Bedenken gegen den durch (15) gekennzeichneten Übergang:

1.) (15) verlangt die Gleichheit zweier Größen, die wesentlich verschiedene Bedeutung haben. y hatten wir ja als Parameter zur Kennzeichnung unserer Probekörper eingeführt. Solch ein Parameter muß natürlich eine c-Zahl sein. $\xi(y)$ hingegen war als die Observable «Ort des durch y gekennzeichneten Probekörpers» eingeführt worden. Die durch (15) geforderte Vereinigung von Teilchen-Index und dynamischer Variabler $\xi(y)$ ist deshalb höchst merkwürdig.

2.) Durch (15) wird der unserer Vorstellung über die ξ-Messung, wie sie oben dargestellt wurde, adäquate mathematische Formalismus zerstört. Vorher konnten wir sagen: y charakterisiert die Einstellung des Injektions-Gerätes; $\xi(y)$ repräsentiert den wirklichen Ort des bei der Einstellung y injizierten Probekörpers. $\xi(y)$ und y sollten wegen statistischer Effekte i.a. nicht zusammenfallen. Dieser Möglichkeit sehen wir uns durch (15) beraubt.

3.) Nach Einführung der Gleichung $\xi(y) = y$ kommt ferner nicht mehr zum Ausdruck, daß wir zur vollständigen Ausmessung des Feldes unendlich viele Probekörper benötigen. Denn jedem Operator entspricht nach den bekannten Regeln der Quantentheorie gerade *ein* Meßprozeß. Es ist nicht zu sehen, wie man mit den 4 Operatoren y_ν die erforderliche Mannigfaltigkeit von Meßprozessen darstellen kann.

4.) Schließlich hält es der Autor für etwas merkwürdig und bedenklich, daß die rechte Seite von (8b) i.a. keine c-Zahl mehr ist, sondern q-Zahl-Charakter erhält. Schon die ganz allgemeine Schreibweise (8) brachte ja zum Ausdruck, daß der Kommutator von F und ξ eine c-Zahl sein sollte.

Aus all diesen Gründen neigt der Autor dazu, Gl. (5) bzw. (15) nicht in die Quantentheorie zu übernehmen; statt dessen möchten wir nur fordern, daß der Erwartungswert $\overline{\xi(y)}$ von $\xi(y)$ gleich y wird:

$$\overline{\xi_\mu(y)} = y_\mu \,. \tag{15a}$$

Als Abschluß dieses Abschnittes sei noch eine spezielle Methode zur Erfüllung der Veratuschungsregeln (8a), (13) und (14) angegeben. Unter Einführung des aus den konventionellen Feldtheorien gut bekannten, sehr großen, 4-dimensionalen Normierungs- und Periodizitätsvolumens schreibe man:

$$\left\{\begin{aligned} F_\nu(y) &= \sum_k p_{\nu,k} \exp\,[iky]\,, \\ \xi_\mu(y') &= \sum_k q_{\mu,k} \exp\,[-iky']\,, \\ G_{\nu\mu}(y-y') &= \sum_k g_{\nu\mu,k} \exp\,[ik(y-y')] \end{aligned}\right. \tag{16}$$

und erhält sofort:

$$\text{(17)} \qquad \begin{cases} [p_{\nu,k},\, q_{\mu,l}] = -\,i\hbar\,\delta_{k,l}\,g_{\nu\mu,k}\,, \\ \text{sowie} \\ [p,\, p] = [q,\, q] \equiv 0\,. \end{cases}$$

Die Relationen (17) kann man im sicher vorliegenden Fall $g_{\nu\mu,k} = \delta_{\nu\mu}\cdot g_k$ sofort erfüllen, indem man z.B. wie in der Wellenmechanik setzt:

$$\text{(18)} \qquad \begin{cases} q_{\mu,l} = q_{\mu,l} \quad (c\text{-Zahlen})\,; \\ p_{\nu,k} = \dfrac{\hbar}{i}\,g_k\,\dfrac{\partial}{\partial q_{\nu,k}}\,. \end{cases}$$

Die Relationen (17) sind besonders interessant wegen der aus (18) folgenden Eigenschaft der $g_{\nu\mu,k}$:

$$\text{(19)} \qquad \sum_k g_{\nu\mu,k} = \delta_{\nu\mu}\,; \qquad \text{d.h.:} \quad \sum_k g_k = 1\,.$$

Die $g_{\nu\mu,k}$ müssen also in ihrer Abhängigkeit von k eine charakteristische, starke Konvergenz zeigen. Mit $g_{\nu\mu,k} \to 0$ werden die entsprechenden p_k, q_k gemäß (17) in zunehmendem Maße klassische Größen. Aus diesem Umstand leiten wir unsere Hoffnung darauf ab, daß eine durch (8*a*) modifizierte Feldtheorie gewisse Divergenz-Schwierigkeiten der klassischen Theorie nicht enthält. Als einfachstes Beispiel kann man das Produkt der mittleren Schwankungsquadrate von $\xi(y)$ und $F(y)$ berechnen (*). Eine solche Größe ist in Theorien mit unendlich vielen Freiheitsgraden in der Regel divergent. Hier bleibt sie konvergent wegen der Eigenschaft (10) bzw. (19) unseres Kommutators.

6. – Schlußbemerkungen.

Wir haben damit gewissermaßen die Kinematik unseres Modell-Feldes an die realen Meß-Möglichkeiten angepaßt. Es bleiben wichtige Probleme wie das der Dynamik dieses Feldes und das der vollständigen Quantisierung des Modelles vorläufig noch ungelöst. Besonders schwierig sind diese Probleme u.a. deshalb, weil es gar nicht trivial zu sein scheint, die Größen $\xi_\mu(y)$ sachgemäß in eine geschlossene Feldtheorie einzubauen. Eine andere Schwierigkeit be-

(*) Man kann diese Rechnung bekanntlich ohne Kenntnis der Bewegungsgleichungen durchführen; es gehen nur die Vertauschungsrelationen ein!

trifft die Quellfunktion $\varphi_0(x)$. Und zwar muß man sich überlegen, ob man Deformationen der Quelldichte bei einwirkenden Kräften zulassen will oder nicht. Dabei muß man beachten, daß in (4) implizite die Annahme eingeführt ist, daß weder Impuls noch Energie vom Feld auf die *inneren* Freiheitsgrade der Quelle übergehen können. Die Quelle besitzt nach (4) nur die Translations-Freiheitsgrade. Auch (9) wäre natürlich mit Deformationen nicht verträglich. Diesen Schwierigkeiten könnte man natürlich entgehen, wenn man wieder punktförmige Probekörper, also $\varphi_0(x) \sim \delta^4(x)$ (*) einführte.

Es ist möglich, daß dies keine neuen Schwierigkeiten hervorruft, solange in (12a) $l_v > 0$ gehalten wird. Diese Frage bedarf jedoch noch einer sorgfältigen Prüfung. Verfasser hofft, einige der offenen Fragen später behandeln zu können.

* * *

Der größte Teil der vorliegenden Untersuchung wurde während des Aufenthaltes des Autors im Vereinigten Institut für Kernforschung in Dubna (UdSSSR) ausgeführt. Es ist dem Autor ein aufrichtiges Bedürfnis, vielen Mitarbeitern dieses Institutes für die erwiesene Gastfreundschaft und für anregende Diskussionen zu danken. Besonders herzlicher Dank für wertvolle Anregungen bzw. Bemerkungen gilt den Herren Professoren Blohinčev und Ning Hu in Dubna.

(*) Unter $\delta^4(x)$ verstehen wir wie üblich das Produkt der 4 Diracschen Delta-Funktionen für $x_0 \ldots x_3$.

RIASSUNTO (*)

Si cerca di introdurre organicamente nel formalismo della teoria del campo le limitazioni di misurabilità che sorgono esplorando un determinato campo con corpi di prova reali. A tal fine, dalle regole di scambio tra posizione e quantità di moto di un corpo di prova si derivano regole di scambio tra le grandezze del campo e la posizione in cui tali grandezze dominano, discutendo il risultato.

(*) *Traduzione a cura della Redazione.*

Nuclear Potential for τ^+-mesons.

T. G. Lim and S. J. Bosgra

Natuurkundig Laboratorium - Universiteit van Amsterdam, The Netherlands

(ricevuto il 26 Gennaio 1958)

Summary. — An analysis of the elastic scattering of τ^+-mesons in G5 nuclear emulsion shows that the nuclear potential by which the τ^+-mesons are scattered is repulsive and that its value is higher than 13 MeV.

1. – Introduction.

In order to examine the scattering of K^+-mesons we used two stacks of Ilford G5 nuclear emulsion which were exposed to the K^+-beam, set up by Kerth and Stork (1) of the Berkeley Bevatron. The stacks consist of 80 sheets of 600 μm pellicles, each with an area of about 100 cm^2. We determined the elastic differential cross-sections of the τ^+-mesons in the angular region $(2 \div 20)°$. The analysis of these forward angles is based on the optical model of the nucleus (2) which was also used in the analysis of the π-meson scattering (3). Information regarding the sign and value of the nuclear potential is thus obtained. The analysis was carried out for the energy region of $(30 \div 90)$ MeV.

2. – Experimental procedure.

The identified τ^+-meson tracks have been searched for scattering events. This was done by means of a hairline in the eyepiece of the microscopes so that any change of direction could easily be detected. All scattering angles

(1) R. W. Birge, R. P. Haddock, L. T. Kerth, J. R. Peterson, J. Sandweiss, D. H. Stork and M. N. Whitehead: *Suppl. Nuovo Cimento*, **4**, 351 (1956).
(2) H. A. Bethe: *Phys. Rev.*, **57**, 1125 (1942).
(3) A. Pevsner and J. Rainwater: *Phys. Rev.*, **100**, 1431 (1955).

which had a projection of 2° or larger in the plane of the emulsion were recorded; the conversion to space angles was carried out by means of a Wulff's net.

The determination of the energy loss was done by counting about 1000 grains before and after each collision. The relative energy loss determination by means of the relative ionization is rather insensitive to personal systematic errors and to the possible inhomogeneity of the emulsion. All scattering events of the K^+-mesons with an energy loss of 10 % or less were classified as elastic.

3. – Correction for the geometric loss.

It can easily be seen that a fraction of the scattering events escapes detection if the plane of scattering is unfavorably oriented and the total number of angles of a certain type (depending on the elevation or dip of the incoming particle) should be corrected for this geometric loss. The situation of a scattering event is illustrated in Fig. 1. Let δ be the smallest projected angle in

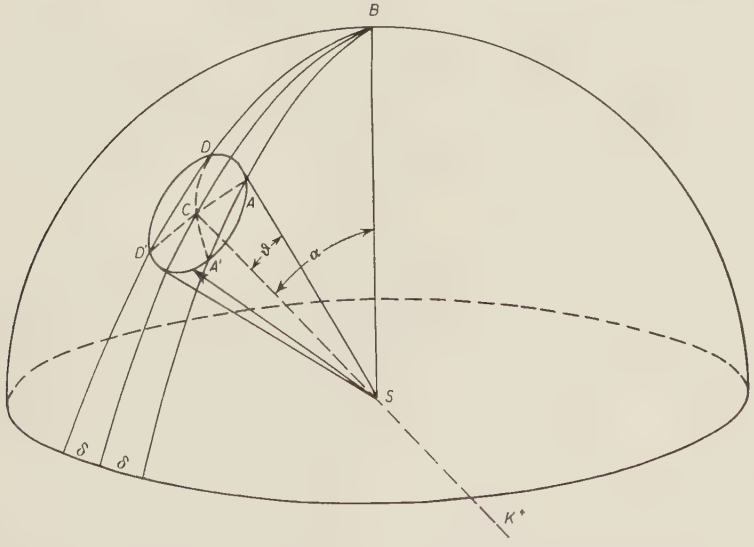

Fig. 1. – A scattering event. A particle of which the line of flight makes an angle α with SB is scattered under an angle ϑ; δ is the smallest angle which is recorded.

the emulsion plane which is recorded. A meson of which the line of flight makes an angle α with the vertical is scattered by a scattering center S. The track after scattering and the former line of flight SC define an angle ϑ.

All possible scattering events with scattering angle ϑ for a constant line of flight SC form a cone with SC as axis, ϑ being the half-angle of opening. The angles which have a projection smaller than δ in the horizontal plane (i.e. the plane of the emulsion) are not recorded. Assuming an equal probability for the scattering around SC, the fraction P which is lost by this way of recording is $(\angle ACD + \angle A'CD')/2\pi$. Call $\varkappa = 1/(1-P)$ the correction factor by which the number of events of a certain type must be multiplied. Keeping δ constant, this correction factor $\varkappa$ is sensitively dependent on ϑ and α for the angles of scattering ϑ near δ. In our computation we took this dependence into account and we corrected every event individually. In this sensitive region the angle α is computed before every collision.

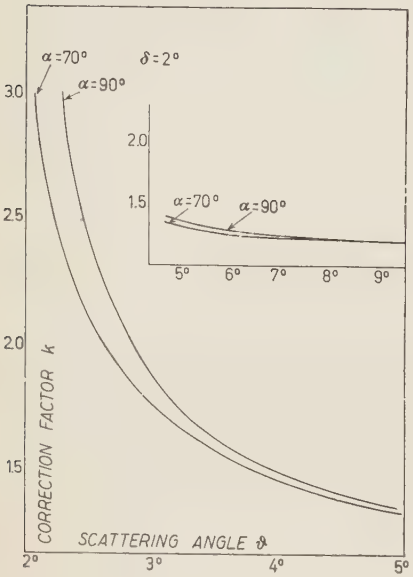

Fig. 2. – Dependence of the geometric correction factor $\varkappa$ on the angles α and ϑ for $\delta = 2°$.

In Fig. 2 two curves are presented which show this dependence of $\varkappa$ on α and ϑ for a value $\delta = 2°$.

4. – Results.

The experimental differential cross-sections for elastic scattering of the τ^+-mesons are compared with the theoretical curves of COSTA and PATERGNANI (4). From Fig. 3 it can be seen that our experimental points lie well above the 13 MeV real potential curve, suggesting that the average nuclear potential for the τ^+-mesons has a repulsive character and a value higher than +13 MeV, probably about 20 MeV.

BISWAS *et al.* (5) deduced a repulsive nuclear potential of about 12 MeV from K^--meson scattering measurements in the energy region of (60 ÷ 100) MeV. They, however, took only into account scattering angles larger than 10°. MARCHI *et al.* (6) investigated K^+-meson scatterings in the energy region of

(4) G. COSTA and G. PATERGNANI: *Nuovo Cimento*, **5**, 448 (1957).

(5) N. N. BISWAS, L. CECCARELLI-FABBRICHESI, M. CECCARELLI, K. GOTTSTEIN, N. VARSHNEYA and P. WALOSCHEK: *Nuovo Cimento*, **5**, 123 (1957).

(6) C. MARCHI, G. QUARENI, A. VIGNUDELLI, G. DASCOLA and S. MORA: *Nuovo Cimento*, **6**, 1790 (1957).

(50 ÷ 120) MeV and considered scattering angles of 3° and larger. They inferred a repulsive nuclear potential of 10 MeV.

HOANG *et al.* (7) carried out measurements between (30 ÷ 65) MeV and dis-

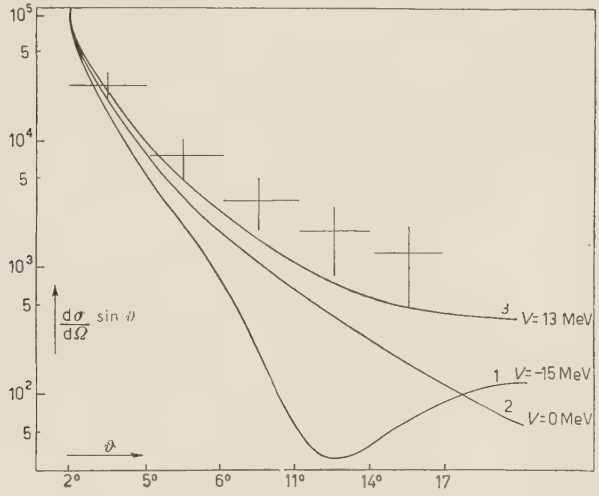

Fig. 3. – Experimental differential cross sections of 67 elastic scatterings of τ^+-mesons in the energy region of (30 ÷ 90) MeV. Drawn curves are calculated theoretically by COSTA and PATERGNANI. They result from the interference between the Coulomb potential and the nuclear potential. Curve 1: nuclear potential: — 15 MeV (attractive). Curve 2: nuclear potential: 0 MeV. Curve 3: nuclear potential: + 13 MeV (repulsive). The errors given are statistical ones.

carded angles less than $7\frac{1}{2}$°. They found a repulsive potential of about 15 MeV. Our measurements are in agreement with the results reported at the Padua Conference by S. GOLDHABER (8). In the energy region of (40 ÷ 100) MeV they found a repulsive potential of about 20 MeV.

* * *

This work is part of the research program of the Netherlands Foundation for Fundamental Research of Matter (F.O.M.) financially supported by the Netherlands Institution for Pure Scientific Research (Z.W.O.).

(7) T. F. HOANG, M. F. KAPLON and R. CESTER: *Phys. Rev.*, **107**, 1698 (1957).
(8) G. IGO, D. G. RAVENHALL, J. J. TIEMANN, J. E. LANNUTTI, G. GOLDHABER, S. GOLDHABER and R. M. THALER: *Proc. of the Padua-Venice Conf.* (September 1957).

The authors wish to express their gratitude to Dr. R. W. BIRGE, Dr. E. J. LOFGREN and the Bevatron Staff in Berkeley for the two stacks exposed to the K^--beam. Thanks are due to Professor Dr. G. W. RATHENAU and Dr. M. BRUIN for many discussions, to Mr. J. P. VAN DER LINDEN and to Mrs. H. A. C. BARREVELD, Mr. T. J. VAN DER LINDE and Mrs. H. E. VAN VLIET of the scanning group for their assistance.

RIASSUNTO (*)

Un'analisi dello scattering elastico dei mesoni τ^+ nelle emulsioni nucleari G5 dimostra che il potenziale nucleare col quale avviene lo scattering dei mesoni τ^+ è repulsivo ed ha valore superiore a 13 MeV.

(*) *Traduzione a cura della Redazione.*

IL NUOVO CIMENTO Vol. VIII, N. 2 16 Aprile 1958

The Solutions of the Low Equation - I.

D. B. Fairlie and J. C. Polkinghorne

Tait Institute of Mathematical Physics - University of Edinburgh, Scotland

(ricevuto il 30 Gennaio 1958)

Summary. — The connection between the manifold of solutions of the Low equation for a non-relativistic system and the existence of « hidden structure » is exhibited.

1. – Introduction.

Castillejo, Dalitz and Dyson (1) have shown that the Low equation for certain simple cases of scattering possesses an infinite number of solutions. Norton (2) has obtained a similar result for a more extensive set of equations. The question of the physical significance and acceptability of all these solutions has been the subject of discussion. Haag (3) has shown that all but the simplest solution appear to lead to eigenstates of the total Hamiltonian that are not orthogonal. On the other hand Dyson (4) has constructed a class of Lee-type models which can be put in one-one correspondence with the solutions of a single basic Low equation. The reconciliation of these two statements is easily found in the observation that Haag's results are obtained under the explicit assumption that the eigenstates of the free Hamiltonian are in one-one correspondence with the asymptotic form of the eigenstates of the total Hamiltonian. The Dyson model does not fulfil this condition as excited states of the scatterer appear as intermediate states but not as asymptotic

(1) L. Castillejo, R. H. Dalitz and F. J. Dyson: *Phys. Rev.*, **101**, 453 (1956).

(2) R. E. Norton: *A Derivation of a Complete Set of Dispersion Relations and the Examination of Their Physical Content* (preprint).

(3) R. Haag: *Nuovo Cimento*, **5**, 203 (1957).

(4) F. J. Dyson: *Phys. Rev.*, **106**, 157 (1957).

states. This observation is made by HAAG in a footnote added in proof. In this note we give an explicit investigation of the relation between the solutions of the Low equation and the existence of such « hidden structure ». In Sect. 2 we show that the use of general Low equation solutions implies that this hidden structure must exist, and in Sect. 3 we give an analysis of the Dyson model in the spirit of HAAG's arguments.

2. – The Low equation.

We consider the Low equation for a non-relativistic system. H_0 is the free Hamiltonian; $H = H_0 + V$ the total Hamiltonian; $|\overset{+}{k}\rangle$ the set of eigenstates of H corresponding to the eigenvalues E_k, and satisfying the condition that

$$\lim_{t\to\infty} \exp[iH_0 t] \exp[-iHt] |\overset{+}{k}\rangle \to |k\rangle , \tag{1}$$

where $|k\rangle$ are eigenstates of H_0 with eigenvalues E_k. We shall assume initially that the states $|k\rangle$ form a complete set of the eigenstates of H_0. We therefore have the relations

$$\sum_k |\overset{+}{k}\rangle\langle\overset{+}{k}| = 1 , \tag{2}$$

$$\sum_k |k\rangle\langle k| = 1 . \tag{3}$$

We find that

$$|\overset{+}{k}\rangle = |k\rangle - \frac{1}{H - E_k + i\varepsilon} V |k\rangle , \tag{4}$$

and using (2) this readily yields

$$\langle\overset{+}{k'}|V|k\rangle = -\sum_{k''} \frac{\langle\overset{+}{k''}|V|k'\rangle^* \langle\overset{+}{k''}|V|k\rangle}{E_{k''} - E_{k'} - i\varepsilon} + \langle k'|V|k\rangle . \tag{5}$$

This is the Low equation for the theory and HAAG has shown how this be reduced to the familiar form for factorizable potentials V.

From (4) we have

$$\langle\overset{+}{k'}|\overset{+}{k}\rangle = \langle\overset{+}{k'}|k\rangle - \frac{1}{E_{k'} - E_k + i\varepsilon} \langle\overset{+}{k'}|V|k\rangle ,$$

and so

$$\langle\overset{+}{k'}|k\rangle = \delta(k' - k) + \frac{1}{E_{k'} - E_k + i\varepsilon} \langle\overset{+}{k'}|V|k\rangle . \tag{6}$$

Equation (7) provides the link between the solutions of the Low equation (5) and the properties of the eigenkets $|\overset{+}{k}\rangle$. In fact HAAG derives two conditions for consistency from this connection which must be satisfied by solutions of (5). The first is the completeness condition. From (2)

$$\sum_{k''} \langle k' | \overset{+}{k''} \rangle \langle \overset{+}{k''} | k \rangle = \langle k' | k \rangle = \delta(k' - k) . \tag{7}$$

From (6) equation (7) is satisfied if and only if

$$A(k', k) = A(k, k')^* , \tag{8}$$

where

$$A(k', k) = \langle \overset{+}{k'} | V | k \rangle + \sum_{k''} \frac{\langle \overset{+}{k''} | V | k' \rangle^* \langle \overset{+}{k''} | V | k \rangle}{E_{k''} - E_{k'} - i\varepsilon} . \tag{9}$$

From (5)

$$A(k', k) = \langle k' | V | k \rangle \tag{10}$$

and so condition (8) follows from the hermiticity of V.

The second condition is obtained from (3) and is

$$\sum_{k''} \langle \overset{+}{k'} | k'' \rangle \langle k'' | \overset{+}{k} \rangle = \langle \overset{+}{k'} | \overset{+}{k} \rangle = \delta(k' - k) . \tag{11}$$

This is satisfied if

$$B(k', k) = B(k, k')^* , \tag{12}$$

where

$$B(k', k) = \langle k' | V | \overset{+}{k} \rangle + \sum_{k''} \frac{\langle \overset{+}{k'} | V | k'' \rangle \langle \overset{+}{k} | V | k'' \rangle^*}{E_{k'} - E_{k''} + i\varepsilon} . \tag{13}$$

Haag terms this the orthogonality condition. We prefer to call this the asymptotic completeness condition, for if (3) holds we readily see that

$$\left| \begin{aligned} \langle \overset{+}{k'} | V | \overset{+}{k} \rangle &= \sum_{k''} \langle \overset{+}{k'} | k'' \rangle \langle k'' | V | \overset{+}{k} \rangle \\ &= B(k', k) , \end{aligned} \right. \tag{14}$$

and so (12) would appear to follow also from the hermiticity of V. However HAAG shows by an explicit calculation that (12) fails for $|\overset{+}{k}\rangle$ constructed from any but the simplest solution of the Low equation. We therefore conclude that for these solutions (3) fails and that there are eigenstates $|\alpha\rangle$ of H_0, not

obtained by the limiting process (1), which together with $|k\rangle$ form a complete set:

$$\sum_k |k\rangle\langle k| + \sum_\alpha |\alpha\rangle\langle\alpha| = 1 . \tag{15}$$

These states $|\alpha\rangle$ express the « hidden structure » that must be associated with the system if one of the general Low equation solutions is to be valid. We then have

$$\begin{aligned} B(k', k) = \langle \overset{+}{k'} | V | \overset{+}{k} \rangle - \sum_\alpha \langle \overset{+}{k'} | \alpha \rangle\langle \alpha | V | \overset{+}{k} \rangle = \\ = [\langle \overset{+}{k'} | V | \overset{+}{k} \rangle - \sum_\alpha \sum_\beta \langle \overset{+}{k'} | \alpha \rangle\langle \alpha | V | \beta \rangle\langle \beta | \overset{+}{k} \rangle] - \\ - \sum_\alpha \sum_{k''} \langle \overset{-}{k'} | \alpha \rangle\langle \alpha | V | k'' \rangle\langle k'' | \overset{+}{k} \rangle , \end{aligned} \tag{16}$$

and the condition (12) fails because V must contain terms linking the $|\alpha\rangle$ and the $|k\rangle$. The simplest example of this is provided by the Dyson model that is discussed in the next section.

3. – The Dyson model.

This model discusses the scattering of particles by a scatterer which is initially in its ground state. The mechanism consists solely of the absorption of a particle to form an excited state of the scatterer and the subsquent re-emission of the particle, the scatterer being required to return to its ground state. In this notation of Sect. 2, the states $|k\rangle$ are the states consisting of particles with energy E_k plus ground state of scatterer, the states $|\alpha\rangle$ are the excited states of the oscillator. These are the elements of the « hidden structure ». For this model the interaction V only has matrix elements between a $|k\rangle$ and an $|\alpha\rangle$ and we write

$$\begin{cases} \langle \alpha | V | k \rangle = Q_\alpha u(k) , \\ \langle k | V | \alpha \rangle = Q_\alpha^* u^*(k) . \end{cases} \tag{17}$$

The Schrödinger equation is equivalent to the set of equations

$$(E_{k'} - E_k)\langle k' | \overset{+}{k} \rangle + u^*(k') \sum_\alpha Q_\alpha^* \langle \alpha | \overset{+}{k} \rangle = 0 , \tag{18}$$

$$(E_\alpha - E_k)\langle \alpha | \overset{+}{k} \rangle + Q_\alpha \sum_{k''} u(k'')\langle k'' | \overset{+}{k} \rangle = 0 . \tag{19}$$

If $f(k)$ is defined by

$$f(k)\frac{u(k')}{u(k)} = \langle \overset{+}{k}|V|k'\rangle = \sum_{\alpha}\langle \overset{+}{k}|\alpha\rangle Q_{\alpha}u(k')\,, \tag{20}$$

then it follows from (5) that $f(k)$ satisfies a Low equation. Moreover

$$\sum_{\alpha}\langle \overset{+}{k'}|\alpha\rangle\langle\alpha|V|\overset{+}{k}\rangle = \sum_{\alpha}\sum_{k''}\langle \overset{+}{k'}|\alpha\rangle\langle\alpha|V|k''\rangle\langle k''|\overset{+}{k}\rangle =$$

$$= \sum_{\alpha}\langle \overset{+}{k'}|\alpha\rangle Q_{\alpha}\sum_{k''}u(k'')\langle k''|\overset{+}{k}\rangle\,.$$

However from equation (19)

$$\sum_{\alpha}Q^{*}_{\alpha}\langle\alpha|\overset{+}{k}\rangle = \left[\sum_{\alpha}\frac{|Q_{\alpha}|^{2}}{E_{k}-E_{\alpha}}\right]\sum_{k''}u(k'')\langle k''|\overset{+}{k}\rangle\,,$$

and so

$$\sum_{\alpha}\langle \overset{+}{k'}|\alpha\rangle\langle\alpha|V|\overset{+}{k}\rangle = \frac{f(k')f^{*}(k)}{u(k')u^{*}(k)}R^{-1}(k)\,, \tag{21}$$

where

$$R(k) = \sum_{\alpha}\frac{|Q_{\alpha}|^{2}}{E_{k}-E_{\alpha}}\,. \tag{22}$$

Dyson [4] shows that $R^{-1}(k)$ is effectively the generalized R-function of Castillejo, Dalitz and Dyson [1] for the Low equation for this model. Thus equations (16) and (21) exhibit directly the connection between the failure of condition (12) and the existence of the generalized R-function (22) generating the manifold of solutions of the Low equation.

* * *

One of us (D.B.F.) wishes to thank the Department of Scientific and Industrial Research for a maintenance grant.

RIASSUNTO (*)

Si mostra la connessione tra la famiglia di soluzioni dell'equazione di Low per un sistema non relativistico e l'esistenza di una « struttura nascosta ».

(*) *Traduzione a cura della Redazione.*

Isotopic Properties of the K-Meson Decay Interaction.

R. F. SAWYER

Harvard University - Cambridge, Massachusetts

(ricevuto il 27 Febbraio 1958)

It has been shown that the weak interaction responsible for θ-decay must contain $\Delta T = \frac{1}{2}, \frac{3}{2}$, and $\frac{5}{2}$ in order to be consistent with the presently observed branching ratio of θ^0 and with the long θ^+ lifetime. We have therefore investigated other properties of the weak interaction which would forbid θ^+-decay and account for the branching ratio $\tau/\tau' = 4$, as would $\Delta T = \frac{1}{2}$.

Symmetry in the strong interactions, beyond that of charge independence, can be the basis for obtaining a selection rule with very general isotopic properties of the weak interaction. We have assumed a universal pion coupling to all heavy fermions; and we have assumed that the fundamental decay coupling involves the heavy fermions only, or heavy fermions connected by a weakly interacting boson. To forbid θ^0-decay we considered three possible combinations of symmetry in the strong K interaction (NΛK, NΣK, ΞΛK, ΞΣK) and in the decay interaction:

1) No restriction on the K coupling and invariance of the weak coupling under the individual unitary transformations: (notation of ref. (2))

$$U_1 = \exp[i\pi Z_3], \qquad U_1^{-1}\psi_{1.0,\frac{1}{2}}U_1 = i\varphi_3\psi_{1.0,\frac{1}{2}},$$

and

$$U_2^{-1}\psi_{1,0}U_2 = iv_1\varphi_1\psi_{\frac{1}{2}}, \qquad U_2^{-1}\psi_{\frac{1}{2}}U_2 = iv_1\varphi_1\psi_{1,0}, \qquad U_2^{-1}\varphi_\pi U_2 = -\varphi_\pi.$$

The pion interaction is invariant under U_1 and U_2. Now we may state that in the lowest order of g_k, but to all orders in g_π, the decay mode θ_+ is forbidden. The proof involves considering only that portion of the K interaction which annihilates the initial K_+ particle; hence a statement in the first order of g_k:

2) A K interaction which leaves the Λ and Σ masses unsplit (2) and a decay interaction invariant under U_1. In this case we have a rule valid to all orders in both g_k and g_π. The source of K^+-decay in this picture is the source of Λ, Σ mass splitting.

(1) M. GELL-MANN: *Nuovo Cimento*, **5**, 758 (1957).
(2) J. SCHWINGER: *Ann. Phys.*, **2**, 407 (1957).

3) A K interaction leaving Λ and Σ unsplit and a decay interaction invariant under the unitary operation

$$U_3\psi_{1.0}U_3^{-1} = \nu_1\psi_{\frac{1}{2}}\,, \qquad U_3\psi_{\frac{1}{2}}U_3^{-1} = \nu_1\psi_{1.0}\,.$$

This forbids θ^+ in first order of g_k. The θ^0-decay is allowed in all three schemes.

In 1) and 2) we have assumed conservation of the quantity Z_3. This is what will be needed to prohibit $\Xi^- \to N^0 + \pi^-$, but also means that Σ^- decay will be forbidden, in the absence of K-meson corrections. However, we may expect K corrections to be of great importance in the Σ decays, where the mass difference is assumed to result from the K coupling.

For a realization of these symmetries we considered an intermediate vector boson coupled universally to heavy fermions. The effective four-fermion interaction for K decay into pions is

$$L_w = g_w(\psi_{\frac{1}{2}}\beta\gamma_\mu M_i\,\psi_{1.0})(\psi_{1.0}\beta\gamma_\mu M_i\,\psi_{1.0} + \psi_{\frac{1}{2}}\beta\gamma_\mu M_i\,\psi_{\frac{1}{2}})\,,$$

where i is the index indicating the charge of the intermediate meson. If the matrices M_i were τ_i $(i = 1, 2, 3)$ we would have $\Delta T = \frac{1}{2}$. The simplest way to introduce $\Delta T = \frac{3}{2}, \frac{5}{2}$ is to sum over $i = 1, 2$, that is, to use a purely charged meson. When parity nonconservation is introduced into M_i, L_w may be split into two parts, one responsible for θ-decay and one for τ-decay. We may choose $M_i = \tau_i(1 + i\gamma_5\nu_3)$ where the ν_3 is used to restore the antisymmetry required of a matrix connecting Fermi fields. If the K interaction is scalar that part of L_w effective in θ-decay is

$$g_w[\psi_{\frac{1}{2}}\beta\gamma_\mu\tau_i\psi_{1.0}][\psi_{1.0}\beta\gamma_\mu\tau_i\psi_{1.0} + \psi_{\frac{1}{2}}\beta\gamma_\mu\tau_i\psi_{\frac{1}{2}}] + \\ + g_w[\psi_{\frac{1}{2}}\beta\gamma_\mu(i\gamma_5\nu_3)\tau_i\psi_{1.0}][\psi_{1.0}\beta\gamma_\mu(i\gamma_5\nu_3)\tau_i\psi_{1.0} + \psi_{\frac{1}{2}}\beta\gamma_\mu(i\gamma_5\nu_3)\tau_i\psi_{\frac{1}{2}}]\,.$$

This θ-decay interaction now fulfills the conditions of 1) and 2). If the K interaction is P. S. it is necessary to change the sign of the $\psi_{\frac{1}{2}}\beta\gamma_\mu M_i\psi_{\frac{1}{2}}$ term in order to have invariance under U_2. The θ-decay interaction in this case would be

$$g_w[\psi_{\frac{1}{2}}\beta\gamma_\mu\tau_i\psi_{1.0}][\psi_{1.0}\beta\gamma_\mu(i\gamma_5\nu_3)\tau_i\psi_{1.0} - \psi_{\frac{1}{2}}\beta\gamma_\mu(i\gamma_5\nu_3)\tau_i\psi_{\frac{1}{2}}] + \\ + g_w[\psi_{\frac{1}{2}}\beta\gamma_\mu(i\gamma_5\nu_3)\tau_i\psi_{1.0}][\psi_{1.0}\beta\gamma_\mu\tau_i\psi_{1.0} - \psi_{\frac{1}{2}}\beta\gamma_\mu\tau_i\psi_{\frac{1}{2}}]\,.$$

Since the $\Lambda\Sigma$ mass splitting is small it is reasonable to assume that the K interaction consists of a term which does not split the Λ and Σ, plus a weaker term which accounts for the mass difference. The conclusions of 1) and 2) may then be combined into the statement that decay is allowed only when higher order effects in the weak, non-splitting term of the K coupling are included. This may be sufficient to explain the transition rate ratio $\theta^+/\theta^0 = 1/500$.

We may, within this universal coupling scheme allow the θ-decay coupling to contain $\Delta T = \frac{5}{2}$ while restricting the τ coupling to $\Delta T = \frac{1}{2}$ and $\frac{3}{2}$. For a scalar K we choose

$$M_i = \tau_i + \tfrac{1}{2}\gamma_5\nu_3[\tau_i, \tau_3]\,. \qquad \text{where } i = 1, 2\,.$$

The terms in L_w with an odd number of γ_5's (τ-decay) now contain no $\Delta T = \frac{5}{2}$, explaining the τ/τ' branching ratio if the final orbital state is sufficiently symmetric.

Rapid Decrease of Cosmic-Ray Intensity (*).

R. A. R. Palmeira (+) and R. W. Williams

Physics Department and Laboratory for Nuclear Science
Massachusetts Institute of Technology - Cambridge, Mass.

(ricevuto il 3 Marzo 1958)

A remarkable sudden decrease in cosmic-ray μ-meson intensity occurred in connection with the magnetic storm and auroral display of the night of 10 February 1958. We have put in operation a high counting rate, high time-resolution meson monitor which enables detailed study of such events. The instrument employs large disks of plastic scintillator [1], and consists of three telescope units, each of which counts coincidences between two layers of the plastic disks. Fig. 1 is a view of one telescope unit; each disk is 107 cm in diameter and 9 cm thick, a layer of four disks is viewed by two Dumont 5 in. 6364 photomultipliers (only one is shown in the drawing) and two-fold coincidence is made between the upper and lower layers with a resolving time of 0.15 microseconds. The efficiency is over 90%, so that a nearly flat « plateau » is obtained at a counting rate corresponding to the known meson intensity. Each layer has a scintillator area of 3.4 m^2, and the two layers are arranged for maximum counting rate: small vertical separation (25 cm) and essentially no absorber between layers. The total absorber thickness, principally the concrete roof of the building, is 50 g cm^{-2}. The outputs of the three telescopes can be recorded individually or added electronically to give a total counting rate of nearly 1000 counts per second. To take advantage of the high resolution which this rate affords, a special recorder has been devised (to be described elsewhere [2]) which accurately registers the number of counts in each 30-second interval; absolute time is known to $\pm$ 3 seconds. The monitor is located at Cambridge, Massachusetts at sea level latitude 41° 23′ N., longitude 71° 08′ W.

At the time of the sudden decrease the sum output of two telescopes was being recorded on the count recorder and the third telescope was on a low-precision counting-rate meter. The record of the count recorder, with counts averaged over 8-minute intervals for convenience, is shown in Fig. 2; the 8-minute average

(*) Supported by the joint program of the O.N.R. and the U.S.A.E.C.

(+) On leave from Centro Brasileiro de Pesquisas Fisicas, Rio de Janeiro, Brazil.

(1) G. Clark, F. Scherb and W. Smith: *Rev. Sci. Inst.*, **28**, 433 (1957).

(2) R. G. D'Arcy: to be published.

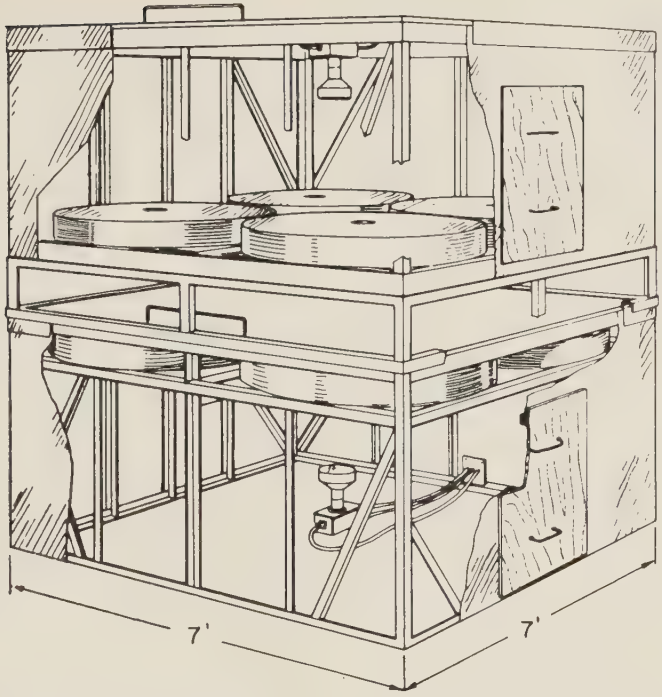

Fig. 1. – Cutaway view of one of the three telescopes which comprise the monitor. There are at present two five-inch phototubes for each layer of scintillator.

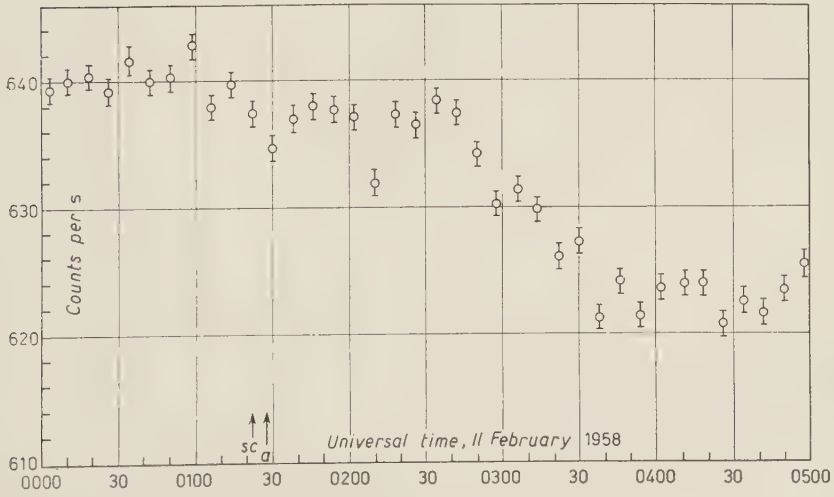

Fig. 2. – The intensity of cosmic-ray μ-mesons at the time of the auroral display of February 10-11, 1958, averaged over 8 min intervals. *SC* indicates the sudden commencement of the magnetic storm; *a* indicates approximately the beginning of the aurora.

counting rates are given in Table I, which includes samples of the recovery of the intensity after the drop. All rates

TABLE I. – *Counting rate of the meson monitor in counts per second, averaged over 8-minute intervals, on 11 February 1958. The standard deviation of each entry is* $\pm$ 1.2 *counts per second.*

Universal Time	Counts per second	Universal Time	Counts per second
0002	639.3	0250	634.3
0010	640.0	0258	630.3
0018	640.5	0306	631.5
0026	639.3	0314	629.9
0034	641.8	0322	626.2
0042	640.0	0330	627.4
0050	640.5	0338	621.3
0058	624.9	0346	624.3
0106	638.0	0354	621.6
0114	639.7	0402	623.7
0122	637.7	0410	624.0
0130	634.8	0418	624.1
0138	637.1	0426	620.9
0146	638.1	0434	622.8
0154	637.7	0442	621.7
0202	637.4	0450	623.6
0210	632.7	0458	625.6
0218	637.4		
0226	636.6	0800	625.6
0234	638.8		
0242	637.5	1100	632.4
		1430	633.1
		1700	638.7

are corrected for barometric changes, the largest correction being 0.46%. The change in height of the upper atmosphere over this period would correspond to a correction of about 0.1%, which has not been made since detailed data are not available. With the exception of the third telescope the instrument has been in operation since August 1957, and has proved to be stable and reliable. A check on the results at the time of the decrease is provided by the third telescope, which has completely independent circuitry, and which showed the same decrease, although with poor precision because of the limitations of the counting-rate meter.

The record (Fig. 2) shows that a small decrease began at about 0100 Universal (Greenwich) Time on 11 February 1958, and the intensity has dropped 0.5% by 0240 U.T. At (0245 $\pm$ 5) U.T. the sharp drop began; the intensity dropped 2.1% in about one hour, leveling off at (0340 $\pm$ 5) U.T. The intensity remained at this level for a few hours (Table I), then rose gradually to its pre-drop value, the total time from the drop being about 14 hours. The magnetic storm began with a « sudden commencement » at 0121 U.T. ([3]), and the aurora began a few minutes later. Presumably the three phenomena correspond to the arrival of ionized gas emitted from the sun during the previous day, but the solar activity of that day was so great that it does not seem possible to identify the specific event that was responsible.

The event reported here resembles previously-reported « Forbush » decreases except that the time scale is shorter ([4]). Theories of these decreases ([5-7]) generally assume the arrival of solar gas clouds carrying magnetic fields which somehow exclude a fraction of the cosmic rays from the vicinity of the earth. The median energy of the primaries of the me-

([3]) Preliminary Report of Solar Activity TR 337, High Altitude Observatory, Univ. of Colorado, Boulder, Colorado.

([4]) For example, for the widely-noted decrease of August 29, 1957, our monitor recorded a 2.8 % decrease in 10 h, and recovery in another 82 h.

([5]) P. MORRISON: *Phys. Rev.*, **101**, 1397 (1956).

([6]) E. N. PARKER: *Phys. Rev.*, **103**, 1518 (1956).

([7]) G. COCCONI, T. GOLD K. GREISEN, S. HAYAKAWA, and P. MORRISON, Procedings of the Varenna Conference, *Nuovo Cimento*, in press.

sons recorded by our apparatus is about 10 GeV; the gyration radius of a 10 GeV proton in a field of B gauss is $3.3 \cdot 10^7 B^{-1}$ cm; and the minimum time in which a magnetic cloud of velocity v carrying a field B could make its effects felt is greater than $3.3 \cdot 10^7 (Bv)^{-1}$ s. This implies, for a typical gas-cloud velocity of 2000 km s^{-1}, and a one-hour decrease a model-independent lower limit for B of $5 \cdot 10^{-5}$ G. The actual lower limit depends on the model assumed; in the diffusion model ([5]), for example, fields from two to three orders of magnitude greater than this would be required; in the gravitational-capture model ([6]) the capture time is longer than one hour, and a more detailed calculation would be required to see whether the model could reproduce the effects reported. The model proposed by Cocconi *et al.* envisions an elongated tongue-shaped magnetic field drawn out from the sun by the outburst of gas, and remaining well-organized out to the earth's orbit. The decrease would then correspond to the tip of this tongue passing over the earth. The three models should give quite different predictions for the anisotropy of the cosmic-ray decreases. It would be very useful to have high-resolution records of these events from different parts of the world.

* * *

We are indebted to R. G. D'Arcy for much of the design and successful completion of the monitor; to W. B. Smith for invaluable assistance; to Professor T. Gold for a helpful discussion; and to Professor B. Rossi for his original suggestion and continued support for this work. One of us (R.A.R.P.) is supported by a fellowship of the Conselho Nacional de Pesquisas, Brasil.

Dynamic Determination of Viscosity.

A. Carrelli and E. Ragozzino
Istituto di Fisica Sperimentale dell'Università - Napoli

(ricevuto il 6 Marzo 1958)

We have repeated the measurements of internal friction coefficient of fluids with the torsional method that is to say in such a condition that the speed in the various layers and its gradient are not constant in time. The new measurements refer to 150 Hz frequency obtained by a frequency static triplicator (*). After having put the 150 Hz single phase current on the section $DABC$ of the set already mentioned in the previous note, we made the verification at this frequency of the following equations:

$$(1) \qquad A = k \frac{1}{\sqrt{\varrho\eta}} \cdot \mathrm{tgh}\left(\sqrt{\frac{\omega_0 \varrho}{\eta}} \cdot s\right)$$

$$(2) \qquad A_{as} \cdot \sqrt{\varrho\eta} = k\,.$$

We must remember that in (1) A is the oscillation amplitude of a cylinder immersed in another coaxial cylinder containing a liquid with density ϱ and viscosity η, s is the thickness of the liquid layer between the two cylinders, ω_0 is the pulsation of the alternate current put on the circuit and k an instrumental constant. The quantity A_{as} which appears in (2) is the asymptotic oscillation amplitude, obtained by using external cylinders with a very big radius.

Referring to the substances already examined at 50 Hz frequency, plotting A against s we obtained some points placed on a right line parallel to the axis of the abscissa. That means that with $\nu = 150$ Hz also for a s value of 16 mm, corresponding to the smallest internal cylinder we used, the amplitude A has already reached the asymptotic value

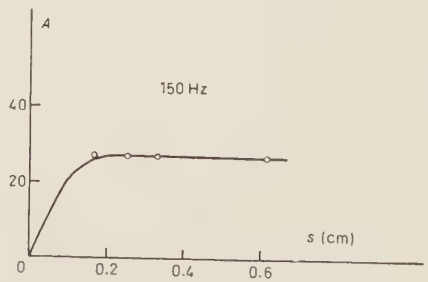

Fig. 1.

and the theoretical curves, traced in accordance with this experimental value, confirm this interpretation (Fig. 1 refers to glycerine).

(*) The set has been invented by Ing. U. Corbino who kindly has put it at our disposal, and we thank him here very deeply.

The experimental verification of (2) with the new frequency has shown that the characteristic of special solutions already studied is much more evident. In fact glycerine, solutions of glycerine in water and some mineral oils still act as (2) (Fig. 2 referring to solutions of glycerine in water of different concen-

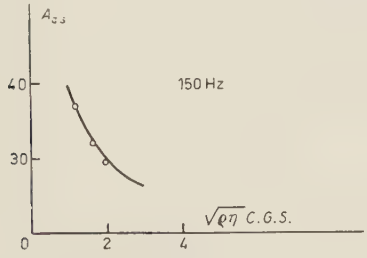

Fig. 2.

trations shows that the experimental values are really on an equilateral hyperbola); on the contrary colloidal solutions of nylon in formic acid and of para in benzol display more evidently their cha-

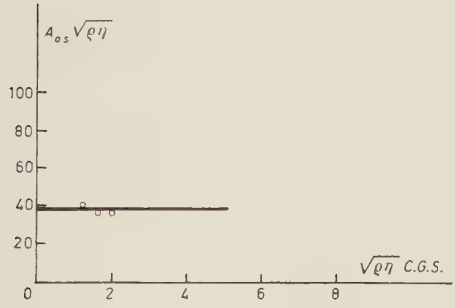

Fig. 3.

racteristic deviations. For the first group of substances the $A_{as}\cdot\sqrt{\varrho\eta}$ products assume, in the limits of the experimental errors, a constant value and form the right line shown in Fig. 3, it does not happen at all for the second group (see the dashed curves of Fig. 4 and 5). In this regard we must notice that for solutions of nylon in formic acid, with $\nu = 50$ Hz, the product $A_{as}\cdot\sqrt{\varrho\eta}$, the value of $\sqrt{\varrho\eta}$ passing from 2 to 4, had a 10% variation; with $\nu = 150$ Hz the pro-

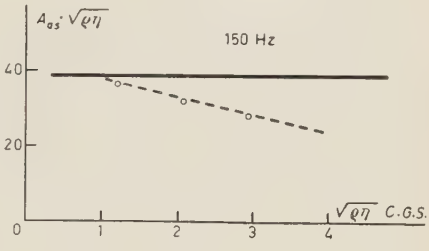

Fig. 4.

duct had a 21% variation (Fig. 4). The product $A_{as}\cdot\sqrt{\eta\varrho}$ for the solutions of para in benzol had a 32% variation the value of $\sqrt{\varrho\eta}$ passing from 2 to 4;

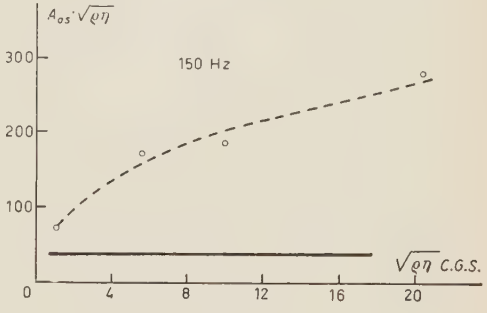

Fig. 5.

with $\nu = 150$ Hz the product had a 86% variation (Fig. 5).

Vaseline in benzol, on the contrary,

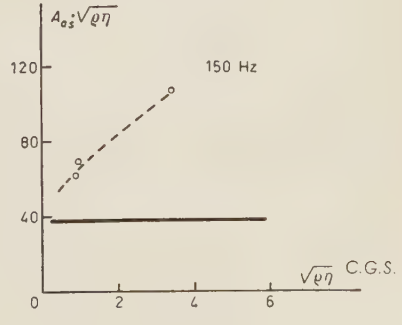

Fig. 6.

still presenting remarkable deviations from the values we can deduce from (2), is not affected by this frequency increase.

With the new frequency we examined other substances. The dispersions of tylose in water act as solutions of para in benzol and vaseline in benzol (Fig. 6); on the contrary some colloidal solutions of polyvinyl alcohol in water, at least the most diluted solutions, act as shown in (2).

We can therefore conclude that some solutions of very complex molecules, with this method of viscosity measurements, do not act regularly from two points of view; with the purpose of studying more completely the question from a theoretical standpoint, we will make other researches at higher frequencies.

On the Coupling between (Λ^0, p) Field and the K-Meson Field (*).

E. M. Ferreira (+)

Department of Mathematics, Imperial College - London

(ricevuto il 20 Marzo 1958)

It can be shown [1] that if the decay $\Lambda^0 \to p + \mu + \nu$ goes through a Fermi coupling with constant of the order of that of β-decay ($= 3 \cdot 10^{-49}$ erg cm^3) then the mean life of the process will be about 200 times longer than the experimental one. That is, for about 200 decays of Λ^0 into $p + \pi$ there will be only one going to $p + \mu + \nu$.

We now ask whether the decay into 3 fermions can proceed through the interaction with the K-meson field, that is $\Lambda^0 \to p + K \to p + \mu + \nu$, the intermediate state being a virtual one. The calculations we have done lead to the following result. If both couplings $(\Lambda^0, p; K)$ and $(\mu, \nu; K)$ are scalar, the expression for the mean life is

$$(1) \qquad 1/\tau = 2 \cdot 10^{104} (4\pi\hbar c)^2 K^{-4} \cdot \cdot (G^2/4\pi\hbar c)(g^2/4\pi\hbar c) ,$$

where all quantities are in c.g.s. units, K is the inverse compton wave length of the K-meson, G is the coupling constant in the vertex $(\Lambda^0, p; K)$ and g is the coupling constant in the vertex $(\mu, \nu; K)$. Using for g the value as given by the rate of the $K \to \mu + \nu$ decay ($g^2/4\pi\hbar c = 2.3 \cdot 10^{-16}$) we get

$$(2) \qquad \tau(G^2/4\pi\hbar c) = 5.3 \cdot 10^{-5} .$$

This means that even if the decay into three fermions occurs in only one thousandth of the cases ($\tau = 1000\tau_{exp}$, with $\tau_{exp} = 2.85 \cdot 10^{-10}$ s) the coupling constant has the quite unreasonably large value of $G^2/4\pi\hbar c = 1.8 \cdot 10^2$.

The calculations have shown that if any other coupling except the scalar one is assumed at any of the two vertices, then the value of $G^2/4\pi\hbar c$ will be larger than that given by (1) or (2).

The implication of these results is that if $G^2/4\pi\hbar c$ has a value about 1, as estimated by Gell-Mann [2] and by Matthews and Salam [3] then the decay $\Lambda^0 \to p + \mu + \nu$ through this mechanism will occur in only one out of $1.8 \cdot 10^5$ cases. The direct Fermi interaction of the type considered by L. Lopes [1] would then be the dominant interaction leading to the three fermions.

(*) Supported by the National Research Council of Brazil.

(+) On leave of absence from the Centro Brasileiro de Pesquisas Fisicas, Rio de Janeiro.

(1) L. Lopes: *An. da Acad. Bras. de Ciencias* (in press).

(2) M. Gell-Mann: *Phys. Rev.*, **106**, 1296 (1957).

(3) P. T. Matthews and A. Salam: *Phys. Rev.* (in press).

For a given value of $G^2/4\pi\hbar c$ the small rate of the decay is in part due to the large value of the K-meson mass in (1) and in part due to the small value of $g^2/4\pi\hbar c$. This last factor can be modified by considering that it is possible that in virtue of some selection rule the decay rate of $K \to \mu + \nu$ is smaller by a factor of the order of 10^2 than the value expected simply from the magnitude of the coupling constants. This consideration would increase the value of $g^2/4\pi\hbar c$ by a factor of 10^2, the right hand side of (2) becoming $5.3 \cdot 10^{-3}$.

* * *

We are indebted to Prof. A. Salam for the suggestion of the present work and to Dr. P. T. Matthews for helpful discussions.

IL NUOVO CIMENTO Vol. VIII, N. 2 16 Aprile 1958

Metodi approssimati per lo studio della diffusione pione-nucleone in onde S.

M. Bassetti

Istituto di Fisica dell'Università - Roma

(ricevuto il 29 Marzo 1958)

È stato recentemente fatto [1] un confronto tra due metodi di approssimazione, quello di Tamm-Dancoff e quello variazionale di Cini-Fubini [2] applicato allo scattering delle onde S nell'urto pione-nucleone per un'interazione del tipo

$$(1) \qquad H_I = g\int \varrho(x)\varrho(x')\boldsymbol{\varphi}(x)\cdot\boldsymbol{\varphi}(x')\,\mathrm{d}x\,\mathrm{d}x' + \lambda\int \varrho(x)\varrho(x')\boldsymbol{\tau}\cdot[\boldsymbol{\varphi}(x)\times\boldsymbol{\pi}(x')]\,\mathrm{d}x\,\mathrm{d}x'\,.$$

Le soluzioni approssimate ottenute con questi due metodi sono confrontate con una soluzione ritenuta esatta ottenuta per questa interazione da Lomon [3]. Poichè all'ordine più basso la soluzione di Tamm-Dancoff si approssima meglio della soluzione variazionale alla soluzione ritenuta esatta si conclude in B.M. affermando che un metodo d'approssimazione non soddisfacente il « crossing theorem » (Tamm-Dancoff) può essere migliore di uno che lo soddisfi (Cini-Fubini).

È chiaro come queste conclusioni perdano la loro validità se si riesce a dimostrare che la soluzione esatta di Lomon non è tale. Un dubbio di questo genere nasce dall'osservazione che Lomon nel trovare la sua soluzione ha adottato un metodo di diagonalizzazione in un numero finito di dimensioni, mentre il problema trattato che ha infinite variabili richiede un numero infinito di dimensioni.

D'altra parte si controlla facilmente se la soluzione di Lomon è esatta semplicemente confrontando il suo sviluppo perturbativo (per semplicità è sufficiente esaminare il caso $g = 0$):

$$\operatorname{tg}\delta_j = \lambda_j A_1 + \lambda_j^2 A_2 + \dots\,, \qquad \lambda_1 = 2\lambda\,, \quad \lambda_3 = -\lambda$$

dove

$$A_1 = \frac{\varkappa\omega(\varkappa)v^2(\varkappa)}{2\pi}\,, \qquad A_2 = \frac{\varkappa v^2(\varkappa)}{4\pi}V + \frac{\varkappa v^2(\varkappa)\omega^2(\varkappa)}{\pi}S(\varkappa)\,,$$

$$V = \frac{1}{2\pi^2}\int_0^{+\infty} v^2(\varkappa')\varkappa'^2\,\mathrm{d}\varkappa'\,, \qquad S(\varkappa) = \frac{1}{2\pi^2}\int_0^{+\infty}\frac{v^2(\varkappa')\varkappa'^2}{\varkappa'^2-\varkappa^2}\,\mathrm{d}\varkappa'\,,$$

(1) B. H. Bransden e R. G. Moorhouse: *Nuovo Cimento*, **6**, 693 (1957), indicato in seguito come B.M.

(2) M. Cini and S. Fubini: *Nuovo Cimento*, **11**, 142 (1954).

(3) E. Lomon: *Nuovo Cimento*, **4**, 106 (1956).

con la soluzione perturbativa usuale della matrice K [4] ottenuta dall'Hamiltoniana (1).

Seguendo i metodi usuali si ottiene (nel caso $T = \frac{3}{2}$) per il secondo sviluppo

$$\operatorname{tg} \delta_3 = \lambda_3 B_1 + \lambda_3^2 B_2 + \dots .$$

Mentre $A_1 = B_1$ si trova facilmente

$$B_2 = A_2 + \frac{\varkappa v^2(\varkappa)}{8\pi^3} \int_0^{+\infty} \frac{v^2(\varkappa')\big(\omega(\varkappa') - \omega(\varkappa)\big)^2}{\big(\omega(\varkappa') + \omega(\varkappa)\big)\omega(\varkappa')} \varkappa'^2 \mathrm{d}\varkappa' .$$

La soluzione di Lomon deve essere perciò considerata anch'essa una approssimazione alla soluzione esatta. Uno studio più sistematico della validità del metodo variazionale nel caso di interazione costituita da due Hamiltoniane è in corso.

---

[4] B. A. Lippmann e J. Schwinger: *Phys. Rev.*, **79**, 469 (1950).

LIBRI RICEVUTI E RECENSIONI

H. PREUSS – *Integraltafeln zur Quantenchemie*. Zweiter Band Springer-Verlag, Göttingen, 1957, pag. IV-143; tabelle. Prezzo L. 5760.

È questo il secondo di una collana di quattro volumi che sarà presto completata in conformità di un programma recentemente pubblicato dall'Autore in *Zeits. f. Elektrochemie*, B **924**, 61 Heft, 8 (1957).

Abbiamo già avuto occasione (*Nuovo Cimento*, **5**, 819 (1957) di segnalare l'interesse che presenta, per lo studio dei problemi di struttura molecolare, una tabulazione, il più completa possibile, degli integrali che coinvolgono le funzioni di Slater e i vari addendi dell'operatore Hamiltoniano; potrà forse interessare il lettore qualche maggiore dettaglio.

Gli integrali che più frequentemente si incontrano nei problemi di fisica molecolare sono dei seguenti quattro tipi:

I) $$\int \varphi_a^* \varphi_b \mathrm{d}\tau ,$$

II) $$\int \varphi_a^* r_c^k \varphi_b \mathrm{d}\tau ,$$

III) $$\int \varphi_a^* \Delta \varphi_b \mathrm{d}\tau ,$$

IV) $$\int \varphi_a^*(1)\varphi_b^*(2)\frac{1}{r_{12}}\varphi_c(1)\varphi_d(2)\mathrm{d}\tau_1 \mathrm{d}\tau_2 ,$$

in cui le φ sono delle funzioni idrogenoidi senza nodi di Slater, gli indici a, b, c, d si riferiscono agli atomi su cui sono centrate le funzioni corrispondenti, quelli 1, 2 specificano gli elettroni e Δ è l'operatore Laplaciano.

Nel primo volume sono riportati i valori degli integrali monocentrici I e II (caso $a = b = c$) per i valori di $K = -2$, -1, 0, 1, 2 e con i parametri α e β uguali e variabili di 0.5 in 0.5 da 0.5 a 10 e vi si trovano tabulati pure gli integrali bicentrici I, II e IV, sempre con funzioni aventi tutte lo stesso parametro di schermo, e per i valori di $\alpha R = 0.5(0.5)7$ (R è la distanza tra i due centri).

Sempre nel primo volume si trova, poi, un certo numero di funzioni ausiliarie, comode per il calcolo di I, II (caso $c = a$, b) e IV, ed alcuni integrali del tipo I, II (caso $c = a$, b) e III valutati con pure funzioni esponenziali anzichè con funzioni di Slater.

In questo secondo volume, invece, sono tabulati gli integrali monoelettronici I e II (caso $c = a$, b) per i casi di costanti di schermo α e β differenti e per i valori αR, $\beta R = 0.5(0.5)8$ e $8(1.0)10$. Come nella prima parte, anche qui si trovano alcuni integrali ausiliari per il calcolo di II.

Sfortunatamente non sembra incluso, nell'attuale programma di Preuss, il calcolo e la tabulazione degli integrali di tipo IV per funzioni di Slater con costanti di schermo diverse, dei quali

sarebbe molto utile per lo meno il caso bicentrico; tuttavia, nel presente volume e in quello di prossima pubblicazione, si potranno trovare gli integrali ausiliari utili per il loro calcolo. Inoltre le funzioni di Slater usate si limitano ai soli due gusci K ed L.

Come per il volume precedente, la veste tipografica è molto buona e i valori numerici sono stati accuratamente controllati dall'Autore.

E. Scrocco

F. E. Borgnis und C. H. Papas – *Randwertprobleme der Mikrowellenphysik*. Springer-Verlag, 1955, pagg. XV+266, con 75 figure, rilegato.

Come indica il titolo questo volume tratta problemi al contorno nella fisica delle microonde; in altre parole, problemi di propagazione ed irraggiamento di onde elettromagnetiche con condizioni al contorno assegnate. La trattazione è basata essenzialmente sui metodi variazionali stazionari introdotti specialmente da Schwinger (vedasi, ad esempio, Lippmann e Schwinger: *Phys. Rev.*, **79**, 469 (1950)); metodi che sono tra i più potenti in questo tipo di problemi e che sono familiari a coloro che conoscono la meccanica quantistica in quanto servono egualmente bene, naturalmente, a trattare problemi di scattering di particelle.

Diamo qui di seguito una lista di alcuni tra i principali problemi trattati: Diffusione di un'onda elettromagnetica da un cilindro, in varie condizioni, e relative espressioni delle sezioni di diffusione; irraggiamento di un cavo coassiale semiinfinito collegato ad uno schermo; comportamento di due cavi coassiali accoppiati aventi sezioni esterne diverse; teoria delle guide d'onda; determinazione delle frequenze proprie di varie cavità risonanti; problemi di irraggiamento di antenne.

Si tratta di un'opera nella quale, con una chiara esposizione, oltre a discutere i problemi suaccennati in tutti i dettagli, si danno i metodi per trattare problemi analoghi; pertanto pensiamo che essa sia indispensabile a coloro che entrano in questo campo e vogliono avere una conoscenza dei metodi matematici che vi si usano.

G. Morpurgo

Direttore responsabile: G. POLVANI Tipografia Compositori - Bologna

Questo fascicolo è stato licenziato dai torchi il 3-V-1958